

**Group 10 Methyl Transfer Reactions toward Catalyst
Development for Oxidative Oligomerization of Methane**

by

Matthew Sean Remy

A dissertation submitted in partial fulfillment
of the requirements for the degree of
Doctor of Philosophy
(Chemistry)
in The University of Michigan
2011

Doctoral Committee:

Professor Melanie S. Sanford, Chair
Professor Mark M. Banaszak Holl
Professor Paul F. Hollenberg
Assistant Professor Nicolai Lehnert

© Matthew Sean Remy

2011

To Courtney, Elyana, and Liam

Acknowledgments

As I near the end of my formal education, I find myself indebted to more people than I can readily count or effectively enumerate. It is impossible for me to truly comprehend the amount of work I have caused for all those involved in my education, but here I offer my thanks with the knowledge that tremendous effort was expended on my behalf. And although I may be just one of many to the majority of those who supported me, all of these people were tremendously important to me.

I must begin by thanking my committee: Prof. Melanie Sanford, Prof. Mark Banaszak Holl, Prof. Nicolai Lehnert, and Prof. Paul Hollenberg. I have been thankful for the mentorship in all things from my research to postdoctoral applications to professional development provided by them all.

Prof. Melanie Sanford gave me the opportunity to grow into a doctor of the philosophy of chemistry. I arrived at the University of Michigan, still a novice in the laboratory and rudimentary in my approach to laboratory work. However, Melanie provided me with an exciting research idea and exceptional guidance throughout my explorations, while giving me the freedom to pursue my interests and turn the project in new directions as new results were uncovered. My approach to scientific writing and presentations has significantly benefitted from Melanie's supervision, and I truly could not have asked for a more enthusiastic and brilliant mentor than Melanie.

I had the privilege of being advised by Prof. Mark Banaszak Holl in my first rotation at the University of Michigan, and I am thankful that opportunity. I spent nearly a semester trying to synthesize an appropriate solvent for the study of enantioselectivity of C-H activation by germynes before I realized I needed to try more than one thing to have a chance at success. It was an important lesson that Prof. Banaszak Holl compassionately guided me through. Prof. Banaszak Holl also has the distinction of introducing me to the world of grant writing during CHEM616. While my idea was naive, it was my first truly original chemistry idea, and I am grateful for that opportunity.

Prof. Nicolai Lehnert was always ready and willing to answer my questions or offer his resources. He was willing to allow me to run calculations on his cluster, and he provided significant insight in N₂ activation for a proposal I prepared.

Prof. Paul Hollenberg was a joy to interact with. He was always welcoming and a consummate gentleman. He was willing to sit down with me and recount the story of his professional development as I was seeking to decide my future, and his encouragement and thoughts were invaluable.

Prof. James Mayer (University of Washington) was also an advisor I am thankful to have worked with. The impact of his advice and guidance during my education were second only to Melanie, and I am thankful for helping me to learn attention to experimental detail. As a reference (and candidate) during my search for a postdoctoral position, Jim was also there during all of my challenges in finally landing a position.

Prof. Thomas Cundari (University of North Texas) gave me the background and technical expertise to enjoy computational chemistry. Thankfully, I know that Tom is my “guru” for all things computational, and throughout my graduate education, Tom responded to each and every one of my questions with amazing haste.

Prof. Adam Matzger also played an influential part in my computational education. He allowed me to use his computational resources, and when I knew nothing about computations, he personally took time to instruct me in the use of computations for modeling chemical reactions.

It is important for me to also thank Professors John Wolfe and Weston Borden (University of North Texas) for allowing me to sit in on their group meetings at various times during my graduate education.

If professors are the fire by which I as a chemist was forged, then my labmates were the whetting stone by which I was honed. I had the privilege of working with a group of the most talented graduate students and postdocs at the University of Michigan, and it was my interactions with them that gave me the greatest joy in my growth as a chemist. It is a special relationship in which both (or multiple) participants are striving to develop the best understanding of the chemistry at hand to mutual benefit of all.

I must thank Amanda Hickman, Brannon Gary, and Dr. Andrew Higgs specifically for their parts in my growth as a chemist. Amanda and I had innumerable

conversations about chemistry, and her insightful questions as a younger graduate student were an amazing opportunity for my growth as a chemist and teacher. Beyond that, Amanda is one of those people who just gets things done, and it was inspiring to see such efficiency and talent in a fellow labmate. Without Brannon Gary, I would have only a fraction of the knowledge of computations that I have now. Having him as someone to bounce questions and ideas off of was an incredibly important part of my education, and I am thankful for his patience in explaining the fundamentals of density functional theory on multiple occasions. Dr. Andrew Higgs and I had spent more time together as first-year graduate students than I did with my wife, Courtney. We spent much time working through classes together and starting in the Sanford lab together. As the two inorganic students joining the lab in 2006, we became great resources for one another in applying the knowledge gained in our classes to the chemistry of the lab. Lunches would have been a shade less bright without Andrew's colorful commentary.

In regards to my chemistry colleagues, I must finish by thanking Dr. Michael Lanci and David Lao from the University of Washington. Without Mike in particular, this project may have taken an entirely different direction, but his mechanistic work on one-electron oxidation of dimethyl-palladium(II) complexes provided invaluable insights in making new C–C bonds from methyl-group 10 complexes. I am proud of our work together and how far we come from the initial conception of the project. Each of us has made significant contributions to the progress of our project, and we did so in a collaboration that was far more than the sum of its parts.

The support staff at University of Michigan's chemistry department make this place feel a bit more like home. While all of the graduate students, professors, and instructors get focused on chemistry, the people in the business office, glassblowing shop, and elsewhere are happy to talk about life outside of confines of chemistry. So not only do they support and make our jobs possible, they bring a bit of the world outside of the walls of the chemistry building to work – and let it show. I thank Roy Wentz for our conversations on religion and his time explaining the art of glassblowing. I am in awe of his craft, and loved watching him work. Rich Gisczack gave me the motivation to go hear a carillon concert in the Burton Memorial Tower that he played. It was a special part of my experience in Ann Arbor, getting to hear the beautiful music of the bells up

close, while partaking a spectacular view of Ann Arbor. Todd Raeker, Doug Cox, and David Rhey made it possible for me do calculations, and Eugenio Alvarado was an invaluable resource in the NMR room. Jim Windak was not only extremely helpful and professional in the instrument lab but also one of the nicest, most accommodating people I have ever met.

Most importantly, I have to thank my family. My dad and mom, Mark and Jamie Remy, never let me think that I could accomplish less than my heart's desire. My in-laws, Bill and Sallie Hosack were always supportive and always gave me reason to believe in my promise as someone who could contribute bountifully to whatever job I undertook. I thank my sister, Heather and my niece, Searra who I love, and who were willing to give me up for nearly a full five years without seeing them so that I could complete this degree.

Courtney, my wife and love of my life, endured with me the struggles of balancing this job, which can be all consuming, and my life with her at home. She patiently let me find a balance that let us both be comfortable, and truly held down the fort at home. Having her to come home to made this experience so much more fulfilling than just the job itself. Her joy of life, friends, and family is contagious, and my most enduring friends from Ann Arbor are those with whom she first formed a relationship. She and our babies, Elyana, Liam, and even Bailey, who we love and cherish together, have given me the great blessing of being able to detach myself fully from my job and focus purely on loving them.

Lastly, I thank God, the Father of life and all that is good, for the blessing of knowing his Son, Christ Jesus, who died for atonement of all sins. Whatever shortfalls I may have as a chemist or a person are consumed by grace and mercy through His sacrifice and my adoption into the sonship of God.

Table of Contents

Dedication.....	ii
Acknowledgments.....	iii
List of Schemes.....	ix
List of Tables	xviii
CHAPTER 1	1
Conversion of Natural Gas to Oxygenates and Higher Alkanes.....	1
1.1 Overview of Natural Gas and Natural Gas Use.....	2
1.2 Indirect Methods for Synthesis of Methanol and Higher Alkanes	4
1.3 Direct Methods for Synthesis of Methanol	5
1.4 Direct Methods for Synthesis of Higher Alkanes.....	7
1.5 Collaboration	10
1.6 References	11
CHAPTER 2	13
Methyl Transfer at Pd(II) Related to Disproportionation Formation of Dimethyl Palladium Species	13
2.1 Background and Significance	13
2.2 Results and Discussion	19
2.3 Conclusions	36
2.4 Experimental Procedures.....	37
2.5 References	45
CHAPTER 3	48
Carbon–Carbon Bond Formation from (tBu-bpy)Pd(CH ₃) ₂ in the Presence of Electron-Deficient Olefins and One-Electron Oxidants	48
3.1 Background and Significance	48

3.2 Results and Discussion	53
3.3 Conclusions	76
3.4 Experimental Procedures	79
3.5 References	81
CHAPTER 4	84
One-Electron Oxidation of Monomethyl Palladium(II) Complexes	84
4.1 Background and Significance	84
4.2 Results and Discussion	87
4.3 Conclusions	108
4.4 Experimental Procedures	111
4.5 References	118
CHAPTER 5	120
Stoichiometric Studies of Disproportionation, One-Electron Oxidation and Reductive Elimination at Platinum.	120
5.1 Background and Significance	120
5.2 Results and Discussion	126
5.3 Conclusions	164
5.4 Experimental Procedures	166
5.5 References	177
CHAPTER 6	180
Nitrogen Insertion into Palladium–Carbon Bonds	180
6.1 Background and Significance	180
6.2 Results and Discussion	182
6.3 Conclusions	190
6.4 Experimental Procedures	190
6.5 References	199

List of Schemes

Scheme 1.1 Oxidative Oligomerization of Methane.....	1
Scheme 1.2 Methods for Reforming Methane to Syn Gas.....	4
Scheme 1.3 Catalytic Cycle for the Shilov System for Methane Oxidation to Methanol..	6
Scheme 1.4 Structure of (bpym)Pt ^{II} (Cl) ₂	7
Scheme 1.5 Breakdown of Chemicals Produced from Ethylene in 1999.....	8
Scheme 1.6 Thermodynamics of Oxidative Coupling of Methane.....	8
Scheme 1.7 Thermodynamics of Methane to Ethane + H ₂	8
Scheme 1.8 Reaction of (tBu-bpy)Pd ^{II} (CH ₃) ₂ (1) with AgI and BQ.....	10
Scheme 1.9 Summary of [(ArDAB)Pt ^{IV} (CH ₃) ₃ (solvent)]PF ₆ Complexes.	11
Scheme 2.1 Schemes for Liquefying Natural Gas.....	13
Scheme 2.2 Fundamental steps for methane oligomerization.....	14
Scheme 2.3 Pathways for C–C Bond Formation from Monomethyl Complexes.....	15
Scheme 2.4 C–H Activation of Methane Leading to Methyl Exchange. ^{7,8}	15
Scheme 2.5 Radical Dimerization to Form Ethane. ⁹	16
Scheme 2.6 Binuclear Reductive Elimination of Ethane. ¹¹	16
Scheme 2.7 Disproportionation Formation of a Dimethyl Complex.	16
Scheme 2.8 Proposed Catalytic Cycle for Pd ^{II} -Catalyzed Homocoupling of Arenes.....	17
Scheme 2.9 Stoichiometric Aryl Disproportionation Leading C–C Bond Formation. ¹⁵ .	17
Scheme 2.10 Computed Aryl Disproportionation for Pd ^{II} -Catalyzed Domino Reactions. ¹⁶	18
Scheme 2.11 Methyl Comproportionation of Pt ^{II} . ²⁰	18
Scheme 2.12 Attempted Disproportionation of 8 in the Absence of Light.....	20
Scheme 2.13 Attempted Disproportionation of 8 in the Presence of Light.....	20
Scheme 2.14 Comproportionation of 6 and 8	20

Scheme 2.15 Hammett Plot for Variation of the Para Substituent on the Pyridine Ligand.	23
Scheme 2.16 Hammett Plot for Variation of the <i>para</i> Substituent on the Phenoxide Ligand.....	25
Scheme 2.17 Synthesis of Methyl Acetyl Complex 9	26
Scheme 2.18 Disproportionation of 9 to Generate Dimethyl Complex 6	26
Scheme 2.19 Summary of Computational and Experimental Measurements of $\Delta G_{\text{disprop}}$	27
Scheme 2.20 Ph–Ph Bond Coupling Driving a Disproportionation Equilibrium.	29
Scheme 2.21 Formation of Ethane Driving a Disproportionation Equilibrium.	29
Scheme 2.22 Monomethyl Complexes Studied in Thermolysis Reactions.....	30
Scheme 2.23 Stability of Monoaryl Complex 14 Toward Disproportionation. ¹⁵	30
Scheme 2.24 Proposed Intermediate in the Synthesis of 10 Related to Thermolysis of 11	33
Scheme 2.25 Thermolysis of (<i>t</i> Bu-bpy)Pd(CH ₃)OAc (12).....	33
Scheme 2.26 Rationale for Using a Substoichiometric Amount of AgOTf.....	34
Scheme 2.27 Reaction of (bpy)Pd(CH ₃) ₂ with O ₂ to Form a Methyl-Peroxo Species.....	35
Scheme 2.28 Decomposition of 16 in Acetone to Produce an Acetyl Complex.....	36
Scheme 3.1 Proposed Catalytic Cycle for Oxidative Oligomerization of Methane.....	48
Scheme 3.2 Common Pathways for C–C Bond Formation.....	49
Scheme 3.3 Thermolysis of (<i>t</i> Bu-bpy)Pd(CH ₃) ₂ (1).....	49
Scheme 3.4 Ethane Formed by C–C Bond Reductive Elimination from Pd ^{II} . ²	50
Scheme 3.5 Oxidative Coupling of 2-phenylpyridine to Arenes Promoted By BQ. ⁵	51
Scheme 3.6 BQ-Promoted Reductive Elimination from a Pd ^{II} -Dimethyl Complex. ⁶	51
Scheme 3.7 Computed ΔG^\ddagger for Ethane Reductive Elimination. ⁶	52
Scheme 3.8 Reaction of Ag ^I with Complex 7 to Ethane. ²⁰	52
Scheme 3.9 Oxidative Pd–CH ₃ Bond Cleavage to Afford Ethane. ²⁰	52
Scheme 3.10 Ce ^{IV} Oxidatively-Induced Reductive Elimination of a C–N Bond. ¹⁸	53
Scheme 3.11 Ag ^I Binding to the <i>dz</i> ² Orbital of (diimine)Pt(CH ₃) ₂ Complexes. ²⁶	54
Scheme 3.12 Alternate Pathways for Ag ^I -Promoted Reductive Elimination.....	54
Scheme 3.13 Reaction (<i>t</i> Bu-bpy)Pd(CH ₃) ₂ (1) with BQ to Afford Ethane.	54

Scheme 3.14 Crossover Study for the Formation of Ethane Promoted by BQ.	55
Scheme 3.15 Scrambling of Methyl Groups in 1 and 1-d₆	55
Scheme 3.16 Oxidation of Pd ⁰ to Pd ^{II} by 1,4-Benzoquinone. ²⁸	56
Scheme 3.17 One-Electron Oxidation Potential for a Pd ^{II/III} Couple. ³⁰	56
Scheme 3.18 Ethane Formation from Ni ^{II} Promoted by Electron-Deficient Arenes. ³¹	57
Scheme 3.19 Proposed Binding of 1,4-Benzoquinone to Complex 1	57
Scheme 3.20 General Structures for Computed (bpy)Pd(CH ₃) ₂ -BQ Intermediates.	58
Scheme 3.21 Singlet and Triplet Electronic States of Pd-BQ Complexes.	58
Scheme 3.22 Calculated (bpy)Pd(CH ₃) ₂ -BQ Intermediate I^I	59
Scheme 3.23 Calculated (bpy)Pd(CH ₃) ₂ -BQ Intermediate I³	60
Scheme 3.24 Calculated (bpy)Pd(CH ₃) ₂ -BQ Intermediate II^I	61
Scheme 3.25 Calculated (bpy)Pd(CH ₃) ₂ -BQ Transition State TS-I^I	62
Scheme 3.26 Calculated (bpy)Pd(CH ₃) ₂ -BQ Transition State TS-I³	62
Scheme 3.27 Calculated (bpy)Pd(CH ₃) ₂ -BQ Transition State TS-II^I	63
Scheme 3.28 Two Components of Olefin Binding to a Metal.	65
Scheme 3.29 Disproportionation of (^t Bu-bpy)Pd(CH ₃)X Followed by BQ-Induced Elimination	68
Scheme 3.30 Reaction of (^t Bu-bpy)Pd(CH ₃)(CH ₂ COCH ₃) (11) with BQ – 24 h.	68
Scheme 3.31 Reaction of (^t Bu-bpy)Pd(CH ₃)(CH ₂ COCH ₃) (11) with BQ – 72 h.	69
Scheme 3.32 Preference for Solvent or Triflate Binding Over BQ at Pd ^{II}	71
Scheme 3.33 Reaction of (^t Bu-bpy)Pd(CH ₃)OAc (15) with BQ.	71
Scheme 3.34 Proposed Oxidation of ArI to Anionic Pd ⁰ Species.	71
Scheme 3.35 Reaction of Complex 1 with AgOTf.	72
Scheme 3.36 Postulated Pd-Ag Adduct in the Reaction 1 with AgPF ₆	73
Scheme 3.37 Molecular Structure of [[(^t Bu-bpy)Pd(CH ₃) ₂] ₃ Tl ₂](PF ₆) ₂ (19).	73
Scheme 3.38 Proposed Inner Sphere Oxidation of Pd ^{II} by Ag ^I	74
Scheme 3.39 One-Electron Oxidant, Ferrocenium Hexafluorophosphate.	74
Scheme 3.40 One-Electron Oxidation of 1 to Produce Ethane.	75
Scheme 3.41 Formation of a Pd ^{IV} -Trimethyl Intermediate Upon One-Electron Oxidation.	75

Scheme 3.42 Independent Synthesis of Pd ^{IV} Complex 20	75
Scheme 3.43 Proposed Mechanism for Generating Complexes 20 and 17 Via One-Electron Oxidation.....	76
Scheme 3.44 One-Electron Oxidation of Dimethyl-platinum Diimine Complexes. ³⁸	76
Scheme 3.45 Synthesis of an Isolable Mononuclear Pd ^{III} Complex. ³⁰	76
Scheme 3.46 Two Concepts for Facilitating Methyl Transfer Between Pd Complexes. .	77
Scheme 3.47 Proposed Catalytic Cycle For Methane Oligomerization Based on One-Electron Oxidation.....	78
Scheme 3.48 Concept for One-Electron Oxidation of Monomethyl Pd Complexes.....	79
Scheme 4.1 Oligomerization of Methane.....	84
Scheme 4.2 C–H Activation of Methane Followed by Oxygenation.....	84
Scheme 4.3 C–C Bond Formation from a Monomethyl-Metal Complex.	85
Scheme 4.4 Disproportionation of (^t Bu-bpy)Pd ^{II} (CH ₃)(CH ₂ COCH ₃) (1). ⁴	85
Scheme 4.5 Computational Optimization of ΔG _{disprop} for (MeDAB)Pd ^{II} (CH ₃)X.	86
Scheme 4.6 A Palladium(IV) Intermediate in the One-Electron Oxidation of 2 . ¹¹	86
Scheme 4.7 One-Electron Oxidation of (^t Bu-bpy)Pd ^{II} (CH ₃)X.....	87
Scheme 4.8 Proposed Palladium(III) in the One-Electron Oxidation of 2	87
Scheme 4.9 Isolable Palladium(III)-Methyl Complexes. ¹²	87
Scheme 4.10 Proposed One-Electron Oxidation of (^t Bu-bpy)Pd ^{II} (CH ₃)(CF ₃) (7).	88
Scheme 4.11 Synthesis of (^t Bu-bpy)Pd ^{II} (CH ₃)(CF ₃) (7).	88
Scheme 4.12 One-Electron Oxidation of (^t Bu-bpy)Pd ^{II} (CH ₃)(CF ₃) (7).	89
Scheme 4.13 Preparation of (^t Bu-bpy)Pd ^{II} (CF ₃)I (9).	89
Scheme 4.14 Effect of CH ₃ versus CF ₃ Substitution on Oxidation Potential. ¹⁸	89
Scheme 4.15 Oxidation of (^t Bu-bpy)Pd ^{II} (CH ₃)(CF ₃) (7) with AcFcBF ₄	90
Scheme 4.16 Synthesis of (^t Bu-bpy)Pd ^{II} (CH ₃)(^t Pr-F ₇) (10).	90
Scheme 4.17 Oxidation of (^t Bu-bpy)Pd ^{II} (CH ₃)(^t Pr-F ₇) (10) with AcFcBF ₄	90
Scheme 4.18 Oxidative Cleavage of the Pd–CH ₃ Bond in (^t Bu-bpy)Pd ^{II} (CH ₃)(CF ₃) (7). 91	
Scheme 4.19 Synthesis of (^t Bu-bpy)Pd ^{II} (CH ₃)OAc (13) by Method 1.	91
Scheme 4.20 Synthesis of (^t Bu-bpy)Pd ^{II} (CH ₃)X via Comproportionation (Method 2). ..	91
Scheme 4.21 C–C versus C–X Bond Formation.....	92

Scheme 4.22 Addition of I ⁻ to Inorganic Products of One-Electron Oxidation.	93
Scheme 4.23 Proposed Pathways for Generating Observed Products Upon One-Electron Oxidation.	94
Scheme 4.24 Oxidation of (^t Bu-bpy)Pd ^{II} (CH ₃)X in the Presence of 1,4-Cyclohexadiene.	95
Scheme 4.25 Path 2, Mechanism A: Disproportionation Followed by Oxidation.	96
Scheme 4.26 Path 2, Mechanism B: Oxidatively-Induced Methyl Transfer.....	96
Scheme 4.27 Monomeric versus Dimeric Monoacetate Palladium(II) Structures.	97
Scheme 4.28 Monomeric Platinum-Monoacetate Complex. ²¹	97
Scheme 4.29 Equilibrium of Monomeric and Dimeric Palladium Monoacetate Complexes. ²²	98
Scheme 4.30 Acetate Transfer Equilibrium between 3 and 21	99
Scheme 4.31 Low Temperature Observation of Intermediates in Oxidation of 13	100
Scheme 4.32 Reaction of 13 and AcFcBF ₄ Proceeding through Mechanism A ₂	101
Scheme 4.33 Reductive Elimination of Ethane from (bpy)Pd ^{IV} (CH ₃) ₃ O ₂ CPh (23).....	101
Scheme 4.34 Reaction of 13 and AcFcBF ₄ Proceeding through Mechanism A ₂	101
Scheme 4.35 Attempted Synthesis of [(^t Bu-bpy)Pd ^{IV} (CH ₃) ₂ OAc(solvent)] ⁺ (17 ^{OAc})....	102
Scheme 4.36 Methyl Group Scrambling in (bpy)Pd ^{IV} (CH ₃) ₃ I. ²⁴	102
Scheme 4.37 Reaction of (^t Bu-bpy)Pd ^{II} (CH ₃)OAc with CD ₃ OTf.....	102
Scheme 4.38 Synthesis of [(^t Bu-bpy)Pd ^{II} (CH ₃) ₂ OAc(acetone)] ⁺ (17 ^{OAc}) with an Electrophilic Source of Acetate.....	103
Scheme 4.39 Low Temperature Observation of a Platinum(IV)-Hydride. ²⁶	103
Scheme 4.40 Use of a Facial Tridentate Tp* Ligand to Stabilize a Pt ^{IV} -Hydride. ²⁷	104
Scheme 4.41 Isolation of a Stable Cationic Pd(IV) Complex. ²⁸	104
Scheme 4.42 Synthesis of (tpa)Pd ^{II} (CH ₃)OAc (28).	104
Scheme 4.43 Synthesis of (tpa)Pd ^{II} (CH ₃)I (27).....	105
Scheme 4.44 Dynamic Exchange of Pyridyl Groups in (tpa)Pd ^{II} (CH ₃)X Complexes. ..	105
Scheme 4.45 One-Electron Oxidation of (tpa)Pd ^{II} (CH ₃)OAc (28).	106
Scheme 4.46 Low Temperature Oxidation of (tpa)Pd ^{II} (CH ₃)OAc (28) with AcFcBF ₄ . 106	
Scheme 4.47 Two Pathways for Oxidation of (tpa)Pd ^{II} (CH ₃)OAc by CH ₃ OTf.....	107
Scheme 4.48 Proposed Synthesis of [(tpa)Pd ^{IV} (CH ₃) ₂ OAc]OAc.....	107

Scheme 4.49 Reaction of (tpa)Pd ^{II} (CH ₃)OAc (28) with CH ₃ OTf.	108
Scheme 4.50 Reaction of (tpa)Pd ^{II} (CH ₃)OAc (32) with PhI(OAc) ₂	108
Scheme 4.51 Picolinate as a Supporting Ligand in One-Electron Oxidation.	110
Scheme 4.52 HX and [(L ₂)Pd ^{II} (CH ₃)(solvent)] ⁺ Formation from a Pd Intermediate.	110
Scheme 4.53 HX and [(L ₂)Pd ^{II} (CH ₃)(solvent)] ⁺ Formation from Pd ^{III}	110
Scheme 4.54 Proposed Catalytic Cycle for Oligomerization of Methane.	111
Scheme 5.1 Oxygenation of Methane Catalyzed by Platinum Salts. ¹	120
Scheme 5.2 Proposed Mechanism for Shilov System for Oxygenation of Methane. ¹ ...	120
Scheme 5.3 C–H Activation of Methane by Pt(II)-Diimine Complexes. ⁴	121
Scheme 5.4 Abbreviation System for 1,4-diaza-1,3-butadiene (DAB) Ligands.	121
Scheme 5.5 C–H Activation as a First Step in Oligomerization of Methane.	121
Scheme 5.6 Proposed Catalytic Cycle for Pd(II)-Catalyzed Homocoupling of Arenes.	122
Scheme 5.7 Methane Activation by [(bpy)Pt(CH ₃)] ⁺ . ¹⁶	122
Scheme 5.8 Two Pathways for Formation of a “Dimethyl”-Platinum Intermediate.	123
Scheme 5.9 Comproportionation of (L) ₂ Pt(CH ₃) ₂ with (L) ₂ (Pt)(X) ₂	123
Scheme 5.10 Effect of Halide on Comproportionation Reaction. ¹⁹	124
Scheme 5.11 Proposed Transition State for Methyl Transfer between Platinum Complexes. ¹⁹	124
Scheme 5.12 Mechanism of Comproportionation of (SMe ₂) ₂ Pt(CH ₃) ₂ and (SMe ₂) ₂ Pt(X) ₂ . ²³	124
Scheme 5.13 X-type Versus L-type Ligand Dissociation in Methyl Transfer Reactions.	125
Scheme 5.14 One-Electron Oxidatively-Induced Methyl Transfer from Pt(II). ²⁴	125
Scheme 5.15 Mechanism of Ethane Elimination from Pt ^{IV} -Phosphine Complexes.	126
Scheme 5.16 Elimination of Ethane from Five-Coordinate Pt ^{IV} with <i>sp</i> ² Nitrogen Chelates. ³³	126
Scheme 5.17 Disproportionation of (^t Bu-bpy)Pd(CH ₃)(CH ₂ COCH ₃). ¹⁷	127
Scheme 5.18 Synthesis of (^t Bu-bpy)Pt ^{II} (CH ₃)OAc.	128
Scheme 5.19 Disproportionation of (^t Bu-bpy)Pt ^{II} (CH ₃)X.	128
Scheme 5.20 Comproportionation of (^t Bu-bpy)Pt ^{II} (CH ₃) ₂ and (^t Bu-bpy)Pt ^{II} (X) ₂	129
Scheme 5.21 Proposed Transition State for Direct Exchange of CH ₃ -for-Cl.	130

Scheme 5.22 Transition State for Methyl Transfer Following Cl ⁻ Dissociation.	130
Scheme 5.23 Methyl Transfer Transition State TS-I^{Pt}	130
Scheme 5.24 Methyl Transfer Transition State TS-II^{Pt}	131
Scheme 5.25 Comproportionation of (^t Bu-bpy)Pd(CH ₃) ₂ and (^t Bu-bpy)Pd(Cl) ₂	132
Scheme 5.26 Methyl Transfer Transition State TS-II^{Pd}	133
Scheme 5.27 Comproportionation of Phenyl to Give (COD)Pt ^{II} (Ph)Cl. ⁴⁴	134
Scheme 5.28 Comproportionation between (COD)Pt ^{II} (Ph) ₂ and [(COD)Pt ^{II} (acetone) ₂] ⁺ . ⁴⁴	134
Scheme 5.29 Comproportionation between (COD)Pt ^{II} (Ph) ₂ and (bpy)Pt ^{II} (Cl) ₂ . ⁴⁴	134
Scheme 5.30 Comproportionation between (bpy)Pt ^{II} (Ph) ₂ and (COD)Pt ^{II} (Cl) ₂ . ⁴⁴	134
Scheme 5.31 Tandem Palladium and Platinum System for Methane Oligomerization.	135
Scheme 5.32 Methyl Transfer from (^t Bu-bpy)Pd ^{II} (CH ₃)Cl to (^t Bu-bpy)Pt ^{II} (CH ₃)Cl.	136
Scheme 5.33 Comparison of Thermodynamic Stability of Pt versus Pd Complexes.	137
Scheme 5.34 Methyl Transfer Transition State TS-II^{Pd-Pt}	138
Scheme 5.35 Methyl Transfer Transition State TS-II^{Pt-Pd}	138
Scheme 5.36 Methyl Transfer from (L ₂)Pt ^{II} (CH ₃)X to (L ₂)Pd ^{II} (X) ₂	139
Scheme 5.37 Tandem Palladium and Platinum System for Methane Oligomerization.	140
Scheme 5.38 Methyl Transfer from (CH ₃ -bpy)Pt ^{II} (CH ₃)I to (NO ₂ -bpy)Pd ^{II} (I) ₂	141
Scheme 5.39 Methyl Transfer from (^t Bu-bpy)Pt(CH ₃)I to (NO ₂ -bpy)Pd(I) ₂	142
Scheme 5.40 Methyl Transfer at Platinum Induced by One-Electron Oxidation.....	143
Scheme 5.41 Synthesis of Platinum-Perfluoroalkyl Complexes by Ligand Displacement.	144
Scheme 5.42 Reaction of (ArDAB)Pt ^{II} (CH ₃) ₂ with Perfluoroalkyl Iodides. ⁴⁵	144
Scheme 5.43 (L ₂)Pt ^{II} (CH ₃) ₂ Complexes Used for Ligand Substitution Reactions.....	144
Scheme 5.44 (L ₂)Pt ^{II} (CH ₃)(R _F) Complexes Utilized in Ligand Exchange.	144
Scheme 5.45 Effect of Perfluoroalkyl Group in One-Electron Oxidation of Pd ^{II}	145
Scheme 5.46 Products of Oxidation of (NBD)Pt ^{II} (CH ₃) ₂ with CF ₃ I. ⁴⁸	145
Scheme 5.47 Attempted Syntheses of (SMe ₂) ₂ Pt ^{II} (CH ₃)(CF ₃).	146
Scheme 5.48 Synthesis of (COD)Pt ^{II} (CH ₃)(ⁿ Bu-F ₉) (14). ⁴⁹	146
Scheme 5.49 Attempted Synthesis of (^t Bu-bpy)Pt ^{II} (CH ₃)(ⁿ Bu-F ₉).	146

Scheme 5.50 Synthesis of (bpy)Pt ^{II} (CH ₃)(ⁿ Bu-F ₉) (16).	147
Scheme 5.51 Comparative Study of “Pt ^{II} (CH ₃) ₂ ” Donors in Synthesis of (py) ₂ Pt ^{II} (CH ₃) ₂ . ⁵⁰	147
Scheme 5.52 Attempted Synthesis of (NBD)Pt ^{II} (CH ₃)(ⁿ Bu-F ₉) (17).	148
Scheme 5.53 Study of Sterics of R _F I on Product Distribution in (COD)Pt ^{II} (CH ₃) ₂ + R _F I.	148
Scheme 5.54 Synthesis of (NBD)Pt ^{II} (CH ₃)(ⁱ Pr-F ₇) (18).	149
Scheme 5.55 Displacement of NBD by Chelating Ligands.	149
Scheme 5.56 Reaction of (NBD)Pt ^{II} (CH ₃)(ⁱ Pr-F ₇) (18) with 4-MePhDAB.	150
Scheme 5.57 Oxidative Addition of R _F I to (ArDAB)Pt ^{II} (CH ₃) ₂	150
Scheme 5.58 Oxidative addition of R _F I to (4-MePhDAB)Pt ^{II} (CH ₃) ₂ . ⁴⁵	150
Scheme 5.59 Syntheses of (ArDAB)Pt ^{II} (CH ₃)(R _F) Complexes, 24 , 25 , and 26	151
Scheme 5.60 Expected Products of One-Electron Oxidation of (L ₂)Pt ^{II} (CH ₃)(X).	151
Scheme 5.61 Summary of all (L ₂)Pt ^{II} (CH ₃)(X) Complexes Synthesized.....	152
Scheme 5.62 Reaction of (^t Bu-bpy)Pt ^{II} (CH ₃)OAc with AcFcBF ₄	153
Scheme 5.63 Reaction of 16 with AcFcBF ₄ in Dichloromethane- <i>d</i> ₂	153
Scheme 5.64 Comparative Oxidation of (bpy)Pt ^{II} (CH ₃)R _F Complexes 16 and 19	153
Scheme 5.65 One-Electron Oxidation of (TMEDA)Pt ^{II} (CH ₃)(ⁱ Pr-F ₇) (20).	154
Scheme 5.66 Stability of (dppe)Pt ^{II} (CH ₃)(ⁱ Pr-F ₇) (21) and (2,6-diClPhDAB)Pt ^{II} (CH ₃)(ⁱ Pr-F ₇) (26) to Oxidation.	154
Scheme 5.67 Reaction of (2,6-diMePhDAB)Pt ^{II} (CH ₃)(ⁱ Pr-F ₇) (24) with AcFcBF ₄	155
Scheme 5.68 Reaction of (2,6-diMePhDAB)Pt ^{II} (CH ₃)(ⁿ Bu-F ₉) (25) with FcBF ₄	155
Scheme 5.69 Synthesis of (2,6-diXDAB)Pt ^{II} (CH ₃)(CF ₃).	156
Scheme 5.70 Proposed Catalytic Cycle for an [(N–N)Pt ^{II} (CH ₃)(solvent)] ⁺ Catalyst.....	157
Scheme 5.71 Ethane Elimination from Platinum(II). ⁵⁴	158
Scheme 5.72 <i>In Situ</i> Synthesis of (ArDAB)Pt ^{IV} (CH ₃) ₃ (solvent)]PF ₆	159
Scheme 5.73 Mechanism of Axial and Equatorial CH ₃ Scrambling in (ArDAB)Pt ^{IV} CH ₃ X.	159
Scheme 5.74 Proposed Stabilization of Five-Coordinate Intermediate in 33	161
Scheme 5.75 Reductive Elimination Transition State TS-33	162
Scheme 5.76 Oxidatively-Induced Methyl Transfer from (ArDAB)Pt ^{II} (CH ₃) ₂	164

Scheme 5.77 Electron-Donating Ligands in Platinum(II) Disproportionation.	165
Scheme 5.78 Electron-Donating Ligands in Platinum-to-Palladium CH Transfer.	165
Scheme 5.79 Generation of a Platinum(II)-Dimethyl Complex Upon Methane Activation.	166
Scheme 6.1 Metal catalyzed amination of aryl halides.	180
Scheme 6.2 Rh-catalyzed C–H Amination. ³	181
Scheme 6.3 Pd-catalyzed Ligand-Directed Functionalization of C–H Bonds.	181
Scheme 6.4 Structure of PhI=NTs oxidant.	181
Scheme 6.5 Proposed Mechanism for Double Nitrogen Insertion into Complex 1	182
Scheme 6.6 Palladium Complexes of Benzo[<i>h</i>]quinoline.	183
Scheme 6.7 Reaction Sequence for Synthesis of Complex 8	184
Scheme 6.8 ORTEP Diagram for Complex 8	185
Scheme 6.9 Amination of Complex 6 with Electronically Diverse Oxidants.	186
Scheme 6.10 Amination of Palladium-8-Ethylquinoline Complex 12	187
Scheme 6.11 Possible Mechanisms for Insertion of “NTs” into the Pd–C Bond.	188
Scheme 6.12 Proposed Catalytic Cycle for Palladium-Catalyzed Amination of C–H Bonds.	190

List of Tables

Table 1.1 Methods for Chemical Liquefaction of Methane.....	2
Table 2.1 Effect of R-group Hybridization on $\Delta G_{\text{disprop}}$	19
Table 2.2 Effect of Tethering L-Type Ligands on $\Delta G_{\text{disprop}}$	21
Table 2.3 Effect of L-Type Ligands on $\Delta G_{\text{disprop}}$	22
Table 2.4 DFT Hammett Study of the Effect of <i>para</i> -Substituted Pyridines on $\Delta G_{\text{disprop}}$	23
Table 2.5 Effect of X-Type Ligands on $\Delta G_{\text{disprop}}$	24
Table 2.6 DFT Hammett Study of the Effect of <i>para</i> -Substituted Phenoxides on $\Delta G_{\text{disprop}}$	25
Table 2.7 Decomposition of Dimethyl Complex 6 Under Ambient Light After 24 h.	26
Table 2.8 Calculation of $\Delta G_{\text{disprop}}$ for Models of Complex 9	27
Table 2.9 Yields of Decomposition Products for Thermolysis of Pd ^{II} -Methyl Complexes Under N ₂	31
Table 2.10 Yields of Decomposition Products for Thermolysis of Pd ^{II} -Methyl Complexes Under O ₂	32
Table 3.1 Calculated Bond Lengths for (bpy)Pd(CH ₃) ₂ -BQ Intermediates.	59
Table 3.2 Calculated ΔH and ΔG for BQ binding to (bpy)Pd(CH ₃) ₂	61
Table 3.3 Calculated ΔH^\ddagger and ΔG^\ddagger for BQ-induced ethane elimination.	64
Table 3.4 Computed Atomic Charges for (bpy)Pd(CH ₃) ₂ -BQ and [(bpy)Pd(CH ₃) ₂ -BQ] [‡]	65
Table 3.5 Products of (^t Bu-bpy)Pd(CH ₃)X Disproportionation and BQ-Induced Elimination	70
Table 3.6 Selected Bond Distances (Å) and Bond Angles (°) for 19	73
Table 4.1 One-Electron Oxidation of (^t Bu-bpy)Pd ^{II} (CH ₃)X.....	92

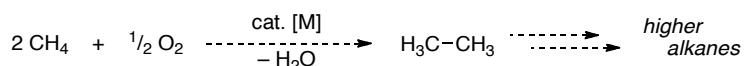
Table 4.2 Proposed Palladium(IV) Intermediates in Path 2 Mechanism.	99
Table 5.1 Comparison of $\Delta G_{\text{disprop}}$ for Pt ^{II} and Pd ^{II} Systems.	127
Table 5.2 Transition State Energies from Methyl Transfer at Pt ^{II}	132
Table 5.3 Transition State Energies from Methyl Transfer at Pd ^{II} and Pt ^{II}	133
Table 5.4 Methyl Transfer from Pt to Pd to Generate (Me-DAB)Pd(CH ₃) ₂	136
Table 5.5 Methyl Transfer from Pd to Pt to Generate (Me-DAB)Pt(CH ₃) ₂	137
Table 5.6 Transition State Energies from Methyl Transfer between Pd ^{II} and Pt ^{II}	138
Table 5.7 Methyl Transfer from (MeDAB)Pt ^{II} (CH ₃)X to (MeDAB)Pd ^{II} (X) ₂	140
Table 5.8 Methyl Transfer from (X-bpy)Pt ^{II} (CH ₃)I to (X'-bpy)Pd ^{II} (I) ₂	141
Table 5.9 Oxidation Potentials of One-Electron Oxidants Employed.	152
Table 5.10 Summary of [(ArDAB)Pt ^{IV} (CH ₃) ₃ (solvent)]PF ₆ Thermolysis Results.	160
Table 5.11 Computation of Reductive Elimination of Ethane from [(ArDAB)Pt ^{IV} (CH ₃) ₃ (solvent)] ⁺	161
Table 5.12 Thermolysis of [(ArDAB)Pt ^{IV} (CH ₃) ₃ (solvent)]PF ₆ in Dichloromethane. ...	163
Table 6.1 Major Products Observed from the Reaction of Complexes 3-6 with PhI=NTs.	184
Table 6.2 Selected Bond Distances (Å) and Bond Angles (°) for Complex 8	186
Table 6.3 Acid Cleavage of Aminated Palladacycles.	189

CHAPTER 1

Conversion of Natural Gas to Oxygenates and Higher Alkanes

The comprehensive goal of the research described in Chapters 2 through 5 of this dissertation is to identify and develop a molecular catalyst for oxidative oligomerization of methane (OOM, Scheme 1.1). Details of the proposed OOM reaction will be enumerated later in this chapter, but the general scheme is introduced at the outset to highlight the overarching purpose of OOM: the chemical conversion of methane to liquid alkane products.

Scheme 1.1 Oxidative Oligomerization of Methane.

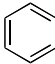
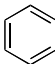


Methane, as the principle component of natural gas,¹⁻³ is a valuable carbon resource that is often relegated to use near its point of origin due to the cost of its transportation.¹ Transforming methane to liquid alkanes represents one solution to the challenge of transportation.

Several methods have been developed for transformation of methane to liquid products. These can be divided into (1) direct methods (whereby methane is converted directly to a liquid alkane product) or (2) indirect methods, (where methane is initially converted to a chemical intermediate(s) followed by reaction of the intermediate(s) to generate liquid products) (Table 1.1). Direct methods include partial oxidation of methane to methanol/methyl esters, conversion of methane to benzene,⁴ and the proposed OOM reaction. Indirect methods include generation of H₂ and CO (synthesis gas) followed by synthesis of methanol or reductive homologation to generate linear alkanes

(the Fischer-Tropsch synthesis),⁵⁻⁸ high temperature (>1400 °C) pyrolysis of methane to acetylene followed by aromatization of acetylene to benzene,⁹ and chlorination of methane with subsequent condensation to generate gasoline and HCl.¹ While of the examples of methane liquefaction listed above each have their own merits and challenges, industrial implementation of nearly all are constrained by a number of factors, including local methane price, capital investment costs, byproducts, and market demand for the liquefied product.

Table 1.1 Methods for Chemical Liquefaction of Methane.

Method	Direct/Indirect	Intermediate(s)	Product
Partial Oxidation	Direct	None	CH ₃ OR
Aromatization	Direct	None	
OOM	Direct	None	Unknown
CH ₃ OH via syn gas	Indirect	H ₂ + CO	CH ₃ OH
Fischer-Tropsch Synthesis	Indirect	H ₂ + CO	Liquid alkanes (diesel fraction)
Pyrolysis	Indirect	H—≡—H	
Chlorination	Indirect	CH ₃ Cl	Gasoline + HCl

This chapter will focus on a comparison of direct and indirect syntheses of methanol/methyl esters and higher (>C1) alkanes as a means of liquefaction of methane for transportation. What follows is a brief discussion of natural gas and natural gas use, with a subsequent comparison of methanol and higher alkane synthesis. The comparison of methanol production to higher alkane production provides an opportunity to discuss challenges of direct conversion in heterogeneous catalysts with advances brought about by study of molecular catalysts.

1.1 Overview of Natural Gas and Natural Gas Use

Natural gas is the most abundant source of naturally-occurring alkanes on the planet.¹⁰ Estimates as of 2009 place the quantity of industrially-relevant natural gas at

186×10^3 billion m^3 . Over the time span from 1970 to 2000, more natural gas was discovered (138×10^3 billion m^3) than consumed (42×10^3 billion m^3).¹¹ These values do not take into account further natural gas holdings that remain technically challenging for large-scale capture and use. The most abundant example of such deposits is methane hydrates collected deep on the ocean floor. Researchers estimate that the natural gas available in these hydrate stores is 190×10^7 billion m^3 (over twice the amount of natural gas found in currently industrially-exploitable deposits). However, its use is pending new developments in sequestration and transportation of the natural gas.

Despite the large abundance of natural gas, its use is typically limited to burning for heat or power rather than as a transportation fuel or feedstock for petrochemicals. A 2009 survey of United States natural gas consumption indicated commercial and residential heating (35%), electric power generation (30%), and industrial usage (32%) made up 97% of natural gas usage.¹² Of the industrial usage, only a marginal amount of natural gas was utilized for synthesis of chemical feedstocks, while the majority of use was for reactor heating, general heating, and power production.¹

These limitations in the use of natural gas are the result of its chemical makeup. Methane, the simplest of alkanes, on average makes up 60–95% of natural gas with ethane (20–1%) making up majority of the balance. The low boiling point of methane (109 K) necessitates compression and cooling for transportation. These transportation constraints limit the markets to which natural gas can be delivered at low cost. Typically, natural gas use is limited to markets nearby its origin or markets directly linked to the point of origin via pipeline. This is especially challenging because many of the major natural gas reservoirs are located in remote regions of the globe, including western Australia, Siberia, and the Amazon Jungle. However, because the deposits are remote, there is little market for using the natural gas for heat or energy, driving down market value of the natural gas.¹

Parmon has provided an illustrative example for the cost incurred transporting natural gas over long distances by pipeline.¹ The natural gas reservoir in the Yamal peninsula of Russia is the largest known, industrially-relevant natural gas reserve in the world. The nearest large market for natural gas is Moscow, some 5,000 km away. Five thousand kilometers is typically considered the maximum economical distance to

transport natural gas via pipeline. The energy required to transport natural gas by pipeline over that distance is equivalent to the energy supplied by burning half of the gas transported. Most of that energy is required for repeated recompression of the gas to 45 to 80 bar at recompression stations, which must be placed approximately every 100 km along a pipeline.¹¹ Energy is also required to separate methane and ethane from higher boiling alkanes before transporting the gas via pipeline to avoid condensation of the heavier alkanes in the pipeline.

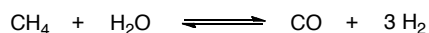
The abundance of natural gas makes it an attractive source for further development of the petrochemical industry. However, the current inability to process methane directly to higher value chemicals and the cost of transporting natural gas over large distances limits opportunities to use natural gas as a high value fuel or chemical feedstock. To monetize remote reservoirs of natural gas, it is important to develop cheap methods of transportation of the gas. Producing liquid products via chemical reaction is one method being aggressively pursued at this moment.

1.2 Indirect Methods for Synthesis of Methanol and Higher Alkanes

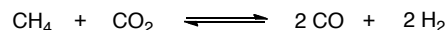
The production of syn gas is a mature industrial technology.^{1,2} Several methods of syn gas production have been developed including steam reforming, dry reforming, partial oxidation, and autothermal reforming (Scheme 1.2).^{13,14} In building syn gas plants, the method of syn gas production is dictated by primarily by the intended products and the scale of the syn gas plant.

Scheme 1.2 Methods for Reforming Methane to Syn Gas.

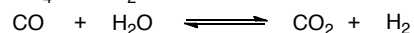
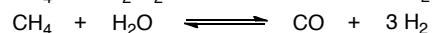
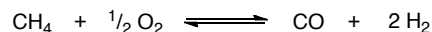
Steam Reforming



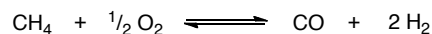
Dry Reforming



Autothermal Reforming



Partial Oxidation



The synthesis of methanol and higher alkanes from syn gas is practiced on 30 million and 18 million tonne/year volumes.¹ Methanol synthesis from H₂ and CO is highly selective (99.9%), and yields of methanol as high as 50% per pass have been reported.¹⁵ Because of the extraordinary selectivity, multiple passes of the syn gas over the catalyst bed are a practical way to reach high conversion. F–T synthesis of produces alkanes in a Schultz-Flory distribution, meaning that the yield of alkane product drops off as the size of the alkane increases. The major fraction of synthesized alkanes is a low-boiling fraction, with methane being the principle product. The major challenges for syn gas technology are: (1) accounting for heat exchange in the reactors and (2) the large capital investment required to build and upkeep the infrastructure. For example, in a F–T plant, two-thirds of the plant’s cost are associated with syn gas production, and a F–T plant costs approximately \$700 million to construct.¹⁶

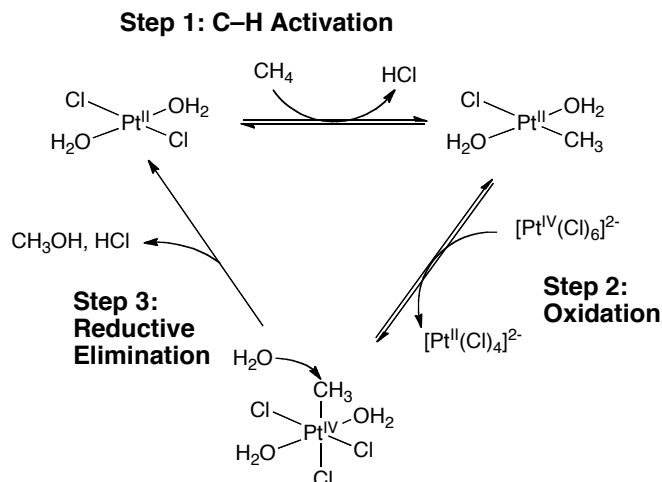
1.3 Direct Methods for Synthesis of Methanol

The direct synthesis of methanol via partial oxidation of methane would circumvent nearly half the cost of a methanol production plant utilizing synthesis gas technology. Heterogeneous catalysts for direct oxidation of methane using O₂ as an oxidant have been limited to ~5% yield with further oxidation products (formaldehyde and CO₂) contributing to the low overall yield and selectivity for methanol.^{17,18} To compete with syn gas production of methanol, the yields of methanol from direct oxidation need to reach ~10%.¹⁹ The low selectivities are attributed to the ease of further reaction of the oxidized products with O₂.

Homogeneous molecular catalysts for direct oxidation of methane to methanol have been explored since Shilov’s initial report on the oxidation of methane using platinum salts in water (Scheme 1.3).²⁰ The oxygenation of methane was proposed to occur via activation of methane by the platinum(II) catalyst (step 1), oxidation of the methyl-platinum(II) complex to platinum(IV) (step 2), and nucleophilic attack of water on the methyl ligand to liberate methanol and regenerate platinum(II) (step 3). The Shilov system was limited by the requirement for platinum(IV) as a stoichiometric oxidant and by catalyst decomposition to platinum metal. However, this discovery has

been foundational for many subsequent developments in homogeneous transition metal catalysts for the direct synthesis of methanol from methane in the decades since its discovery.

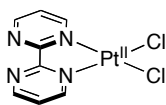
Scheme 1.3 Catalytic Cycle for the Shilov System for Methane Oxidation to Methanol.



In one of the largest advances in the direct oxidation of methane, Periana used $\text{Hg}(\text{SO}_4)_2$ as catalyst in concentrated H_2SO_4 to generate methyl bisulfate ($\text{CH}_3\text{OSO}_3\text{H}$) in 85% selectivity and 43% overall yield.²¹ Previously, Sen used palladium(II) salts in trifluoroacetic acid to mediate conversion of methane to methyl trifluoroacetate ($\text{CH}_3\text{O}_2\text{CF}_3$).^{22,23} Further optimization of the catalyst to $(\text{bpym})\text{Pt}^{\text{II}}(\text{Cl})_2$ (Scheme 1.4) with use of SO_3 as an oxidant produced methyl bisulfate in 81% selectivity and 73% overall yield.²⁴ The reaction was proposed to occur by a similar mechanism to the Shilov cycle.

The outstanding selectivity for a single oxidation of methane to the methyl ester form in these reactions is attributed to the electron-withdrawing ester group, which is proposed to deactivate the oxidized product to further C–H activation and oxidation. However, even for the promising $(\text{bpym})\text{Pt}^{\text{II}}(\text{Cl})_2$ system, industrial implementation has been terminated. The SO_3 oxidant and $(\text{bpym})\text{Pt}^{\text{II}}(\text{Cl})_2$ catalyst required strictly anhydrous conditions, and the use of concentrated H_2SO_4 as a solvent requires addition capital investments to build and maintain corrosion-resistant reactors.

Scheme 1.4 Structure of (bpym)Pt^{II}(Cl)₂.

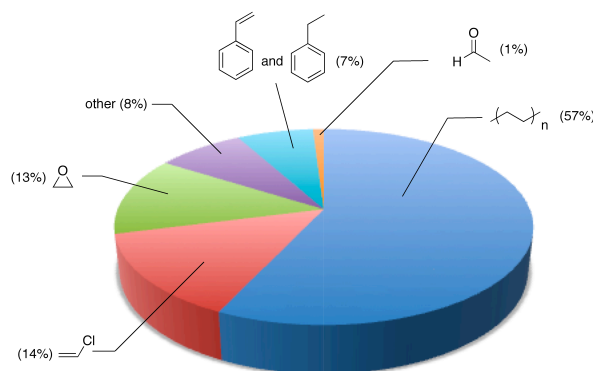


Much like the Shilov system inspired subsequent research toward homogeneous catalysts for methane oxidation, the protecting group strategy has marked a major advance in selective methane partial oxidation to oxygenates. Subsequently, a wealth of research aimed at engineering this strategy into an industrially practicable system has been published.²⁵⁻³¹

1.4 Direct Methods for Synthesis of Higher Alkanes

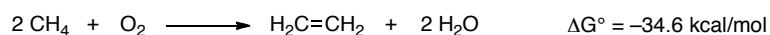
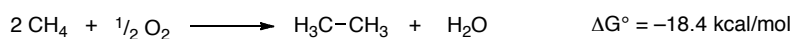
The only currently viable industrial methodology for synthesis of higher alkanes from natural gas is the Fischer-Tropsch synthesis. Initial progress has been made toward methodologies for direct coupling of methane to higher alkanes. Examples include direct catalytic methane oligomerization using a tantalum hydride fragment bound to the surface of dehydrated silica³² and a hybrid oxygenation-dimerization approach where homogeneous catalysts have been developed for synthesis of acetic acid (CH₃CO₂H).^{33,34} Reacting methane with superacids has also generated methane coupling products.³⁵ By far, the most substantial amount of research conducted has been toward direct oxidative coupling of methane (OCM) to ethylene and ethane.³⁶⁻⁴² Targeting the production of ethylene directly from methane is not surprising considering ethylene is a feedstock for roughly 30% of all petrochemicals.¹⁵ Worldwide usage of ethylene in 1999 comprised the synthesis of polyethylene (57%), vinyl chloride (14%), ethylene oxide (13%), ethylbenzene and styrene (7%), and acetaldehyde (1%) (Scheme 1.5).¹⁵

Scheme 1.5 Breakdown of Chemicals Produced from Ethylene in 1999.

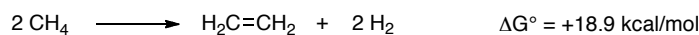


The oxidative coupling of methane (OCM) is significantly exothermic. $\Delta G^0(400\text{ K})$ of oxidative coupling of methane is -18.4 kcal/mol to ethane and -34.6 kcal/mol to ethylene (Scheme 1.6). In contrast, for a non-oxidative process in which H_2 is released, $\Delta G^0(400\text{ K})$ is $+8.6\text{ kcal/mol}$ to ethane and $+18.9\text{ kcal/mol}$ to ethylene (Scheme 1.7). The reaction proceeds by homolytic cleavage of methane C–H bonds over a mixed-metal oxide catalyst such as $\text{SrO/La}_2\text{O}_3$ or $\text{Mn/Na}_2\text{WO}_4/\text{SiO}_2$ to generate methyl radicals, which then dimerize to generate C2 products. Oxygen is used as a limiting reagent in this process to avoid combustion to CO_2 . This limits OCM to producing C2 products, as conversion to higher alkanes (C3 and above) is unfavorable compared to complete combustion to CO_2 .

Scheme 1.6 Thermodynamics of Oxidative Coupling of Methane.



Scheme 1.7 Thermodynamics of Methane to Ethane + H_2 .



The best catalysts under these conditions are capable of generating C2 products in $\sim 80\%$ selectivity and 25% yield on a laboratory scale.⁴³ These values are expected to decrease upon scale-up⁴⁴ due to the challenges of heat management of the exothermic reaction in a larger catalyst bed.³⁶ In order to make the process industrially viable, it is

estimated that selectivity for C2 products and yield must be approximately >80% and 16-30%, respectively, with a single pass of the methane over the catalyst.⁴⁵ However, in 1988, Labinger calculated the maximum yield for current OCM catalysts to be 30% yield.⁴⁶ A more recent 2003 report by Green, which used a more complex algorithm for determining the maximum yield, actually lowered the theoretical maximum to 28% yield for C2 products. The authors concluded that until new classes of catalysts were designed or an alternate mechanism was developed, the yields and selectivity needed for an industrially-applicable process could not be achieved.

Interestingly, Green also pointed out that researchers have been almost exclusively focused on increasing the activity of the OCM catalysts by making them better H atom abstractors. Like the synthesis of methanol from methane, OCM has reached a point where it needs a substantial advance to ignite the field. Current economics have sparked a new flurry of activity toward OCM with researchers using the most modern techniques for heterogeneous catalyst preparation,⁴⁷ but no major advances have been reported. To date, no homogeneous catalyst has been developed for OCM or oxidative oligomerization of methane (OOM). Whereas homogeneous catalyst development helped open a new paradigm in catalyst development for methane oxygenation, homogeneous catalyst development has the potential to provide new insights into the field of methane coupling.⁴⁸

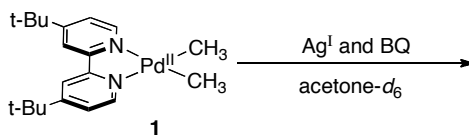
In Chapter 2, I describe our initial foray into homogeneous OOM catalyst design that is based on the related dimerization of arenes by homogeneous palladium complexes. In Chapters 3 through 5, our approach to catalyzing this reaction evolves as our fundamental studies toward oxidation revealed an oxidatively-induced methyl transfer event. The overarching goal of this catalyst development is to catalytically generate liquid alkanes from methane. To that end, this dissertation describes fundamental studies of methyl-metal complexes as models for the expected products of C–H activation.^{20,49} Conversion of the methyl ligands into ethane is a model for the necessary C–C bond-forming reaction of OOM. The fundamental studies described herein are a starting point for achieving catalytic OOM.

1.5 Collaboration

Throughout my pursuit toward developing a catalyst for the oxidative oligomerization of methane, I have had the privilege of collaborating with Prof. James M. Mayer and Dr. Michael P. Lanci. It is the combination of our efforts that has brought this project to its current state. Thus, it is important to point out the contributions Dr. Lanci, which are included herein to highlight and provide context for my own data.

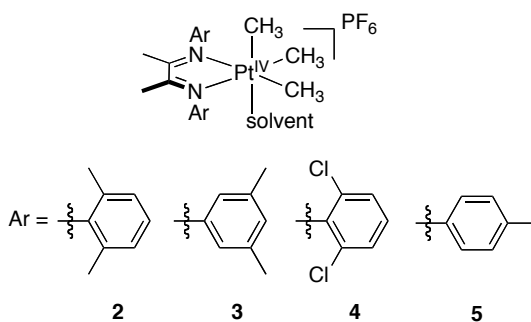
In Chapter 3, I discovered reactions of (*t*-Bu-bpy)Pd^{II}(CH₃)₂ (**1**) (*t*-Bu-bpy = 4,4'-di-*tert*-butyl-2,2'-bipyridine) with Ag^I and 1,4-benzoquinone (BQ) that produced ethane. Dr. Lanci characterized all of the products of the reactions and provided evidence for the mechanism of each reaction. All work related to the oxidation of **1** by ferrocenium hexafluorophosphate was performed by Dr. Lanci.

Scheme 1.8 Reaction of (*t*-Bu-bpy)Pd^{II}(CH₃)₂ (**1**) with Ag^I and BQ.



In Chapter 5, Dr. Lanci demonstrated facile evolution of ethane from [(2,6-diMePhDAB)Pt^{IV}(CH₃)₃(solvent)]⁺ (**2**). He also provided computations on the energetic differences of ethane elimination between the related complexes **2** and [(3,5-diMePhDAB)Pt^{IV}(CH₃)₃(solvent)]⁺ (**3**). My work on [(2,6-diClPhDAB)Pt^{IV}(CH₃)₃(solvent)]⁺ (**4**) and [(4-MePhDAB)Pt^{IV}(CH₃)₃(solvent)]⁺ (**5**) and computations on **4** served to support our hypothesis that 2,6-substitution of the ligands was necessary for the inducing facile ethane elimination.

Scheme 1.9 Summary of [(ArDAB)Pt^{IV}(CH₃)₃(solvent)]PF₆ Complexes.



1.6 References

- (1) Deroune, E. G., Ed.; Parmon, V., Ed.; Lemos, F., Ed.; Ribeiro, F. R., Ed. *Sustainable Strategies for the Upgrading of Natural Gas: Fundamentals, Challenges, and Opportunities*; Springer: Dordrecht, The Netherlands, 2005.
- (2) Marks, T. J. et. Al. *Chem. Rev.* **2001**, *101*, 953.
- (3) Crabtree, R. H. *Chem. Rev.* **1995**, *95*, 987.
- (4) Choudhary, T. V.; Aksoylu, E.; Goodman, D. W. *Catal. Rev.* **2003**, *45*, 151.
- (5) Khodakov, A. Y.; Chu, W.; Fongarland, P. *Chem. Rev.* **2007**, *107*, 1692.
- (6) Dry, M. E. *Catal. Today* **2002**, *71*, 227.
- (7) Jager, B.; Espinoza, R. *Catal. Today* **1995**, *23*, 17.
- (8) Rofer-DePoorter, C. K. *Chem. Rev.* **1981**, *81*, 447
- (9) Weill, J.; Chevron, F.; Raimbault, C.; Genier, R. Renesme, G.; Capogna, L.; Muller, Y. *Rev. Inst. Fr. De Pétrole* **1992**, *47*, 255.
- (10) International Energy Agency (2009) Natural Gas Information. Copyrighted data used in accordance with the terms and conditions for subscribers.
- (11) Institut Français du Pétrole (2002) Fundamentals of Natural Gas.
- (12) Energy Information Administration (2009) Annual Energy Review.
- (13) Rostrup-Nielsen, J. R.; Sehested, J.; Nørskov, J. K. *Adv. Catal.* **2002**, *47*, 65.
- (14) Aasberg-Peterson, K.; Bak Hansen, J.-H.; Christensen, T. S.; Dybkjær, I.; Seier Christiansen, P.; Stub Nielsen, C.; Winter Madsen, S. E. L.; Rostrup-Nielsen, J. R. *App. Catal. A* **2001**, *221*, 379.
- (15) Weissermel, K.; Arpe, H.-J.; Lindley, C. R., trans.; Hawkins, S., trans. *Industrial Organic Chemistry: 4th Ed*; Wiley-VCH: Weinheim, Germany, 2003.
- (16) Eur. Chem. News 2003, February 10, 22.
- (17) Wolf, D. *Angew.Chem., Int. Ed.* **1998**, *37*, 24.
- (18) Baerns, M.; Ross, J. R. H.; Thomas, J. A., Ed.; Zamaraev, K. I., Ed. *Perspectives in Catalysis*, Blackwell, Oxford, **1992**.
- (19) Parkyns, N. D.; Warburton, C. I.; Wilson, J. D.; *Catal. Today* **1993**, *18*, 385.
- (20) Shilov, A. E.; Shul'pin, G. B. *Chem. Rev.* **1997**, *97*, 2879.
- (21) Periana, R. A.; Taube, D. J.; Evitt, E. R.; Löffler, D. G.; Wentreck, P. R.; Voss, G.; Masuda, T. *Science* **1993**, *259*, 340.

-
- (22) Kao, L. C.; Hutson, A. C.; Sen, A. *J. Am. Chem. Soc.* **1991**, *113*, 700.
- (23) Gretz, E.; Oliver, T. F.; Sen, A. *J. Am. Chem. Soc.* **1987**, *109*, 8109.
- (24) Periana, R. A.; Taube, D. J.; Gamble, S.; Taube, H.; Satoh, T.; Fujii, H. *Science* **1998**, *280*, 560.
- (25) Palkovits, R.; Antonietti, M.; Kuhn, P.; Thomas, A.; Schüth, F. *Angew. Chem., Int. Ed.* **2009**, *48*, 6909.
- (26) Michalkiewicz, B.; Kosowski, P. *Catal. Commun.* **2007**, *8*, 1939
- (27) Cheng, J.; Li, Z.; Haught M.; Tang, Y. *Chem. Commun.* **2006**, 4617.
- (28) Mukhopadhyay, S.; Zerella, M.; Bell, A. T. *Adv. Synth. Catal.* **2005**, *347*, 1203
- (29) Bar-Nahum, I.; Khenkin, A. M.; Neumann, R. *J. Am. Chem. Soc.* **2004**, *126*, 10236.
- (30) C. J., Jones, Taube, D.; Ziatdinov, V. R.; Periana, R. A.; Nielsen, R. J.; Oxgaard, J.; Goddard, W. A. *Angew. Chem., Int. Ed.* **2004**, *43*, 4626.
- (31) Shul'pin, G. B.; Nizova, G. V.; Kozlov, Y. N.; Gonzalez Cuervo, L.; Süss-Fink, G. *Adv. Synth. Catal.* **2004**, *346*, 317.
- (32) Soulivong, D.; Norsic, S.; Taoufik, M.; Copéret, C.; Thivolle-Cazat, J.; Chakka, S.; Basset, J. M. *J. Am. Chem. Soc.* **2008**, *130*, 5044.
- (33) Periana, R. A.; Mironov, O.; Taube, D.; Bhalla, G.; Jones, C. J. *Science* **2003**, *301*, 814.
- (34) Jia, C. G.; Kitamura, T.; Fujiwara, Y. *Acc. Chem. Res.* **2001**, *34*, 633
- (35) Olah, G. A. *Acc. Chem. Res.* **1987**, *20*, 422.
- (36) Lunsford, J. H. *Catal. Today* **2000**, *63*, 165.
- (37) Mleczko, L.; Baerns, M. *Fuel Proc. Tech.* **1995**, *42*, 217.
- (38) Maitra, A. M. *App. Catal. A* **1993**, *104*, 11.
- (39) Wolf, E. E., Ed. *Methane Conversion by Oxidative Processes*; Van Nostrand Reinhold: New York, New York, 1992.
- (40) Amenomiya, Y.; Birss, V. I.; Goledzinowski, M.; Galuszka, J.; Sanger, A. R. *Catal. Rev. Sci. Eng.* **1990**, *32*, 163.
- (41) Hutchings, G. J.; Scurrrell, M. S.; Woodhouse, J. R. *Chem. Soc. Rev.* **1989**, *18*, 251.
- (42) Lee, J. S.; Oyama, S. T. *Catal. Rev. Sci. Eng.* **1988**, *30*, 249.
- (43) Holmen, A. *Catal. Today* **2009**, *142*, 2.
- (44) Su, Y. S.; Ying, J. Y.; Green, W. H., Jr. *J. Catal.* **2003**, *218*, 321.
- (45) Gradassi, M. J.; Green, N. W. *Fuel Proc. Technol.* **1995**, *42*, 65.
- (46) Labinger, J. A. *Catal. Lett.* **1988**, *1*, 371.
- (47) "Ethylene from Ethane" *Chem. and Eng. News*. 2011, January 17.
- (48) Labinger, J. A. *J. Mol. Catal. A* **2004**, *220*, 27.
- (49) Lersch, M.; Tilset, M. *Chem. Rev.* **2005**, *105*, 2471.

CHAPTER 2

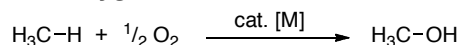
Methyl Transfer at Pd(II) Related to Disproportionation Formation of Dimethyl Palladium Species

2.1 Background and Significance

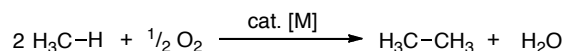
Methane, the principal constituent of natural gas, is the most abundant alkane on the planet.¹ Transformation of methane into a liquid would allow for far greater usage of natural gas as a fuel (see Chapter 1 for a more detailed discussion). As a result, liquefaction of natural gas is a grand challenge for scientists. While substantial efforts have been made toward liquefying methane by oxygenation (Path A, Scheme 2.1), little progress has been made toward the oxidative oligomerization of methane (Path B, Scheme 2.1).

Scheme 2.1 Schemes for Liquefying Natural Gas.

Path A: Oxygenation of Methane

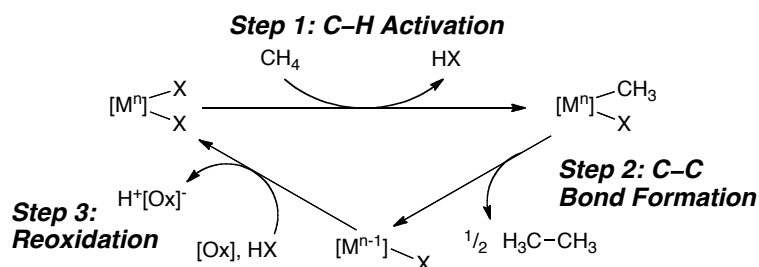


Path B: Oxidative Oligomerization of Methane



For the homogeneous oxidative oligomerization of methane, we propose a catalyst must perform three fundamental steps: 1) C-H activation, 2) C-C bond formation, and 3) oxidation to regenerate the catalyst (Scheme 2.2).

Scheme 2.2 Fundamental steps for methane oligomerization.

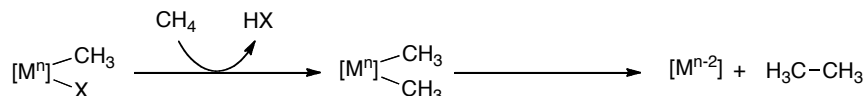


As depicted in Scheme 2.2, a catalyst must first activate methane (Step 1). C-H activation of methane has been studied extensively.²⁻⁶ In methane functionalization reactions catalyzed by late transition metals, methane activation is often proposed to proceed through a monomethyl intermediate, formed by cleavage of a C-H bond to make a new M-C bond (Step 1, Scheme 2.2).

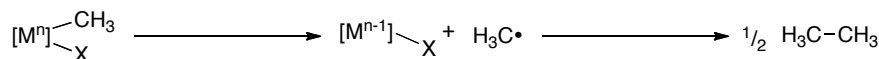
For subsequent oligomerization, a significant challenge is formation of a C-C bond from the monomethyl intermediate. Four general pathways exist for forming a new C-C bond from a monomethyl species: 1) C-H activation to form a dimethyl-metal complex followed by reductive elimination (Scheme 2.3, Path A), 2) radical dimerization of methyl radicals (Scheme 2.3, Path B), 3) bimolecular C-C bond reductive elimination (Scheme 2.3, Path C), and 4) methyl transfer between two metal centers to generate a dimethyl-metal intermediate followed by reductive elimination (Scheme 2.3, Path D).

Scheme 2.3 Pathways for C–C Bond Formation from Monomethyl Complexes.

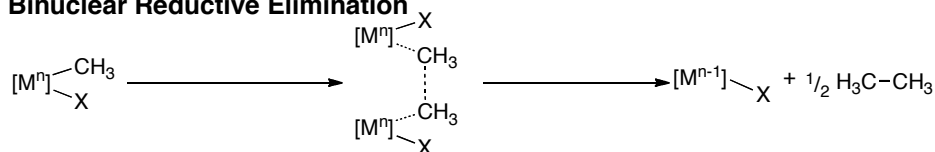
Path A: C–H Activation



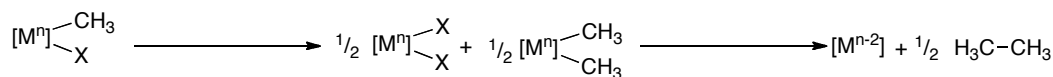
Path B: Radical Homocoupling



Path C: Binuclear Reductive Elimination

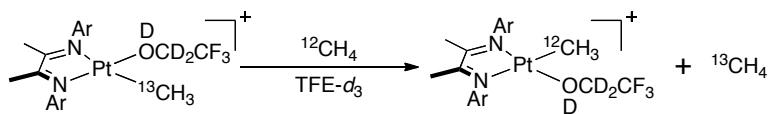


Path D: Disproportionation Followed by Reductive Elimination



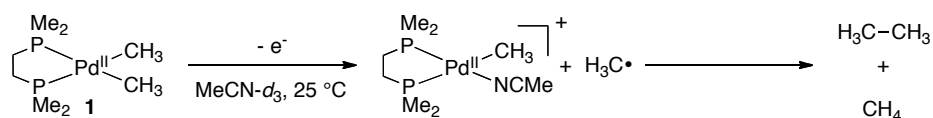
For group 10 metals, C–H activation of methane by a monomethyl complex to generate a dimethyl species is unknown (Path A, Scheme 2.3). Bercaw and Tilset have shown through labeling studies that C–H activation of methane by [(diimine)Pt(CH₃)(solvent)]⁺ complexes results in exchange of the methyl group rather than formation of a dimethyl-platinum species (Scheme 2.4).^{7,8}

Scheme 2.4 C–H Activation of Methane Leading to Methyl Exchange.^{7,8}



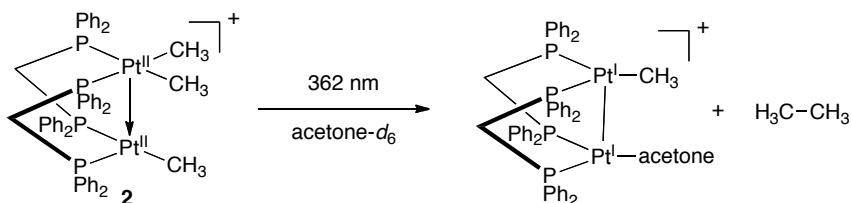
Radical dimerization (Path B, Scheme 2.3) has been proposed upon one-electron oxidation of dimethyl palladium complex **1** (Scheme 2.5).⁹ In this reaction, the Pd–C bond is homolytically cleaved to generate a methyl radical which then undergoes reaction with a proximal Pd–C bond to generate ethane. Formation of ethane in this proposed mechanism is reliant on the presence of a nearby Pd–C bond to trap the reactive methyl radical. In the absence of a trap, free methyl radicals generated form only a small amount ethane instead giving up to 120:1 CH₄ to ethane ratio.¹⁰

Scheme 2.5 Radical Dimerization to Form Ethane.⁹



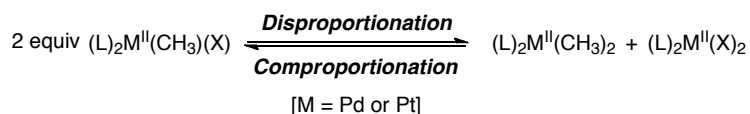
Bimolecular C–C bond-forming reductive elimination (Path C, Scheme 2.3) has been proposed for systems in which the two metal centers are tethered by bridging ligands. Methyl/methyl-*d*₃ labeling studies of complex **2** suggest that C–C bond formation is at least partly attributable to intramolecular reductive elimination across two Pt metal centers (Scheme 2.6).¹¹ However, although intramolecular reductive elimination was proposed for **2**, there is a significant gap in understanding the excited state behavior of this complex upon photolysis, leaving open the possibility of reductive elimination from a single Pt^{II} center.

Scheme 2.6 Binuclear Reductive Elimination of Ethane.¹¹



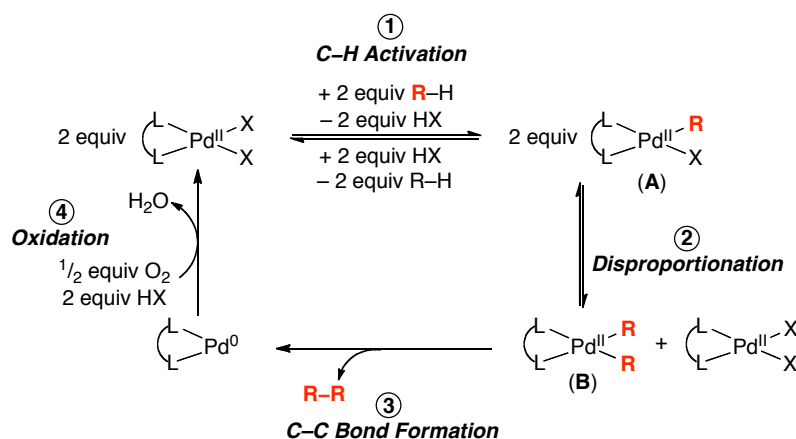
Methyl transfer between metal centers to generate a dimethyl–metal intermediate from which unimolecular C–C reductive elimination can occur (Path D, Scheme 2.3) is directly related to proposed mechanisms for aryl–aryl homocouplings.^{12–15} In these reactions, two metal centers undergo a methyl-for-X metathesis (called disproportionation) that converts two equiv of (L)₂(M)(CH₃)(X) into one equiv of each (L)₂(M)(CH₃)₂ and (L)₂(M)(X)₂ (Scheme 2.7).

Scheme 2.7 Disproportionation Formation of a Dimethyl Complex.

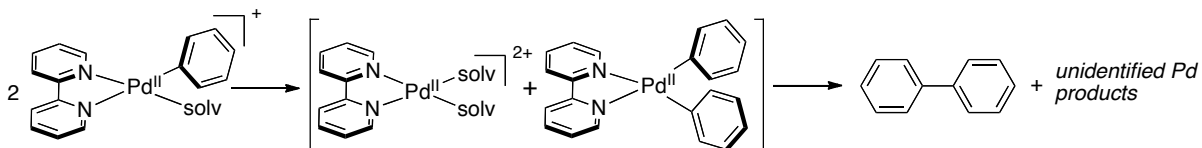


The proposed catalytic cycle for palladium-catalyzed homocoupling of arenes requires the disproportionation of 2 equiv of $(L)_2Pd(R)(X)$ to generate 1 equiv of $(L)_2Pd(R)_2$ and 1 equiv of $(L)_2Pd(X)_2$ (Step 2, Scheme 2.8). In related stoichiometric studies, of the formation of biaryl coupling products from monoaryl Pd^{II} species have been postulated to occur via an initial disproportionation to a diaryl- Pd^{II} intermediate (Scheme 2.8).¹⁵ Computational evidence has also been presented for disproportionation leading to aryl-aryl bond formation in Pd-catalyzed domino reactions (Scheme 2.9).¹⁶ The authors contend that disproportionation between **3** and **4** is more favorable than the previously proposed mechanism which involved oxidative addition of Ph-I at **4** to generate a Pd^{IV} intermediate. Further examples of disproportionation have been directly observed at both Pd^{II} (with $R = Ph$,^{13,17} alkynyl¹⁸) and at Pt^{II} (with $R = Ph$).¹⁹ Although alkynyl and aryl disproportionations are good precedents, the oxidative oligomerization of methane requires disproportionation of methyl ligands. When we initiated this research, the disproportionation of analogous Pd^{II} or Pt^{II} -methyl species was not known.

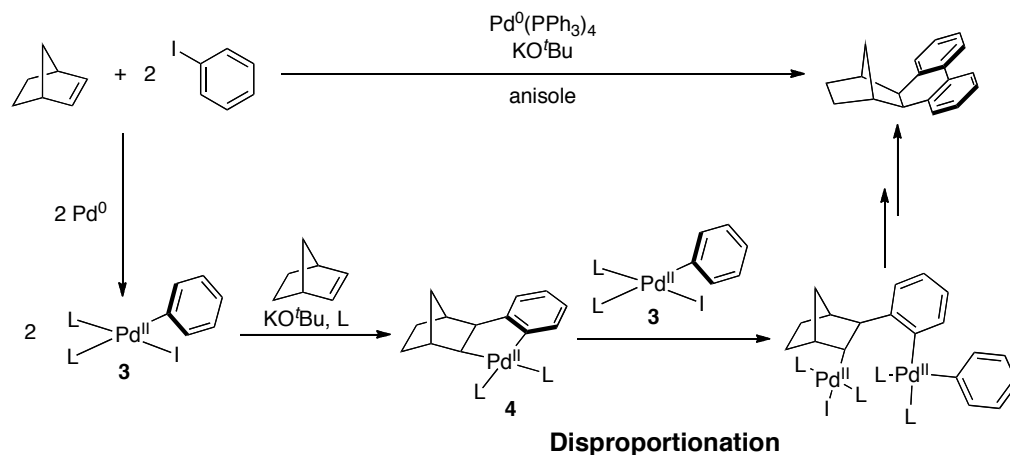
Scheme 2.8 Proposed Catalytic Cycle for Pd^{II} -Catalyzed Homocoupling of Arenes.



Scheme 2.9 Stoichiometric Aryl Disproportionation Leading C-C Bond Formation.¹⁵

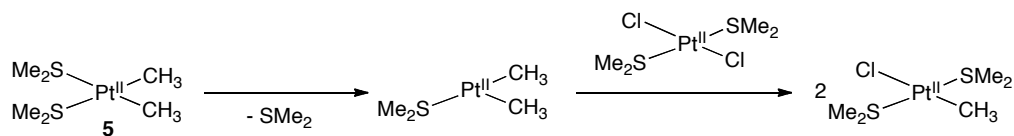


Scheme 2.10 Computed Aryl Disproportionation for Pd^{II}-Catalyzed Domino Reactions.¹⁶



Importantly, comproportionation, the microscopic reverse of disproportionation, is known for the reaction of Pt^{II} dimethyl complexes with their Pt^{II} dihalide counterparts (Scheme 2.11).²⁰ Kinetic studies of this reaction showed that loss of a dimethyl sulfide ligand from **5** precedes methyl transfer. These studies indicate that π systems present in sp^2 and sp group transfers are not required in group transfer reactions. Further precedent for comproportionation has been shown at Pd^{II} centers with R = Ph,^{17,21} alkynyl¹⁸ and at Pt^{II} centers with R = Ph,²²⁻²⁴ alkynyl,^{25,26} and CH₃.^{27,28} These studies suggest that methyl group disproportionation is kinetically feasible but appears to be thermodynamically unfavorable.

Scheme 2.11 Methyl Comproportionation of Pt^{II}.²⁰



In pursuit of facilitating methyl disproportionation, we took two approaches to assess the reaction of monomethyl-palladium complexes to form dimethyl-palladium complexes. First, we initiated density functional theory (DFT) calculations (B3LYP/CEP-31G(d))^{29,30} to evaluate the thermodynamics associated with methyl disproportionation at square-planar complexes as a function of the ligands L and X. Secondly, we sought to thermolyze monomethyl complexes in order to probe for the

characteristic reactivity of any dimethyl palladium complex that formed via disproportionation.

2.2 Results and Discussion

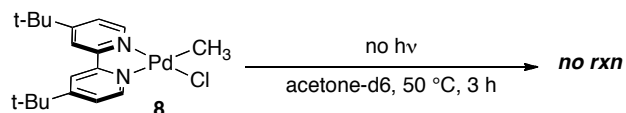
We first examined the relative thermodynamics of methyl, phenyl, and alkynyl group disproportionation at (MeDAB)Pd^{II}(R)(Cl) (MeDAB = N,N^o-dimethyl-1,4-diazabutene). This diimine was selected because Pt and Pd complexes containing related ligands are known to promote both stoichiometric³¹ and catalytic^{31,32} C–H activation reactions. Tilset had also shown simplified diimine structures to be valid models in computations of platinum C–H activation intermediates.⁸ The singlet ground-state structures for (MeDAB)Pd(R)(Cl), (MeDAB)Pd(R)₂, and (MeDAB)Pd(Cl)₂ were optimized for each R ligand in the gas phase at 298 K and 1 atm. Solvent corrections in acetone were performed as single-point energy calculations on the optimized gas-phase structures using the integral equation formalism of the polarizable continuum model (IEFPCM). $\Delta G_{\text{disprop}}$ was then calculated on the basis of these optimized ground-state energies. As summarized in Table 2.1, the disproportionation reactions with R = Ph, CH₃ are thermodynamically uphill at 298 K, while when R = alkynyl the disproportionation is thermoneutral. Significantly, ΔG for methyl disproportionation is >3 kcal/mol further uphill than the analogous phenyl reaction (Table 1, entries 1 and 2). Notably, for all R groups, the acetone solvent correction had minimal effect (< 1 kcal/mol) on the calculated values of ΔG .

Table 2.1 Effect of R-group Hybridization on $\Delta G_{\text{disprop}}$.

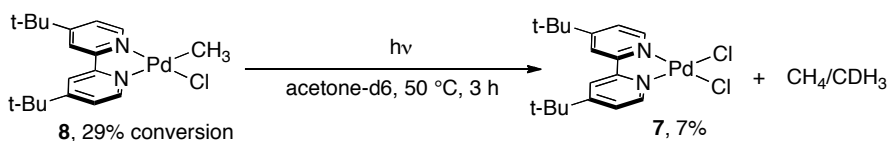
$\Delta G_{\text{disprop}}$ (kcal/mol)			
Entry	R	gas phase	IEFPCM (acetone)
1	CH ₃	11.7	11.0
2	C ₆ H ₅	7.6	7.8
3	C ₂ H	0.0	0.1

The data in Table 2.1 indicate that K_{eq} for the disproportionation of (MeDAB)Pd(CH₃)(Cl) should be approximately 8×10^{-9} in acetone. To experimentally test this prediction, we synthesized the related complexes (^tBu-bpy)Pd(CH₃)₂ (**6**), (^tBu-bpy)Pd(Cl)₂ (**7**), and (^tBu-bpy)Pd(CH₃)(Cl) (**8**) and examined their reactivity in methyl group transfer reactions. As predicted, isolated samples of (^tBu-bpy)Pd(CH₃)(Cl) (**8**) did not react to form detectable quantities of complex **6** under any conditions examined. Thermolyzing **8** for 18 h at 50 °C in acetone-*d*₆ in the absence of light resulted in no change by ¹H NMR spectroscopy with **8** still being observed in 99% yield relative to internal standard (Scheme 2.12). When thermolyzed under identical conditions but in the presence of ambient room light, **8** decomposed slightly, with 71% **8** remaining after 18 h and 7% **7** being formed along with CH₄ and CDH₃ (Scheme 2.13). However, **6** was not detected at any point during the reaction. Furthermore, stirring a 1:1 mixture of **6** and **7** in acetone-*d*₆ at 50 °C for 18 h led to the complete consumption of **6** and **7** and formation of (^tBu-bpy)Pd(CH₃)(Cl) (**8**) in quantitative yield (99% as determined by ¹H NMR spectroscopy) (Scheme 2.14). These experimental observations are all consistent with the calculated equilibrium constant, which greatly favors the comproportionation reaction.

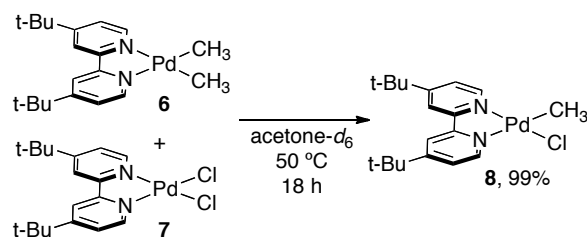
Scheme 2.12 Attempted Disproportionation of **8** in the Absence of Light



Scheme 2.13 Attempted Disproportionation of **8** in the Presence of Light.



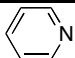
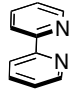
Scheme 2.14 Comproportionation of **6** and **8**.



We next used DFT calculations to probe the influence of the L-type ligand (L) on $\Delta G_{\text{disprop}}$ for complexes of general structure $(L)_2\text{Pd}(\text{CH}_3)(\text{Cl})$. The *cis* isomers were examined in these calculations, since the vast majority of group 10 complexes that promote C–H activation contain *cis*-chelating L-L ligands.³¹⁻³⁵ Importantly, as shown in Table 2.2, covalently tethering the *cis* L-type ligands had only a minimal impact on $\Delta G_{\text{disprop}}$.

Table 2.2 Effect of Tethering L-Type Ligands on $\Delta G_{\text{disprop}}$.

$$2 \begin{array}{c} \text{L} \\ \diagdown \\ \text{Pd} \\ \diagup \\ \text{L} \end{array} \begin{array}{c} \text{CH}_3 \\ \diagdown \\ \text{I} \end{array} \xrightleftharpoons{\Delta G_{\text{disprop}}} \begin{array}{c} \text{L} \\ \diagdown \\ \text{Pd} \\ \diagup \\ \text{L} \end{array} \begin{array}{c} \text{CH}_3 \\ \diagdown \\ \text{CH}_3 \end{array} + \begin{array}{c} \text{L} \\ \diagdown \\ \text{Pd} \\ \diagup \\ \text{L} \end{array} \begin{array}{c} \text{I} \\ \diagdown \\ \text{I} \end{array}$$

Entry	L	$\Delta G_{\text{disprop}}$ (kcal/mol)
1		10.6
2		11.1

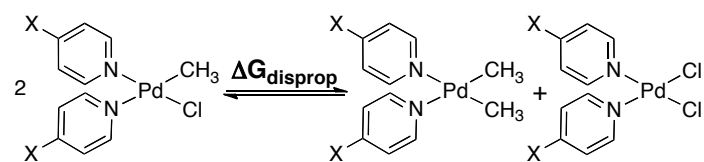
Ground-state structures for *cis*- $(L)_2\text{Pd}(\text{CH}_3)_2$, *cis*- $(L)_2\text{Pd}(\text{CH}_3)(\text{Cl})$, and *cis*- $(L)_2\text{Pd}(\text{Cl})_2$ were obtained from geometry optimizations for a variety of monodentate L-type donors, and $\Delta G_{\text{disprop}}$ was determined for each ligand L in the gas phase. As summarized in Table 2.3, $\Delta G_{\text{disprop}}$ remained >7 kcal/mol with all of the ligands examined. Nonetheless, L did have a significant influence on the value of $\Delta G_{\text{disprop}}$, with strongly σ -donating ligands such as 1,3-dimethylimidazol-2-ylidene (Me_2Im), PH_3 , $\text{C}_5\text{H}_5\text{N}$, and NH_3 (entries 1-5) providing the most favorable equilibria for this transformation. Gratifyingly, chelating carbenes,³⁵ diamines,³⁶ diimines,³¹ bipyridine derivatives,³⁴ and phosphines^{23,37} are all known to support group 10 metal complexes capable of alkane activation. In contrast, weaker σ -donors such as MeCN , SH_2 , and OH_2 (entries 6, 8, and 10) as well as strong π -acceptors such as PF_3 , CO , and ethylene (entries 7, 9, and 11) provided much larger values of $\Delta G_{\text{disprop}}$ in this system.

Table 2.3 Effect of L-Type Ligands on $\Delta G_{\text{disprop}}$.
$$2 \begin{array}{c} \text{L} \diagup \text{Pd} \text{---} \text{CH}_3 \\ \text{L} \diagdown \text{---} \text{Cl} \end{array} \xrightleftharpoons{\Delta G_{\text{disprop}}} \begin{array}{c} \text{L} \diagup \text{Pd} \text{---} \text{CH}_3 \\ \text{L} \diagdown \text{---} \text{CH}_3 \end{array} + \begin{array}{c} \text{L} \diagup \text{Pd} \text{---} \text{Cl} \\ \text{L} \diagdown \text{---} \text{Cl} \end{array}$$

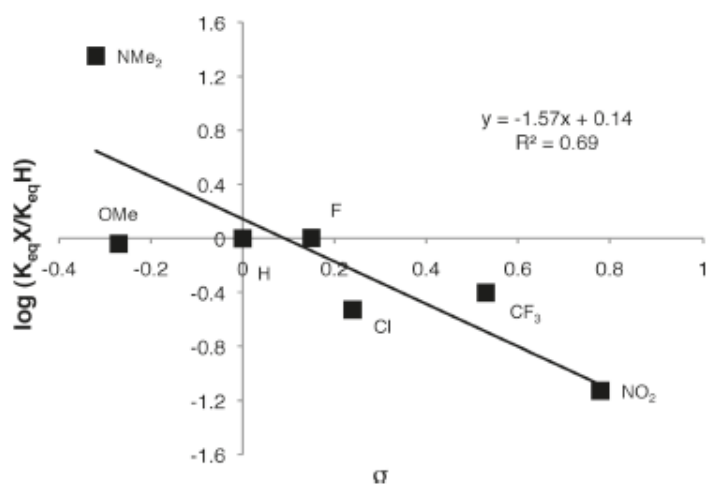
Entry	L	$\Delta G_{\text{disprop}}$ (kcal/mol)
1	Me ₂ Im ^a	7.7
2	PH ₃	10.4
3	CH ₃ N=CH ₂	11.3
4	NH ₃	11.4
5	NC ₅ H ₆	11.7
6	SH ₂	15.0
7	PF ₃	15.8
8	OH ₂	15.9
9	CO	16.8
10	CH ₃ CN	17.4
11	C ₂ H ₄	18.5

^a Me₂Im = 1,3-dimethylimidazol-2-ylidene

To more systematically probe the electronic influence of the L-type ligand on $\Delta G_{\text{disprop}}$, we computationally examined a series of pyridine ligands containing diverse *para* substituents. As summarized in Table 2.4, more electron rich pyridines generally provided smaller values of $\Delta G_{\text{disprop}}$. A Hammett plot of the data versus σ showed a modest correlation ($R^2 = 0.69$), with a ρ value of -1.57 (Scheme 2.15). However, it is important to note that even with $X = \text{N}(\text{CH}_3)_2$, $\Delta G_{\text{disprop}}$ remained relatively large (nearly 10 kcal/mol).

Table 2.4 DFT Hammett Study of the Effect of *para*-Substituted Pyridines on $\Delta G_{\text{disprop}}$.

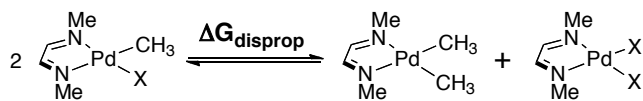
Entry	X	σ	$\Delta G_{\text{disprop}}$ (kcal/mol)
1	N(CH ₃) ₂	-0.32	9.9
2	OCH ₃	-0.27	11.8
3	H	0	11.7
4	F	0.15	11.7
5	Cl	0.24	12.4
6	CF ₃	0.53	12.3
7	NO ₂	0.73	13.3

Scheme 2.15 Hammett Plot for Variation of the Para Substituent on the Pyridine Ligand.

The influence of the X-type ligands on $\Delta G_{\text{disprop}}$ was also examined by DFT, using MeDAB as a chelating L-L ligand. Again, ground-state structures were optimized in the gas phase for (MeDAB)Pd(CH₃)(X), (MeDAB)Pd(CH₃)₂, and (MeDAB)Pd(X)₂, and $\Delta G_{\text{disprop}}$ was determined on the basis of these data. As summarized in Table 2.5, $\Delta G_{\text{disprop}}$ showed a reasonable correlation with the basicity of X. For example, with weakly basic X ligands such as iodide, bromide, chloride, and trifluoroacetate, $\Delta G_{\text{disprop}}$ was ≥ 11.7 kcal/mol (entries 1-4). However, $\Delta G_{\text{disprop}}$ decreased by close to 8 kcal/mol upon moving to alkoxide and phenoxide ligands (entries 6 and 7). Furthermore, when X was changed

to a C-bound enolate, $\Delta G_{\text{disprop}}$ was only 1.2 kcal/mol (entry 8). This value corresponds to a K_{eq} value of 0.14, indicating that the disproportionation should be readily detectable by ^1H NMR spectroscopy.

Table 2.5 Effect of X-Type Ligands on $\Delta G_{\text{disprop}}$.



Entry	X	pK_a^a	$\Delta G_{\text{disprop}}$ (kcal/mol)
1	I	-10	11.8
2	Br	-9	12.1
3	Cl	-8	11.7
4	CF_3CO_2	-0.3	12.4
5	CH_3CO_2	4.8	8.1
6	$\text{C}_6\text{H}_5\text{O}$	10.0	4.4
7	CH_3O	15.5	2.0
8	$\text{CH}_3\text{C}(\text{O})\text{CH}_2$	26.5	1.2
9	NH_2	38	0.1

^a pK_a of the conjugate acid of X

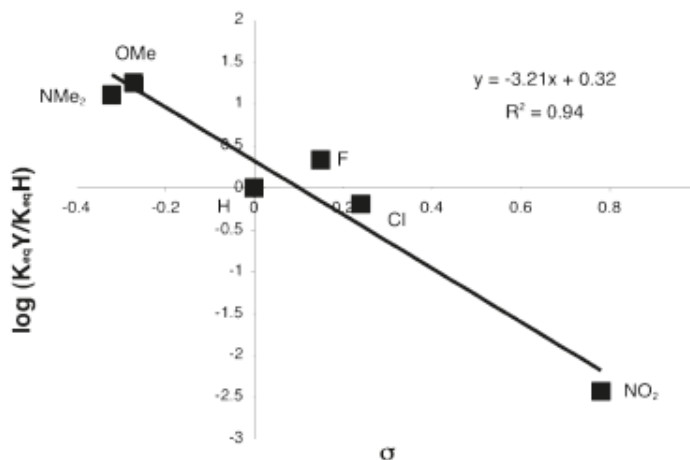
To further study the effect of the X-type ligand on $\Delta G_{\text{disprop}}$, DFT calculations were carried out on the complexes $(\text{MeDAB})\text{Pd}(\text{CH}_3)(\text{OAr})$, where OAr is a series of *para*-substituted phenoxides. An excellent correlation was observed between $\Delta G_{\text{disprop}}$ and the σ value of the *para* substituent, with $\rho = -3.21$ ($R^2 = 0.94$) (Table 2.6 and Figure 2.16). This indicates that disproportionation is strongly favored with more electron rich alkoxide ligands. All of the observed trends in $\Delta G_{\text{disprop}}$ as a function of X can be rationalized on the basis that as this ligand becomes more and more similar to CH_3 [$\text{pK}_a = 48$, $\Delta G_{\text{disprop}} = 0$ (by definition)], the free energy for disproportionation approaches zero.

Table 2.6 DFT Hammett Study of the Effect of *para*-Substituted Phenoxides on $\Delta G_{\text{disprop}}$.

$\text{OAr} = \text{---O---C}_6\text{H}_4\text{---Y}$

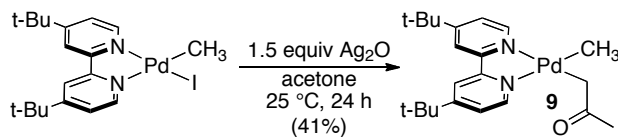
Entry	Y	σ	$\Delta G_{\text{disprop}}$ (kcal/mol)
1	N(CH ₃) ₂	-0.32	2.9
2	OCH ₃	-0.27	2.7
3	H	0	4.4
4	F	0.15	4.0
5	Cl	0.24	4.7
6	NO ₂	0.78	7.7

Scheme 2.16 Hammett Plot for Variation of the *para* Substituent on the Phenoxide Ligand.



The DFT calculations above suggested that the disproportionation equilibrium should be detectable with $X = \text{CH}_2\text{COCH}_3$, and we sought to experimentally confirm this by studying the Pd^{II} methyl enolate complex (*t*Bu-bpy)Pd(CH₃)(CH₂COCH₃) (**9**). An analytically pure sample of **9** was prepared by the reaction of (*t*Bu-bpy)Pd(CH₃)(I) with 1.5 equiv of Ag₂O in acetone at room temperature in the absence of light (Scheme 2.17).¹⁹

Scheme 2.17 Synthesis of Methyl Acetonyl Complex **9**.



Monitoring the monomethyl complex **9** by ^1H NMR spectroscopy for 7 h at 25 °C showed no reaction. Heating monomethyl complex **9** for 50 °C for 3 h in the absence of light also gave no evidence for disproportionation. However, when complex **9** was dissolved in $\text{THF-}d_8$ at 25 °C in a Teflon®-sealed NMR tube in ambient (room) light, disproportionation was observed to generate a 86:1:1.4 ratio of **9**:**6**: $(^t\text{Bu-bpy})\text{Pd}(\text{CH}_2\text{COCH}_3)_2$ (**10**) after 6 h and a 36:1:1.2 ratio of **9**:**6**:**10** after 24 h, as determined by ^1H NMR spectroscopy (Scheme 2.18). The observed ratio **9**:**6** after 24 h would correspond to $\Delta G = 4.2$ kcal/mol; however, competing decomposition of **6** over the course of the disproportionation means that this can only serve as an estimate of the thermodynamics associated with this reaction. To confirm the decomposition of **6** under the reaction conditions, solutions of independently synthesized **6** were subjected to the conditions of the disproportionation reaction for 24 h and were analyzed by ^1H NMR spectroscopy. Table 2.7 shows the amount of **6** remaining after standing in ambient light for 24 h in acetone- d_6 , benzene- d_6 , and tetrahydrofuran- d_8 .

Scheme 2.18 Disproportionation of **9** to Generate Dimethyl Complex **6**.

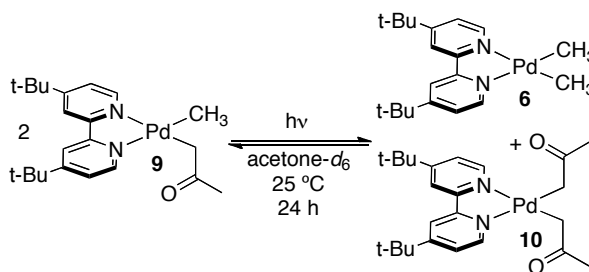
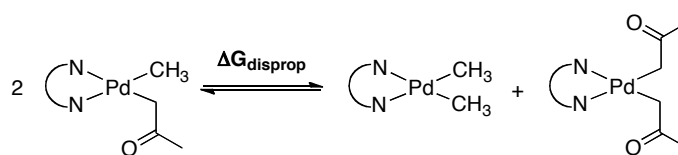


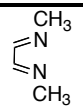
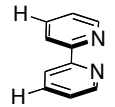
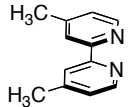
Table 2.7 Decomposition of Dimethyl Complex **6** Under Ambient Light After 24 h.

	Solvent		
	acetone- d_6	benzene- d_6	tetrahydrofuran- d_8
% 6 Remaining	47	13	63

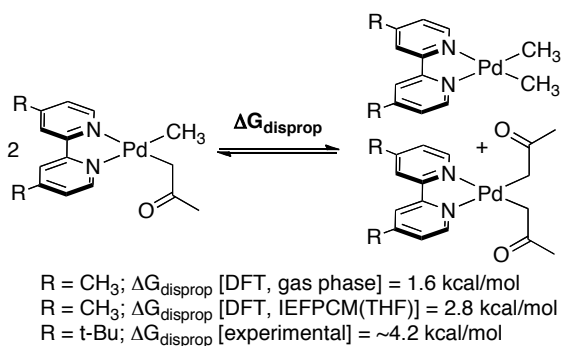
For comparison to the observed disproportionation, DFT calculations were performed on multiple methyl-acetyl-palladium models for **9** (Table 2.8). The closest approximation to **9**, (4,4'-dimethyl-2,2'-dipyridyl)Pd(CH₃)(CH₂COCH₃) (Table 2.8, Entry 3) predicts $\Delta G_{\text{disprop}} = 1.6$ kcal/mol for disproportionation. Further application of an IEFPCM (integral equation formalism of the polar continuum model) solvent correction in THF predicts $\Delta G_{\text{disprop}} = 2.8$ kcal/mol, which is in reasonable agreement with our experimental data (Scheme 2.19).

Table 2.8 Calculation of $\Delta G_{\text{disprop}}$ for Models of Complex **9**.



Entry	Ligand	$\Delta G_{\text{disprop}}$ (kcal/mol)
1		1.2
2		2.2
3		1.6

Scheme 2.19 Summary of Computational and Experimental Measurements of $\Delta G_{\text{disprop}}$.



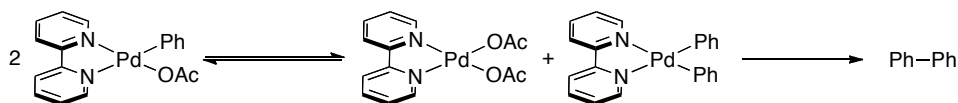
The importance of light in the disproportionation of **9** is not fully understood, and to my knowledge, no detailed photochemical studies of palladium alkyl complexes have

been undertaken that provide a sufficient explanation of the photomchemistry observed for complex **9**. One hypothesis that explains the requirement of light is that light is necessary to labelize a ligand to facilitate disproportionation. In support of this hypothesis, Kaim, in the process of elucidating the electronic structure Pt(II)-dialkyl and Pt(IV)-tetraalkyl complexes with cis-chelating diimine ligands, has observed light-induced platinum-methyl bond homolysis in the Pt(IV) examples that is attributed to the lowest energy electronic transition from a axial Pt-CH₃ σ -bonding orbital (HOMO) to a π^* ligand orbital (LUMO).³⁸ Under the same conditions, the square planar Pt(II) complexes are stable. Not surprisingly, the lowest energy transition for the Pt(II) complexes is that of a metal based *d* orbital (presumably the *dz*² orbital) to a π^* ligand orbital. While the Pt(II)-dialkyl complexes reported are stable, the related Pd(II)-alkyl complexes including (t-Bu-bpy)Pd^{II}(CH₃)(CH₂COCH₃) are expected to have higher-lying Pd-C σ -bonding orbitals, thus requiring less energy for excitation of electrons from the Pd-C bonding orbitals and potentially enabling photolabelization of the carbon ligands. In fact, there are several examples of Pd-alkyl complexes that undergo photodecomposition in chlorinated solvents.³⁹⁻⁴¹ What remains unclear are the relative destabilization of the Pd-CH₃ bond versus the Pd-X bond in complexes of the general formula (t-Bu-bpy)Pd^{II}(CH₃)X and whether light-induced bond homolysis in these platinum examples can be extended to arguments about photolabelization of Pd-C bonds. In the case of **9** specifically, it is unclear whether the highest occupied Pd-C σ -bonding orbital is Pd-CH₃ or Pd-CH₂COCH₃ in character. Analysis of the ground state molecular orbitals suggests that the filled σ -bonding orbitals for Pd-CH₃ and Pd-CH₂COCH₃ are nearly degenerate. However, to fully characterize the electronic transitions from the Pd-CH₃ or Pd-CH₂COCH₃ σ -bonding orbitals to the LUMO or other unoccupied orbitals will require that time dependent density functional theory calculations (TD-DFT) calculations be employed.

These studies offer valuable insights into the influence of ligands on the thermodynamics of methyl disproportionation. However, it is important to note that if the dimethyl species is kinetically accessible, only small equilibrium concentrations of (L)₂Pd(CH₃)₂ should be required to achieve catalytic turnover via the mechanism in Scheme 2.8. This is exemplified by the oxidative coupling of benzene catalyzed by

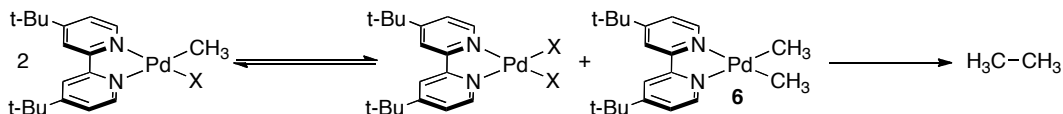
(bpy)Pd(OAc)₂. This transformation proceeds efficiently, despite an unfavorable calculated $\Delta G_{\text{disprop}}$ of 1.7 kcal/mol for (bpy)Pd(Ph)(OAc). In this case, the disproportionation equilibrium is believed to be rapid and reversible and a subsequent irreversible C–C bond-forming step drives the reaction in the forward direction (Scheme 2.20).

Scheme 2.20 Ph–Ph Bond Coupling Driving a Disproportionation Equilibrium.



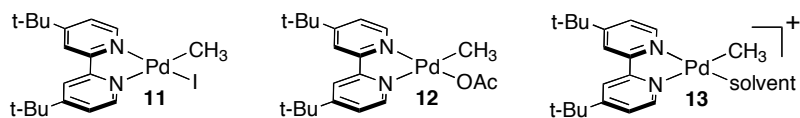
As such, for monomethyl palladium complexes, (^tBu-bpy)Pd(CH₃)X, where $\Delta G_{\text{disprop}}$ was computed to be unfavorable (>7 kcal/mol) we attempted to drive the disproportionation equilibrium toward products by thermally decomposing the product, (^tBu-bpy)Pd(CH₃)₂ (**6**). Under these conditions, if **6** was formed in small quantities via disproportionation, subsequent decomposition of this dimethyl complex would drive the disproportionation equilibrium toward products (Scheme 2.21).

Scheme 2.21 Formation of Ethane Driving a Disproportionation Equilibrium.

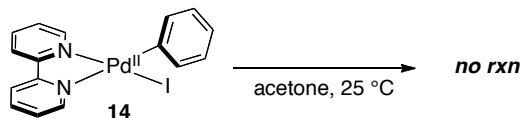


Monomethyl palladium complexes **11** and **12** and cationic complex **13** were chosen for comparison to the reactivity of dimethyl complex **6** (Scheme 2.22). Iodide complex **11** was chosen due to its similarity to monoaryl iodide palladium complexes studied by Osakada in aryl disproportionation reactions.¹⁵ Osakada has shown that monophenyl iodide palladium complex **14** is stable in acetone-*d*₆ (Scheme 2.23). However, upon abstraction of iodide with AgBF₄, spontaneous C–C bond formation is observed after 1 h at 25 °C. He hypothesized that abstraction of the iodide facilitates disproportionation to make a diphenyl intermediate that undergoes reductive elimination to form a new C–C bond (Scheme 2.8). Hence, cationic complex **13** was also studied. Acetate complex **12** was chosen because it is the methyl analogue of aryl complexes proposed as intermediates in the homocoupling of arenes.^{42,43}

Scheme 2.22 Monomethyl Complexes Studied in Thermolysis Reactions.

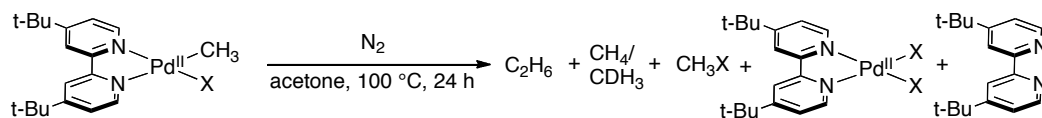


Scheme 2.23 Stability of Monoaryl Complex **14** Toward Disproportionation.¹⁵



These monomethyl palladium(II) complexes and dimethyl complex **6** were thermolyzed at 100 °C for 24 h in Teflon®-sealed J. Young NMR tubes either under 1 atm N₂ or under 1 atm O₂, and the results were analyzed by ¹H NMR spectroscopy. The results are reported in Table 2.9 (under N₂) and Table 2.10 (under O₂). It should be noted that for monomethyl starting materials, the maximum yield of ethane is 50% because two equiv of the starting complex are required to form 1 equiv of ethane. A calibration for determining the total amount of ethane produced in these had previously been determined for ethane-producing reactions in acetone-*d*₆.⁴⁴

Table 2.9 Yields of Decomposition Products for Thermolysis of Pd^{II}-Methyl Complexes Under N₂.



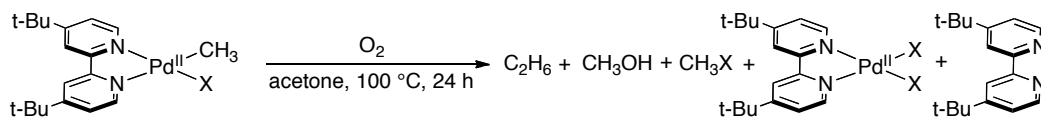
Entry	X	Starting Material	C ₂ H ₆	CH ₄ /CDH ₃	CH ₃ X	PdX ₂ (^t Bu-bpy)	^t Bu-bpy
1	CH ₃	0	20	9	–	–	103
2	I	63	0	0	19	6	30
3 ^a	OAc	0	15	1	0	0	64
	Solvent						
4 ^b	(0.9 equiv Ag ⁺) Solvent	0	13	4	0	39	60
5 ^{b,c}	(1.1 equiv Ag ⁺)	0	5	3	0	47	0

^a55% HOAc and 30% (^tBu-bpy)Pd(OAc)(CD₂COCD₃) were also identified.

^bYields of inorganic products were determined after addition of 4 equiv. KI.

^cAn unidentified symmetric inorganic product was observed in 51% yield.

Table 2.10 Yields of Decomposition Products for Thermolysis of Pd^{II}-Methyl Complexes Under O₂.



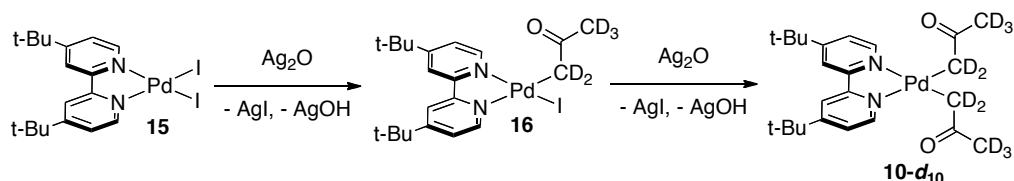
Entry	X	Starting Material	C ₂ H ₆	CH ₃ OH	CH ₃ X	PdX ₂ (^t Bu- ^t Bu-bpy)	^t Bu-bpy
1	CH ₃	0	2	48	–	–	75
2	I	26	0	22	0	6	0
3	OAc	0	18	21	0	0	63
	Solvent						
4	(0.9 equiv Ag ⁺) Solvent	41	4	27	6	57	0
5	(1.1 equiv Ag ⁺) Solvent	0	0	41	0	51	49

For iodide complex **11**, thermolysis under N₂ produced starting material (63%) and (^tBu-bpy)PdI₂ (**15**, 6%) as the only inorganic products observed. Free ^tBu-bpy (30%) was also observed along with deposition of metallic palladium on the NMR tube suggesting that free bipyridine is the result of reduced palladium products being formed. Methyl iodide (19%) was the only product derived from the CH₃ ligand identified in this reaction. Methyl halogen reductive elimination has been observed in the Shilov process for methane functionalization, and the topic of C–halogen reductive elimination from Pd^{II} and Pt^{II} has recently been reviewed.⁴⁵ However, it is interesting to note that C–halogen reductive elimination typically has been shown to occur for Pd^{IV} and Pt^{IV} complexes. Reductive elimination of *sp*² C–halogen from Pd^{II} bonds generally requires bulky ancillary ligands.^{46–49}

Thermolysis of **11** under O₂ led to incomplete conversion of the starting material (74% conversion), and methanol was the only organic product observed (22%). A trace of (^tBu-bpy)PdI₂ (**15**, 6%) and an asymmetric, bipyridine-ligated product (51%) were the major inorganic byproducts. The asymmetric complex had two inequivalent pyridine and

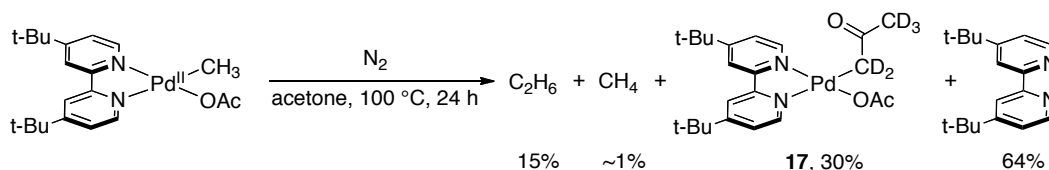
no related methyl resonance, and the product had been observed before in the incomplete reaction of **15** with Ag_2O to synthesize diacetyl complex **10** (Scheme 2.24). It is proposed to be $(^t\text{Bu-bpy})\text{Pd}(\text{CD}_2\text{COCD}_3)\text{I}$ (**16**). Complex **16** is the result of loss of a CH_3 ligand from **11** and activation of the acetone solvent.

Scheme 2.24 Proposed Intermediate in the Synthesis of **10** Related to Thermolysis of **11**.



For acetate complex **12**, thermolysis at $100\text{ }^\circ\text{C}$ for 24 h under N_2 (entry 3, Table 2.9) resulted in complete consumption of **12**. Ethane (15%) and methane ($\sim 1\%$) were produced in low yields, and free $^t\text{Bu-bpy}$ (63%) and metallic palladium were observed. An inorganic product containing asymmetric bipyridyl rings and an acetate ligand was also observed (30%). Subjection of the NMR sample to mass spectral analysis gave evidence for $(^t\text{Bu-bpy})\text{Pd}(\text{CD}_2\text{COCD}_3)\text{OAc}$ (**17**, Scheme 2.25) as the identity of the asymmetric product. Complex **17** is directly analogous to complex **16** formed in the thermolysis of $(^t\text{Bu-bpy})\text{Pd}(\text{CH}_3)\text{I}$ (**11**) under O_2 . Acetic acid (55%) was also a byproduct of this reaction.

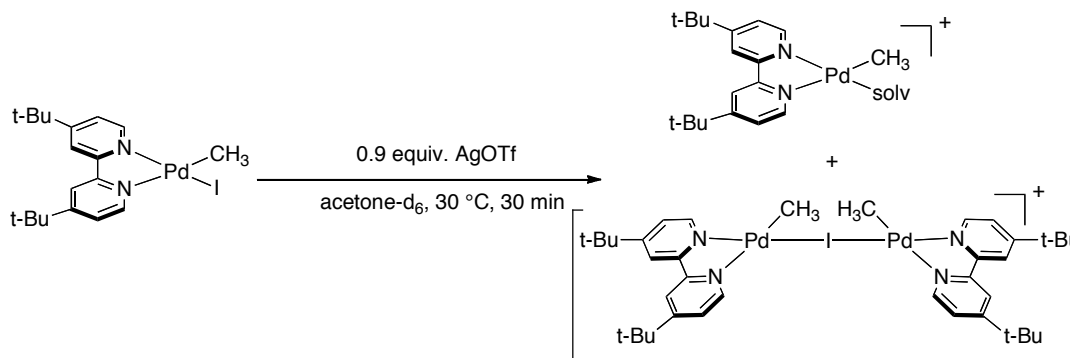
Scheme 2.25 Thermolysis of $(^t\text{Bu-bpy})\text{Pd}(\text{CH}_3)\text{OAc}$ (**12**).



The analogous thermolysis of **12** under O_2 (entry 3, Table 2.10) provided ethane (18%) in slightly higher yield than the reaction of **12** under N_2 and methanol in 21%. When comparing the ethane formed in this reaction (18%) versus the amount formed in the thermolysis of **12** under N_2 (15%) this result is somewhat surprising. All other thermolyses performed under O_2 gave lower yields of ethane than the related reactions under N_2 . Free $^t\text{Bu-bpy}$ (63%), **17** (23%) and acetic acid (72%) were also observed.

Cationic complex **13** was synthesized via iodide abstraction from **11** in acetone- d_6 . Iodide complex **11** was reacted with AgOTf for 30 min in acetone- d_6 , and the resulting mixture was filtered through Celite to remove AgI. The filtrate was then dispensed into a Teflon®-sealed J. Young NMR tube and thermolyzed. This reaction was run with both a substoichiometric amount (0.9 equiv) and a superstoichiometric amount (1.1 equiv) of AgOTf. The rationale for using a substoichiometric amount of AgOTf was that residual iodide could act as a bridging ligand for two palladium centers, potentially facilitating methyl transfer (Scheme 2.26). Related structures have been proposed as intermediates in comproportionation reactions of Group 10 metal complexes.^{17,28}

Scheme 2.26 Rationale for Using a Substoichiometric Amount of AgOTf



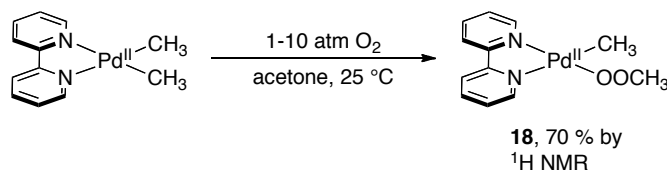
Thermolysis of these two solutions under N_2 generated ethane and methane as organic products as well as free t -Bu-bpy. Resonances related to inorganic byproducts were significantly broadened at room temperature, presumably due to exchange processes. In order to ease characterization, KI (4 equiv) was added to convert all cationic inorganic products into monomethyl iodide complex **11** and (t -Bu-bpy) PdI_2 (**15**). In the reaction where 0.9 equivalents of AgOTf were used (entry 4, Table 2.9), **11** (8%) and **15** (39%) were observed along with free t -Bu-bpy (60%). However, in the reaction where 1.1 equiv of AgOTf (entry 5, Table 2.9) was used, **11** and t -Bu-bpy were not observed. Diiodide complex **15** (47%) and an unidentified complex (53%) were formed instead. The unidentified complex had equivalent pyridine rings by 1H NMR suggesting symmetry about the palladium center, and no related methyl resonance was detected.

Interestingly, the reaction containing residual iodide produced more ethane (13%) than reaction with no iodide present (5%).

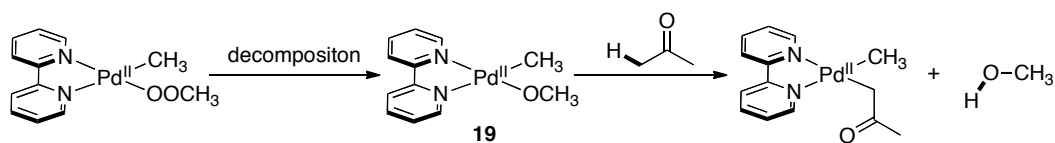
For thermolysis under O₂, complete abstraction of the iodide (1.1 equiv AgOTf, entry 5, Table 2.10) gave better conversion (100%) compared to the reaction with residual iodide (59% conversion based on yield of **11**). Methanol was formed in higher yield (41% versus 27%) and after quenching with KI, diiodide complex **15** (51%) and ^tBu-bpy (49%) were the only other observed products of the reaction where 1.1 equiv of AgOTf were used (entry 5, Table 2.10). In the reaction with residual iodide (entry 4, Table 2.10), addition of KI after thermolysis afforded only **11** (41%) and **15** (57%) as inorganic products. Small amounts of ethane (4%), CH₄ (~2%), and methyl iodide (6%) were also formed in this reaction.

When dimethyl complex **6** was thermolyzed for 24 h, complete consumption of **6** was observed. Free bipyridine ligand (103%), ethane (20%), CH₄ (~9%) were observed as decomposition products (entry 1, Table 2.9). Reaction of **6** at analogous conditions under 1 atm of O₂ led to complete decomposition after 24 h with methanol (48%) being formed as the major organic product (entry 1, Table 2.10). Goldberg and coworkers have shown that related complex (bpy)Pd(CH₃)₂ reacts with O₂ in benzene to give methyl peroxide complex **18** (Scheme 2.27).⁵⁰ This complex decomposes to methoxy complex **19** in benzene, but in acetone the bpy analogue of acetyl complex **9** is formed.⁵¹ This is proposed to occur via deprotonation of the acetone solvent by the methoxide product (Scheme 2.28). In our system, when allowed to stand for 1 h under 1 atm of O₂, no change was observed in starting dimethyl complex **6** by ¹H NMR spectroscopic analysis. From our studies it is unclear whether methanol formation is the result of the intermediacy of a methyl peroxo complex or by methyl radical trapping by O₂.

Scheme 2.27 Reaction of (bpy)Pd(CH₃)₂ with O₂ to Form a Methyl-Peroxo Species.



Scheme 2.28 Decomposition of **16** in Acetone to Produce an Acetyl Complex.



The results of these experiments suggest that thermolysis is not an effective means of ethane production, even for dimethyl complex **6**. While ethane is produced by thermolysis of monomethyl complexes, as in the case of **6**, the low overall yields of gaseous products and simultaneous formation of CH₄ and CDH₃ in the reaction do not allow a definitive conclusion of whether the products are the result of disproportionation to form **6** *in situ*. Side reactions, such as C–heteroatom bond formation and solvent activation, further complicate establishing whether disproportionation is occurring during thermolysis of monomethyl complexes.

2.3 Conclusions

In summary, we have conducted DFT calculations to gain insights into the influence of supporting ligands on the disproportionation chemistry of cis-(L)₂Pd(CH₃)(X). In general, these calculations predict that strongly electron donating L and X ligands will afford the largest equilibrium populations of the disproportionation products. On the basis of these calculations, we have identified the first experimental example of methyl disproportionation at Pd^{II}, with (tBu-bpy)Pd(CH₃)(CH₂COCH₃) (**9**) as the starting material.

Attempts to trap (tBu-bpy)Pd(CH₃)₂ (**6**) as a product of monomethyl disproportionation via thermolysis showed poor yields of ethane. The formation of other gaseous products, CH₄ and CDH₃, suggest that methyl radicals are involved in the thermal decomposition of the methyl-palladium complexes. Thermolysis in the presence of O₂ generated methanol as the major organic product, in most cases suppressing the formation of ethane. In order to proceed toward a system for oxidative oligomerization of methane, it was evident that further studies toward the efficient production of ethane were necessary. Details of that exploration are presented in Chapter 3.

2.4 Experimental Procedures

2.4.1 Instrumentation

NMR spectra were obtained on a Varian Inova 500 (499.90 MHz for ^1H ; 125.70 MHz for ^{13}C) or a Varian Inova 400 (399.96 MHz for ^1H ; 100.57 MHz for ^{13}C) spectrometer. ^1H NMR chemical shifts are reported in parts per million (ppm) relative to TMS with the residual solvent peak used as an internal reference. Multiplicities are reported as follows: singlet (s), doublet (d), and doublet of doublets (dd). Infrared spectra were obtained on a Perkin-Elmer FT-IR Spectrum BX spectrometer. Microanalyses were performed by Atlantic Microlab, Inc. Mass spectra were collected on a Micromass Electrospray-ionization-time of flight mass spectrometer.

2.4.2 Materials and Methods

All manipulations were performed using standard Schlenk or glovebox procedures unless otherwise noted. Acetone and acetone- d_6 (Cambridge Isotopes) were refluxed over calcium sulfate overnight and then distilled, freeze-pump-thaw degassed, and stored over 4 Å molecular sieves. All other solvents were purchased from Fisher or EMD and dispensed from an Innovative Technologies solvent purification system equipped with columns packed with activated alumina, copper catalyst, and molecular sieves. 4,4'-Di-*tert*-butyl-2,2'-bipyridine (*t*Bu-bpy) was purchased from Aldrich, Ag_2O was purchased from Alfa Aesar, Na_2PdCl_4 was purchased from Pressure Chemical, and all other materials were used as purchased from Aldrich or Acros. Ambient light refers to light emitted from two fluorescent tube lights in a fume hood.

J. Young NMR tubes were Norell (# S-5-600-7) brand purchased from Chemglass®. These tubes match the internal volume of those used in production of the calibration curve for ethane in acetone- d_6 produced previously.⁴⁴ Because of the large T^1 of ethane and the internal standards used, the following acquisition parameters were used for ^1H NMR spectroscopic analysis: scans = 2, acquisition time = 5 s, and relaxation

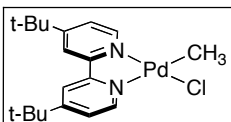
delay = 180 s. At these long relaxation delays, steady state scans are not needed, and that parameter was set to zero.

2.4.3 Computational Methods

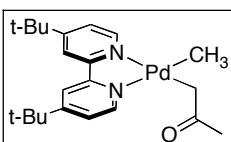
All density functional theory (DFT) calculations were carried out using the Gaussian 03 suite of programs.⁵² The B3LYP (Becke's three-parameter hybrid functional⁵³ using the LYP correlation functional containing both local and nonlocal terms of Lee, Yang, and Parr)⁵⁴ functional, Stevens (CEP-31G) valence basis sets, and effective core potentials were employed.^{55,56} The CEP-31G valence basis sets are valence triple- ζ for palladium and double- ζ for main group elements. All main group elements were augmented with a d-polarization function: $\xi_d = 0.8$ for carbon, nitrogen, oxygen, and fluorine; $\xi_d = 0.55$ for phosphorus; $\xi_d = 0.65$ for sulfur; $\xi_d = 0.75$ for chlorine; $\xi_d = 0.451$ for bromine; and $\xi_d = 0.302$ for iodine. The closed-shell (diamagnetic) complexes were modeled using the restricted Kohn–Sham formalism. All geometries were optimized without symmetry constraint and were confirmed as minima by the absence of imaginary frequencies. Thermochemistry was determined at 298.15 K and 1 atm using unscaled B3LYP/CEP-31G(d) vibrational frequencies. Solvent corrections were performed as single-point energy calculations on optimized gas-phase structures using the integral equation formalism of the polarizable continuum model (IEFPCM).^{57–60}

2.4.4 Syntheses

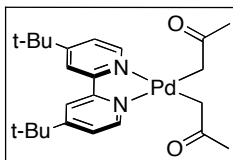
The Pd complexes (*t*Bu-bpy)Pd(CH₃)₂ (**6**),⁶¹ (*t*Bu-bpy)Pd(CH₃)(I) (**11**)⁶¹, and (*t*Bu-bpy)Pd(I)₂ (**15**)⁶² were prepared by analogous procedures to those reported in the literature for the corresponding derivatives containing unsubstituted 2,2'-bipyridine, and spectroscopic data matched those of previous reports for **6**,⁶³ **11**,⁴⁴ and **15**.⁶⁴ (*t*Bu-bpy)Pd(Cl)₂ (**7**) was prepared according to literature procedure.⁶⁵



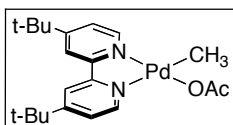
(*t*-Bu-bpy)Pd(CH₃)(Cl) (8): (*t*-Bu-bpy)Pd(CH₃)₂ (51 mg, 0.126 mmol, 1.1 equiv), (*t*-Bu-bpy)Pd(Cl)₂ (51 mg, 0.114 mmol, 1 equiv), acetone (15 mL), and a magnetic stirbar were added to a 20 mL vial. The reaction vessel was wrapped in foil and heated at 50 °C for 18 h. After removing the vial from the glovebox, the reaction mixture was filtered through a plug of Celite into a 100 mL round bottom flask, and hexanes was added to precipitate the product. The pale yellow precipitate was collected on a frit, washed with hexanes, and dried under vacuum to afford **8** as a pale yellow powder (81 mg, 84% yield). This complex has been previously synthesized, and the characterization data match those reported in the literature.⁶⁶



(*t*-Bu-bpy)Pd(CH₃)(CH₂COCH₃) (9): (*t*-Bu-bpy)Pd(CH₃)(I) (212 mg, 0.41 mmol, 1 equiv) was suspended in dry acetone (10 mL). Ag₂O (124 mg, 0.61 mmol, 1.5 equiv) and a magnetic stir bar were added, and the reaction was stirred for 24 h at 25 °C. The resulting suspension was passed through a plug of Celite. The filtrate was concentrated, pentanes (15 mL) was added, and the solution was cooled to –32 °C overnight. The resulting yellow precipitate was collected on a frit, washed with cold pentanes, and dried under vacuum to afford **9** as a yellow powder (75 mg, 41% yield). ¹H NMR (acetone-*d*₆): δ 9.37 (d, *J* = 6.0 Hz, 1H), 8.61 (d, *J* = 6.0 Hz, 1H), 8.51 (d, *J* = 1.5 Hz, 1H), 8.46 (d, *J* = 2.0 Hz, 1H), 7.73 (dd, *J* = 6.0 Hz, 1.5 Hz, 1H), 7.70 (dd, *J* = 6.0 Hz, 2.0 Hz, 1H), 2.37 (s, 2H), 1.98 (s, 3H), 1.44 (two peaks, 18H), 0.52 (s, 3H). ¹³C NMR (acetone-*d*₆): δ 208.4, 164.0, 163.5, 156.7, 155.3, 151.2, 148.2, 124.1, 123.9, 120.5, 119.8, 36.2, 36.1, 30.5, 30.4, 29.7. The ¹³C signals for the two different *tert*-butyl groups appear to be coincidentally overlapping. IR (KBr) 1611 cm⁻¹ (C=O). Anal. Calcd for C₂₂H₃₂N₂OPd: C, 59.12; H, 7.22; N, 6.27. Found: C, 59.29; H, 7.15; N, 6.27.

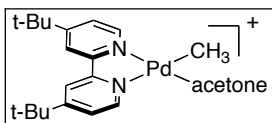


(*t*-Bu-bpy)Pd(CH₂COCH₃)₂ (10): (*t*-Bu-bpy)Pd(I)₂ (269 mg, 0.43 mmol, 1 equiv), Ag₂O (422 mg, 1.82 mmol, 4.3 equiv), dry acetone (5 mL) and a magnetic stir bar were loaded into a 25 mL Schlenk flask. The reaction mixture was refluxed for 24 h, then filtered through Celite and concentrated under vacuum. The red-brown residue was dissolved in benzene (4 mL) and filtered through a plug of Celite. This solution was then layered with pentanes (15 mL) and stored at –32 °C overnight. The resulting yellow precipitate was collected on a frit, washed with cold pentanes, and dried under vacuum to afford **10** as a yellow powder (24.9 mg, 12% yield). ¹H NMR (acetone-*d*₆): δ 9.31 (d, *J* = 5.7 Hz, 2H), 8.49 (d, *J* = 1.8 Hz, 2H), 7.75 (dd, *J* = 5.7 Hz, 1.8 Hz, 2H), 2.56 (s, 4H), 2.07 (s, 6H), 1.45 (s, 18H). ¹³C NMR (acetone-*d*₆): δ 209.5, 164.3, 156.2, 151.2, 124.1, 120.3, 36.2, 30.5, 30.4, 30.1. IR (KBr) 1612 cm⁻¹ (C=O). Anal. Calcd for C₂₄H₃₄N₂O₂Pd: C, 58.59; H, 7.01; N, 5.73. Found: C, 58.82; H, 6.98; N, 5.77.



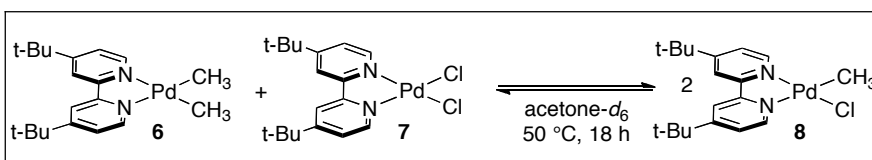
(*t*-Bu-bpy)Pd(CH₃)(O₂CCH₃) (12): (*t*-Bu-bpy)Pd(CH₃)(I) (121 mg, 0.23 mmol, 1 equiv) was suspended in dry acetone (10 mL). AgOAc (40 mg, 0.24 mmol, 1 equiv) and a magnetic stir bar were added, and the reaction was stirred for 3 h at 25 °C. The resulting suspension was passed through a plug of Celite. The acetone filtrate was concentrated under vacuum, and the residue was dissolved in benzene (5 mL). The benzene solution was passed through a plug of Celite, and filtrate was cooled to -32 °C. The frozen benzene solution was dried under vacuum to afford **12** as a pale yellow solid (78 mg, 75%). ¹H NMR (acetone-*d*₆): δ 8.53 (d, *J* = 2.0 Hz, 1H), 8.52 (d, *J* = 6.0 Hz, 1H), 8.51 (d, *J* = 1.5 Hz, 1H), 8.41 (d, *J* = 5.5 Hz, 1H), 7.72 (dd, *J* = 5.5 Hz, 1.5 Hz, 1H), 7.69 (dd, *J* = 6.0 Hz, 2.0 Hz, 1H), 1.91 (s, 3H), 1.44 (s, 9H), 1.43 (s, 9H), 0.68 (s, 3H). ¹³C NMR (acetone-*d*₆): δ 175.4, 164.3, 164.1, 157.8, 153.8, 150.2, 148.7, 124.5, 124.3, 121.4, 120.0, 36.3, 30.5, 30.3, 24.7, -0.9. The ¹³C signals for the two different *tert*-butyl groups

appear to be coincidentally overlapping. Anal. Calcd for C₂₂H₃₂N₂OPd: C, 56.19; H, 6.74; N, 6.24. Found: C, 55.90; H, 6.70; N, 6.10.

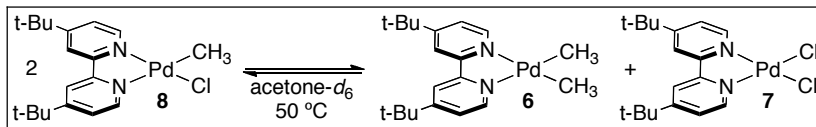


[(^tBu-bpy)Pd(CH₃)(acetone)]OTf (13): (^tBu-bpy)Pd(CH₃)(I) (14 mg, 27 μmol, 1 equiv) was suspended in dry acetone-*d*₆ (5.0 mL) to give a 5.4 mM solution. AgOTf (7.7 mg, 30 μmol, 1.1 equiv) and a magnetic stir bar were added, and the reaction was stirred for 30 min at 25 °C. The resulting suspension was passed through a plug of Celite, and the acetone-*d*₆ filtrate (0.55 mL) was directly dispensed into NMR tubes for thermolysis experiments. ¹H NMR (acetone-*d*₆): δ 8.69 (d, *J* = 2.0 Hz, 1H), 8.68 (d, *J* = 2.0 Hz, 1H), 8.57 (d, *J* = 6.0 Hz, 1H), 8.24 (d, *J* = 6.0 Hz, 1H), 7.83 (dd, *J* = 6.5 Hz, 2.0 Hz, 1H), 7.77 (dd, *J* = 5.5 Hz, 2.0 Hz, 1H), 1.46 (s, 9H), 1.44 (s, 9H), 0.83 (s, 3H). Note: The presence of any residual iodide or H₂O cause the peak at 8.24 ppm to broaden into the baseline and the Pd–CH₃ peak at 0.834 ppm to shift up to 0.1 ppm.

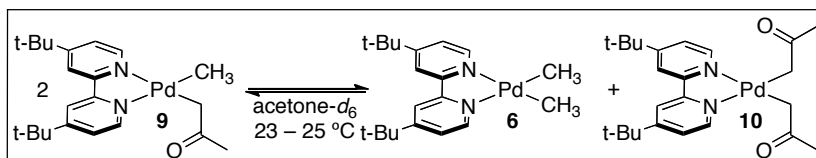
2.4.5 Reaction Details



Comproportionation of 6 and 7. A solution of complex **6** (0.1 mL, 3.7 mg in 1.0 mL acetone-*d*₆, 9.1 mM), a solution of complex **7** (0.4 mL, 3.1 mg in 3.0 mL acetone-*d*₆, 2.2 mM) and a solution of 1,3,5-trimethoxybenzene (internal standard, 50 μL of a 20.2 mM solution in acetone-*d*₆) were added to a screw cap NMR tube that was then sealed with a Teflon-lined cap. The reaction was monitored by ¹H NMR spectroscopy at room temperature. When not in the NMR spectrometer for data acquisition, the sample was maintained at 50 °C and in the absence of light. After 18 h, complex **8** was the only product observed in 99% yield relative to the internal standard.



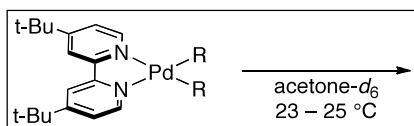
Disproportionation of 8. (*with light*) Complex **8** (2.3 mg, 5.4 μmol) was weighed into a screw cap NMR tube. Acetone- d_6 (0.5 mL) and 1,3,5-trimethoxybenzene (internal standard, 50 μL of a 20.2 mM solution in acetone- d_6) were added, and the tube was sealed with a Teflon-lined cap. The reaction was monitored by ^1H NMR spectroscopy at room temperature. When not in the NMR spectrometer for data acquisition, the sample was maintained at 50 $^\circ\text{C}$ and was exposed to ambient (room) light. After 18 h in acetone- d_6 , **8** remained (71% relative to the starting integration of this material versus the internal standard). Some decomposition of **8** had also clearly taken place. The dichloride complex **7** (7%), free $t\text{-Bu-bpy}$ (6%), and two other unidentified $t\text{-Bu-bpy}$ products were also observed along with CH_4 and CH_3D after 18 h. However, the dimethyl complex **6** was not observed at any time during the course of the reaction. (*without light*) Above procedure is followed, but NMR tube is wrapped in foil when not in the NMR. In the absence of light, 101% **8** remained by ^1H NMR, indicating no disproportionation and no decomposition had occurred.



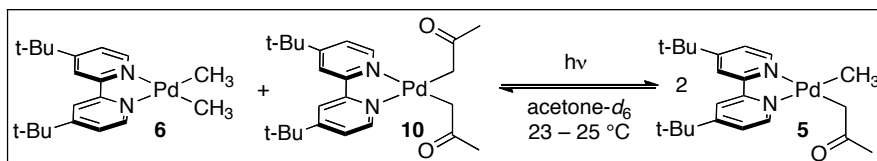
Disproportionation of 9. Complex **9** (2.4 mg, 5.4 μmol) was weighed into a screw cap NMR tube. Acetone- d_6 /THF- d_8 (0.5 mL) and 1,3,5-trimethoxybenzene (internal standard, 50 μL of a 20.2 mM solution in acetone- d_6 /THF- d_8) were added, and the tube was sealed with a Teflon-lined cap. The reaction was monitored by ^1H NMR spectroscopy at room temperature. When not in the NMR spectrometer for data acquisition, the sample was maintained at between 23 and 25 $^\circ\text{C}$ and was exposed to ambient (room) light.

[†] Decomposition of **6** was observed in all solvents tested under the reaction conditions. Specifically, light induced decomposition of **6**. This decomposition prohibited establishment of a stable equilibrium, and therefore any ΔG or K_{eq} values derived from

experimental data are only estimates at a given time. Because decomposition of **6** is minimized in THF, disproportionation in THF provided the best experimental estimates of K_{eq} . In contrast, decomposition studies in acetone showed that small amounts of **9** are formed as **6** decomposed making acetone a particularly challenging solvent in which to study disproportionation.

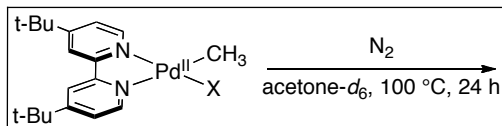


Decomposition Studies of 6 and 10. Decomposition studies were completed in various deuterated solvents. The appropriate palladium complex (7.4 μmol) was dissolved in the appropriate solvent (1 mL) and this stock solution was used immediately. A portion of this stock solution (50 μL) was combined with 1,3,5-trimethoxybenzene (internal standard, 25 μL of a 20.2 mM solution in the corresponding deuterated solvent) and the deuterated solvent (450 μL) in a screw cap NMR tube. The tube was sealed with a Teflon-lined cap. The reaction was monitored by ^1H NMR spectroscopy at room temperature. When not in the NMR spectrometer for data acquisition, the sample was maintained at 23 – 25 $^\circ\text{C}$ and was exposed to ambient (room) light.

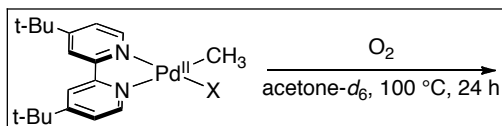


Comproportionation of 6 and 10. Complexes **6** (1.1 mg, 2.7 μmol) and **10** (1.3 mg, 2.7 μmol) were weighed into a screw cap NMR tube. Acetone- d_6 (1.0 mL) and 1,3,5-trimethoxybenzene (internal standard, 50 μL of a 20.2 mM solution in acetone- d_6) were added, and the tube was sealed with a Teflon-lined cap. The reaction was monitored by ^1H NMR spectroscopy at room temperature. When not in the NMR spectrometer for data acquisition, the sample was maintained at 23 and 25 $^\circ\text{C}$ and was exposed to ambient (room) light.

2.4.6 Thermolysis Reaction Details



Thermolysis of Complexes 6, 11, and 12 Under N₂: The palladium complex (3.0 μmol) was weighed into a J. Young NMR tube. Acetone (0.65 mL) was added along with 1,1,2-trichloroethane[‡] (internal standard, 15 μL of 215 mM solution in acetone-*d*₆) or 1,3,5-trimethoxybenzene (internal standard, 15 μL of 48 mM solution in acetone-*d*₆), and the tube was sealed with a Teflon stopcock. The solutions were protected from light, and initial NMR spectra were recorded. The tubes were heated at 100 °C in a foil-wrapped Erlenmeyer flask filled with silicon oil in a darkened fume hood. After heating for 24 h, NMR spectra were recorded to determine yields decomposition products versus the initial spectra.



Thermolysis of Complexes 6, 11, and 12 Under O₂: The palladium complex (3.0 μmol) was weighed into a J. Young NMR tube. Acetone (0.65 mL) was added along with 1,1,2-trichloroethane[‡] (internal standard, 15 μL of 215 mM solution in acetone-*d*₆) or 1,3,5-trimethoxybenzene (internal standard, 15 μL of 48 mM solution in acetone-*d*₆), and the tube was sealed with a Teflon stopcock. Each tube was frozen with N_{2(l)}, evacuated, and thawed. This was repeated for a total of three cycles, and the tubes were backfilled with O₂. The solutions were protected from light, and initial NMR spectra were recorded. The tubes were heated at 100 °C in a foil-wrapped Erlenmeyer flask filled with silicon oil in a darkened fume hood. After heating for 24 h, NMR spectra were recorded to determine yields of decomposition products versus the initial spectra.

Thermolysis of Complex 13 Under N₂ or O₂: (*t*-Bu-bpy)Pd(CH₃)(I) (14 mg, 27 μmol, 1 equiv) was suspended in dry acetone-*d*₆ (5.0 mL) to give a 5.4 mM solution. AgOTf, either 0.9 equivalents (6.5 mg, 25 μmol) or 1.1 equivalents (7.7 mg, 30 μmol), and a

magnetic stir bar were added, and the reaction was stirred for 30 min at 25 °C. The resulting suspension was passed through a plug of Celite, and the acetone-*d*₆ filtrate (0.55 mL) was directly dispensed into NMR tubes for thermolysis experiments. Further setup follows procedures for Complexes **6**, **11**, and **12** under N₂ and O₂.

‡ Importantly, reaction of Complexes **6** and **11** with 1,1,2-trichloroethane as an internal standard resulted in decomposition of the internal standard and formation of chlorinated products **7** and **8**. In these reactions, 1,3,5-trimethoxybenzene was used as the internal standard to derive the yield of the decomposition products.

2.5 References

- (1) Deroune, E. G., Ed.; Parmon, V., Ed.; Lemos, F., Ed.; Ribeiro, F. R., Ed. Sustainable Strategies for the Upgrading of Natural Gas: Fundamentals, Challenges, and Opportunities; Springer: Dordrecht, The Netherlands, 2005.
- (2) Periana, R. A.; Bhalla, G.; Tenn, W. J., III; Young, K. J. H.; Liu, X. Y.; Mironov, O.; Jones, C. J.; Ziatdinov, V. *J. Mol. Cat. A* **2004**, *220*, 7.
- (3) Crabtree, R. H. *J. Organometallic Chem.* **2004**, *689*, 4083.
- (4) Labinger, J. A.; Bercaw, J. E. *Nature* **2002**, *417*, 507.
- (5) Crabtree, R. H. *J. Chem. Soc., Dalton Trans.* **2001**, 2437.
- (6) Shilov, A. E.; Shul'pin, G. *Chem. Rev.* **1997**, *97*, 2879.
- (7) Owen, J. S.; Labinger, J. A.; Bercaw, J. E. *J. Am. Chem. Soc.* **2006**, *128*, 2005.
- (8) Heiberg, H.; Johansson, L.; Gropen, O.; Ryan, O. B.; Swang, O.; Tilset, M. *J. Am. Chem. Soc.* **2000**, *122*, 10831.
- (9) Seligson, A. L.; Trogler, W. C. *J. Am. Chem. Soc.* **1992**, *114*, 7085.
- (10) Pieck, R.; Steacie, E. W. R. *Can. J. Chem.* **1995**, *33*, 1304.
- (11) Hill, R. H.; Puddephatt, R. J. *Organometallics* **1983**, *2*, 1474.
- (12) Ackerman, L. J.; Sadighi, J. P.; Kurtz, D. M.; Labinger, J. A.; Bercaw, J. E. *Organometallics* **2003**, *22*, 3884.
- (13) Suzaki, Y.; Osakada, K. *Organometallics* **2003**, *22*, 2193.
- (14) Konze, W. V.; Scott, B. L.; Kubas, G. J. *J. Am. Chem. Soc.* **2002**, *124*, 12550.
- (15) Yagyu, T.; Hamada, M.; Osakada, K.; Yamamoto, T. *Organometallics* **2001**, *20*, 1087.
- (16) Cárdenas, D. J.; Martín-Matute, B.; Echavarren, A. M. *J. Am. Chem. Soc.* **2006**, *128*, 5033
- (17) Suzaki, Y.; Yagyu, T.; Osakada, K. *J. Organometallic Chem.* **2007**, *692*, 326.
- (18) Osakada, K.; Hamada, M.; Yamamoto, T. *Organometallics* **2000**, *19*, 458.
- (19) Suzaki, Y.; Yagyu, T.; Yamamura, Y.; Mori, A.; Osakada, K. *Organometallics* **2002**, *21*, 5254.
- (20) Scott, J. D.; Puddephatt, R. J. *Organometallics* **1983**, *2*, 1643.
- (21) Casado, A. L.; Casares, J. A.; Espinet, P. *Organometallics* **1997**, *16*, 5730.

-
- (22) Suzaki, Y.; Osakada, K. *Bull. Chem. Soc. Jpn.* **2004**, *77*, 139.
- (23) Peters, R. G.; White, S.; Roddick, D. M. *Organometallics* **1998**, *17*, 4493.
- (24) Eaborn, C.; Odell, K. J.; Pidcock, A. *J. Chem. Soc., Dalton Trans.* **1978**, 357.
- (25) Osakada, K.; Yamamoto, T. *Coord. Chem. Rev.* **2000**, *198*, 379.
- (26) Cross, R. J.; Gemmill, J. *J. Chem. Soc., Dalton Trans.* **1984**, 205.
- (27) Puddephatt, R. J.; Thompson, P. J. *J. Chem. Soc., Dalton Trans.* **1977**, 1219.
- (28) Puddephatt, R. J.; Thompson, P. J. *J. Chem. Soc., Dalton Trans.* **1975**, 1810.
- (29) Foley, N. A.; Lail, M.; Lee, J. P.; Gunnoe, T. B.; Cundari, T. R. Peterson, J. L. *J. Am. Chem. Soc.* **2007**, *129*, 6765.
- (30) Veige, A. S.; Slaughter, L. M.; Wolczanski, P. T.; Matsunaga, N.; Decker, S. A.; Cundari, T. R. *J. Am. Chem. Soc.* **2001**, *123*, 6419.
- (31) Lerch, M.; Tilset, M. *Chem. Rev.* **2005**, *105*, 2471.
- (32) Hickman, A. J.; Villalobos, J. A.; Sanford, M. S. *Organometallics* **2009**, *28*, 5316.
- (33) Bar-Nahum, I.; Khenkin, A. M.; Neumann, R. *J. Am. Chem. Soc.* **2004**, *126*, 10236.
- (34) Periana, R. A.; Taube, D. J.; Gamble, S.; Taube, H.; Satoh, T.; Fujii, H. *Science* **1998**, *280*, 560.
- (35) Muehlhofer, M.; Strassner, T.; Herrmann, W. A. *Angew. Chem., Int. Ed.* **2002**, *41*, 1745.
- (36) Holtcamp, M. W.; Henling, L. M.; Day, M. W.; Labinger, J. A.; Bercaw, J. E. *Inorg. Chim. Acta* **1998**, *270*, 467.
- (37) Hackett, M.; Whitesides, G. M. *J. Am. Chem. Soc.* **1988**, *110*, 1449.
- (38) Kaim, W.; Klein, A.; Hasenzahl, S.; Stoll, H.; Zális, S.; Fiedler, J. *Organometallics* **1998**, *17*, 237.
- (39) Scarel, A.; Durand, J.; Franchi, D.; Zangrando, E.; Mestroni, G.; Milani, B.; Gladiali, S.; Carfagna, C.; Binotti, B.; Bronco, S.; Gragnoli, T. *J. Organometallic Chem.* **2005**, *690*, 2106.
- (40) Bastero, A.; Claver, C.; Ruiz, A.; Catillón, S.; Bo, C.; Zangrando, E. *Chem. Eur. J.* **2004**, *10*, 3747.
- (41) Bastero, A.; Ruiz, A.; Claver, C.; Milani, B.; Zangrando, E. *Organometallics* **2002**, *21*, 5820.
- (42) Iretskii, A. V.; Sherman, S. C.; White, M. G.; Kevlin, J. C.; Schiraldi, D. A. *J. Catal.* **2000**, *193*, 49.
- (43) Shiotani, A.; Itatani, H.; Inagaki, T. *J. Mol. Catal.* **1986**, *34*, 57.
- (44) Lanci, M. P.; Remy, M. S.; Kaminsky, W.; Mayer, J. M.; Sanford, M. S. *J. Am. Chem. Soc.* **2009**, *131*, 15618.
- (45) Vigalok, A.; Kaspri, A. *Top. Organometallic Chem.* **2010**, *31*, 19.
- (46) Yandulov, D. V.; Tran, N. T. *J. Am. Chem. Soc.* **2007**, *129*, 1342.
- (47) Roy, A. H.; Hartwig, J. F. *Organometallics* **2004**, *23*, 1533.
- (48) Roy, A. H.; Hartwig, J. F. *J. Am. Chem. Soc.* **2003**, *125*, 13944.
- (49) Roy, A. H.; Hartwig, J. F. *J. Am. Chem. Soc.* **2001**, *123*, 1232.
- (50) Boisvert, L.; Denney, M. C.; Kloek Hanson, S.; Goldberg, K. I. *J. Am. Chem. Soc.* **2009**, *131*, 15802.
- (51) Kloek Hanson, S. *Synthesis and Reactivity Studies of Late Transition Metal Complexes Relevant to C-H Bond Activation and Functionalization*, Ph.D. Thesis, University of Washington, Seattle, 2007
- (52) Frisch, M. J.; Trucks, G. W.; Schlegel, H. B.; Scuseria, G. E.; Robb, M. A.; Cheeseman, J. R.; Montgomery Jr., J. A.; Vreven, T.; Kudin, K. N.; Burant, J. C.; Millam, J. M.; Iyengar, S. S.; Tomasi, J.; Barone, V.; Mennucci, B.; Cossi, M.; Scalmani, G.; Rega, N.; Petersson, G. A.; Nakatsuji, H.; Hada, M.;

Ehara, M.; Toyota, Fukuda, R.; Hasegawa, J.; Ishida, T.; Nakajima, T.; Honda, Y.; Kitao, O.; Nakai, H.; Klene, M.; Li, X.; Knox, J. E.; Hratchian, H. P.; Cross, J. B.; Adamo, C.; Jaramillo, J.; Gomperts, R.; Stratman, R. E.; Yazyev, O.; Austin, A. J.; Cammi, R.; Pomellia, C.; Ochterski, J. W.; Ayala, P. Y.; Morokuma, K.; Voth, G. A.; Salvador, P.; Dannenberg, J. J.; Zakrzewski, V. G.; Dapprich, S.; Daniels, A. D.; Strain, M. C.; Farkas, O.; Malick, D. K.; Rabuck, A. D.; Raghavachari, K.; Foresman, J. B.; Ortiz, J. V.; Cui, Q.; Baboul, A. G.; Clifford, S.; Cioslowski, J.; Stefanov, B. B.; Liu, G.; Liashenko, A.; Piskorz, P.; Komaromi, I.; Martin, R. L.; Fox, D. J.; Keith, T.; Al-Laham, M. A.; Peng, C. Y.; Nanayakkara, A.; Challacombe, M.; Gill, P. M. W.; Johnson, B.; Chen, W.; Wong, M. W.; Gonzalez, C.; Pople, J. A. *Gaussian 03*, Revision C.02; Gaussian, Inc.: Wallingford, CT, 2004.

(53) Becke, A. D. *J. Chem. Phys.* **1993**, *98*, 1372

(54) Lee, C.; Yang, W.; Parr, R. G. *Phys. Rev.* **1998**, *B37*, 785.

(55) Stevens, W. J.; Basch, H.; Krauss, M. *J. Chem. Phys.* **1984**, *81*, 6026

(56) Stevens, W. J.; Krauss, M.; Basch, H.; Jasien, P. G. *Can. J. Chem.* **1992**, *70*, 612

(57) Cancès, M. T.; Mennucci, B.; Tomasi, J. *J. Chem. Phys.* **1997**, *107*, 3032.

(58) Mennucci, B.; Tomasi, J. *J. Chem. Phys.* **1997**, *106*, 5151.

(59) Mennucci, B.; Cancès, E.; Tomasi, J. *J. Chem. Phys. B.* **1997**, *101*, 10506.

(60) Tomasi, J.; Mennucci, B.; Cancès, E. *J. Mol. Struct. (Theochem)* **1999**, *464*, 211.

(61) Byers, P. K.; Canty, A. J.; Jin, H.; Kruis, D.; Markies, B. A.; Boersma, J.; Van Koten, G.; Hill, G. S.; Irwin, M. J.; Rendina, L. M.; Puddephatt, R. J. *Inorg. Synth.* **1998**, *32*, 162.

(62) Engelter, C.; Thornton, D. A. *Transition Met. Chem.* **1990**, *15*, 212.

(63) Byers, P. K.; Canty, A. J.; Crespo, M.; Puddephatt, R. J.; Scott, J. D. *Organometallics* **1988**, *7*, 1363.

(64) Ball, N. D.; Sanford, M. S. *J. Am. Chem. Soc.* **2009**, *131*, 3796.

(65) Foley, S. R.; Shen, H.; Qadeer, U. A.; Jordan, R. F. *Organometallics* **2004**, *23*, 600

(66) Shen, H.; Jordan, R. F. *Organometallics* **2003**, *22*, 1878.

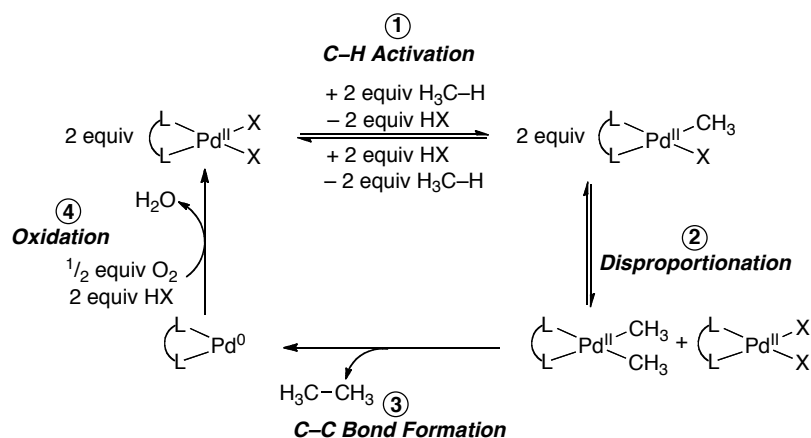
CHAPTER 3

Carbon–Carbon Bond Formation from (*t*Bu-bpy)Pd(CH₃)₂ in the Presence of Electron-Deficient Olefins and One-Electron Oxidants

3.1 Background and Significance

In designing a homogenous catalyst for the oxidative oligomerization of methane, we have proposed the necessary fundamental steps to be 1) C–H activation of methane to give a monomethyl-metal complex, 2) formation of a dimethyl intermediate via disproportionation, 3) C–C bond-forming reductive elimination of ethane, and 4) reoxidation of the metal (Scheme 3.1). Studies shown in Chapter 2 focused on accomplishing the formation of a Pd^{II}-dimethyl intermediate but also uncovered the need to develop new chemistry for efficiently achieving C–C coupling to generate ethane from dimethyl-palladium complexes.

Scheme 3.1 Proposed Catalytic Cycle for Oxidative Oligomerization of Methane.

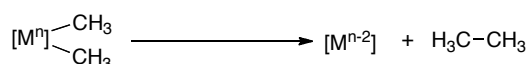


Carbon–carbon bond formation at palladium centers is one of the most important transformations in organometallic chemistry, as it serves as the product forming step in Pd-catalyzed cross-couplings, allylic substitutions, C–H functionalizations, and numerous

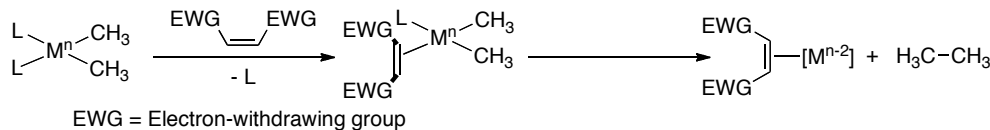
other processes.¹ There are three general pathways for palladium-mediated C–C bond formation from Pd^{II}(R)₂ intermediates (R = alkyl or aryl): 1) direct C–C bond-forming reductive elimination (Path A, Scheme 3.2), 2) C–C bond-forming reductive elimination promoted by electron deficient olefins (Path B, Scheme 3.2), or 3) oxidatively-induced C–C coupling (Path C, Scheme 3.2).

Scheme 3.2 Common Pathways for C–C Bond Formation.

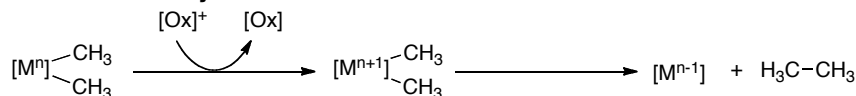
Path A: Direct C–C Bond Formation



Path B: C–C Bond Formation Promoted by Electron Deficient Olefins

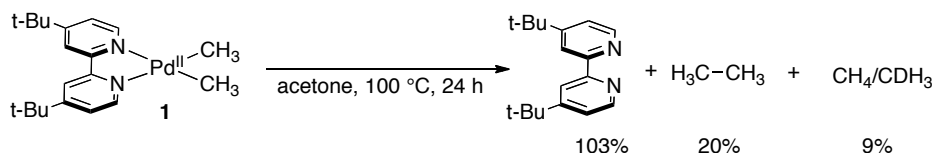


Path C: Oxidatively-Induced C–C Bond Formation

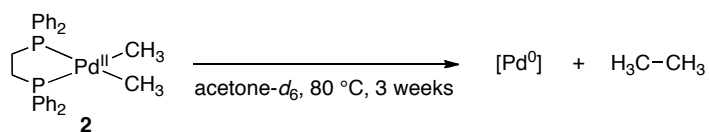


In Chapter 2, thermolysis of (*t*-Bu-bpy)Pd(CH₃)₂ (**1**) was discussed (Scheme 3.3). Direct C–C bond-forming reductive elimination was shown to be inefficient with 20% H₃C–CH₃ being formed at 100% conversion of **1** over 24 h at 100 °C in acetone-*d*₆. Reaction of a similar diphosphine-ligated complex **2** was reported to occur over the course of three weeks at 80 °C in acetone-*d*₆ (Scheme 3.4),² highlighting the inefficiency of direct *sp*³–*sp*³ C–C bond formation from *cis*-chelated Pd^{II} complexes.

Scheme 3.3 Thermolysis of (*t*-Bu-bpy)Pd(CH₃)₂ (**1**).



Scheme 3.4 Ethane Formed by C–C Bond Reductive Elimination from Pd^{II}.²

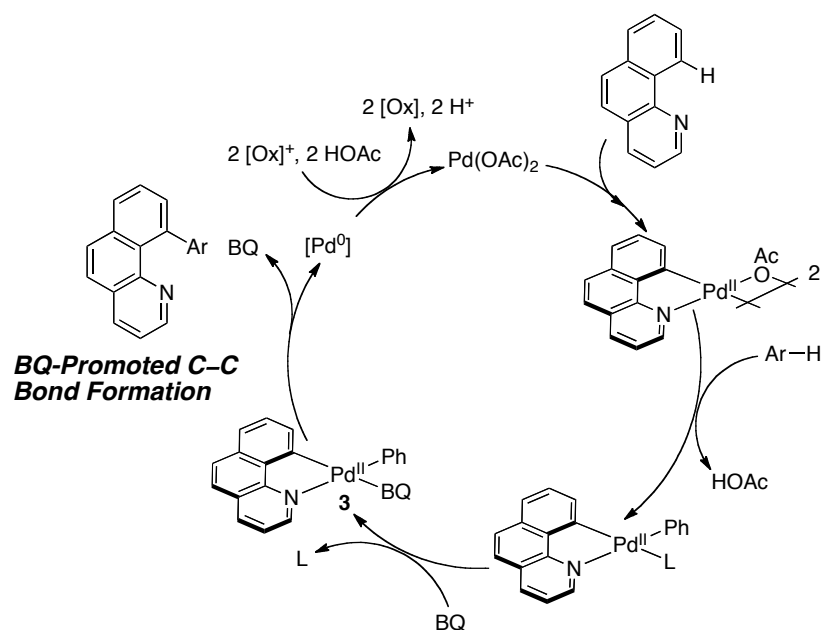


Hartwig has reviewed rates of C–C bond-forming reductive elimination and found that sp^2 – sp^2 couplings are generally faster than sp^3 – sp^3 couplings for complexes bearing monodentate ligands.³ For example, spontaneous reductive elimination of biphenyl (sp^2 – sp^2 coupling) is known to occur from bipyridine-ligated palladium(II).⁴ So while direct C–C bond formation is facile for sp^2 – sp^2 C–C couplings and sp^2 – sp^3 C–C couplings, development of efficient methods of sp^3 – sp^3 C–C bond formation from *cis*-chelated complexes still requires significant study.

In palladium-catalyzed reactions to form new C–C bonds, several common additives have been shown to promote C–C bond-forming reductive elimination. Two prevalent classes of additives include electron deficient olefins^{5–12} and one-electron oxidants such as Ag(I)^{13–17} or Ce(IV).¹⁸

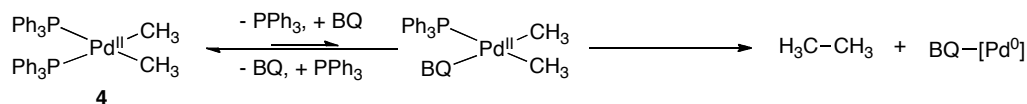
Amongst electron deficient olefins, 1,4-benzoquinone (BQ) is ubiquitous as a promoter of C–C reductive elimination.^{5–12} A study from the Sanford lab showed BQ to be crucial in the rate-determining C–C bond-forming step during the catalytic oxidative coupling of arenes (Scheme 3.5).^{5,7} In this system, kinetic studies indicated that BQ induced reductive elimination after binding Pd^{II} within the square plane palladium diaryl complex (Complex 3, Scheme 3.5).

Scheme 3.5 Oxidative Coupling of 2-phenylpyridine to Arenes Promoted By BQ.⁵

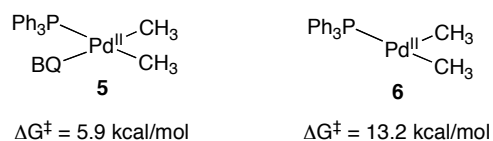


A computational and experimental study by Espinet showed that BQ underwent ligand substitution of PPh_3 in the dimethyl complex $(\text{PPh}_3)_2\text{Pd}(\text{CH}_3)_2$ (**4**) in a related process to promote subsequent reductive elimination of ethane (Scheme 3.6).⁶ The effect of BQ binding was proposed to be stabilization of the reductive elimination transition state, lowering the kinetic barrier for C–C bond formation. Strikingly, these computations showed that the ΔG^\ddagger for reductive elimination from four-coordinate BQ complex **5** is 7.3 kcal/mol lower than 3-coordinate complex **6**, which is related to the generally accepted intermediates involved in aryl cross-coupling reductive elimination (Scheme 3.7).³ Subsequently, kinetic studies of complex **4** were performed at 23 °C in acetone- d_6 with and without BQ. The results show 100% conversion of **4** within 17 minutes in the presence of BQ while the analogous reaction without BQ reached only 60% conversion after 2 h.

Scheme 3.6 BQ-Promoted Reductive Elimination from a Pd^{II} -Dimethyl Complex.⁶

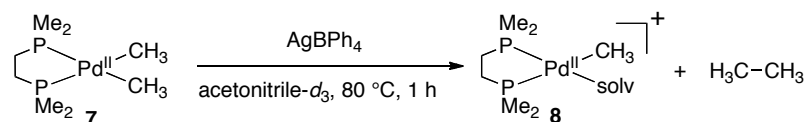


Scheme 3.7 Computed ΔG^\ddagger for Ethane Reductive Elimination.⁶

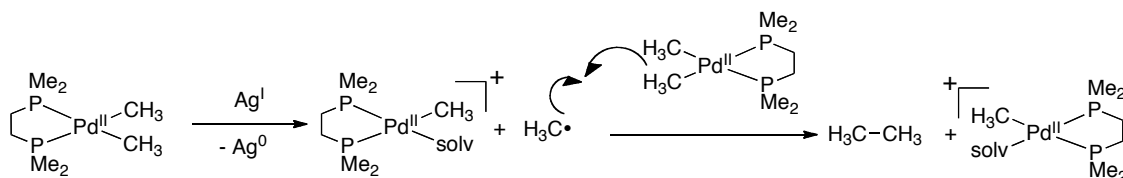


One-electron oxidants, such as Ag^{I} are common additives in Pd-catalyzed transformations,^{13–17} but often their role is attributed to functions other than oxidation. However, Ag^{I} has been shown to induce C–C bond formation from $\text{Pd}^{\text{II}}\text{--R}$ complexes (Scheme 3.8).^{19,20} For example, dimethyl complex $(\text{dmpe})\text{Pd}(\text{CH}_3)_2$ (**7**) reacted with Ag^{I} in acetonitrile for 1 h at room temperature to generate cationic monomethyl complex **8** and ethane.²⁰ The mildness of these reaction conditions compared to thermolysis of related complex **2** is remarkable (Scheme 3.4). The reaction was proposed to occur via one-electron oxidation of the Pd–C bond followed by trapping of the alkyl radical by a proximal Pd–C bond (Scheme 3.9).

Scheme 3.8 Reaction of Ag^{I} with Complex **7** to Ethane.²⁰



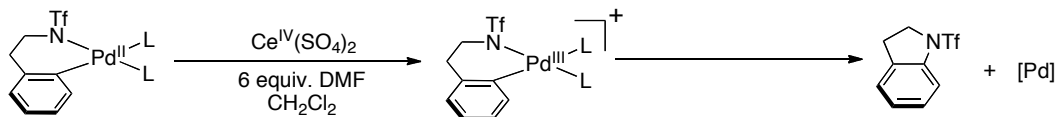
Scheme 3.9 Oxidative Pd–CH₃ Bond Cleavage to Afford Ethane.²⁰



In a related Pd-catalyzed C–N bond-forming reaction, the one-electron oxidant Ce^{IV} was used to promote the C–N bond formation (Scheme 3.10).¹⁸ The one-electron oxidation of Pd^{II} to Pd^{III} or two sequential one-electron oxidations to give Pd^{IV} from Pd^{II} are proposed to facilitate subsequent C–N bond formation. These precedents suggest that withdrawing electron density from the a Pd^{II} metal center, either by binding of an electron-deficient olefin or by oxidation, should also facilitate ethane formation from $(\text{L}_2)\text{Pd}(\text{CH}_3)_2$ complexes relevant to the oligomerization of methane to occur under mild

conditions. It was our goal to identify the most effective promoting agents for C–C bond formation from $(L_2)Pd(CH_3)_2$ and study mechanisms of reactivity in these systems.

Scheme 3.10 Ce^{IV} Oxidatively-Induced Reductive Elimination of a C–N Bond.¹⁸



3.2 Results and Discussion

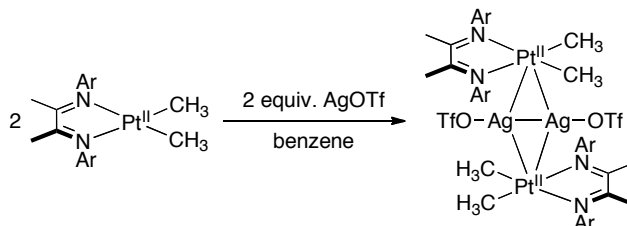
In choosing a dimethyl complex for study of C–C bond formation, it was important to consider the entire proposed catalytic cycle for oxidative oligomerization of methane. Thus, the model complex needed a ligand framework that was relevant to C–H activation and disproportionation. Diimine complexes are known to promote C–H activation of methane^{21–23} and act as supporting ligands in disproportionation reactions.^{24,25} Specifically, our stoichiometric studies toward methyl disproportionation focused on complexes of *t*-Bu-bpy (4,4'-*di*-*tert*butyl-2,2'-bipyridine).²⁴ Hence, dimethyl complex (*t*-Bu-bpy) $Pd(CH_3)_2$ (**1**) was identified as a model complex for study of C–C bond formation in the presence of promoters.

The structure of **1** prompted a number of questions in regard to the action of promoters. In the examples of BQ-promoted C–C formation discussed above, BQ is proposed to displace a ligand in the square plane of the metal before inducing C–C bond reductive elimination. In complex **1**, no ligand appears labile enough to allow BQ to ligate the complex within the square plane, so it was unclear whether BQ could promote ethane formation from **1**.

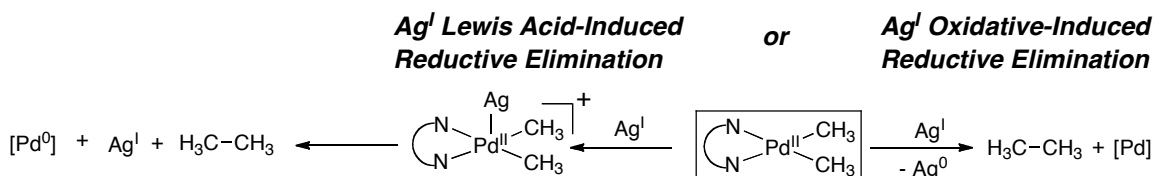
With regard to Ag^I -promoted C–C bond formation, studies of (diimine) $Pt^{II}(CH_3)_2$ complexes indicated that Ag^I was able to act as a Lewis acid by binding to the dz^2 orbital of the metal (Scheme 3.11).^{26,27} These crystallographically characterized complexes were stable at room temperature. For complex **1**, similar reactivity would require Ag^+ to bind via the Pd dz^2 orbital. Precedent for such interaction at Pd was unknown, and it was further questioned whether Ag^I binding the palladium dz^2 orbital as a Lewis acid would induce C–C bond formation by reducing the electron density at Pd^{II} or whether single-

electron oxidation by Ag^{I} would cause C–C bond formation analogous to the oxidation of **7** (Scheme 3.12). In the former case, Ag^{I} could be used catalytically as a Lewis acid to promote reductive elimination. In the latter case, Ag^{I} would be a stoichiometric oxidant.

Scheme 3.11 Ag^{I} Binding to the d_{z^2} Orbital of (diimine) $\text{Pt}(\text{CH}_3)_2$ Complexes.²⁶



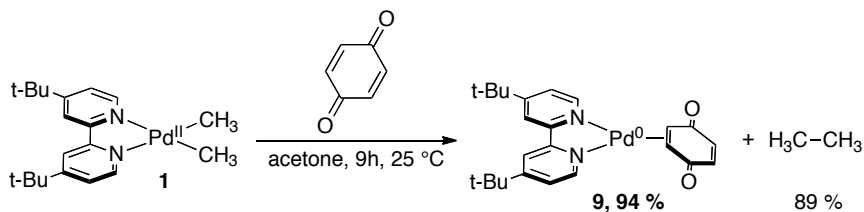
Scheme 3.12 Alternate Pathways for Ag^{I} -Promoted Reductive Elimination.



3.2.1 1,4-Benzoquinone-Promoted C–C Bond Formation

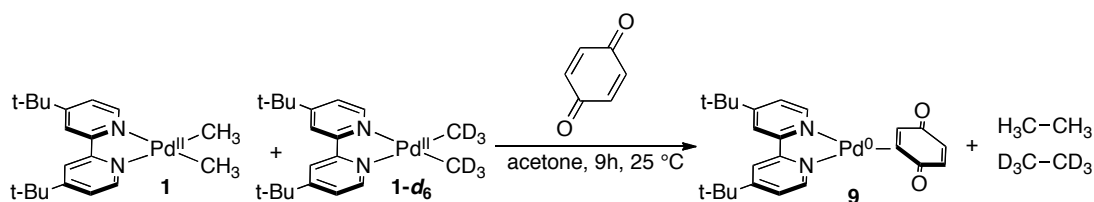
Initially, dimethyl complex **1** was reacted with benzoquinone (BQ) in acetone- d_6 . Over the course of 9 h at 25 °C, the reaction generated ethane (89%), and a symmetric palladium complex (94%). The symmetric palladium complex was identified by Dr. Michael Lanci as (*t*Bu-bpy) $\text{Pd}^0(\text{BQ})$ (**9**) (Scheme 3.13). Only 3.5% hydroquinone (HQ), the two-electron reduced form of BQ, was observed in this reaction. These results suggested that BQ-promoted C–C bond formation occurred from a single metal center, without oxidation **1**.

Scheme 3.13 Reaction (*t*Bu-bpy) $\text{Pd}(\text{CH}_3)_2$ (**1**) with BQ to Afford Ethane.

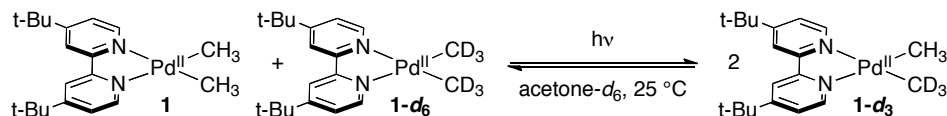


Crossover studies were performed to confirm that ethane elimination occurred from a single metal center. The reaction of **1** and **1-d₆** with BQ was performed by Dr. Michael Lanci, and at initial timepoints there was no evidence for crossover to form ethane-*d*₃ (Scheme 3.14). Initially, only ethane-*d*₀ and ethane-*d*₆ were observed. These studies were complicated, however, by methyl exchange between starting material **1** and **1-d₆** to form the mixed label **1-d₃** complex at longer reaction times. This scrambling occurred in the absence and in the presence of BQ (Scheme 3.15). Protection from light slowed the scrambling process between **1** and **1-d₆**, but did not eliminate **1-d₃** from forming at longer reaction times.

Scheme 3.14 Crossover Study for the Formation of Ethane Promoted by BQ.



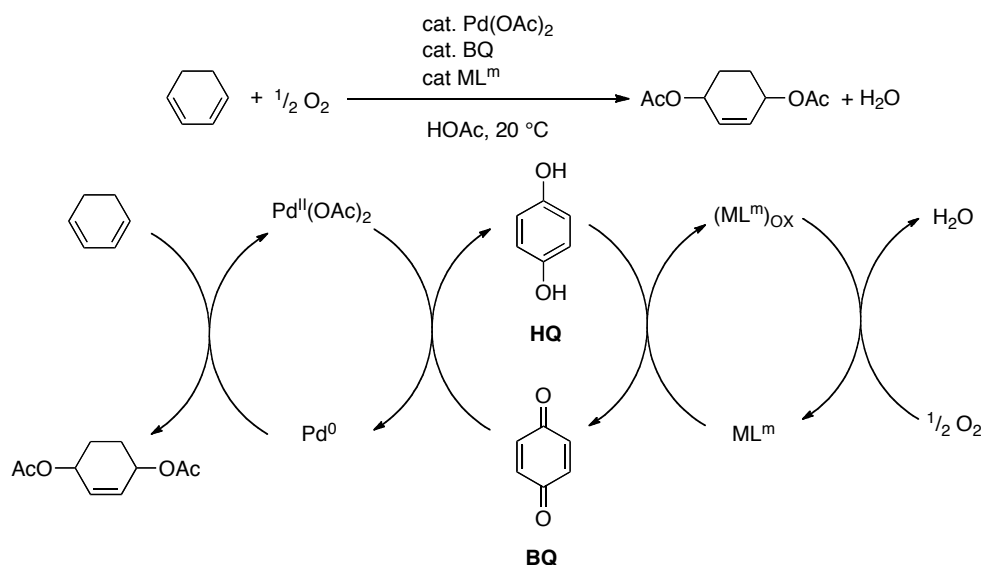
Scheme 3.15 Scrambling of Methyl Groups in **1** and **1-d₆**.



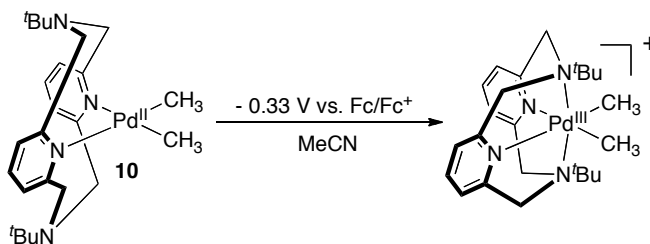
These studies demonstrated that BQ is an effective promoter of C–C bond formation, even in the case of **1** although the mechanism of this reaction was not apparent. BQ has been shown to oxidize Pd⁰ to Pd^{II} with concomitant formation of hydroquinone (HQ) (Scheme 3.16).²⁸ Bäckvall has shown that in the catalytic diacetoxylation of 1,3-dienes, Pd⁰ is reoxidized to Pd^{II} by BQ. In this system, BQ is used catalytically because HQ is reoxidized by O₂ through an electron relay (ML^m) such as a metal phthalocyanine. When considering the role of BQ in promoting reductive elimination from complex **1**, it is unclear though whether BQ (E⁰ = -0.41 V vs Fc/Fc⁺ in MeCN)²⁹ is a strong enough oxidant for oxidations of Pd^{II} to Pd^{III} (E⁰ (**10**) = -0.33 V vs. Fc/Fc⁺ in MeCN) (Scheme 3.17).³⁰ Complex **10** is the only dialkyl group 10 complex that produces a reversible oxidation wave, presumably because of the stabilizing pendant

amine groups in the ligand. However, it is unclear to what extent the presence of the pendant amine groups affects the oxidation potential of **10** vs **1**. When Dr. Lanci performed cyclic voltammetry experiments of **1**, an irreversible oxidation wave at +0.58 V (vs. Fc/Fc⁺ in acetone) was observed. If the irreversible potential for oxidation of **1** is indicative of the potential for oxidation of **1**, one-electron oxidation of **1** by BQ would have a K_{eq} of 1.9×10^{-17} . Even if the oxidation potential of **1** can be approximated by that of **10**, K_{eq} for electron transfer would be 4.5×10^{-2} . These electrochemical studies, the small quantities of HQ observed, and observation of **9** suggested that oxidation of **1** by BQ is not occurring.

Scheme 3.16 Oxidation of Pd⁰ to Pd^{II} by 1,4-Benzoquinone.²⁸



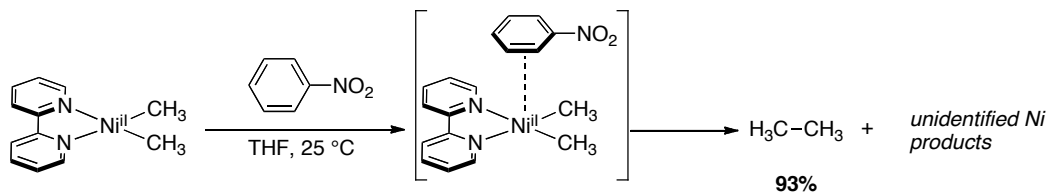
Scheme 3.17 One-Electron Oxidation Potential for a Pd^{II/III} Couple.³⁰



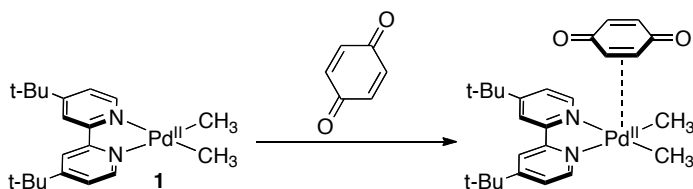
Related studies of ethane reductive elimination from square planar (bpy)Ni(CH₃)₂ complexes have shown that electron deficient arenes promote ethane formation (Scheme 3.18).³¹ These complexes are stable at 25 °C, however, in the presence of electron deficient arenes, ethane is liberated. The authors proposed arene binding to the Ni^{II}

center as the means by which the electron deficient arenes promoted ethane elimination. Our results in the crossover study of **1** and **1-d₆** showed the C–C bond formation occurred from a single metal center much like the methyl coupling from Ni^{II}. This suggests that a similar, bimolecular interaction between **1** and BQ could lead to ethane formation from **1** (Scheme 3.19).

Scheme 3.18 Ethane Formation from Ni^{II} Promoted by Electron-Deficient Arenes.³¹



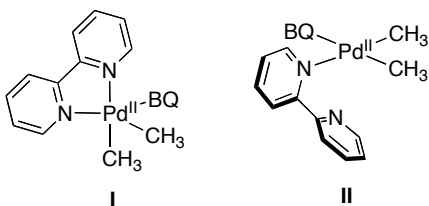
Scheme 3.19 Proposed Binding of 1,4-Benzoquinone to Complex **1**.



3.2.2 Calculations of Pd–BQ Binding

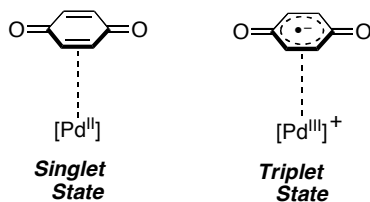
To further understand BQ interaction with **1**, density functional theory (DFT) calculations were carried out. (bpy)Pd(CH₃)₂ was used as a simplified model of **1** for the purposes of the calculations. Two BQ-bound structures were optimized as potential intermediates (Scheme 3.20). The exact computed geometries of structures **I** and **II** depended on the electronic configuration (singlet vs. triplet) applied in the calculation. However, generally, intermediate **I** was a five-coordinate complex of BQ and (bpy)Pd(CH₃)₂, and intermediate **II** was a four coordinate complex where BQ had displaced an arm of the bipyridine ligand.

Scheme 3.20 General Structures for Computed (bpy)Pd(CH₃)₂-BQ Intermediates.



To identify whether interaction of BQ with palladium was an oxidative process, intermediates **I** and **II** were calculated as restricted singlet (denoted as **I**^I or **II**^I), unrestricted singlet, and triplet electronic configurations (denoted as **I**³ or **II**³) (Scheme 3.21). Unrestricted singlet calculations allow open-shell electronic states with a singlet spin state. For all singlet calculations, restricted and unrestricted calculations produced exactly the same geometries and energies, so discussion of singlet calculations will be limited to the restricted calculations. Preference for a singlet state would imply that interaction of BQ and palladium occurs via dative olefin coordination to palladium. In contrast, preference for the triplet state would indicate a charge-separated state where an electron was promoted from palladium to BQ to generate a species with a delocalized radical π -anion and a cationic palladium(III) metal center.

Scheme 3.21 Singlet and Triplet Electronic States of Pd-BQ Complexes.



Density functional calculations, specifically those applying the functional B3LYP, are the most commonly applied computations in similar calculations. Examples include modeling of ethane elimination from dimethyl-palladium(II) phosphine complexes,⁶ charge separation in ruthenium-*ortho*-quinone complexes,^{32,33} charge separation in uranium-benzophenone complexes,³⁴ and orbital occupancies in iridium(I) complexes of dithio-*p*-benzoquinone.³⁵ Thus, we sought to calculate BQ binding to (bpy)Pd^{II}(CH₃)₂ using the functional B3LYP and CEP-31G(d) basis set combination we had previously employed for modeling of methyl disproportionation at palladium(II).

Singlet intermediate **I^I** was calculated as a trigonal bipyramidal palladium center with BQ, one methyl, and one pyridine in the trigonal plane and the second methyl and second pyridine as the axial ligands (Scheme 3.22). Compared to the Pd–CH₃ bond lengths of (bpy)Pd(CH₃)₂ (2.05 Å), the axial methyl Pd–CH₃ bond (2.06 Å) in **I^I** is only 0.01 Å longer. In contrast, the Pd–CH₃ bond in trigonal plane is 2.11 Å, substantially longer. The bound C=C bond of BQ (1.42 Å) was elongated in comparison with the C=C double bonds of unbound BQ (1.37 Å), while the unbound C=C bond of BQ in **I^I** was unaffected (1.37 Å). Key bond lengths for all calculated intermediates are tabulated in Table 3.1.

Scheme 3.22 Calculated (bpy)Pd(CH₃)₂–BQ Intermediate **I^I**.

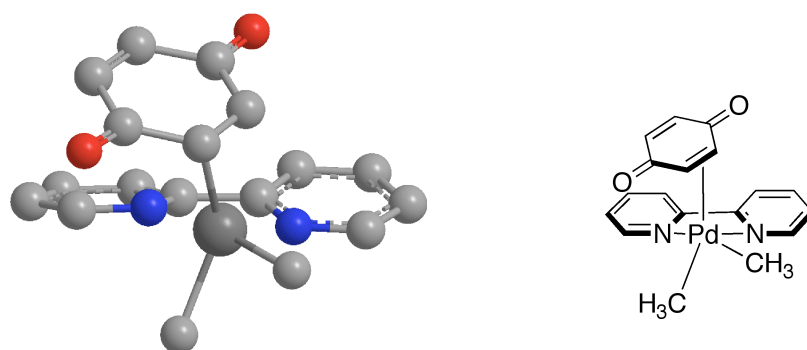


Table 3.1 Calculated Bond Lengths for (bpy)Pd(CH₃)₂–BQ Intermediates.

Complex	Bond Length (Å)			
	Pd–C1	Pd–C2	BQ C=C ^a	BQ C=C ^b
(bpy)Pd ^{II} (CH ₃) ₂	2.05	–	–	–
[(bpy)Pd ^{III} (CH ₃) ₂] ⁺	2.06	–	–	–
BQ	–	–	1.37	–
I^I	2.11 ^c	2.06 ^d	1.42	1.37
I³	2.08 ^e	2.07 ^d	1.41	1.39
II^I	2.09 ^e	2.07 ^d	1.40	1.37

^a bound to palladium

^b unbound

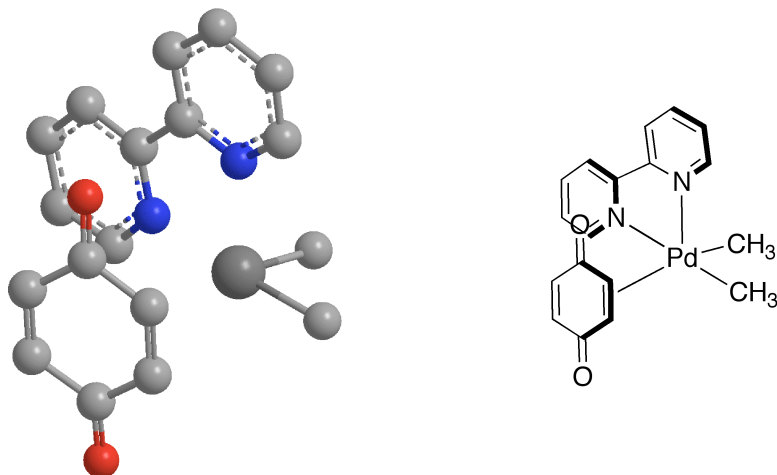
^c in the trigonal plane

^d trans to pyridine

^e trans to BQ

The triplet state, \mathbf{I}^3 was calculated as a square pyramidal palladium center with one arm of the bipyridine ligand acting as the axial ligand (Scheme 3.23). Palladium–CH₃ bond lengths of [(bpy)Pd^{III}(CH₃)₂]⁺ (2.06 Å) were calculated for comparison to \mathbf{I}^3 . The Pd–CH₃ bond trans to BQ (2.08 Å) was elongated slightly in comparison to the Pd–CH₃ bond trans to pyridine (2.07 Å). In contrast to \mathbf{I}^1 , the C=C bond lengths of BQ in \mathbf{I}^3 were elongated for both bound (1.41 Å) and unbound (1.39 Å) as expected for a delocalized π -anion radical. Attempts to find minimum energy geometry of the \mathbf{II}^3 always resulted in minimization to \mathbf{I}^3 .

Scheme 3.23 Calculated (bpy)Pd(CH₃)₂–BQ Intermediate \mathbf{I}^3 .



Intermediate \mathbf{II}^1 was calculated as a square planar complex presenting cis BQ and pyridine ligands (Scheme 3.24). Clearly only one arm of the bipyridine ligand is coordinated to palladium as the torsional angle between the pyridine groups is 35°. Upon binding of BQ, the Pd–CH₃ bond trans to BQ (2.09 Å) was elongated as was the trans-pyridine Pd–CH₃ bond (2.07 Å). Like \mathbf{I}^1 , the bound BQ C=C bond (1.40 Å) was elongated while the length of the unbound C=C bond (1.37 Å) was unaffected.

Scheme 3.24 Calculated (bpy)Pd(CH₃)₂-BQ Intermediate **II'**.

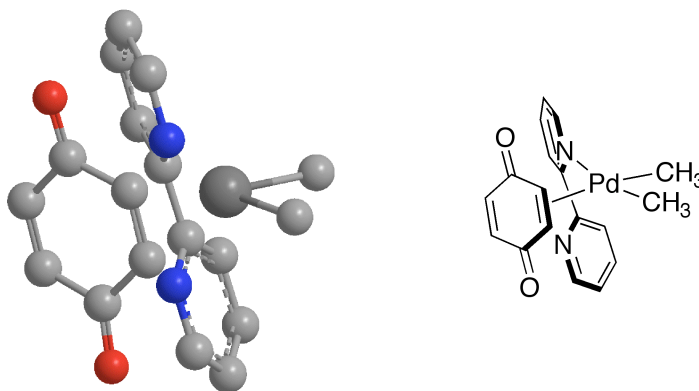


Table 3.2 summarizes ΔH and ΔG for BQ binding to palladium for all intermediates calculated. The large difference in ΔH and ΔG is the result of the added unfavorable entropy correction in ΔG from a decrease in entropy caused by producing one complex from two separate molecules. **I'** is substantially favored over the triplet state **I³** by 18.9 kcal/mol (ΔH) and 18.8 kcal/mol (ΔG). **I'** is only marginally favored over **II'** by 1.1 kcal/mol (ΔH) and 0.8 kcal/mol (ΔG). Inclusion of solvation calculations on ΔG raised the energies of **I'** and **II'** by 3.8 kcal/mol and 7.1 kcal/mol respectively while only lowering the ΔG of **I³** by 2.2 kcal/mol. With solvation, the minimum difference in energy between **I³** and **II²** still disfavored **I³** by 8.7 kcal/mol.

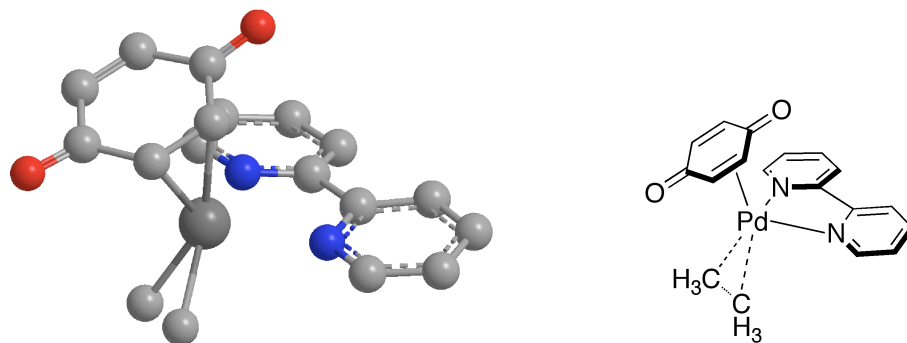
Table 3.2 Calculated ΔH and ΔG for BQ binding to (bpy)Pd(CH₃)₂.

Intermediate	ΔH (kcal/mol)	ΔG (kcal/mol)	ΔG_{+solv} (kcal/mol)
I'	2.6	14.4	18.2
I³	21.5	33.2	31.0
II'	3.7	15.2	22.3

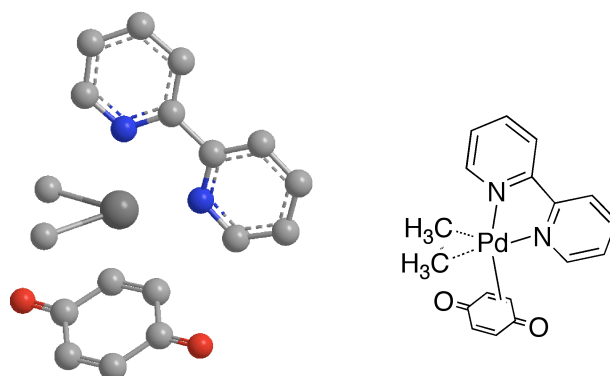
Transition structures were calculated for reductive elimination of ethane from (bpy)Pd(CH₃)₂(BQ) and for direct ethane elimination from (bpy)Pd(CH₃)₂. Like the calculations for Pd-BQ intermediates, transition structures were calculated for five-coordinate Pd-BQ complexes (**TS-I**) and four-coordinate Pd-BQ complexes (**TS-II**). The calculations were performed on singlet (**TS-X'**) and triplet (**TS-X³**) electronic energies.

TS-I' and **TS-I³** are pictured in Scheme 3.25 and Scheme 3.26 respectively. Reductive elimination in **TS-II'** occurs from a pseudo-tetrahedral geometry like those reported by Espinet for 4-coordinate transition states of ethane reductive elimination from related $(\text{PPh}_3)(\text{BQ})\text{Pd}(\text{CH}_3)_2$ (Scheme 3.27).⁶ Attempts to calculate **TS-II³** always resulted in minimization to the same geometry as **TS-I³**.

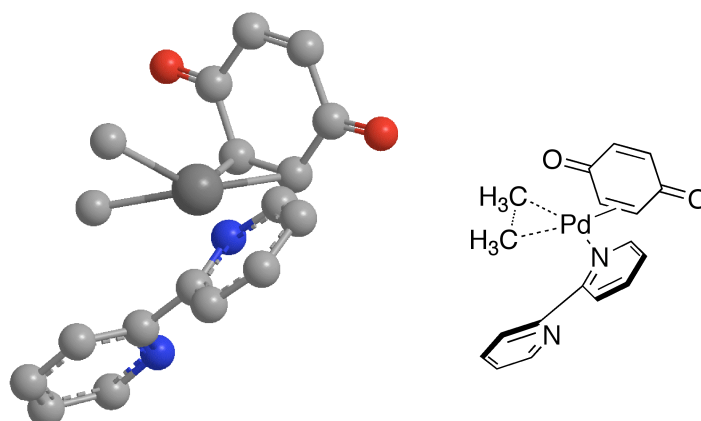
Scheme 3.25 Calculated $(\text{bpy})\text{Pd}(\text{CH}_3)_2\text{-BQ}$ Transition State **TS-I'**.



Scheme 3.26 Calculated $(\text{bpy})\text{Pd}(\text{CH}_3)_2\text{-BQ}$ Transition State **TS-I³**.



Scheme 3.27 Calculated (bpy)Pd(CH₃)₂-BQ Transition State **TS-II'**.



Energies for reductive elimination transition states are recorded in Table 3.3 as the difference in energy between the transition state and starting materials, (bpy)Pd(CH₃)₂ and BQ or in the case of elimination from (bpy)Pd(CH₃)₂, the difference in energy between (bpy)Pd(CH₃)₂ and [(bpy)Pd(CH₃)₂][‡]. Triplet transition state, **TS-I'** is substantially higher in energy than **TS-I'** and **TS-II'**, while direct reductive elimination from [(bpy)Pd(CH₃)₂][‡] is enthalpically 15.4 kcal/mol less favorable than **TS-I'** but only 3.0 kcal/mol less favorable in free energy. Reductive elimination from [(bpy)Pd(CH₃)₂][‡] is a unimolecular process while elimination from **TS-I'** requires BQ to bind to palladium. The entropic penalty paid is enough to make the transition states only differ by 3.0 kcal/mol in free energy. **TS-I'** and **TS-II'** are only separated by 1.0 kcal/mol (ΔH^\ddagger) and 0.4 kcal/mol (ΔG^\ddagger) in favor of **TS-II'**. A suitable transition state for direct reductive elimination from [(bpy)Pd^{III}(CH₃)₂][‡] could not be found. All of the transition states are characterized by increasing Pd-CH₃ bond lengths, contracting H₃C-CH₃ bond lengths, and elongating C=C bond lengths for the bound BQ double bond.

Table 3.3 Calculated ΔH^\ddagger and ΔG^\ddagger for BQ-induced ethane elimination.

Transition State	ΔH^\ddagger (kcal/mol)	ΔG^\ddagger (kcal/mol)	$\Delta G_{+\text{solv}}^\ddagger$ (kcal/mol)
$[(\text{bpy})\text{Pd}(\text{CH}_3)_2]^\ddagger$	34.4	33.3	36.0
TS-I'	19.0	30.3	34.5
TS-I³	37.7	49.2	45.4
TS-II'	18.0	29.9	33.3

Transition state calculations including solvation effects on ΔG were also performed. Similar to calculation of $(\text{bpy})\text{Pd}(\text{CH}_3)_2(\text{BQ})$ intermediates, solvation decreased the difference in energy between the singlet energy transition states and triplet transition state **TS-I³**. The difference in energy between **TS-I'** and **TS-I³**, 11.1 kcal/mol, still suggests the singlet state is substantially favored the over triplet state reaction pathway. With solvation effects, the difference in ΔG^\ddagger between singlet transition states **TS-I'** and **TS-II'** and direct reductive elimination from $(^t\text{Bu-bpy})\text{Pd}(\text{CH}_3)_2$ is narrowed to 1.5 kcal/mol and 2.7 kcal/mol for the BQ-ligated transition states. Favored by 2.7 kcal/mol, reaction proceeding through **TS-II'** is predicted to occur at rate approximately two orders of magnitude faster than direct elimination from $[(\text{bpy})\text{Pd}(\text{CH}_3)_2]^\ddagger$ by the Eyring equation.

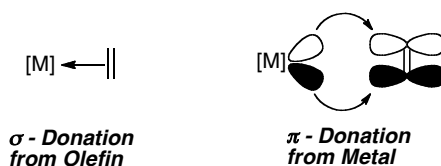
Natural bond orbital charge analysis was pursued as a further characterization of benzoquinone's interaction with palladium (Table 3.4).³⁶ The charge on palladium in $(\text{bpy})\text{Pd}^{\text{II}}(\text{CH}_3)_2$ and the olefinic carbons of BQ were calculated as benchmarks for interpreting Pd–BQ complexes. The charge of BQ olefinic carbons is reported as the average of the two carbons for each double bond. Charge analysis was limited to the singlet state computations. Increasing positive charge indicates electron density is being removed from the atom in question. In contrast, as the charge becomes more negative electron density increases on the atoms in question.

Table 3.4 Computed Atomic Charges for (bpy)Pd(CH₃)₂-BQ and [(bpy)Pd(CH₃)₂-BQ][‡]

Complex	Computed Atomic Charge		
	Pd	BQ-C _{bound} ^a	BQ-C _{unbound} ^a
(bpy)Pd ^{II} (CH ₃) ₂	+0.48	–	–
BQ	–	-0.22	–
I ^I	+0.73	-0.35	-0.22
II ^I	+0.57	-0.29	-0.22
TS-I ^I	+0.57	-0.38	-0.23
TS-II ^I	+0.56	-0.38	-0.22

^a atomic charge shown is the average of charge for the two olefinic carbons

Upon binding of BQ, the charge on palladium clearly increases relative to (bpy)Pd(CH₃)₂ (+0.48) in both **I**^I (+0.73) and **II**^I (+0.57). The effect of BQ binding on the palladium charge is significantly more profound in **I**^I. A commensurate decrease in charge is observed for the bound olefinic carbons in **I**^I (-0.35) and **II**^I (-0.29) relative to unbound BQ (-0.22). The increasing charge on palladium and decreasing charge on BQ carbon atoms bound to palladium indicate that BQ is removing electron density from Pd in the Pd-BQ complexes and the charge is building up on the carbons of the bound olefin carbons. This buildup charge is consistent with the elongated C=C bonds calculated for the bound BQ, which can be described by the Dewar-Chatt-Duncanson model for olefin binding to metals (Scheme 3.28).^{37,38} In this description, electron density is donated from the metal into the C=C π* orbital, elongating the C=C double bond.

Scheme 3.28 Two Components of Olefin Binding to a Metal.

In comparison, the analogous transition structures **TS-I**^I and **TS-II**^I show decreased charge on palladium (+0.57 and +0.56 respectively) and diminished charge on the bound C=C bond carbons (-0.38 for both transition structures). The decreased charge on palladium is expected because elimination of H₃C-CH₃ is a reductive process on the

metal, reducing the oxidation state of palladium(II) to palladium(0). The increase in electron density on BQ indicates BQ is acting as reservoir for electron density, accepting electron density from the metal into C=C π^* orbitals.

In summary, these calculations suggest that BQ promotes reductive elimination of ethane from (bpy)Pd(CH₃)₂ by removing electron density from the metal center rather than by acting as an oxidant. This is in agreement with experimental observations. However, the calculations do not show a clear energetic preference for reductive elimination from a four- versus five-coordinate intermediate. Strictly based on the numbers, BQ binding to (bpy)Pd(CH₃)₂ would form **I'** in an endothermic reaction. Dissociation of one pyridine in **I'** would lead to **II'**, and elimination of ethane would occur from four-coordinate transition state **TS-II'**.

Unfortunately, the calculations fail to accurately predict the difference in energy between direct ethane elimination from **1** and BQ-induced elimination from **1**. Experimentally, the ΔG^\ddagger for ethane elimination is roughly estimated to be 21 kcal/mol (at 298 K) for BQ-induced elimination and 32 kcal/mol (at 373 K) for direct ethane elimination based on the total time of reaction. These computations (at 298 K) suggest that the overall difference between direct ethane elimination and elimination occurring through **TS-II'** is only 2.7 kcal/mol. This discrepancy between theory and experiment suggests two scenarios: 1) the calculations are improperly calibrated to describe BQ-induced reductive elimination, or 2) our limited understanding of how BQ interacts with (t-Bu-bpy)Pd^{II}(CH₃)₂ led us to improperly model the reaction. Regarding the former point, as noted above similar methods (functionals and basis sets) have been used to compute BQ adducts of transition metals. Specifically, our values for ΔG^\ddagger of ethane elimination track well with those calculated by Espinet.⁶ However, changes in the basis set employed have given markedly different results for orbital occupancies in calculations of Ir(I)(dithio-*p*-BQ) complexes.³⁵ Similarly, computations on the mechanism of hydrogen atom transfer between O₂ and reduced quinone species calculated with complete active space self consistent field (CASSCF) methods provides results that better paralleled experiment than related computations employing DFT.³⁹ These precedents suggest that further optimization of method (DFT functional or higher levels of theory) or basis sets should be pursued to confirm similar trends in computations of ethane

elimination from (*t*Bu-bpy)Pd^{II}(CH₃)₂. Alternatively, the methods by which unrestricted calculations (open shell, singlet) were performed could be more thoroughly explored. DFT calculations have an inherent bias for spin pairing, and more effort may be necessary to optimize the open shell singlet geometries for BQ-induced elimination of ethane. In regard to the second reason posited for the discrepancy between theory and experiment, a better understanding of the reactions kinetics could shed light on the interactions between (*t*Bu-bpy)Pd^{II}(CH₃)₂ and BQ that would allow more accurate modeling to be accomplished. As an example, in computations of a Vitamin E-BQ donor-acceptor complex, it was important to model the excited state behavior of the complex to accurately model charge transfer between the donor and acceptor.⁴⁰ Finally, optimization of ground state (bpy)Pd^{II}(CH₃)₂-BQ complexes was challenging because of the propensity for BQ dissociation during the course of the optimization. Although many geometries and conformations were calculated, perhaps a lower-energy conformation could be calculated with further probing.

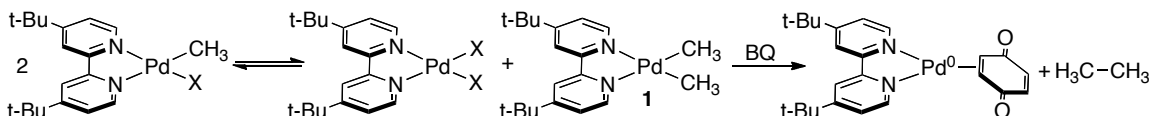
In summary, DFT calculations employing the B3LYP/CEP-31G(d) functional/basis set combination failed to accurately predict the difference in ΔG^\ddagger between direct ethane elimination from (bpy)Pd^{II}(CH₃)₂ and BQ-induced ethane elimination from (bpy)Pd^{II}(CH₃)₂ that is estimated from experimental values. The calculated value for $\Delta G_{+soln}^\ddagger$ (36.0 kcal/mol) of direct ethane elimination is only +4 kcal/mol from the experimental estimate (32.0 kcal/mol), while the calculated $\Delta G_{+soln}^\ddagger$ of BQ-induced ethane elimination (33.3 kcal/mol) is +12.3 kcal/mol from the experimental estimate (21 kcal/mol). These results suggest the computations are accurate for modeling ethane elimination in the absence of BQ, but are ill-suited or incorrect in modeling the interactions between (bpy)Pd^{II}(CH₃)₂ and BQ.

3.2.3 Driving Equilibrium Formation of (*t*Bu-bpy)Pd(CH₃)₂ with BQ

In Chapter 2, experiments were described that attempted to show disproportionation to form **1** from monomethyl palladium complexes (Scheme 2.21). The conclusion of those studies was that thermolysis was not an effective means for decomposition of **1**, so interpretations suggesting disproportionation to **1** from

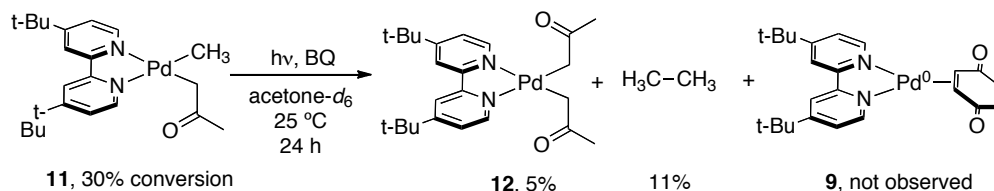
monomethyl complexes were unable to be made. Now knowing that BQ effectively promotes decomposition of **1** to generate ethane and well-defined inorganic products, we sought to drive disproportionative formation of **1** from monomethyl complexes by decomposing **1** with BQ (Scheme 3.29).

Scheme 3.29 Disproportionation of (^tBu-bpy)Pd(CH₃)X Followed by BQ-Induced Elimination

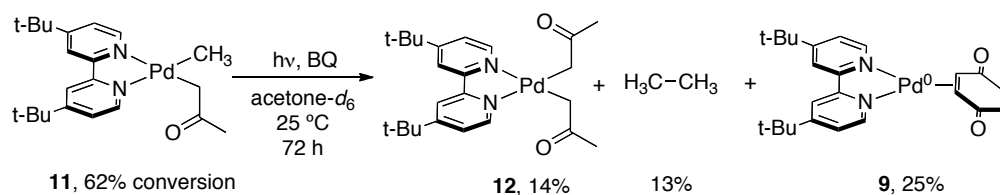


Acetyl complex (^tBu-bpy)Pd(CH₃)(CH₂COCH₃) (**11**), which was shown to undergo disproportionation to form **1**,²⁴ was reacted with BQ at 25 °C in acetone-*d*₆. After 24 h, **11** (30% conversion) decomposed to form diacetyl complex **12** (5%), and ethane (11%) (Scheme 3.30). Neither Pd⁰-BQ complex **9** nor other C-C coupled products (for example, 2-butanone and 2,5-hexane-di-one) were not observed. Over 72 h, **11** (62% conversion) reacted further to produce **12** (14%), ethane (13%), and **9** (25%) (Scheme 3.31). In the absence of light, no reaction between **11** and BQ occurred under these conditions. These results suggested that other (^tBu-bpy)Pd(CH₃)X complexes, where disproportionation to form **1** was not observed spectroscopically, may react with BQ if rapid, reversible disproportionation to form **1** was occurring. If **1** was formed and able to react with BQ on the timescale of disproportionation, BQ-induced elimination of ethane should drive the disproportionation equilibrium toward formation of Pd⁰-BQ, ethane, and (^tBu-bpy)PdX₂.

Scheme 3.30 Reaction of (^tBu-bpy)Pd(CH₃)(CH₂COCH₃) (**11**) with BQ – 24 h.

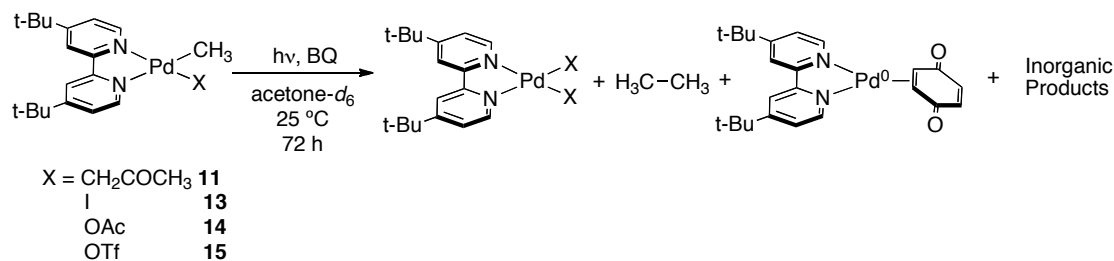


Scheme 3.31 Reaction of (^tBu-bpy)Pd(CH₃)(CH₂COCH₃) (**11**) with BQ – 72 h.



To that end, monomethyl complexes (^tBu-bpy)Pd(CH₃)I (**13**), (^tBu-bpy)Pd(CH₃)OAc (**14**) and (^tBu-bpy)Pd(CH₃)OTf (**15**) were reacted with BQ at 25 °C for 72 h in acetone-*d*₆ in J. Young NMR tubes under ambient light. The results of these reactions are recorded in Table 3.5. No reaction of **13** or **14** was observed in the absence of light. Triflate complex **15** decomposed similarly under ambient light and in the absence of light.

Table 3.5 Products of (*t*-Bu-bpy)Pd(CH₃)X Disproportionation and BQ-Induced Elimination



Entry	Complex	% Yield					
		C ₂ H ₆	CH ₃ X	Starting Material	(<i>t</i> -Bu-bpy)Pd(X) ₂	(<i>t</i> -Bu-bpy)Pd(BQ) (13)	Other Inorganic Products
1	11 (CH ₂ COCH ₃)	13	0	38	14	25	0
2	13 (I)	0	21	70	10	0	14 ^a
3	14 (OAc)	22	0	39	14	0	38 ^{b,c}
4	15 (OTf)	0	0	22	0	0	–

^a free *t*-Bu-bpy (14%) + Pd(0)

^b (*t*-Bu-bpy)Pd(CH₃)(CH₂COCH₃) – 10%

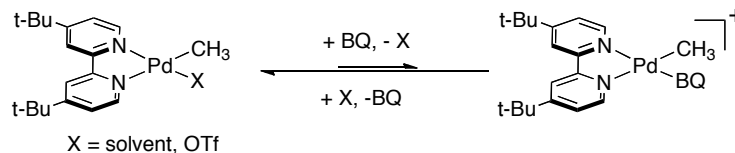
^c (*t*-Bu-bpy)Pd(CH₂COCH₃)OAc – 28%

NMR spectroscopic analysis of the reactions of iodide complex **13** and triflate complex **15** after 72 h showed 30% and 78% conversion respectively. No ethane or **9** (Pd⁰-BQ) were observed in these reactions, but 21% methyl iodide was formed in the reaction of **13**.

When triflate complex **15** was reacted with BQ at 25 °C an initial ¹H NMR spectrum showed no shift of the resonances for **15**, suggesting that room temperature binding of BQ to the complex was not occurring to a measurable extent. In fact, only one well-characterized example of BQ binding to Pd^{II} has been reported.⁴¹ In acetone solvent, this likely indicates preferential binding of solvent or triflate over BQ (Scheme 3.32). Reaction of **15** (78% conversion) over 72 h at 25 °C produced no identifiable

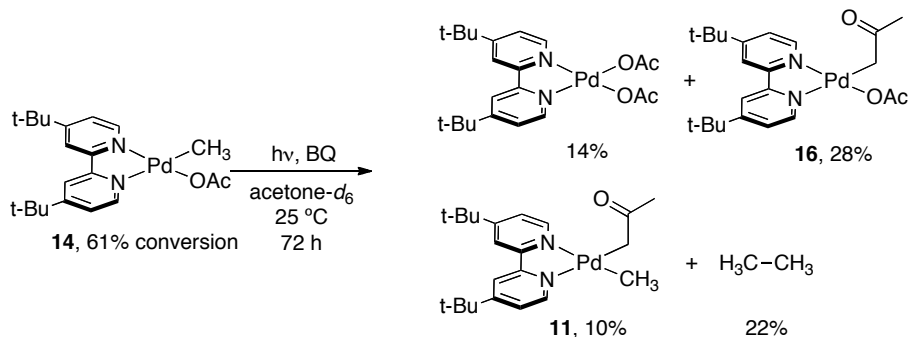
inorganic products and no ethane while reaction of **13** produced (^tBu-bpy)Pd(I)₂ (10%) and free ^tBu-bpy (14%).

Scheme 3.32 Preference for Solvent or Triflate Binding Over BQ at Pd^{II}.

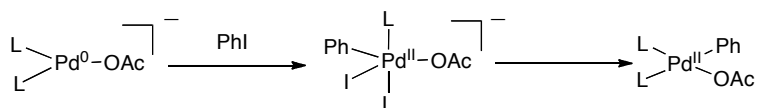


When acetate complex **14** and BQ stood at 25 °C for 72 h, 61% of **14** reacted to give ethane (22%), (^tBu-bpy)Pd(OAc)₂ (**14**, 14%), and acetyl complexes **11** (10%) and (^tBu-bpy)Pd(CH₂COCH₃)(OAc) (**16**, 28%) (Scheme 3.33). Interpretation of the source of ethane in this reaction is complicated by the presence of **11**, but surprisingly, more ethane is formed in this reaction than the reaction **11** with BQ. Pd⁰-BQ complex **13** was not observed. One explanation could be that **13**, in the presence of OAc⁻, is unstable to oxidation by BQ. In fact, in the reaction of **15** with BQ shows 54% BQ converted to HQ suggesting BQ acted as an oxidant in the reaction. Jutand has shown by electrochemical experiments that oxidation addition of an aryl halide to Pd⁰ in cross-coupling reactions could proceed by first forming an anion Pd⁰-X complex (Scheme 3.34).⁴² Likewise, oxidation of Pd⁰ by BQ may be facilitated by the presence of OAc⁻.

Scheme 3.33 Reaction of (^tBu-bpy)Pd(CH₃)OAc (**15**) with BQ.



Scheme 3.34 Proposed Oxidation of ArI to Anionic Pd⁰ Species.

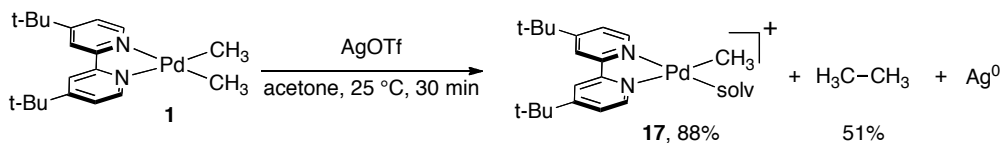


In summary, reaction of **11** with BQ proceeded as expected. Complex **11** disproportionated slowly to **1** and **12** as previously shown, followed by BQ-induced elimination of ethane from **1**. However, mass balance for this reaction was poor (77% Pd, 64% CH₃, and 66% CH₂COCH₃). Gratifyingly, ethane was also formed in the reaction of acetate complex **14** with BQ. Mass balance is excellent in this latter reaction (91% Pd, 93% CH₃, 94% OAc), but the observation of acetyl complexes **11** and (t-Bu-bpy)Pd(CH₂COCH₃)OAc (**16**) derived from solvent activation complicated interpretations of the origin of ethane. Similarly, the lack of Pd⁰-BQ complex **9** is not in agreement with BQ-induced elimination of ethane from **1**. The presence of an 1:1.2 ratio of HQ to BQ suggests BQ is acting as an oxidant in this reaction, reoxidizing Pd⁰ to Pd^{II}, and it was proposed that OAc⁻ facilitated the reoxidation by forming an anionic Pd⁰-OAc complex.

3.2.4 Ag^I-Promoted C-C Bond Formation

Dimethyl palladium complex **1** was reacted with AgOTf in acetone-*d*₆ in a J. Young NMR tube and results of the reaction were analyzed by ¹H NMR spectroscopy. After 0.5 h at 25 °C, ethane (51%) and cationic monomethyl palladium complex (**17**, 88%) were observed along with deposition of metallic Ag⁰ (Scheme 3.35). It should be noted that in this reaction 50% yield of ethane is quantitative, because each metal center contributes only one CH₃ group to the ethane product. Therefore, two equivalents of starting complex are needed to make one equivalent of ethane.

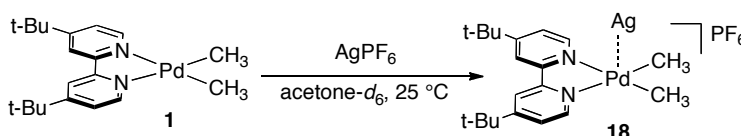
Scheme 3.35 Reaction of Complex **1** with AgOTf.



Subsequently, Dr. Michael Lanci observed the formation of a new species upon the reaction of AgPF₆ with **1** by ¹H NMR spectroscopy at 25 °C after 20 min. This species was postulated to be Pd-Ag adduct **18**, but the complex was too unstable to be

isolated (Scheme 3.36). After 75 min, the reaction was observed to give ethane and 17 Ag⁰ (silver mirror). Further, he reacted dimethyl complex **1** with TlBF₄ to produce a similar species by ¹H NMR spectroscopic analysis that was stable enough to be isolated. X-ray diffraction of a single crystal showed a Pd–Tl sandwich complex (**19**) with two Tl bound to the *dz*² orbitals of three molecules of **1** (Scheme 3.37).⁴³ Selected bond distances and angles are given in Table 3.6.

Scheme 3.36 Postulated Pd–Ag Adduct in the Reaction **1** with AgPF₆.



Scheme 3.37 Molecular Structure of [[(t-Bu-bpy)Pd(CH₃)₂]₃Tl₂](PF₆)₂ (**19**).

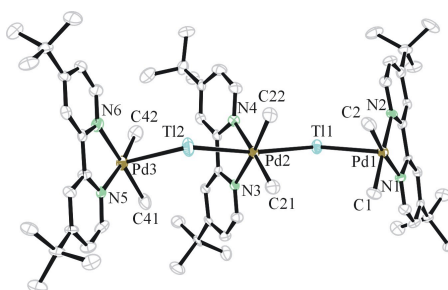


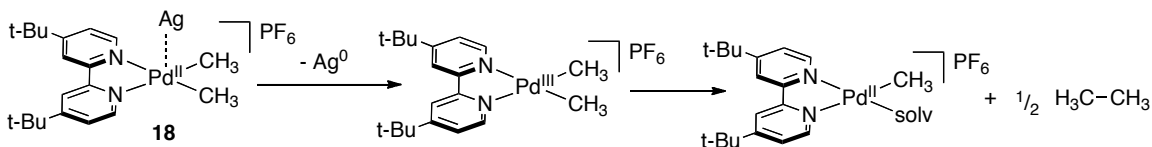
Table 3.6 Selected Bond Distances (Å) and Bond Angles (°) for **19**.

Bond Lengths (Å)		Bond Angles (°)	
Tl1–Pd1	2.7963(9)	Pd1–Tl1–Pd2	132.93
Tl1–Pd2	2.9320(6)	Tl1–Pd2–Tl2	170.92
Tl2–Pd2	2.9942(6)	Pd2–Tl2–Pd3	131.39
Tl2–Pd3	2.8299(7)		

Formation of monomethyl complex **17** suggested that the reactivity of Pd–Ag complex **18** was more complicated than a unimolecular, Lewis acid induced reductive elimination to yield ethane. Deposition of metallic Ag⁰ suggested that Ag^I, upon binding Pd^{II}, was acting as an inner sphere oxidant in this reaction (Scheme 3.38). These results

directly parallel the reaction of phosphine-ligated complex **7** with AgBPh₄ (Scheme 3.8).²⁰

Scheme 3.38 Proposed Inner Sphere Oxidation of Pd^{II} by Ag^I.

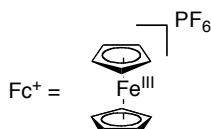


We desired to compare the reactivity of **1** with Ag^I to that reported for (dmpe)Pd(CH₃)₂ (**7**) with Ag^I, where ethane formation was proposed to be the result of oxidative cleavage of the Pd–CH₃ bond. Although Ag⁺ binding to the Pd *dz*² orbital followed by electron transfer was suggested by these studies, further mechanistic analyses proved challenging. The stability of intermediate **18** at low temperatures hindered attempts to observe any subsequent intermediates along the reaction pathway. Therefore in further experiments, we sought to oxidize **1** by one electron via an outer sphere mechanism to circumvent intermediates such as **18** and gain further mechanistic understanding of one-electron oxidation of **1**.

3.2.5 Fc⁺-Promoted C–C Bond Formation

It should be noted at the outset, that all reactions of **1** and one-electron oxidant ferrocenium hexafluorophosphate (Fc⁺) (Scheme 3.39) and related reactions were conducted by Dr. Michael Lanci⁴³ but are included here for the importance of further mechanistic discussion regarding the oxidative oligomerization of methane.

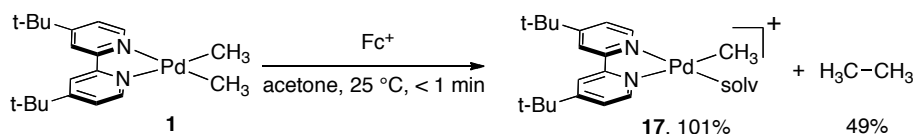
Scheme 3.39 One-Electron Oxidant, Ferrocenium Hexafluorophosphate.



Reaction of an acetone-*d*₆ solution of **1** with a deep blue acetone solution of Fc⁺ resulted in rapid bleaching of the blue color of Fc⁺ on the timescale of diffusion. The

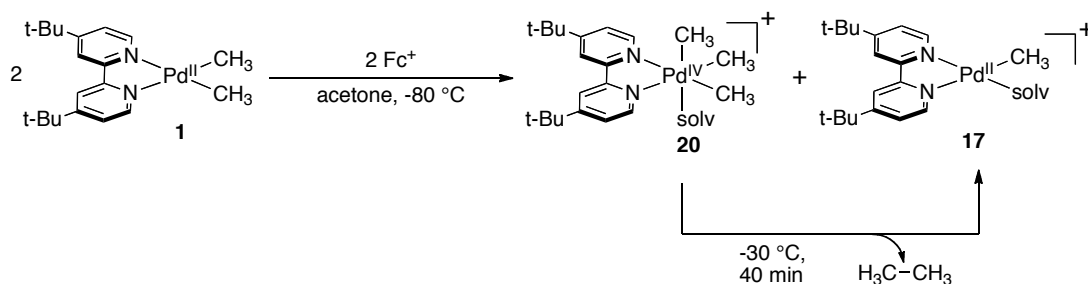
reaction was analyzed by ^1H NMR spectroscopy and showed formation of ethane (49%), cationic monomethyl complex **17** (101%) and ferrocene as the only observable products (Scheme 3.40). These reaction products are directly analogous to those observed in the reaction of **1** with Ag^{I} .

Scheme 3.40 One-Electron Oxidation of **1** to Produce Ethane.

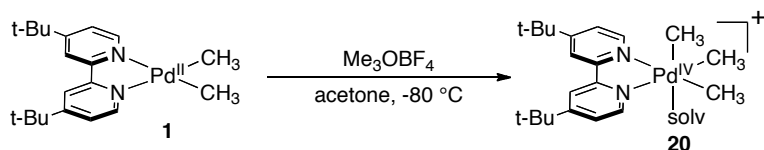


Subsequent reaction of **1** and Fc^+ in a septum-sealed NMR tube at $-80\text{ }^\circ\text{C}$ in the NMR spectrometer resulted in the formation of 0.5 equivalents of $[(\text{t-Bu-bpy})\text{Pd}^{\text{IV}}(\text{CH}_3)_3(\text{solvent})]^+$ (**20**) and 0.5 equivalents of **17**, as observed by ^1H NMR spectroscopy. Upon warming to $-30\text{ }^\circ\text{C}$, Pd^{IV} complex **20** reductively eliminated ethane over 40 min to give an additional 0.5 equivalents of **17** (Scheme 3.41). Independent synthesis of **20** by addition of **1** to an acetone- d_6 solution of Me_3OBF_4 at $-80\text{ }^\circ\text{C}$ verified the identity of **20** (Scheme 3.42).

Scheme 3.41 Formation of a Pd^{IV} -Trimethyl Intermediate Upon One-Electron Oxidation.



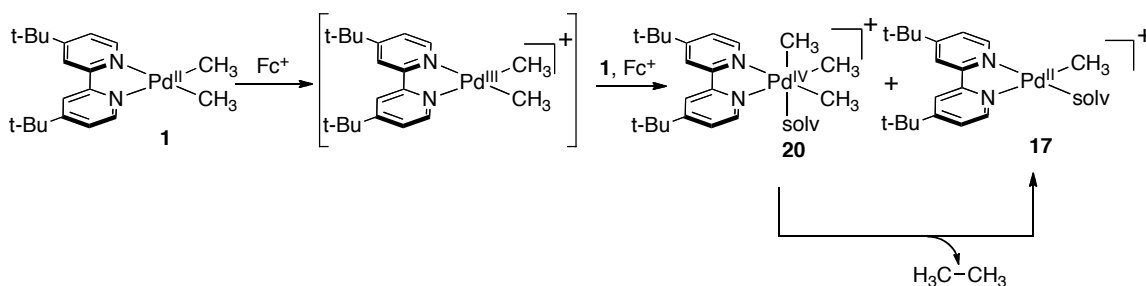
Scheme 3.42 Independent Synthesis of Pd^{IV} Complex **20**.



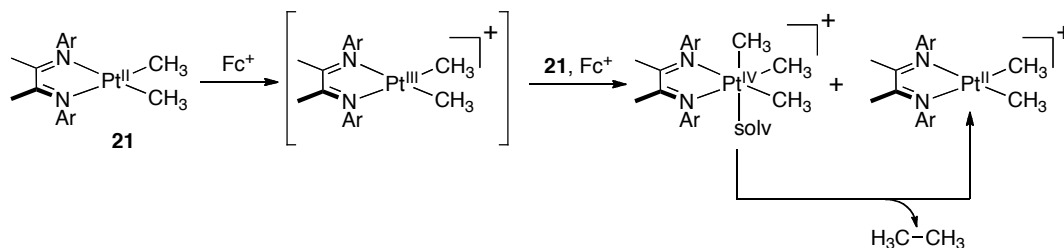
The reaction of **1** with Fc^+ was proposed to proceed through a Pd^{III} intermediate that further reacted with a second equivalent of **1** and Fc^+ to give products **20** and **17**

where a methyl transfer had taken place (Scheme 3.43). Similar reactivity and mechanistic proposals were published by Tilset for the reaction of related (diimine)Pt(CH₃)₂ (**21**) complexes with Fc⁺ (Scheme 3.44).⁴⁴ Subsequent to our work, Mirica published an elegant synthesis of the first isolated mononuclear organometallic Pd^{III} complex (**10**) (Scheme 3.45).³⁰ The reaction models our proposed Pd^{III} well, giving further credence to the participation of a Pd^{III} intermediate in the one-electron oxidation of **1**.

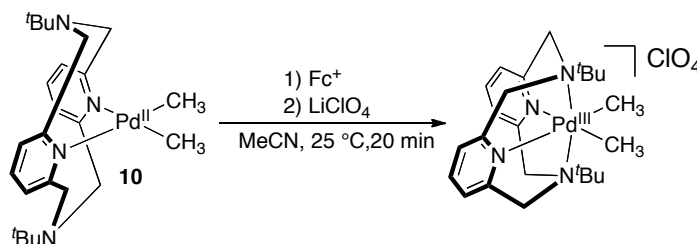
Scheme 3.43 Proposed Mechanism for Generating Complexes **20** and **17** Via One-Electron Oxidation.



Scheme 3.44 One-Electron Oxidation of Dimethyl-platinum Diimine Complexes.⁴⁴



Scheme 3.45 Synthesis of an Isolable Mononuclear Pd^{III} Complex.³⁰



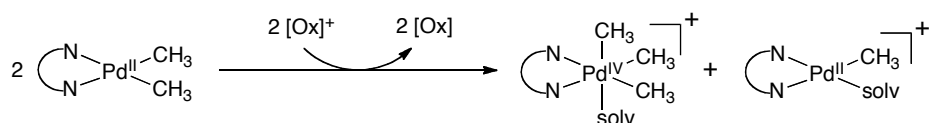
3.3 Conclusions

Reaction of (*t*-Bu-bpy)Pd^{II}(CH₃)₂ (**1**) with BQ or Ag^I each induced elimination of ethane. BQ-promoted reaction of **1** was demonstrated to be a bimolecular process between BQ and **1** resulting in the formation of 89% ethane and Pd⁰ product (*t*-Bu-bpy)Pd(BQ) (**9**, 94%). Complex **1** and Ag^I reacted to form an intermediate proposed to be a Pd^{II}-Ag adduct which further underwent an electron transfer process to generate ethane (51%) and cationic monomethyl complex [(*t*-Bu-bpy)Pd(CH₃)(acetone)]⁺ (**17**, 88%). Further studies with outer sphere, one-electron oxidant, ferrocenium hexafluorophosphate, demonstrated that oxidation of **1** by one electron resulted in an oxidative methyl transfer process to generate [(*t*-Bu-bpy)Pd^{II}(CH₃)(acetone)]⁺ (**17**) and [(*t*-Bu-bpy)Pd^{IV}(CH₃)₃(acetone)]⁺ (**20**) with subsequent elimination of ethane from **20**.

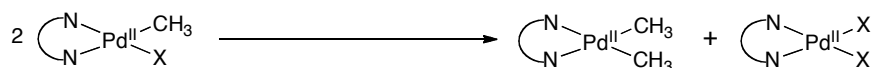
These mechanistic studies fundamentally altered the way in which we thought about accomplishing oxidative oligomerization of methane. Because one-electron oxidation was shown to drive methyl transfer (Path A, Scheme 3.46) it is possible that we could circumvent the need to drive disproportionation between Pd^{II} complexes by thermodynamics of the methyl transfer event (Path B, Scheme 3.47). Thus, one-electron oxidation provides a possible solution to the challenge of methyl disproportionation between metal centers while also inducing subsequent C-C bond formation.

Scheme 3.46 Two Concepts for Facilitating Methyl Transfer Between Pd Complexes.

Path A: Methyl Transfer Driven by Oxidation



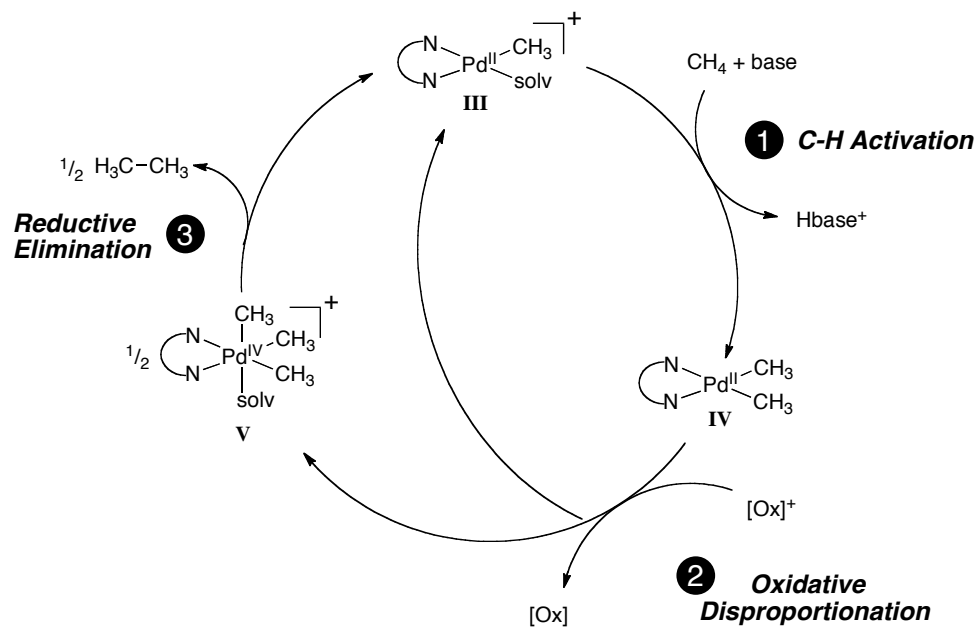
Path B: Methyl Transfer Driven by Thermodynamics



Based on the observed reactivity of **1** with Fc⁺, we proposed a new catalytic cycle for methane oligomerization (Scheme 3.47). In this cycle, a cationic monomethyl complex **III** would perform C-H activation of CH₄ to form a dimethyl complex (**IV**). Complex **IV** can then undergo a one-electron oxidation to generate 0.5 equivalents of **III**

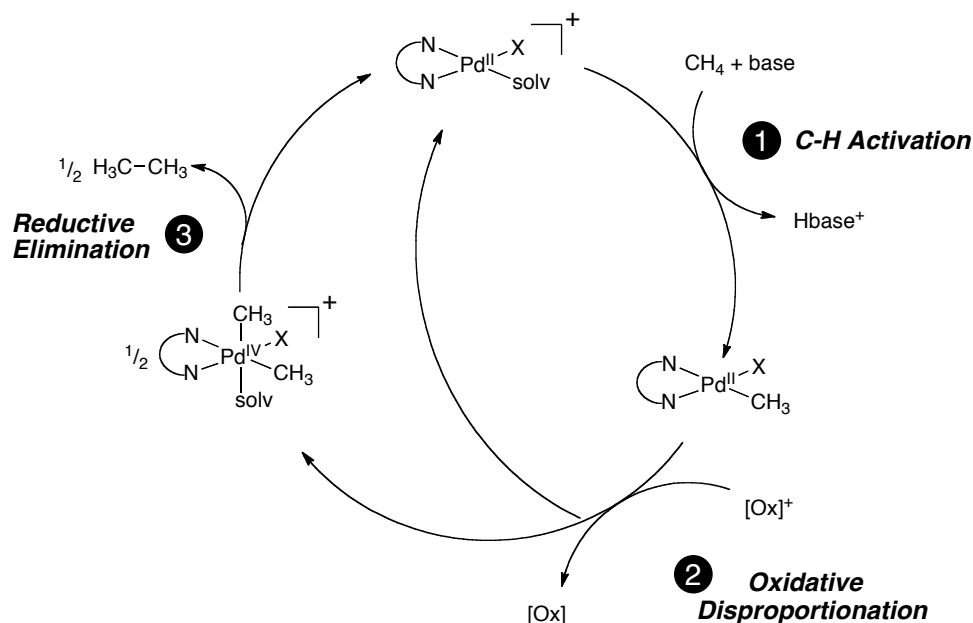
and 0.5 equivalents of Pd^{IV} trimethyl complex **V**. Reductive elimination of ethane from **V** then affords another 0.5 equivalents of **III**.

Scheme 3.47 Proposed Catalytic Cycle For Methane Oligomerization Based on One-Electron Oxidation.



In this proposal, oxidation not only reoxidizes the metal but also provides a driving force for methyl transfer to generate an intermediate that can undergo subsequent elimination of ethane. However, one key challenge in this proposal is development of C–H activation conditions to afford a dimethyl intermediate (see Chapter 2 for a brief discussion of the challenges). Alternatively, the knowledge that one-electron oxidation facilitates methyl transfer could be applied to systems where formation of a dimethyl species is not a prerequisite. If one-electron oxidation of (tBu-bpy)Pd^{II}(CH₃)X induced methyl transfer analogous to the oxidation of **1**, ethane could be effectively produced from a monomethyl starting material (Scheme 3.48). Further discussion of the application of one-electron oxidation of monomethyl species toward oligomerization of methane can be found in Chapter 4.

Scheme 3.48 Concept for One-Electron Oxidation of Monomethyl Pd Complexes.



3.4 Experimental Procedures

3.4.1 Instrumentation

NMR spectra were obtained on a Varian Inova 500 (499.90 MHz for ^1H ; 125.70 MHz for ^{13}C) or a Varian Inova 400 (399.96 MHz for ^1H ; 100.57 MHz for ^{13}C , 376.34 MHz for ^{19}F) spectrometer. ^1H and ^{19}F NMR chemical shifts are reported in parts per million (ppm) relative to TMS with the residual solvent peak used as an internal reference. ^{19}F NMR spectra are referenced on a unified scale, where the single primary reference is the frequency of the residual solvent peak in the ^1H NMR spectrum. Multiplicities are reported as follows: singlet (s), doublet (d), doublet of doublets (dd), and doublet of doublet of doublets (ddd).

3.4.2 Materials and Methods

All manipulations were performed using standard Schlenk or glovebox procedures unless otherwise noted. Acetone and acetone- d_6 (Cambridge Isotopes) were refluxed over calcium sulfate overnight and then distilled, freeze-pump-thaw degassed,

and shaken over 4 Å molecular sieves immediately before use. 1,1,2-Trichloroethane was refluxed over CaH₂ overnight and then distilled, freeze-pump-thaw degassed and stored over 4 Å molecular sieves. All other solvents were purchased from Fisher or EMD and dispensed from an Innovative Technologies solvent purification system equipped with columns packed with activated alumina, copper catalyst, and molecular sieves. 4,4'-Di-*tert*-butyl-2,2'-bipyridine (*t*Bu-bpy) was purchased from Aldrich, silver triflate was purchased from Strem, Na₂PdCl₄ was purchased from Pressure Chemical, and all other materials were used as purchased from Aldrich or Acros. Benzoquinone was sublimed before use.

See Chapter 2 for specific NMR instrumentation settings and particular NMR tubes used in ethane-evolving reactions.

3.4.3 Computational Methods

See Chapter 2 for details on ground state and solvation calculations. Transition states were optimized as saddle points using the Berny algorithm.^{45,46} Transition states were confirmed by visual inspection of the single imaginary frequency. Ground and transition state structures of Pd–BQ complexes were also calculated for unrestricted singlet and triplet electronic states. For geometry optimizations of triplet state structures that produced markedly different geometries from the calculated singlet state structures, single point triplet energies were determined for the singlet state geometry optimized structures. The energies were markedly higher than the geometry optimized triplet structures. Natural bond orbital (NBO)³⁶ analysis of atomic charge was carried on the optimized structures described above.

3.4.4 Syntheses

(*t*Bu-bpy)Pd(CH₃)₂ (**1**) (*t*Bu-bpy = 4,4'-di-*tert*-butyl-bipyridine) and (*t*Bu-bpy)Pd(CH₃)I (**13**) were synthesized following previous published procedures.⁴⁷ The syntheses of (*t*Bu-bpy)Pd(CH₃)OAc (**14**) and (*t*Bu-bpy)Pd(CH₃)(CH₂COCH₃) (**11**) were reported in Chapter 2.

3.4.5 Reaction Details – (^tBu-bpy)Pd(CH₃)₂ + BQ/Ag^I

(^tBu-bpy)Pd(CH₃)₂ (1) + Benzoquinone (BQ) or silver triflate (AgOTf). The palladium complex (3.0 μmol) was weighed into a J. Young NMR tube. Acetone (0.55 mL) was added along with 1,3,5-trimethoxybenzene (internal standard, 15 μL of 48 mM solution in acetone-*d*₆). Benzoquinone (0.1 mL of a 31 mM solution in acetone-*d*₆) or AgOTf (0.1 mL of a 31 mM solution in acetone-*d*₆) was added, and the tube was sealed with a Teflon stopcock. The solutions were protected from light, and initial NMR spectra were recorded. Reactions proceeded at 25 °C and were monitored ¹H NMR spectroscopy.

3.4.6 Reaction Details – (^tBu-bpy)Pd(CH₃)X + BQ

Reaction of Complexes (^tBu-bpy)Pd(CH₃)(CH₂COCH₃) (11), (^tBu-bpy)Pd(CH₃)I (13), (^tBu-bpy)Pd(CH₃)OAc (14), and (^tBu-bpy)Pd(CH₃)OTf (15) with BQ: The palladium complex (3.0 μmol) was weighed into a J. Young NMR tube. Acetone (0.55 mL) was added along with 1,1,2-trichloroethane (internal standard, 15 μL of 215 mM solution in acetone-*d*₆) or 1,3,5-trimethoxybenzene (internal standard, 15 μL of 48 mM solution in acetone-*d*₆). Benzoquinone (0.1 mL of a 31 mM solution in acetone-*d*₆) was added, and the tube was sealed with a Teflon stopcock. The solutions were protected from light, and initial NMR spectra were recorded. The NMR tubes were then exposed to ambient light of two fluorescent bulbs in a hood. After standing for 24 h and 72 h, NMR spectra were recorded to determine yields decomposition products versus the initial spectra.

3.5 References

- (1) Crabtree, R. H. *The Organometallic Chemistry of the Transition Metals* Hoboken: Wiley Interscience, 1995.
- (2) Gillie, A.; Stille, J. K. *J. Am. Chem. Soc.* **1980**, *102*, 4933.
- (3) Hartwig, J. F. *Inorg. Chem.* **2007**, *46*, 1936.
- (4) Yagyu, T.; Hamada, M.; Osakada, K.; Yamamoto, T. *Organometallics* **2001**, *20*, 1087.
- (5) Hull, K. L.; Sanford, M. S. *J. Am. Chem. Soc.* **2009**, *131*, 9651.
- (6) Perez-Rodriguez, M.; Braga, A. A. C.; Garcia-Melchor, M.; Perez-Temprano, M. H.; Casares, J. A.; Ujaque, G.; de Lera, A. R.; Alvarez, R.; Maseras, F.; Espinet, P. *J. Am. Chem. Soc.* **2009**, *131*, 3650.

-
- (7) Hull, K. L.; Sanford, M. S. *J. Am. Chem. Soc.* **2007**, *129*, 11904.
- (8) Chen, X.; Li, J.-J.; Hao, X.-S.; Goodhue, C. E.; Yu, J.-Q. *J. Am. Chem. Soc.* **2006**, *128*, 78.
- (9) Albeniz, A. C.; Espinet, P.; Martin-Ruiz, B. *Chem. Eur. J.* **2001**, *7*, 2481.
- (10) Szabo, K. J. *Organometallics* **1998**, *17*, 1677.
- (11) Backvall, J. E.; Bystrom, S. E.; Nordberg, R. E. *J. Org. Chem.* **1984**, *49*, 4619.
- (12) Temple, J. S.; Riediker, M.; Schwartz, J. *J. Am. Chem. Soc.* **1982**, *104*, 1310.
- (13) Potavathri, S.; Dumas, A. S.; Dwight, T. A.; Naumiec, G. R.; Hammann, J. M.; DeBoef, B. *Tetrahedron Lett.* **2008**, *49*, 4050.
- (14) Chi, S. H.; Hwang, S. J.; Chang, S. *J. Am. Chem. Soc.* **2008**, *130*, 9254.
- (15) Stuart, D. R.; Villemure, E.; Fagnou, K. *J. Am. Chem. Soc.* **2007**, *129*, 12072.
- (16) Chen, X.; Goodhue, C. E.; Yu, J. Q. *J. Am. Chem. Soc.* **2006**, *128*, 12634.
- (17) Takahashi, M.; Masui, K.; Sekiguchi, H.; Kobayashi, N.; Mori, A.; Funahashi, M.; Tamaoki, N. *J. Am. Chem. Soc.* **2006**, *128*, 10930.
- (18) Mei, T.-S.; Wang, X.; Yu, J.-Q. *J. Am. Chem. Soc.* **2009**, *131*, 10806.
- (19) Kraatz, H. B.; van der Boom, M. E.; Ben-David, Y.; Milstein, D. *Isr. J. Chem.* **2001**, *41*, 163.
- (20) Seligson, A. L.; Trogler, W. C.; *J. Am. Chem. Soc.* **1992**, *114*, 7085.
- (21) Owen, J. S.; Labinger, J. A.; Bercaw, J. E. *J. Am. Chem. Soc.* **2006**, *128*, 2005.
- (22) Heiberg, H.; Johansson, L.; Gropen, O.; Ryan, O. B.; Swang, O.; Tilset, M. *J. Am. Chem. Soc.* **2000**, *122*, 10831.
- (23) Periana, R. A.; Taube, D. J.; Gamble, S.; Taube, H.; Satoh, T.; Fujii, H. *Science* **1998**, *280*, 560.
- (24) Remy, M. S.; Cundari, T. R.; Sanford, M. S. *Organometallics* **2010**, *29*, 1522.
- (25) Suzuki, Y.; Yagyu, T.; Osakada, K. *J. Organometallic Chem.* **2007**, *692*, 326.
- (26) Moret, M.-E.; Chen, P. *J. Am. Chem. Soc.* **2009**, *131*, 5675.
- (27) Arsenault, G. L.; Anderson, C. M.; Puddephatt, R. J. *Organometallics* **1988**, *7*, 2094.
- (28) Piera, J.; Bäckvall, J.-E. *Angew. Chem., Int. Ed.* **2008**, *47*, 3506.
- (29) Tsutsui, S.; Sakamoto, K.; Yoshida, H.; Kunai, A. *J. Organometallic Chem.* **2005**, *690*, 1324.
- (30) Khusnutdinova, J. R.; Rath, N. P.; Mirica, L. M. *J. Am. Chem. Soc.* **2010**, *132*, 7303.
- (31) Yamamoto, T.; Abla, M.; Murakami, Y. *Bull. Chem. Soc., Jpn.* **2002**, *75*, 1997.
- (32) Lever, A. B. P. *Coord. Chem. Rev.* **2010**, *254*, 1397.
- (33) Baranovski, V. I.; Sizova, O. V. *Chem. Phys. Lett.* **1999**, *315*, 130.
- (34) Lam, O. P.; Anthon, C.; Heinemann, F. W.; O'Connor, J. M.; Meyer, K. *J. Am. Chem. Soc.* **2008**, *130*, 6567.
- (35) Moussa, J.; Lev, D.; Boubekeur, K.; Rager, M. N.; Amouri, H. *Angew. Chem., Int. Ed.* **2006**, *45*, 3854.
- (36) Foster, J. P.; Weinhold, F. *J. Am. Chem. Soc.* **1980**, *102*, 7211.
- (37) Dewar, M. J. S. *Bull. Soc. Chim. Fr.* **1951**, *18*, C79.
- (38) Chatt, J.; Duncanson, L. A. *J. Chem. Soc.* **1953**, 2929.
- (39) Bobrowski, M.; Liwo, A.; Hirao, K. *J. Phys. Chem. B* **2007**, *111*, 3543.

-
- (40) Li, X.-Y.; Hu, C.-X.; Li, M.-L.; Liu, Z.-G. *Jol. Mol. Struct.* **2004**, *674*, 257.
- (41) Albéniz, A. C.; Espinet, P.; Martín-Ruiz, B. *Chem.–Eur. J.* **2001**, *7*, 2481.
- (42) Amatore, C.; Jutand, A. *Acc. Chem. Res.* **2000**, *33*, 314.
- (43) Lanci, M. P.; Remy, M. S.; Kaminsky, W.; Mayer, J. M.; Sanford, M. S. *J. Am. Chem. Soc.* **2009**, *131*, 15618.
- (44) Johansson, L.; Ryan, O. B.; Romming, C.; Tilset, M. *Organometallics* **1998**, *17*, 3957.
- (45) Reed, A. E.; Weinhold, F. *J. Chem. Phys.* **1983**, *78*, 4066.
- (46) Peng, C.; Ayala, P. Y.; Schlegel, H. B.; Frisch, M. J. *J. Comp. Chem.* **1996**, *17*, 49.
- (47) Byers, P. K.; Canty, A. J.; Jin, H.; Kruis, D.; Markies, B. A.; Boersma, J.; van Koten, G. *Inorg. Synth.*, **1998**, *32*, 162.

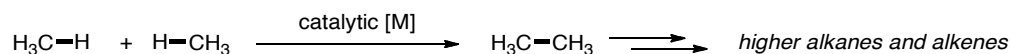
CHAPTER 4

One-Electron Oxidation of Monomethyl Palladium(II) Complexes

4.1 Background and Significance

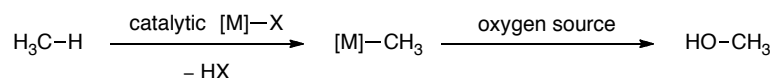
Oxidative oligomerization of methane is fundamentally a process that requires breaking of two C–H bonds and making a new C–C bond (Scheme 4.1). The simplest example of this process is dimerization of methane to produce ethane.

Scheme 4.1 Oligomerization of Methane.

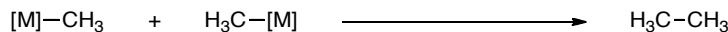


The first fundamental step in oligomerization of methane must be activation of an alkane C–H bond. Many catalysts have been utilized for methane functionalization, and in cases where heterolytic C–H bond cleavage occurs, a monomethyl-metal intermediate is generally proposed.^{1,2} Typically, research efforts have focused on oxygenating the methyl ligand with the oxidant or solvent serving as a source of oxygen (Scheme 4.2).^{2,3}

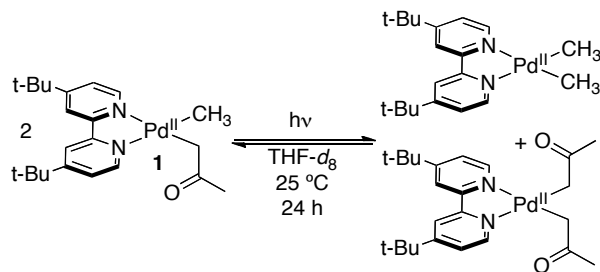
Scheme 4.2 C–H Activation of Methane Followed by Oxygenation.



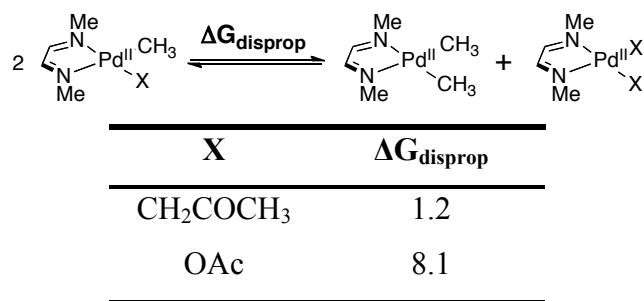
In the oligomerization of methane, the functionalization step requires formation of a new C–C bond (Scheme 4.3). One of the significant challenges of this process is developing a method for generating a new C–C bond from a complex bearing only a single alkyl group. One pathway that would allow this reactivity is a disproportionative alkyl transfer between two alkyl-metal complexes (see Chapter 2 for a more detailed discussion of other possible pathways).

Scheme 4.3 C–C Bond Formation from a Monomethyl-Metal Complex.

Two general methods for disproportionation of methyl ligands have been described: disproportionation driven by thermodynamics and disproportionation driven by one-electron oxidation. Disproportionation driven by thermodynamics, which is typically an endergonic process, has been accomplished by carefully tuning the ligand environment of a monomethyl palladium complex (Scheme 4.4).⁴ (*t*-Bu-bpy)Pd^{II}(CH₃)(CH₂COCH₃) (**1**, *t*-Bu-bpy = 4,4'-ditertbutyl-2,2'-bipyridine) was found to undergo an equilibrium CH₃-for-CH₂COCH₃ metathesis to generate half an equivalent of (*t*-Bu-bpy)Pd^{II}(CH₃)₂. However, this method of disproportionation limits supporting ligands that can be employed in the catalyst. For example, when optimizing Δ*G* of disproportionation (Δ*G*_{disprop}) using density functional calculations, an acetonyl (CH₂COCH₃) ligand minimized Δ*G*_{disprop} for a model palladium system, (MeDAB)Pd^{II}(CH₃)X (Scheme 4.5). Acetate (OAc), which is a common ligand in related aryl homocouplings,^{5–10} provided a Δ*G*_{disprop} value 6.9 kcal/mol higher than CH₂COCH₃.

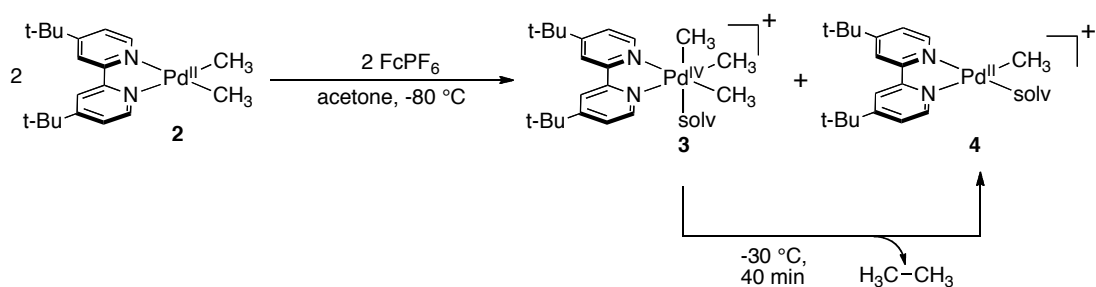
Scheme 4.4 Disproportionation of (*t*-Bu-bpy)Pd^{II}(CH₃)(CH₂COCH₃) (**1**).⁴

Scheme 4.5 Computational Optimization of $\Delta G_{\text{disprop}}$ for (MeDAB)Pd^{II}(CH₃)X.



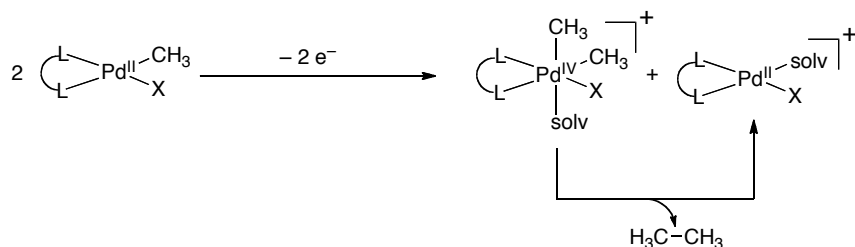
Alternatively, we have shown that the one-electron oxidation of (^tBu-bpy)Pd^{II}(CH₃)₂ (**2**) with ferrocenium hexafluorophosphate (FcPF₆) induces methyl transfer to produce 0.5 equivalents of [(^tBu-bpy)Pd^{IV}(CH₃)₃(acetone)]⁺ (**3**) and 0.5 equivalents of [(^tBu-bpy)Pd^{II}(CH₃)(acetone)]⁺ (**4**) at -80 °C on the timescale of mixing (Scheme 4.6).¹¹ At -30 °C, ethane was eliminated from **3** to produce an additional 0.5 equivalents of **4**. In total, 0.5 equivalents of ethane and 1 equivalent of **4** were generated.

Scheme 4.6 A Palladium(IV) Intermediate in the One-Electron Oxidation of **2**.¹¹



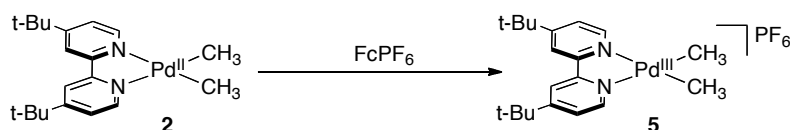
Only one CH₃ group from **2** participated in generating ethane. This result suggested one-electron oxidation of complexes of the general formula (^tBu-bpy)Pd^{II}(CH₃)X could similarly afford ethane via methyl transfer. Development of such chemistry would enable monomethyl complexes, derived from activation of methane, to transfer a methyl group, forming a reactive intermediate from which C–C bond formation could occur (Scheme 4.7). Further, such a reaction could allow greater flexibility in the X-type ligands compared to disproportionation driven by thermodynamics.

Scheme 4.7 One-Electron Oxidation of (*t*Bu-bpy)Pd^{II}(CH₃)X.

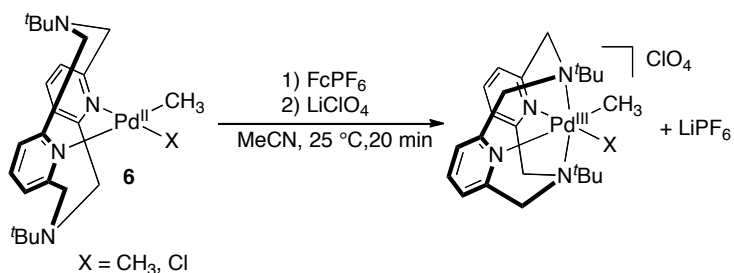


Mirica provided preliminary evidence that one-electron oxidation could generate the desired reactivity. The reaction of **2** with FcPF₆, the reaction was proposed to proceed via an initial one-electron oxidation of **2** to generate palladium(III) complex **5** (Scheme 4.8).¹¹ Mirica demonstrated that one-electron oxidation of (N₄)Pd^{II}(CH₃)X (**6**, X = CH₃, Cl) produced isolable Pd^{III} organometallic complexes (Scheme 4.9).¹² In this reaction, the presence of pendent coordinating amines stabilized the Pd^{III} oxidation state, presumably hindering subsequent methyl transfer.

Scheme 4.8 Proposed Palladium(III) in the One-Electron Oxidation of **2**.



Scheme 4.9 Isolable Palladium(III)-Methyl Complexes.¹²

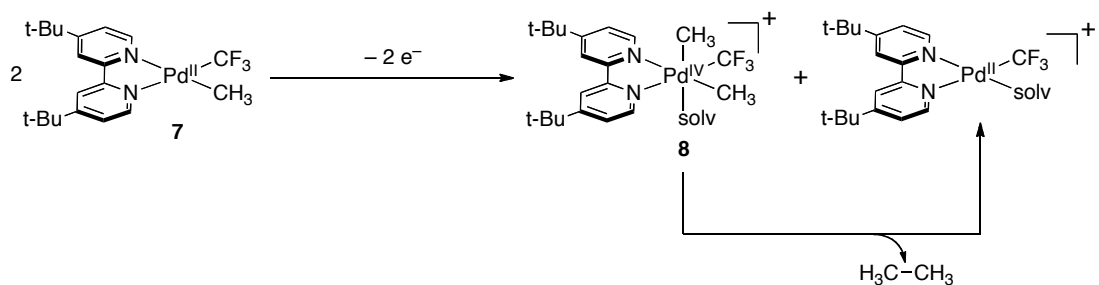


4.2 Results and Discussion

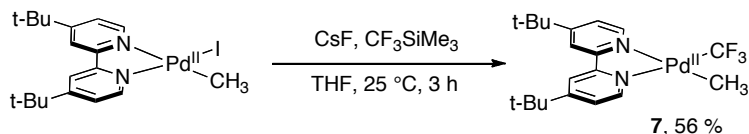
Palladium complexes of *t*Bu-bpy (*t*Bu-bpy = 4,4'-ditertbutyl-2,2'-bipyridine) have served as good models for studies of disproportionation and one-electron oxidatively-induced methyl transfer from starting dimethyl complex (*t*Bu-bpy)Pd^{II}(CH₃)₂ (**2**).^{4,11} In an attempt to achieve analogous methyl transfer reactivity with a monomethyl palladium

complex we sought to only minimally perturb the system. Monomethyl complex (*t*-Bu-bpy)Pd^{II}(CH₃)(CF₃) (**7**) was identified as a target monomethyl complex that met this criterion (Scheme 4.10). Replacing one CH₃ with CF₃ maintained the same N,N,C,C coordination sphere as **2**. Further, efficient C–CF₃ bond formation is an ongoing challenge in organometallic catalysis.^{13–15} If [(*t*-Bu-bpy)Pd^{II}(CH₃)₂(CF₃)(solvent)]⁺ (**8**) was formed by analogy to the one-electron oxidation of **2**, we expected C–CH₃ bond formation to outcompete C–CF₃ bond formation. Using Grushin’s method for synthesis of (L₂)Pd^{II}(Ar)(CF₃) complexes,¹⁶ (*t*-Bu-bpy)Pd^{II}(CH₃)I was reacted with cesium fluoride and Ruppert’s reagent (CF₃Si(CH₃)₃) in THF to provide **7** (Scheme 4.11).

Scheme 4.10 Proposed One-Electron Oxidation of (*t*-Bu-bpy)Pd^{II}(CH₃)(CF₃) (**7**).



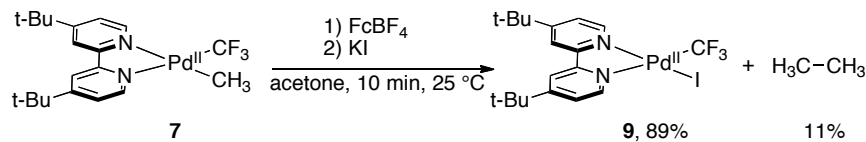
Scheme 4.11 Synthesis of (*t*-Bu-bpy)Pd^{II}(CH₃)(CF₃) (**7**).



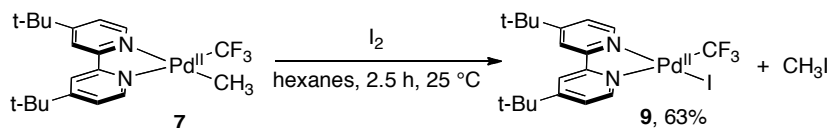
One-electron oxidation of **7** was carried out by reaction of this complex with ferrocenium tetrafluoroborate (FcBF₄) in acetone-*d*₆ in a J. Young NMR tube at room temperature (Scheme 4.12). This reaction required 10 min whereas reaction of **2** with FcBF₄ occurred within the time of mixing. ¹H NMR spectroscopic analysis indicated ethane (11%) and an asymmetric (*t*-Bu-bpy)Pd^{II} complex were formed as products. The asymmetric complex was consistent with [(*t*-Bu-bpy)Pd^{II}(CF₃)(acetone)]BF₄ by ¹H and ¹⁹F NMR analysis. This is analogous to the product **4** that is formed in the one-electron oxidation of **2**. Addition of NaI to the reaction solution produced (*t*-Bu-bpy)Pd^{II}(CF₃)I (89 %, **9**), which matched an independently prepared sample of **9** (Scheme 4.13).¹⁷ It is important to note that two equivalents of starting complex are required to form one

equivalent of ethane in these reactions. This limits the maximum yield of ethane to 50% relative to the number of moles of starting palladium complex.

Scheme 4.12 One-Electron Oxidation of (*t*-Bu-bpy)Pd^{II}(CH₃)(CF₃) (**7**).



Scheme 4.13 Preparation of (*t*-Bu-bpy)Pd^{II}(CF₃)I (**9**).



In comparing the qualitative rates of oxidation of **2** and **7** by FcBF₄, it was assumed that the higher oxidation potential for **7** provided a less favorable equilibrium oxidation of **7** compared to **2**. Studies of CF₃ versus CH₃ substitution of Ni–R and Cu–R complexes have indicated that the M–CF₃ oxidation potentials are approximately 0.6 V higher than the corresponding M–CH₃ analogues (Scheme 4.14).¹⁸

Scheme 4.14 Effect of CH₃ versus CF₃ Substitution on Oxidation Potential.¹⁸

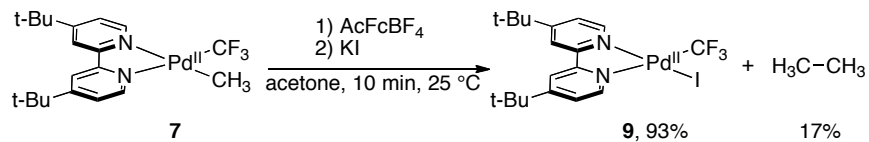
R	E ^o (V)	Solvent
CH ₃	0.65	THF
Cl	1.04	CH ₂ Cl ₂

R	E ^o (V)	Solvent
CH ₃	-0.17	THF
Cl	0.55	CH ₂ Cl ₂

To counteract this unfavorable change in oxidation potential, we next used the stronger ferrocene-based oxidant acetylferrocenium tetrafluoroborate (AcFcBF₄, E^o = 0.27 V versus Fc/Fc⁺) in place of FcBF₄ (E^o = 0 V).¹⁹ Treatment of **7** with AcFcBF₄ resulted in complete reaction within the time of mixing (Scheme 4.15). ¹H NMR analysis

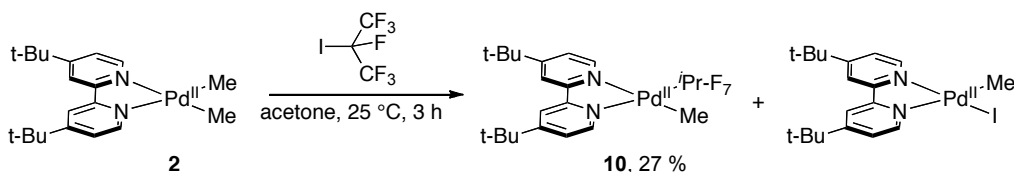
indicated both ethane (17 %) and **9** (93 %) were formed in higher yields than reaction of **7** with FcBF₄.

Scheme 4.15 Oxidation of (*t*-Bu-bpy)Pd^{II}(CH₃)(CF₃) (**7**) with AcFcBF₄.



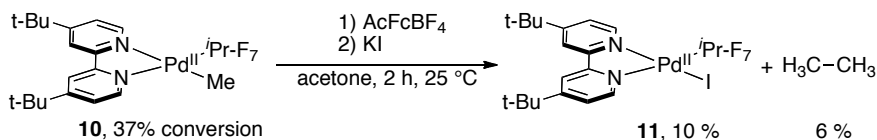
The effect of larger pefluoralkyl groups was also studied. Heptafluoroisopropyl (*i*-Pr-F₇) complex (*t*-Bu-bpy)Pd^{II}(CH₃)(*i*-Pr-F₇) (**10**) was synthesized by reaction of (*t*-Bu-bpy)Pd^{II}(CH₃)₂ with *i*-Pr-F₇-I (Scheme 5.16). The reaction produced **10** along with minor amounts of (*t*-Bu-bpy)Pd^{II}(CH₃)I (formed by oxidative addition of the CH₃I byproduct to the starting material **2**).

Scheme 4.16 Synthesis of (*t*-Bu-bpy)Pd^{II}(CH₃)(*i*-Pr-F₇) (**10**).



One-electron oxidation of **10** with AcFcBF₄ at room temperature in acetone-*d*₆ produced ethane (6%) and (*t*-Bu-bpy)Pd^{II}(*i*-Pr-F₇)I (**11**, 10%) at 37% conversion of **10** after 2 h (Scheme 4.17).

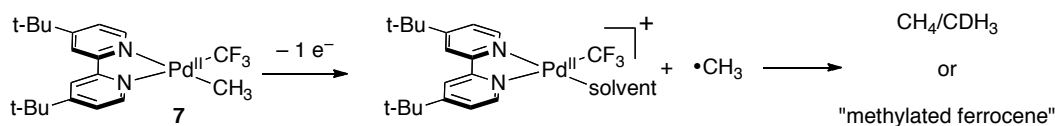
Scheme 4.17 Oxidation of (*t*-Bu-bpy)Pd^{II}(CH₃)(*i*-Pr-F₇) (**10**) with AcFcBF₄.



It is unclear where the CH₃ group balance is in the reactions of **7** and **10** with one-electron oxidants. In the reaction of **7** with AcFcBF₄, only 34% of the Pd-CH₃ groups are accounted for based on the yield of ethane. The high yield of [(*t*-Bu-bpy)Pd^{II}(CF₃)(acetone)]⁺ (93%) and lack of detectable CF₃-containing organics suggests C-CF₃ bond formation is not occurring. Oxidative cleavage of the Pd-CH₃ bond to

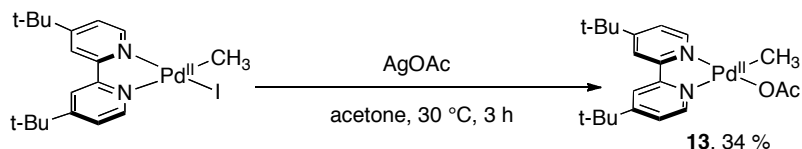
afford methane or methylated ferrocene is another possible path for loss of CH₃ (Scheme 4.18).²⁰ However, methane isotopologues CH₄ and CDH₃ were not observed, and the peaks of the iron(II) product acetyl ferrocene are clearly observed without appearance of methylated ferrocene.

Scheme 4.18 Oxidative Cleavage of the Pd–CH₃ Bond in (t-Bu-bpy)Pd^{II}(CH₃)(CF₃) (**7**).

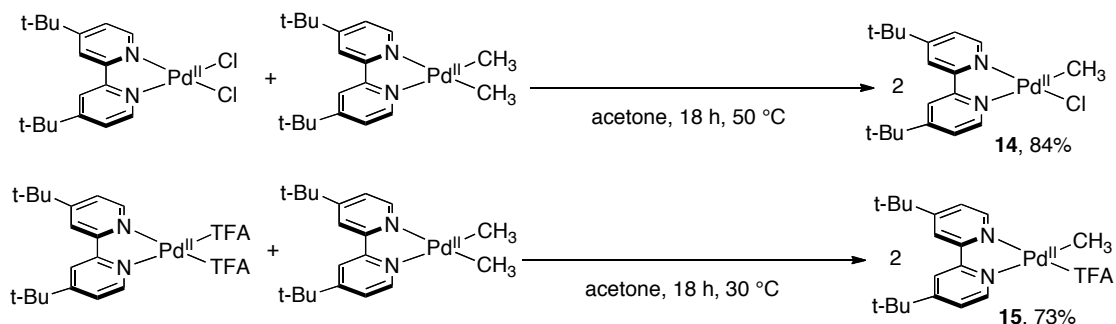


In order to pursue these results further and explore the generality of this one-electron oxidation, complexes of the general formula (t-Bu-bpy)Pd^{II}(CH₃)X were synthesized and reacted with AcFcBF₄. Syntheses of the complexes was accomplished either via reaction of (t-Bu-bpy)Pd^{II}(CH₃)I (**12**) with an appropriate AgX salt (Method 1, Scheme 4.19) or comproportionation of (t-Bu-bpy)Pd(CH₃)₂ and (t-Bu-bpy)Pd^{II}(X)₂ (Method 2, Scheme 4.20). (t-Bu-bpy)Pd^{II}(CH₃)OAc (**13**, OAc = acetate) was prepared in 34% yield by Method 1, and (t-Bu-bpy)Pd^{II}(CH₃)Cl (**14**, 84%) and (t-Bu-bpy)Pd^{II}(CH₃)TFA (**15**, 73%, TFA = trifluoroacetate) were prepared by Method 2.

Scheme 4.19 Synthesis of (t-Bu-bpy)Pd^{II}(CH₃)OAc (**13**) by Method 1.

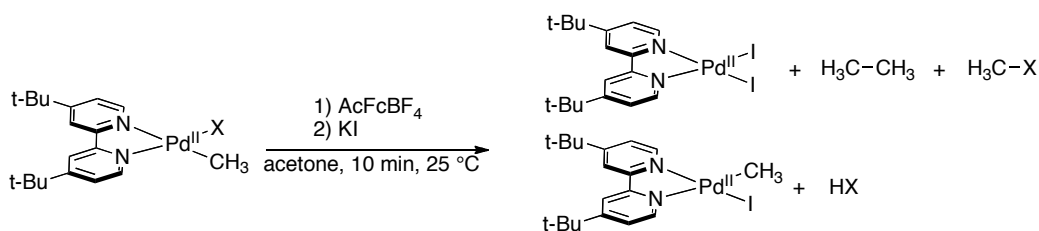


Scheme 4.20 Synthesis of (t-Bu-bpy)Pd^{II}(CH₃)X via Comproportionation (Method 2).



Oxidations of (*t*-Bu-bpy)Pd^{II}(CH₃)X complexes with AcFcBF₄ were performed under identical conditions to the reaction of **7** with AcFcBF₄ (Table 4.1). Strikingly, in all cases, except X = I, ethane was the major organic product with C–X bond formation occurring in <5% yield in all other cases (Scheme 4.21). The reaction of **13** is especially notable, with 70% of the starting methyl group being accounted for as the desired ethane product while H₃C–OAc was not observed.

Table 4.1 One-Electron Oxidation of (*t*-Bu-bpy)Pd^{II}(CH₃)X.

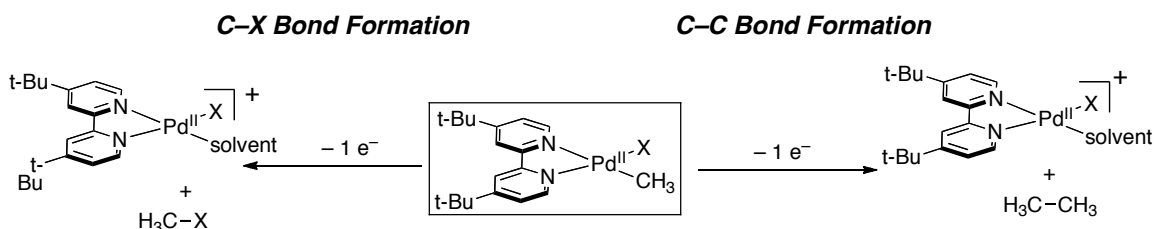


Compound	X	C ₂ H ₆	CH ₃ X	(N ₂)Pd ^{II} (CH ₃)(I)	(N ₂)Pd ^{II} (I) ₂	HX	<i>t</i> -Bu-bpy
7	CF ₃	17	0	0	93 ^a	0	0
12	I	11	28	17 ^b	77	-	0
13	OAc	35	0	22	53	25	0
14	Cl	15	< 5	36	67	-	0
15	TFA	19	0	12	57	-	16

^a observed as (*t*-Bu-bpy)Pd^{II}(CF₃)I (**9**)

^b (*t*-Bu-bpy)Pd^{II}(CH₃)I (**12**) was not present before addition of I

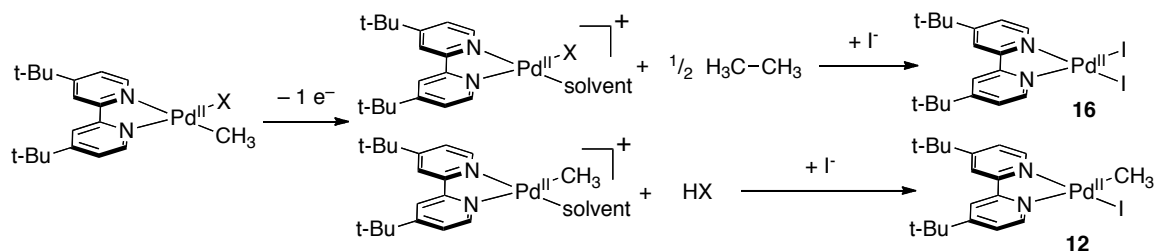
Scheme 4.21 C–C versus C–X Bond Formation.



The identities of the inorganic products in reactions of (*t*-Bu-bpy)Pd^{II}(CH₃)X (X = I, Cl, TFA) with AcFcBF₄ were largely uninterpretable based on ¹H NMR analysis of the crude reaction mixtures. Resonances for the inorganic products were significantly broadened, presumably due to ligand exchange reactions of the cationic products occurring on the timescale of the NMR experiments. Addition of NaI (4 equivalents) to

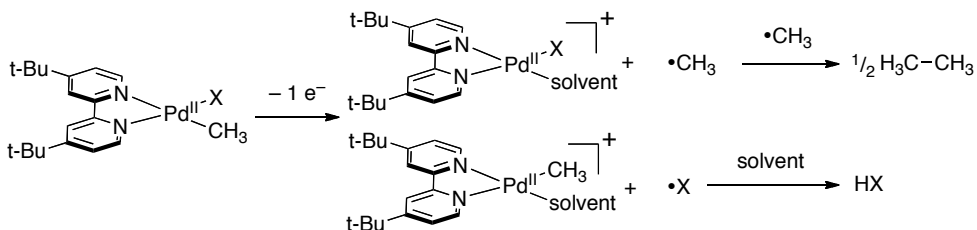
these solutions converted the inorganic products to $(t\text{-Bu-bpy})\text{Pd}^{\text{II}}(\text{I})_2$ (**16**) and $(t\text{-Bu-bpy})\text{Pd}^{\text{II}}(\text{CH}_3)\text{I}$ (**12**). Yields of **16** were interpreted as yields of $[(t\text{-Bu-bpy})\text{Pd}^{\text{II}}(\text{X})(\text{solvent})]^+$ for the crude reaction (Scheme 4.22). Similarly, the yield of **12** was associated with $[(t\text{-Bu-bpy})\text{Pd}^{\text{II}}(\text{CH}_3)(\text{solvent})]^+$. To explain the origin of the inorganic products and the preference for C–C bond formation, two general classes of reaction were considered: reactions involving oxidative cleavage of palladium–ligand bonds (Path 1, Scheme 4.23) or reactions involving methyl group transfer (Path 2, Scheme 4.23).

Scheme 4.22 Addition of I[−] to Inorganic Products of One-Electron Oxidation.

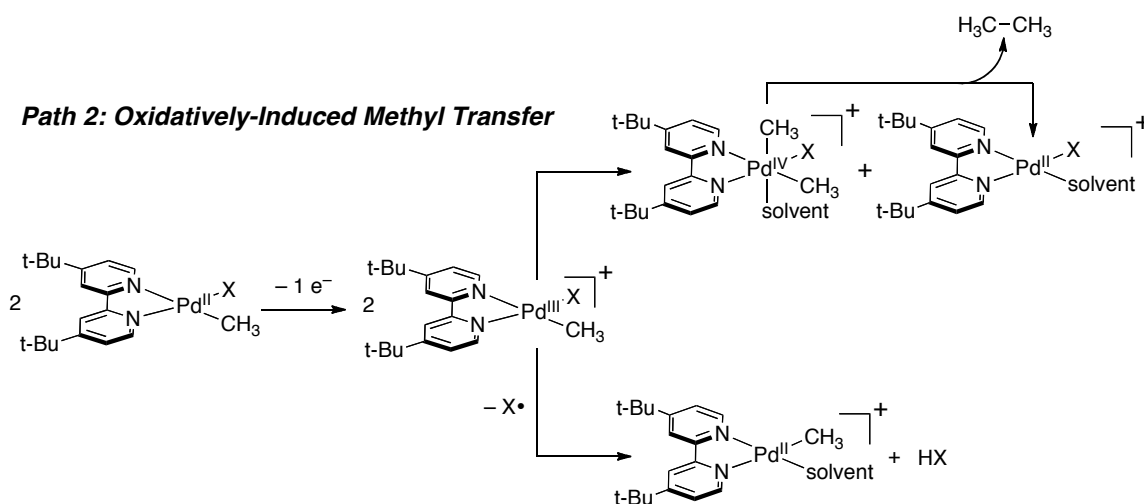


Scheme 4.23 Proposed Pathways for Generating Observed Products Upon One-Electron Oxidation.

Path 1: Oxidatively-Induced Pd–R or Pd–CH₃ Bond Cleavage



Path 2: Oxidatively-Induced Methyl Transfer

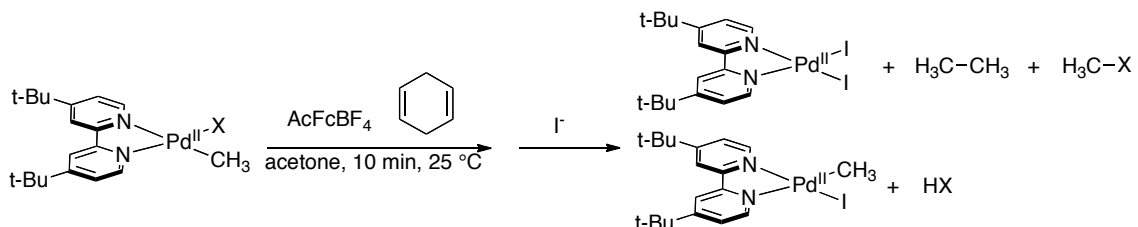


A mechanism involving oxidative cleavage of the Pd–C or Pd–X bond of (^tBu-bpy)Pd(CH₃)X results from AcFcBF₄ inducing homolytic cleavage of either the Pd–C or the Pd–X bond (Scheme 4.23, Path 1).²⁰ Doing so affords either [(^tBu-bpy)Pd^{II}(X)(solvent)]⁺ and CH₃• or [(^tBu-bpy)Pd(CH₃)(solvent)]⁺ and X•. The radical product could then dimerize with another radical, react with a nearby Pd–X or Pd–C bond, or abstract deuterium from solvent. Reaction by this pathway should provide methane in addition to ethane. However methane is not observed in any of these reactions.

To probe the presence of radicals, complexes **7** and **12–14** were reacted with AcFcBF₄ in the presence of 1,4-cyclohexadiene (CHD) (Scheme 4.24). CHD is an H atom donor known to react with methyl radicals at a rate of 1.3 x 10⁵ in acetone. A detailed analysis of similar reaction conditions for the reaction of **2** with FcPF₆ in the

presence of CHD indicated a CH₄:C₂H₆ ratio of >4:1 should be obtained if the reaction proceeded through a radical manifold.¹¹ The yields of ethane with CHD differed by no more than ± 6% from the reactions without CHD. No methane was observed.

Scheme 4.24 Oxidation of (*t*Bu-bpy)Pd^{II}(CH₃)X in the Presence of 1,4-Cyclohexadiene.



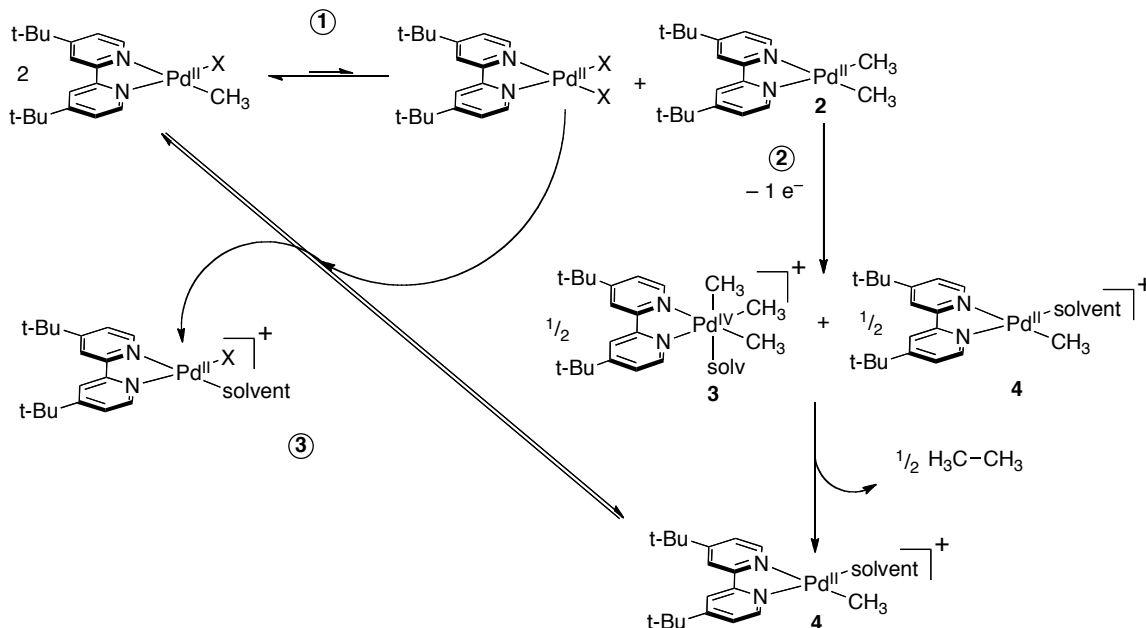
The one-electron oxidations of monomethyl complexes in the presence of CHD and lack of methane suggest that ethane and cationic complex [(*t*Bu-bpy)Pd^{II}(X)(solvent)]⁺ are not formed as the result of oxidative Pd–C bond cleavage. These studies do not rule out oxidative cleavage of the Pd–X bond leading to the generation of [(*t*Bu-bpy)Pd^{II}(CH₃)(solvent)]⁺ and HX.

The second class of reaction mechanism (Scheme 4.23, Path 2) concerned oxidatively-induced transfer of a methyl group. Mechanistic hypotheses for this class of reaction were inspired by our previous observations of disproportionation of (*t*Bu-bpy)Pd^{II}(CH₃)X complexes (Chapter 2)⁴ and one-electron oxidation of (*t*Bu-bpy)Pd^{II}(CH₃)₂ (Chapter 3).¹¹ The mechanistic descriptions presented next are idealized to explain ethane and [(*t*Bu-bpy)Pd^{II}(X)(solvent)]⁺ formation. Further discussion of the origin of [(*t*Bu-bpy)Pd^{II}(CH₃)(solvent)]⁺ and HX as reaction products will be addressed in the detailed study of **13** with AcFcBF₄.

In Mechanism A (Scheme 4.25), equilibrium disproportionation of two equivalents of (*t*Bu-bpy)Pd^{II}(CH₃)X yields one equivalent of (*t*Bu-bpy)Pd^{II}(CH₃)₂ (**2**) and one equivalent of (*t*Bu-bpy)Pd^{II}(X)₂ (Step 1). One-electron oxidation of **2** yields palladium(IV) complex **3** and [(*t*Bu-bpy)Pd^{II}(CH₃)(solvent)]⁺ (**4**) with subsequent elimination of ethane from **3** (Step 2). A ligand exchange equilibrium then occurs between **4** and (*t*Bu-bpy)Pd^{II}(X)₂ to generate [(*t*Bu-bpy)Pd^{II}(X)(solvent)]⁺ and (*t*Bu-bpy)Pd^{II}(CH₃)X (Step 3). Further one-electron oxidations of (*t*Bu-bpy)Pd^{II}(CH₃)X could

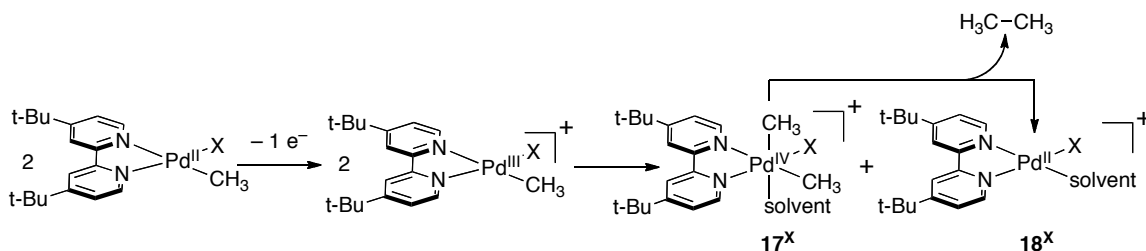
proceed until all CH₃ groups were consumed, resulting in production of 1 equivalent of [(^tBu-bpy)Pd^{II}(X)(solvent)]⁺ and 50% ethane relative to the starting palladium complex.

Scheme 4.25 Path 2, Mechanism A: Disproportionation Followed by Oxidation.



Mechanism B (Scheme 4.26) is directly analogous to one-electron oxidation of (^tBu-bpy)Pd^{II}(CH₃)₂ (2). In this mechanism, one-electron oxidation of (^tBu-bpy)Pd^{II}(CH₃)X promotes an oxidative methyl transfer generating 0.5 equivalents of [(^tBu-bpy)Pd^{IV}(CH₃)₂X(solvent)]⁺ (17^X) and 0.5 equivalents of [(^tBu-bpy)Pd^{II}X(solvent)]⁺ (18^X). Complex 17^X eliminates ethane generating another 0.5 equivalents of 18^X. The reaction should yield a total of one equivalent 18^X and 50% ethane relative to the starting palladium complex.

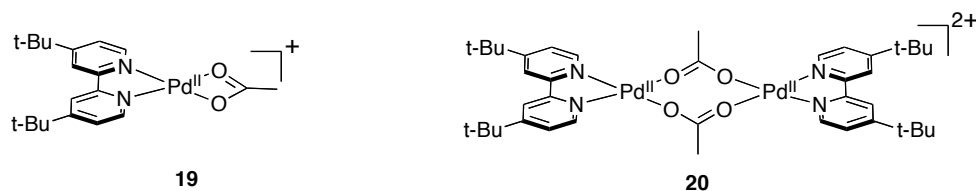
Scheme 4.26 Path 2, Mechanism B: Oxidatively-Induced Methyl Transfer.



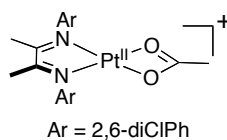
Because of the high yields of ethane and inorganic products in the one-electron oxidation of (*t*-Bu-bpy)Pd^{II}(CH₃)OAc (**13**) and the stability of the inorganic product prior to trapping with I⁻, **13** was selected as an ideal candidate for further mechanistic study. At room temperature, the reaction of **13** with AcFcBF₄ produced two complexes, a symmetric “[(*t*-Bu-bpy)Pd^{II}(OAc)]⁺” species (53% yield) and the unsymmetrical compound [(*t*-Bu-bpy)Pd^{II}(CH₃)(solvent)]⁺ (22% yield). Notably, [(*t*-Bu-bpy)Pd^{II}(CH₃)(solvent)]⁺ was formed in commensurate yield (22%) to acetic acid (25%). The yields of products suggest “[(*t*-Bu-bpy)Pd(OAc)]⁺” is formed upon ethane elimination, and [(*t*-Bu-bpy)Pd(CH₃)(solvent)]⁺ is formed upon HOAc elimination.

Based on the data collected, it was not possible to definitively assign the “[(*t*-Bu-bpy)Pd^{II}(OAc)]⁺” product as [(*t*-Bu-bpy)Pd^{II}(κ-O,O-OAc)]⁺ (**19**) or acetate-bridged dimer [(*t*-Bu-bpy)Pd^{II}(μ-OAc)]₂²⁺ (**20**, Scheme 4.27). In studies of (diimine)platinum-acetate complexes, Chen identified the monomeric κ-O,O-OAc as the favored structure (Scheme 4.28).²¹ Bis-carbene-palladium-acetate complexes were found to be fluxional between dimeric and monomeric forms by ¹H NMR but dimeric in the solid state (Scheme 4.29).²² Based on these precedents and the characterization achieved so far, it is not possible to confirm the identify of the monoacetate product in the reaction of **13** with AcFcBF₄ as **19** or **20**, but for ease of discussion, the monoacetate product will be referred to as the monomeric structure **19**.

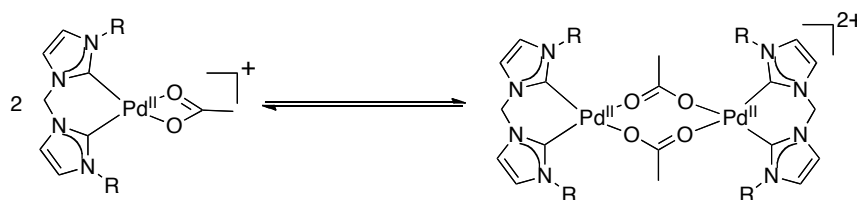
Scheme 4.27 Monomeric versus Dimeric Monoacetate Palladium(II) Structures.



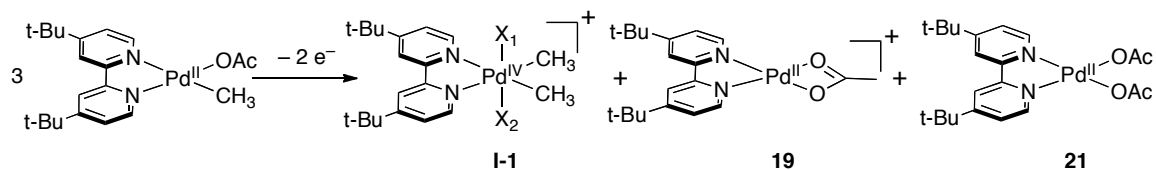
Scheme 4.28 Monomeric Platinum-Monoacetate Complex.²¹



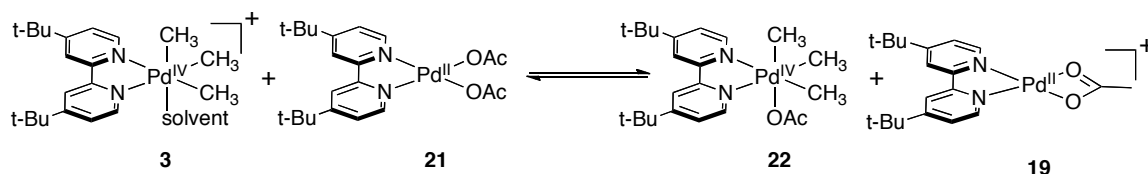
Scheme 4.29 Equilibrium of Monomeric and Dimeric Palladium Monoacetate Complexes.²²



If oxidation of **13** occurred by a methyl transfer mechanism (path 2), intermediate, high-valent palladium complexes should be formed.¹¹ As depicted in Mechanism A, oxidatively-induced methyl transfer should give one of two scenarios: Mechanism A₁, a 1:1:1 ratio of [(^tBu-bpy)Pd^{IV}(CH₃)₃(solvent)]⁺ (**3**), **19**, and (^tBu-bpy)Pd^{II}(OAc)₂ (**21**, entry 1, Table 4.2), or Mechanism A₂ a 1:2 ratio of (^tBu-bpy)Pd^{IV}(CH₃)₃OAc (**22**) and **19** (entry 2, Table 4.2). The preference between Mechanisms A₁ and A₂ would be determined by the equilibrium of acetate transfer between **3** and **21** (Scheme 4.30). Mechanism B should produce a 1:1 ratio of [(^tBu-bpy)Pd^{IV}(CH₃)₂OAc(solvent)]⁺ (**17**^{OAc}) and **19** (entry 3, Table 4.2). The mechanisms should be distinguished by formation of either a trimethyl-palladium(IV) (Mechanism A) or a dimethyl-palladium(IV) (Mechanism B) and the ratios of inorganic products produced upon one-electron oxidation.

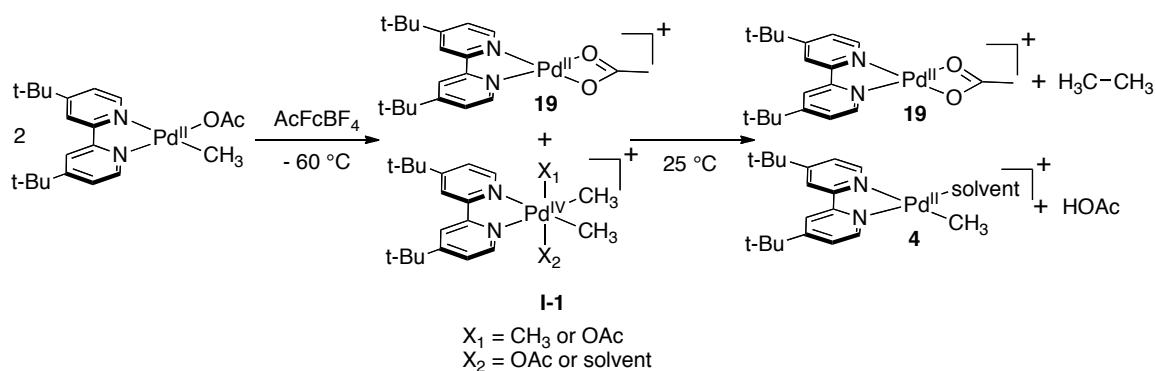
Table 4.2 Proposed Palladium(IV) Intermediates in Path 2 Mechanism.

Entry	I-X	Ratio I-X : 19 : 21	Suggested Mechanism
1	X ₁ = CH ₃ , X ₂ = solvent	1:1:1	Mechanism A ₁
2	X ₁ = CH ₃ , X ₂ = OAc	1:2:0	Mechanism A ₂
3	X ₁ = OAc, X ₂ = solvent	1:1:0	Mechanism B

Scheme 4.30 Acetate Transfer Equilibrium between **3** and **21**.

To probe for these intermediates, the reaction of **13** was carried out at low temperature in an NMR spectrometer, and the reactions were analyzed by ¹H NMR spectroscopy. Oxidation of **13** with AcFcBF₄ at -80 °C in acetone-*d*₆ produced an uninterpretable, broad spectrum. Increasing the temperature to -60 °C, gave a sharpened NMR spectrum, revealing ethane, [(*t*-Bu-bpy)Pd(CH₃)(acetone)]BF₄ (**4**), and a second Pd-CH₃ resonance (**I-1**, 0.69 ppm), which slowly decayed by 15%, while yielding 29% more ethane over 40 minutes at -60 °C (Scheme 4.31). Cationic Pd-OAc species **19** was also observed in the initial NMR spectrum and grew in by 23% over 40 minutes at -60 °C. A complex set of aromatic and aliphatic resonances precluded definitive assignment of a mechanism based on product ratio and also prohibited confirmation of the presence or absence of (*t*-Bu-bpy)Pd^{II}(OAc)₂ (**21**). No starting complex **13** was observed. Upon warming to room temperature, the ¹H NMR spectrum simplified to a typical mixture of ethane, acetic acid, **19**, and **4**.

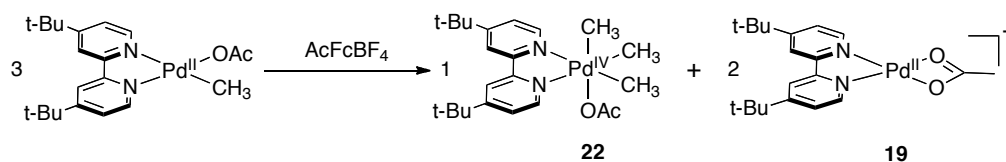
Scheme 4.31 Low Temperature Observation of Intermediates in Oxidation of **13**.



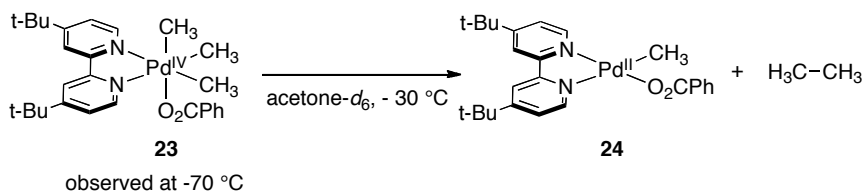
As noted above, the presence of a trimethyl-palladium(IV) would be indicative of Mechanism A versus Mechanism B where a dimethyl-palladium(IV) should be observed. The observation of a single methyl resonance for **I-1** suggests one of three scenarios: 1) a symmetric dimethyl complex was formed (entry 3, Table 4.2), 2) a trimethyl complex was formed and the axial and equatorial methyl resonances exchange on the NMR timescale (entries 1 or 2, Table 4.2), or 3) a trimethyl complex was formed and the second methyl resonance was obscured by a congested ^tBu region of the spectrum (entries 1 or 2, Table 4.2). Of the trimethyl-palladium intermediates proposed, dynamic methyl exchange is most expected for **3**. However, complex **3** has been reported in the literature, and at -60 °C in acetone-*d*₆ the axial and equatorial Pd-CH₃ resonances are observed as distinct resonances. In the reaction of **13** with AcFcBF₄, the reported diagnostic Pd-CH₃ resonances for **3** are not observed, ruling out Mechanism A₁.¹¹

For Mechanism A₂, (*t*Bu-bpy)Pd^{II}(CH₃)₃OAc (**22**) is the expected palladium(IV) intermediate (Scheme 4.32). The benzoate analogue of **22** is known, and its ¹H NMR spectrum has been reported in acetone-*d*₆ (Scheme 4.33).²³ The Pd-CH₃ resonances were reported at 1.69 ppm for equatorial methyls and 0.61 ppm for the axial methyl of complex **23** at -70 °C. The equatorial resonances of **22** are shifted 0.08 ppm from the single observed Pd-CH₃ resonance (0.69 ppm) observed on reaction of **13** and AcFcBF₄ in acetone-*d*₆. Warming benzoate complex **23** to -30 °C resulted in exclusive formation of ethane and (bpy)Pd^{II}(CH₃)(O₂CPh) (**24**). This precedent is supportive of Mechanism A₂, but our experiments have yet to provide conclusive evidence for this mechanism in the one-electron oxidation of (*t*Bu-bpy)Pd^{II}(CH₃)₃OAc.

Scheme 4.32 Reaction of **13** and AcFcBF₄ Proceeding through Mechanism A₂.

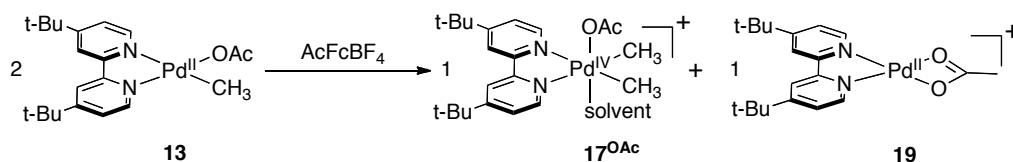


Scheme 4.33 Reductive Elimination of Ethane from (bpy)Pd^{IV}(CH₃)₃O₂CPh (**23**).

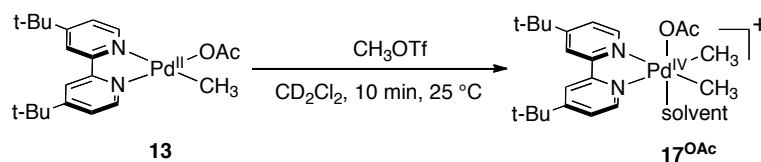


In Mechanism B, [(t-Bu-bpy)Pd^{II}(CH₃)₂OAc(acetone)]⁺ (**17**^{OAc}) is the expected intermediate (Scheme 4.34). No palladium complexes with a similar coordination environment were known, so independent synthesis of **17**^{OAc} was necessary for comparison to the reaction mixture. Preparation of **17**^{OAc} was attempted by reaction of **13** with CH₃OTf, in analogy to the synthesis of cationic trimethyl complex **3** (Scheme 4.35).¹¹ Surprisingly, reaction of **13** with CH₃OTf at 25 °C in methylene chloride-*d*₂ afforded CH₃OAc and [(t-Bu-bpy)Pd^{II}(CH₃)(acetone)]⁺ (**4**) exclusively. These results are in direct contrast to one-electron oxidation of **13**, which afforded ethane without any detectable CH₃OAc. Reaction of **13** with CH₃OTf at -80 °C showed that **13** converts to **4** and CH₃OAc without observed intermediates, suggesting that either no Pd(IV) was being formed in the reaction or that the Pd(IV) intermediate was too unstable to observe under these conditions.

Scheme 4.34 Reaction of **13** and AcFcBF₄ Proceeding through Mechanism A₂.

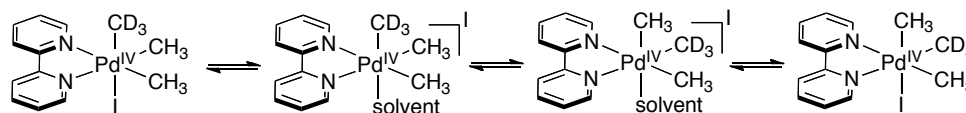


Scheme 4.35 Attempted Synthesis of $[(t\text{-Bu-bpy})\text{Pd}^{\text{IV}}(\text{CH}_3)_2\text{OAc}(\text{solvent})]^+$ (17^{OAc}).

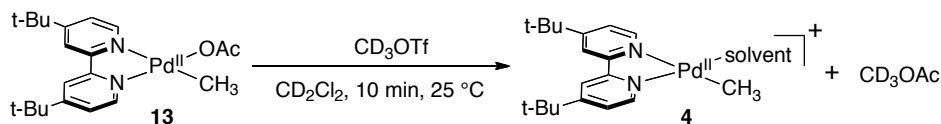


Reaction of **13** with CD_3OTf was devised as a secondary test of whether 17^{OAc} was formed in the reaction in the **13** with CH_3OTf . In the reaction of CD_3I with $(\text{bpy})\text{Pd}(\text{CH}_3)_2$ in acetone- d_6 at $-60\text{ }^\circ\text{C}$, the methyl groups of the $\text{Pd}(\text{IV})$ product, $(\text{bpy})\text{Pd}(\text{CH}_3)_2(\text{CD}_3)\text{I}$, were shown to rapidly interconvert through a cationic intermediate (Scheme 4.36).^{11,24} Reductive elimination produced a mixture of $\text{H}_3\text{C}-\text{CH}_3$ and $\text{H}_3\text{C}-\text{CD}_3$.¹¹ By analogy, reaction of **13** with CD_3OTf should provide a mixture of CH_3OAc and CD_3OAc if the assumption is made that the positions of CH_3 and CD_3 dynamically exchange for intermediate 17^{OAc} . The reaction of **13** with CD_3OTf in methylene chloride- d_2 at room temperature exclusively gave CD_3OAc (Scheme 4.37). This result is consistent with a mechanism involving direct attack of the OAc ligand of **13** (rather than generation of a Pd^{IV} intermediate).

Scheme 4.36 Methyl Group Scrambling in $(\text{bpy})\text{Pd}^{\text{IV}}(\text{CH}_3)_3\text{I}$.²⁴



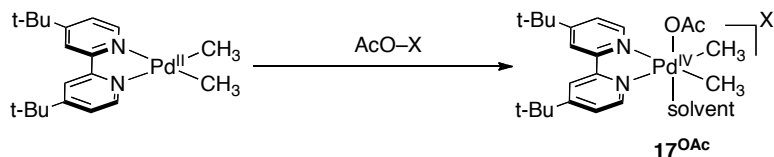
Scheme 4.37 Reaction of $(t\text{-Bu-bpy})\text{Pd}^{\text{II}}(\text{CH}_3)\text{OAc}$ with CD_3OTf .



Addition of an electrophilic source of acetate to $(t\text{-Bu-bpy})\text{Pd}^{\text{II}}(\text{CH}_3)_2$ (**2**) is another conceptual synthetic route to proposed intermediate 17^{OAc} (Scheme 4.38). Iodobenzene diacetate ($\text{PhI}(\text{OAc})_2$) has been used to synthesize a number of isolable $\text{Pd}(\text{IV})$ complexes.²⁵ However, the challenge for synthesis of cationic complex 17^{OAc} is oxidation of **2** with an oxidant that delivers a single acetate and leaves an open

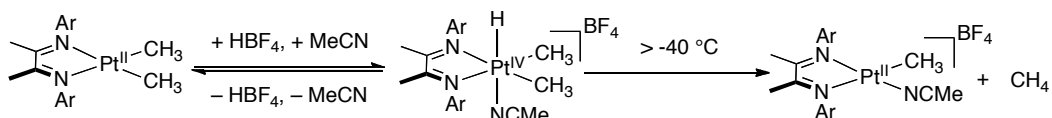
coordination site on palladium. To my knowledge, there are no known two-electron oxidants that deliver a single acetate; thus, we were unable to pursue this route.

Scheme 4.38 Synthesis of $[(t\text{-Bu-bpy})\text{Pd}^{\text{II}}(\text{CH}_3)_2\text{OAc}(\text{acetone})]^+$ (**17^{OAc}**) with an Electrophilic Source of Acetate.

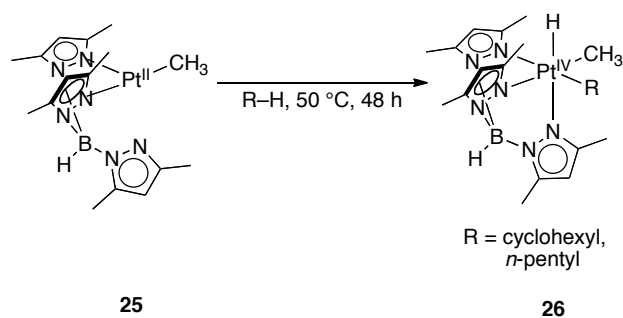


Low temperature ^1H NMR spectroscopic studies of one-electron oxidation of **13** suggest the intermediates are too unstable to isolate. In order to stabilize the observed intermediate, **I-1** for isolation, we sought to modify the bipyridine ligand scaffold. Tripodal ligands have been previously shown to stabilize otherwise unstable high-valent metal complexes. For example, Tilset has shown that platinum-hydride intermediates generated by protonation of a dimethyl-platinum complex bearing a bidentate diimine ligand are highly unstable (Scheme 4.39).²⁶ Observation of the platinum-hydride was only possible in the presence of excess acetonitrile, but even then, these complexes were observed only as transient species at $-40\text{ }^\circ\text{C}$, prior to reductive elimination of methane. In contrast, Goldberg has shown that complex **25**, bearing a tripodal ligand, undergoes C–H activation of alkanes to generate a similar hydride complex **26**, which is stable up to $63\text{ }^\circ\text{C}$ (Scheme 4.40).²⁷ The improved stability of **26** is attributed to the tridentate, facial ligand trispyrazolylborate (Tp^*).

Scheme 4.39 Low Temperature Observation of a Platinum(IV)-Hydride.²⁶

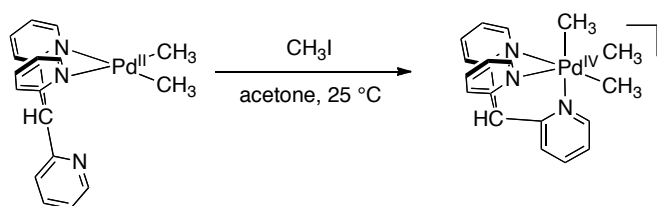


Scheme 4.40 Use of a Facial Tridentate Tp* Ligand to Stabilize a Pt^{IV}-Hydride.²⁷



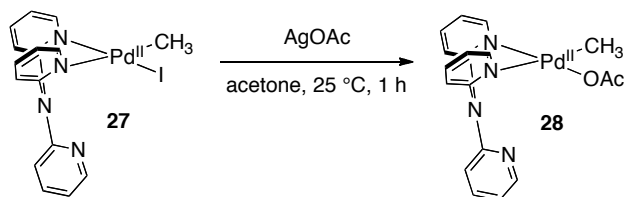
Similarly, Canty has employed the tripodal ligand tris(2-pyridyl)methane to isolate the cationic intermediate proposed in oxidative addition of CH₃I to (N–N)Pd^{II}(CH₃)₂ complexes (Scheme 4.41).²⁸ Whereas (bpy)Pd^{IV}(CH₃)₃I eliminated ethane at temperatures above -20 °C, [(tpm)Pd^{IV}(CH₃)₃]I was completely stable at room temperature.²⁹

Scheme 4.41 Isolation of a Stable Cationic Pd(IV) Complex.²⁸

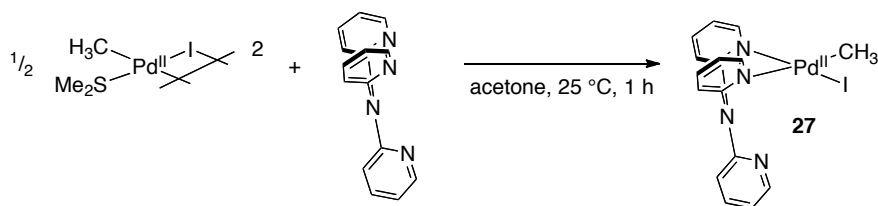


This same rationale was applied to stabilization of potential intermediate **I-1**. Palladium methyl acetate complex **28** was synthesized by metathesis of acetate for iodide between (tpa)Pd(CH₃)I (tpa = tris(2-pyridyl)amine) and AgOAc (Scheme 4.42). Iodide complex (**27**) was synthesized by ligand substitution of tpa onto starting complex [(SMe₂)Pd^{II}(CH₃)(μ-I)]₂ (Scheme 4.43).

Scheme 4.42 Synthesis of (tpa)Pd^{II}(CH₃)OAc (**28**).

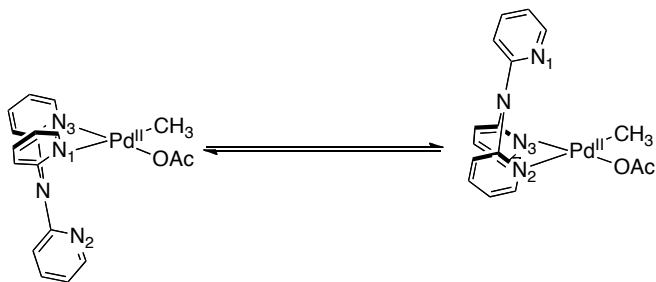


Scheme 4.43 Synthesis of (tpa)Pd^{II}(CH₃)I (**27**).



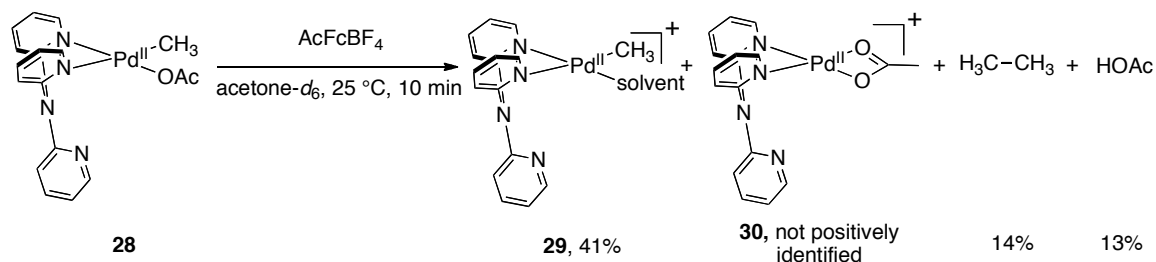
¹H NMR spectroscopic analysis of complex **28** showed a single methyl resonance and broadened aromatic peaks that coalesced into 4 peaks at 50 °C suggestive of dynamic exchange between all of the pyridine rings. Complex **27** exhibited a set of four sharp aromatic resonances and broadened baseline aromatic resonances at 25 °C. This suggests that one of the three pyridines of the tpa ligand remains bound while the other two pyridyl ligands rapidly exchange (Scheme 4.44). The pyridine trans to the strongest trans effect ligand will be the most labile and most likely to be in dynamic exchange. For complex **27**, the methyl ligand is a stronger trans effect ligand than acetate, suggesting the pyridine trans to the methyl ligand should be more more labile than the pyridine trans to acetate or iodide. The free and bound pyridine groups could be resolved at -25 °C for complex **27**.

Scheme 4.44 Dynamic Exchange of Pyridyl Groups in (tpa)Pd^{II}(CH₃)X Complexes.



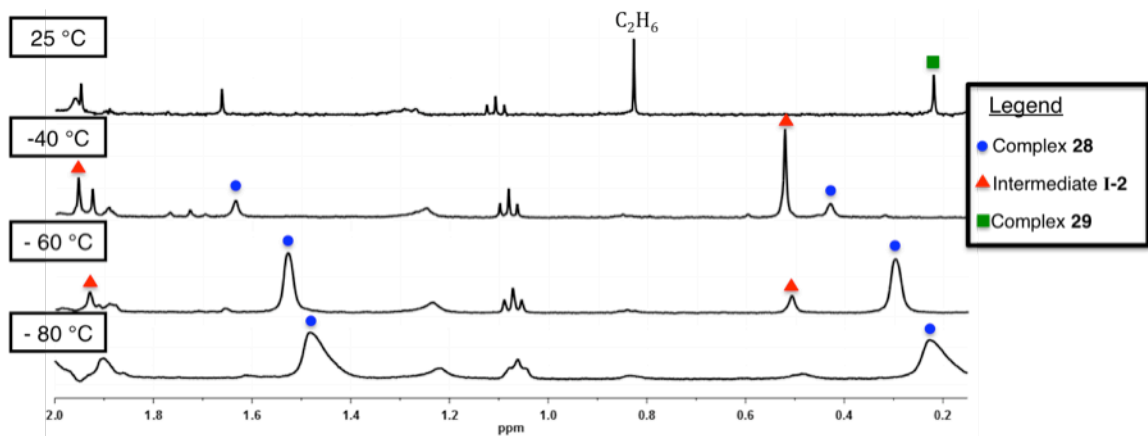
One-electron oxidation of **28** at 25 °C provided a similar distribution of products to ^tBu-bpy complex **13** albeit in lower yields (Scheme 4.45). Notably, no CH₃OAc is formed in the one-electron oxidation of **28**, but HOAc (13%) is formed along with ethane (14%) and [(tpa)Pd^{II}(CH₃)(acetone)]⁺ (**29**, 41%). No monoacetate product, [(tpa)Pd^{II}(κ-O,O-OAc)]⁺ (**30**) could be identified.

Scheme 4.45 One-Electron Oxidation of (tpa)Pd^{II}(CH₃)OAc (**28**).



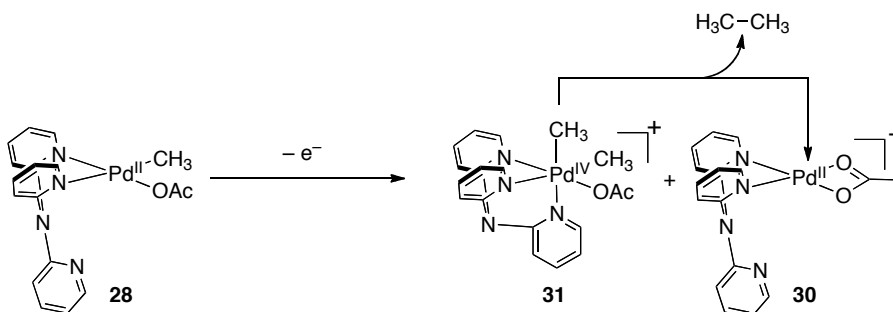
The formation of ethane along with decomposition of **28** upon oxidation with AcFcBF₄ at 25 °C demonstrates that methyl transfer intermediates are still not stable at ambient temperatures even with the stabilizing tpa ligand. Reaction of **28** at -80 °C in an NMR spectrometer showed only starting complex **28** (Scheme 4.46). As the temperature was increased to -60 °C, a minor set of acetate and methyl ¹H NMR resonances began to grow in. At -40 °C, the minor set became the dominant set although no formation of **30** was observed. The methyl and acetate resonances were observed in a 2:1 ratio respectively and were assigned as intermediate **I-2**. Further elevation of the temperature showed **I-2** to be only stable up -40 °C before ethane and **29** began to form. Importantly, no clear identification could be made for a monoacetate palladium product.

Scheme 4.46 Low Temperature Oxidation of (tpa)Pd^{II}(CH₃)OAc (**28**) with AcFcBF₄.



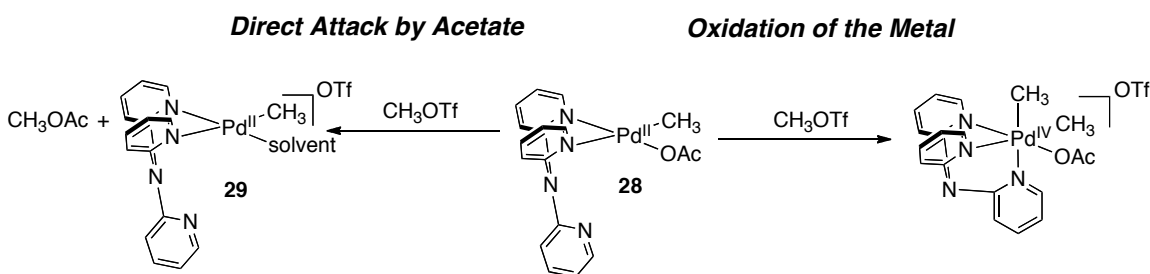
The 2:1 ratio of resonances, tentatively assigned as methyl and acetate resonances, respectively, suggest Mechanism B is operative. If the reaction follows Mechanism B, **30** is the expected product of one-electron oxidation being formed in 50%

yield along with 50% $[(\text{tpa})\text{Pd}^{\text{II}}(\text{CH}_3)_2\text{OAc}]^+$ (**31**) (Scheme 4.47). Decomposition of **31** would then yield ethane and a full equivalent of **30**. Oxidation of **28** with AcFcBF_4 Proceeding through Mechanism B.

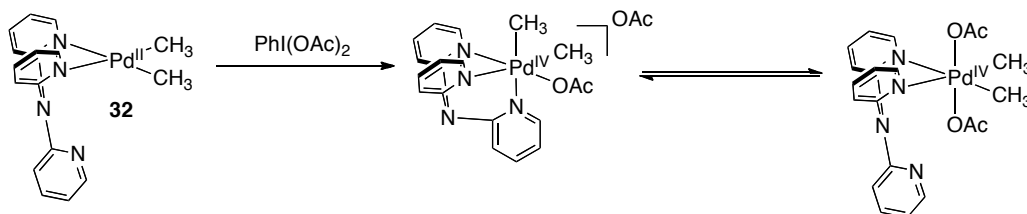


While the use of *tpa* in place of *t*Bu-*bpy* did not stabilize the reaction intermediates enough to allow isolation, *tpa* could potentially facilitate independent synthesis of proposed intermediate complexes. For example, in the synthesis of $[(\text{tpa})\text{Pd}^{\text{II}}(\text{CH}_3)_2\text{OAc}]^+$ by reaction of **28** with CH_3OTf , the pendent arm of *tpa* could lower the energy of an oxidative addition pathway relative to a path where acetate directly attacks CH_3OTf (Scheme 4.48). Also, oxidation of $(\text{tpa})\text{Pd}(\text{CH}_3)_2$ (**32**) with $\text{PhI}(\text{OAc})_2$ could allow synthesis of $[(\text{tpa})\text{Pd}^{\text{II}}(\text{CH}_3)_2\text{OAc}]\text{OAc}$ if the pendant pyridine arm of *tpa* outcompetes a second equivalent of acetate binding palladium (Scheme 4.49).

Scheme 4.47 Two Pathways for Oxidation of $(\text{tpa})\text{Pd}^{\text{II}}(\text{CH}_3)\text{OAc}$ by CH_3OTf .

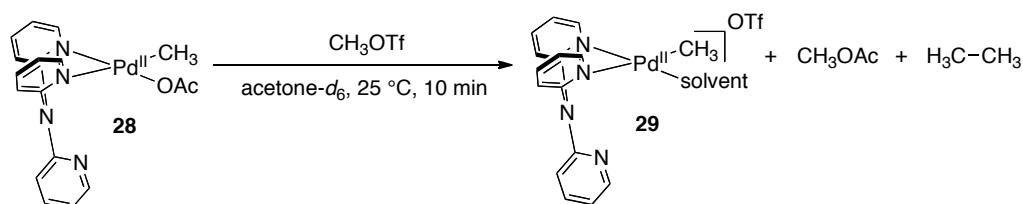


Scheme 4.48 Proposed Synthesis of $[(\text{tpa})\text{Pd}^{\text{IV}}(\text{CH}_3)_2\text{OAc}]\text{OAc}$.



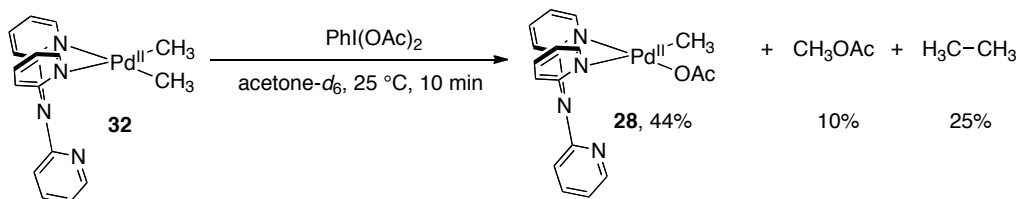
As with reactions of CH₃OTf with (tBu-bpy)Pd^{II}(CH₃)OAc (**13**), if intermediate **I-2** is formed in an independent synthesis of [(tpa)Pd^{IV}(CH₃)₂OAc]⁺, it should decompose to give products analogous to one-electron oxidation of (tpa)Pd^{II}(CH₃)OAc (**28**). Reaction of **28** with CH₃OTf in acetone-*d*₆ at 25 °C immediately proceeded to give monomethyl cationic complex **29** and CH₃OAc as products (Scheme 4.50). This exclusive selectivity for C–O bond formation parallels the reaction of **13** with CH₃OTf, suggesting direct attack of the acetate ligand on CH₃OTf.

Scheme 4.49 Reaction of (tpa)Pd^{II}(CH₃)OAc (**28**) with CH₃OTf.



Oxidation of dimethyl complex **32** with PhI(OAc)₂ in acetone-*d*₆ at 25 °C gives a mixture of CH₃OAc, ethane, and **29** within ten minutes (Scheme 4.51). The formation of CH₃OAc is in contrast to one-electron oxidation of **28**. Even if intermediate **I-2** is produced in this reaction, the decomposition may be complicated by the second equivalent of acetate that would not be present in the one-electron oxidation of **28**.

Scheme 4.50 Reaction of (tpa)Pd^{II}(CH₃)OAc (**32**) with PhI(OAc)₂.



4.3 Conclusions

One of the major challenges of methane oligomerization is carbon-carbon bond formation from monomethyl intermediates. Development of a one-electron oxidation of monomethyl complexes provided an answer to that challenge. Oxidation of complexes of the general formula (tBu-bpy)Pd^{II}(CH₃)X with acetylferrocenium tetrafluoroborate (AcFcBF₄) at 25 °C provided ethane within the time of mixing of the complex and the

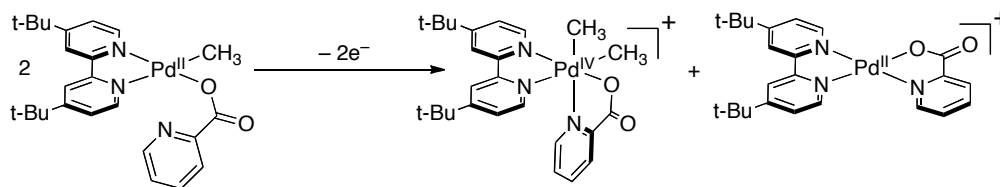
oxidant. The lack of methane, even in the presence of a radical trap, provided evidence against a mechanism where ethane was produced via a dimerization of methyl radicals.

Further mechanistic studies suggested that one-electron oxidation of (^tBu-bpy)Pd^{II}(CH₃)OAc (**13**) proceeds via an oxidatively-induced methyl transfer reaction to generate a high-valent palladium intermediate. Two mechanistic pathways were proposed: 1) equilibrium disproportionation at Pd^{II} to give (^tBu-bpy)Pd^{II}(CH₃)₂ which then subsequently undergoes an oxidatively-induced methyl transfer to generate (^tBu-bpy)Pd^{IV}(CH₃)₃OAc, and 2) oxidatively-induced methyl transfer from (^tBu-bpy)Pd^{II}(CH₃)OAc to generate [(^tBu-bpy)Pd^{IV}(CH₃)₂OAc(solvent)]⁺. Low temperature oxidation of **13** allowed observation of a Pd-CH₃ intermediate which slowly decomposed even at -60 °C, but the data collected precluded definitive identification of the intermediate or reaction pathway.

To stabilize the observed intermediate, an (L₂)Pd^{II}(CH₃)OAc complex where L₂ = the facial, tridentate ligand tris(2-pyridyl)amine (tpa) was prepared and oxidized. The intermediate produced in the one-electron oxidation of (tpa)Pd^{II}(CH₃)OAc was observed to be stable up -40 °C where onset of ethane elimination occurred. While tpa did not stabilize the intermediate enough to allow isolation, the observed 2:1 ratio for integrations of the methyl:acetate resonances were suggestive of the presence of [(tpa)Pd^{IV}(CH₃)₂OAc]⁺.

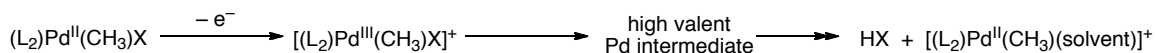
Future attempts to stabilize the observed intermediate will proceed along at least three avenues of study: 1) changing the stabilizing tridentate ligand from tpa to tris(pyrazolyl)methane, 2) changing the X-type ligand in (L₂)Pd^{II}(CH₃)X (L₂ = facial tridentate ligand), or 3) appending stabilizing groups to the carboxylate ligand in (^tBu-bpy)Pd^{II}(CH₃)(O₂CR). Changing the X in (tpa)Pd^{II}(CH₃)X to X = CF₃¹³ or trifluoroacetate (TFA)³⁰ could potentially stabilize the intermediate enough to allow isolation or further characterization. In the system (^tBu-bpy)Pd^{II}(CH₃)(O₂CR), R = 2-pyridyl, oxidation of (^tBu-bpy)Pd^{II}(CH₃)(pic) (pic = picolinate) could generate [(^tBu-bpy)Pd^{IV}(CH₃)₂(pic)]⁺ (Scheme 4.52). Similar neutral palladium(IV) complexes are stable at temperatures up to 25 °C when bearing a bis-bidentate ligand system.^{30,31}

Scheme 4.51 Picolinate as a Supporting Ligand in One-Electron Oxidation.

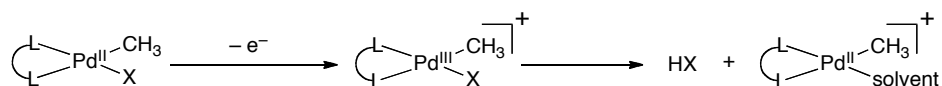


To make one-electron oxidation of $(L_2)Pd^{II}(CH_3)X$ useful for the oligomerization of methane it is important to understand the origin of the $HX/[(L_2)Pd^{II}(CH_3)(solvent)]^+$ in order to mitigate it. Preliminarily, the low temperature oxidation of $(tpa)Pd^{II}(CH_3)OAc$ suggests that $HOAc$ and $[(tpa)Pd^{II}(CH_3)(solvent)]^+$ are formed only after decomposition of the observed intermediate (Scheme 4.53). Alternatively, HX and $[(L_2)Pd^{II}(CH_3)(solvent)]^+$ could be generated from decomposition of the proposed palladium(III) intermediates (Scheme 4.54). Preparation of stable intermediates could provide a foothold to more closely explore the details of these transformations.

Scheme 4.52 HX and $[(L_2)Pd^{II}(CH_3)(solvent)]^+$ Formation from a Pd Intermediate.

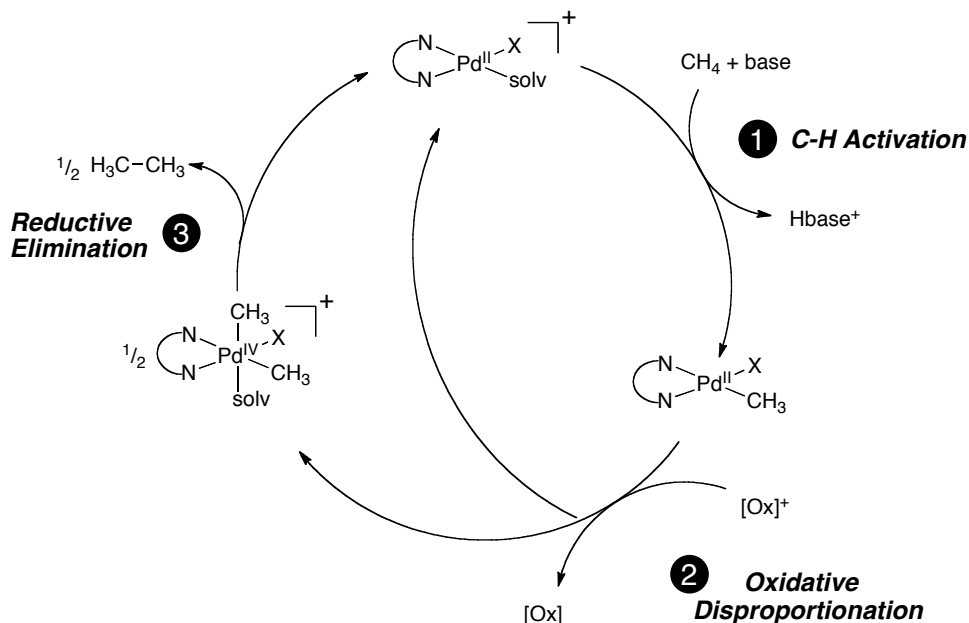


Scheme 4.53 HX and $[(L_2)Pd^{II}(CH_3)(solvent)]^+$ Formation from Pd^{III} .



Development of one-electron oxidations of monoalkyl complexes has the potential to be an important part of catalyzing the oligomerization of methane (Scheme 4.55). In a single reaction, methyl transfer and elimination of ethane occur. To complete the catalytic cycle, palladium must activate methane.

Scheme 4.54 Proposed Catalytic Cycle for Oligomerization of Methane.



4.4 Experimental Procedures

4.4.1 Instrumentation

NMR spectra were obtained on a Varian Inova 500 (499.90 MHz for ^1H ; 125.70 MHz for ^{13}C) or a Varian Inova 400 (399.96 MHz for ^1H ; 100.57 MHz for ^{13}C , 376.34 MHz for ^{19}F) spectrometer. ^1H and ^{19}F NMR chemical shifts are reported in parts per million (ppm) relative to TMS with the residual solvent peak used as an internal reference. ^{19}F NMR spectra are referenced on a unified scale, where the single primary reference is the frequency of the residual solvent peak in the ^1H NMR spectrum. Multiplicities are reported as follows: singlet (s), doublet (d), doublet of doublets (dd), and doublet of doublet of doublets (ddd).

4.4.2 Materials and Methods

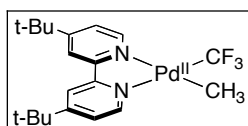
All manipulations were performed using standard Schlenk or glovebox procedures unless otherwise noted. Acetone and acetone- d_6 (Cambridge Isotopes) were refluxed over calcium sulfate overnight and then distilled, freeze-pump-thaw degassed, and shaken over 4 Å molecular sieves immediately before use. Methylene chloride- d_2

(Cambridge Isotopes) and 1,1,2-trichloroethane were refluxed over CaH₂ overnight and then distilled, freeze-pump-thaw degassed and stored over 4 Å molecular sieves. Sodium iodide was dried at 150 °C under vacuum for 16 h. All other solvents were purchased from Fisher or EMD and dispensed from an Innovative Technologies solvent purification system equipped with columns packed with activated alumina, copper catalyst, and molecular sieves. 4,4'-Di-*tert*-butyl-2,2'-bipyridine (*t*Bu-bpy) was purchased from Aldrich, Na₂PdCl₄ and PdCl₂ were purchased from Pressure Chemical, methyl triflate, ferrocene, PhI(OAc)₂ and 2-heptafluoropropyl iodide were purchased from Acros, methyl triflate-*d*₃ was purchased from Cambridge Isotopes, and all other materials were used as purchased from Aldrich or Acros.

See Chapter 2 for specific NMR instrumentation settings and particular NMR tubes used in ethane-evolving reactions.

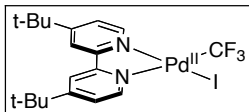
4.4.3 Syntheses

Acetylferrocene,³² FcBF₄,¹⁹ AcFcBF₄,¹⁹ tri(2-pyridyl)amine,³³ (*t*Bu-bpy)Pd^{II}(OAc)₂,³⁴ (*t*Bu-bpy)Pd^{II}(TFA)₂,³⁴ [(CH₃)(SMe₂)Pd^{II}(μ-I)]₂,³⁵ and [(pyridazine)Pd^{II}(CH₃)₂]_n³⁵ were prepared according to literature procedures. The Pd complexes (*t*Bu-bpy)Pd^{II}(CH₃)₂ (**2**), [(*t*Bu-bpy)Pd^{II}(CH₃)(acetone)]OTf (**4**), (*t*Bu-bpy)Pd^{II}(CH₃)I (**12**), (*t*Bu-bpy)Pd^{II}(I)₂ (**16**), (*t*Bu-bpy)Pd^{II}(CH₃)OAc (**13**), and (*t*Bu-bpy)Pd^{II}(CH₃)Cl (**14**) were prepared as described in Chapter 2.

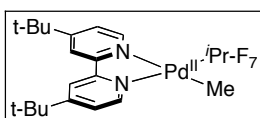


(*t*Bu-bpy)Pd^{II}(CH₃)(CF₃) (7): (*t*Bu-bpy)Pd^{II}(CH₃)I (188 mg, 0.37 mmol, 1 equiv) and freshly ground and dried cesium fluoride (226 mg, 1.49, 4.1 equiv) were suspended in THF (8 mL) in a 25 mL Schlenk flask containing a magnetic stir bar. (CH₃)₃Si(CF₃) (55 μL, 0.37 mmol, 1 equiv) was added via syringe and reaction was stirred vigorously for 4 h. Solvent was removed under vacuum, and the residue was suspended in CH₂Cl₂ (5 mL) and passed through a plug of Celite. Pentanes (15 mL) was added to the filtrate and the solution was stored at -32 °C overnight. The resulting solid was collected on a frit,

washed with cold pentanes, and dried under vacuum to afford **7** as a brown, microcrystalline solid (94 mg, 56% yield). ^1H NMR (500 MHz, acetone- d_6): δ 8.94 (dd, $^3J = 6.0$ Hz, $J_{\text{H-F}} = 1.5$ Hz, 1H), 8.60 (d, $^3J = 5.5$ Hz, 1H), 8.56 (d, $^4J = 1.5$ Hz, 1H), 8.54 (d, $^4J = 2.0$ Hz, 1H), 7.76 (dd, $^3J = 5.5$ Hz, $^4J = 1.5$ Hz, 1H), 7.75 (dd, $^3J = 6.0$ Hz, $^4J = 2.0$ Hz, 1H), 1.45 (2 peaks, 18H), 0.62 (s, 3H). ^{19}F NMR (376 MHz, acetone- d_6): δ -21.3.

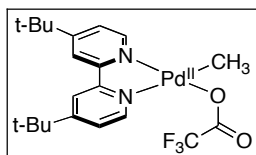


(*t*-Bu-bpy)Pd^{II}(CF₃)I (8): In air and with no attempt to avoid moisture, (*t*-Bu-bpy)Pd^{II}(CH₃)(CF₃) (39 mg, 0.09 mmol, 1 equiv) was suspended in hexanes (10 mL), and I₂ (23 mg, 0.09 mmol, 1.1 equiv.) was added. A magnetic stir was added, and the reaction stirred for 2.5 h. The resulting solid was filtered, washed with hexanes, and dried under vacuum to afford **9** as a tan solid (30.7 mg, 63% yield). ^1H NMR (400 MHz, acetone- d_6): δ 9.74 (d, $^3J = 5.6$ Hz, 1H), 8.84 (d, $^3J = 6.0$ Hz, 1H), 8.61 (d, $^4J = 2.0$ Hz, 1H), 8.57 (d, $^4J = 1.6$ Hz, 1H), 7.90 (dd, $^3J = 6.4$ Hz, $^4J = 2.0$ Hz, 1H), 7.72 (dd, $^3J = 6.0$ Hz, $^4J = 2.0$ Hz, 1H), 1.48 (s, 9H), 1.44 (s, 9H). ^{19}F NMR (376 MHz, acetone- d_6): δ -12.7.

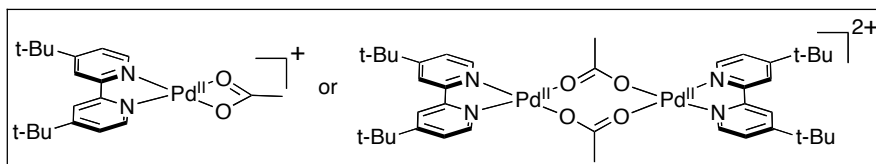


(*t*-Bu-bpy)Pd^{II}(CH₃)(*i*Pr-F₇) (10): (*t*-Bu-bpy)Pd^{II}(CH₃)₂ (200 mg, 0.50 mmol, 1 equiv) was suspended in pentanes (20 mL) in a 100 mL Schlenk flask. 2-heptafluoropropyl iodide (71 μL , 0.50 mmol, 1 equiv) was added, and the reaction stirred at 25 $^\circ\text{C}$ for 16 h. Solvent was removed under vacuum, and the residue was dissolved in acetone (5 mL). Pentanes (15 mL) was added and the resulting solid was filtered out. The filtrate was condensed. Benzene (5 mL) was added, frozen, and placed under vacuum leaving **10** as an orange powder (76 mg, 27% yield). ^1H NMR (500 MHz, acetone- d_6): δ 8.93 (dd, $^3J = 7.5$ Hz, $J_{\text{H-F}} = 6.5$, 1H), 8.62 (d, $^3J = 6.0$ Hz, 1H), 8.55 (d, $^4J = 2.0$ Hz, 1H), 8.52 (d, $^4J = 2.0$ Hz, 1H), 7.79 (dd, $^3J = 6.0$ Hz, $^4J = 2.0$ Hz, 1H), 7.74 (ddd, $^3J = 5.5$ Hz, $^4J = 1.0$ Hz,

$J_{\text{H-F}} = 1.0$ Hz). ^{19}F NMR (376 MHz, acetone- d_6): δ -67.5 (d, $^3J_{\text{F-F}} = 7.9$ Hz, 6H), -196.8 (septet, $^3J_{\text{F-F}} = 7.9$ Hz).

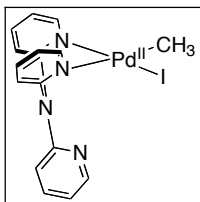


(*t*-Bu-bpy)Pd^{II}(CH₃)(TFA) (15): (*t*-Bu-bpy)Pd^{II}(TFA)₂ (40 mg, 0.07 mmol, 1 equiv) and (*t*-Bu-bpy)Pd^{II}(CH₃)₂ (29 mg, 0.07, 1.1 equiv) were suspended in acetone (5 mL) in a 20 mL vial containing a magnetic stir bar. The reaction was stirred at 30 °C for 16 h. Pentanes (15 mL) was added, and the solution was stored at -32 °C for 2 h. The resulting solid was filtered, washed with pentanes, and dried under vacuum to afford **15** as a white powder (48 mg, 73% yield). ^1H NMR (400 MHz, acetone- d_6): δ 8.58 (d, $^4J = 1.6$ Hz, 1H), 8.57 (d, $^4J = 1.6$ Hz, 1H), 8.54 (d, $^3J = 6.0$ Hz, 1H), 8.26 (d, $^3J = 5.6$ Hz, 1H), 7.80 (dd, $^3J = 5.6$ Hz, $^4J = 1.6$ Hz, 1H), 7.74 (dd, $^3J = 6.0$ Hz, $^4J = 2.4$ Hz, 1H), 1.45 (s, 9H), 1.44 (s, 9H), 0.77 (s, 3H). ^{13}C NMR (100 MHz, acetone- d_6): δ 165.0, 164.9, 161.6 (q, $^2J_{\text{C-F}} = 34.4$ Hz), 158.0, 153.8, 150.5, 148.1, 124.9, 124.8, 121.9, 120.6, 117.1 (q, $^1J_{\text{C-F}} = 290$ Hz), 36.4, 36.4, 30.5, 30.4, 0.3. ^{19}F NMR (376 MHz, acetone- d_6): δ -74.8. Anal. Calcd for C₂₁H₂₇F₃N₂O₂Pd: C, 50.16; H, 5.41; N, 5.57. Found: C, 50.18; H, 5.47; N, 5.52.

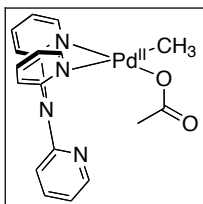


[(*t*-Bu-bpy)Pd^{II}(OAc)]⁺ (19): (*t*-Bu-bpy)Pd^{II}(OAc)₂ (102 mg, 0.21 mmol, 1 equiv) was suspended in CH₂Cl₂ (5 mL), and a magnetic stir bar was added. Methyl triflate (24 μL , 0.21 mmol, 1 equiv) was added and the solution was stirred for 1 h at 30 °C. Pentanes (15 mL) was added to precipitate a yellow solid. The solid was filtered, washed with pentanes, and dried under vacuum to afford **19** as yellow powder (105.1 mg, 87% yield). This yield includes 7% of an additional asymmetric impurity observed by ^1H NMR. ^1H NMR (500 MHz, acetone- d_6): δ 8.41 (d, $^4J = 2.5$ Hz, 2H), 8.30 (d, $^3J = 6.5$ Hz, 2H), 7.79 (dd, $^3J = 6.0$ Hz, $^4J = 2.0$ Hz, 2H), 2.42 (s, 3H), 1.32 (s, 18H). ^1H NMR (400 MHz,

methylene chloride- d_2): δ 8.12 (d, $^3J = 7.5$ Hz, 2H), 7.88 (d, 4J coupling was not resolved in this spectrum, 2H), 7.76 (dd, $^3J = 8.0$ Hz, 4J coupling was not resolved in this spectrum, 2H), 2.46 (s, 3H), 1.31 (s, 18H).

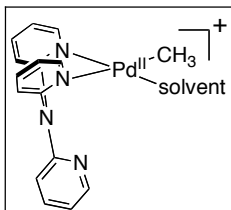


(tpa)Pd^{II}(CH₃)I (27): Without any precautions to avoid moisture, an acetone (5 mL) solution of [(CH₃)(SMe₂)Pd^{II}(μ -I)]₂ (326 mg, 0.49 mmol, 1 equiv) containing a magnetic stir bar was sparged with N₂ for 1 minute. Tri(2-pyridyl)amine (240 mg, 0.97 mmol, 2 equiv) was added to the solution and the reaction was stirred for 1 h. The resulting solution was filtered through a plug of Celite. Et₂O (20 mL) was added to the filtrate, and the solution was stored at -32 °C for 2 h. The resulting solid was collected on a frit, washed with Et₂O, and dried under vacuum to afford **27** as a yellow powder (245 mg, 51% yield). ¹H NMR (400 MHz, acetone- d_6 , 50 °C): δ 0.73 (s, 3H). Four broad overlapping peaks, δ 9.00, 8.59, 8.01, 7.39. ¹H NMR (400 MHz, acetone- d_6 , 25 °C): δ 0.72 (s, 3H), broad peaks, δ 9.14 (1H), 8.65 (1H), [8.23, 8.12, 8.04, 7.93, 7.68, 7.50 (multiple peaks, 8H)], 6.99 (1H), 6.70 (1H).

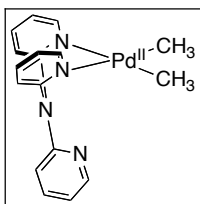


(tpa)Pd^{II}(CH₃)OAc (28): (tpa)Pd^{II}(CH₃)I (97 mg, 0.20 mmol, 1 equiv) was suspended in dry CH₂Cl₂ (5 mL). AgOAc (33 mg, 0.20 mmol, 1 equiv) and a magnetic stir bar were added, and the reaction was stirred for 3 h at 25 °C. The resulting suspension was passed through a plug of Celite. Et₂O (10 mL) was added to the filtrate and the solution was stored at -32 °C overnight. The precipitate was collected on a frit, washed with cold Et₂O, dried under vacuum to afford **28** as a tan, microcrystalline solid (71 mg, 104% yield). ¹H NMR (400 MHz, acetone- d_6 , -25 °C): δ 8.75 (d, $^3J = 6.0$ Hz, 1H), 8.63 (dd, $^3J = 5.6$ Hz, $^4J = 1.6$ Hz, 1H), 8.22 (ddd, $^3J = 7.6$ Hz, 7.6 Hz, $^4J = 1.6$ Hz, 1H), 8.18 (d, $^3J = 4.4$ Hz,

1H), 8.14 (d, $^3J = 7.6$ Hz, 1H), 8.02 (d, $^3J = 8.0$ Hz, 1H), 7.96 (d, $^3J = 7.6$ Hz, 1H), 7.71 (dd, $^3J = 7.1$ Hz, 7.1 Hz, 1H), 7.60 (ddd, $^3J = 7.4$ Hz, 5.6 Hz, $^4J = 1.2$ Hz, 1H), 7.55 (dd, $^3J = 5.6$ Hz, 1H), 7.02 (dd, $^3J = 6.1$ Hz, 5.2 Hz, 1H), 6.79 (d, $^3J = 8.4$ Hz, 1H), 1.78 (s, 3H), 0.59 (s, 3H).



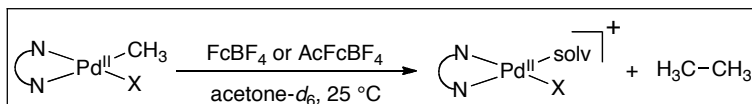
[(tpa)Pd^{II}(CH₃)(acetone)]OTf (29): A solution of (tpa)Pd^{II}(CH₃)(OAc) (0.5 mL of a 5 mM solution in acetone-*d*₆) and methyl triflate (0.1 mL of a 27 mM solution in acetone-*d*₆) were added to a screw cap NMR tube which was sealed with Teflon®-lined cap. ¹H NMR (400 MHz, acetone-*d*₆, -60 °C): δ 9.73 (dd, $^3J = 5.6$ Hz, $^4J = 1.6$ Hz, 1H), 8.80–8.75 (2 peaks, 2H), 8.70 (dd, $^3J = 6.0$ Hz, $^4J = 1.6$ Hz, 1H), 8.27 (ddd, $^3J = 7.2$ Hz, 6.0 Hz, $^4J = 1.6$ Hz, 1H), 8.12 (ddd, $^3J = 8.8$ Hz, 7.2 Hz, $^4J = 1.6$ Hz, 1H), 7.72 (dd, $^3J = 5.6$ Hz, $^4J = 1.2$ Hz, 1H), 7.59 (ddd, $^3J = 8.8$ Hz, 7.2 Hz, $^4J = 1.6$ Hz, 1H), 7.55 (ddd, $^3J = 7.2$ Hz, 7.2 Hz, $^4J = 1.2$ Hz, 1H), 7.48 (d, $^3J = 8.4$ Hz, 1H), 6.95 (dd, $^3J = 6.8$ Hz, 6.8 Hz, 1H), 6.90 (d, $^3J = 8.8$ Hz, 1H), 0.80 (s, 3H).



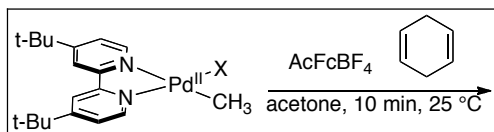
(tpa)Pd^{II}(CH₃)₂ (32): [(pyridazine)Pd(CH₃)₂]_n (21mg, 0.10 mmol, 1 equiv), tri(2-pyridyl)amine (27 mg, 0.11 mmol, 1.1 equiv) and a magnetic stir bar were added to a 20 mL vial. Acetone (1 mL) was added, and the reaction was stirred for 1 hr. The acetone solution was filtered through a plug of Celite and washed with acetone (2 mL). Pentanes (15 mL) was added to the filtrate to precipitate a white solid. The precipitate was collected on a frit, washed with pentanes, and dried under vacuum to afford **32** as a flocculent, white solid (21 mg, 46% yield). ¹H NMR (400 MHz, acetone-*d*₆, -20 °C): δ 8.63 (dd, $^3J = 5.2$ Hz, $^4J = 1.6$ Hz, 2H), 8.15-8.10 (two peaks, 3H), 7.92 (d, $^3J = 8.4$ Hz,

2H), 7.63 (ddd, $^3J = 8.4$ Hz, 7.2 Hz, $^4J = 2.0$ Hz, 1H), 7.56 (ddd, $^3J = 7.2$ Hz, 5.6 $^4J = 1.2$ Hz, 2H), 6.92 (dd, $^3J = 6.8$ Hz, 5.2 Hz, 1H), 6.60 (d, $^3J = 8.8$ Hz, 1H), 0.03 (s, 6H). ^1H NMR (400 MHz, acetone- d_6 , 25 °C): δ 0.05 (s, 6H) Four broad peaks, δ 8.63, 8.08, 7.87, 7.51.

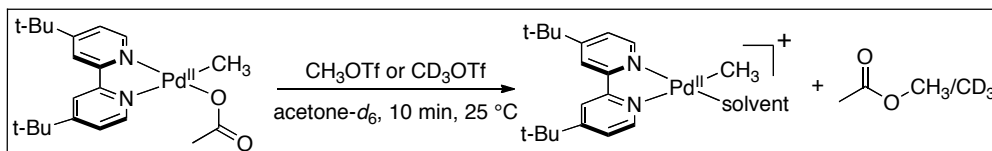
4.4.4 Reaction Details



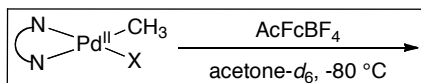
One-Electron Oxidation of 7, 12–15, 28 with FcBF₄ or AcFcBF₄. Solutions of complex (0.5 mL of a 5 mM solution in acetone- d_6) and 1,1,2-trichloroethane (internal standard, 15 μL of a 215 mM solution in acetone- d_6) were added to a J. Young NMR tube, and an initial ^1H NMR spectrum was taken. A solution of oxidant (0.1 mL of a 25 mM solution in acetone- d_6) was added, and the J. Young tube was immediately sealed with a Teflon® stopcock. After NMR spectroscopic analysis was performed, the NMR tube was returned to the glovebox, and ~ 4 equiv. NaI or KI was added to the reaction to quench remaining oxidant and trap cationic products. The resulting solutions were analyzed by NMR spectroscopy.



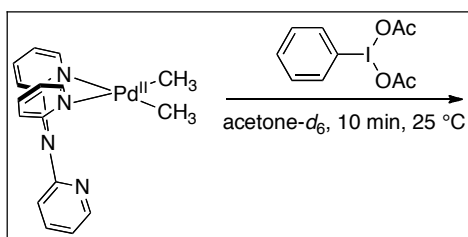
One-Electron Oxidation of 7, 12–15, 28 with AcFcBF₄ in the Presence of 1,4-Cyclohexadiene. Procedure for one-electron oxidation with FcBF₄ or AcFcBF₄ was followed, only 2.5 μL of 1,4-cyclohexadiene was added prior to one-electron oxidation of the monomethyl starting material.



Reaction of 13 with Methyl Triflate and Methyl Triflate-*d*₃. The general procedure for synthesis of [(tpa)Pd^{II}(CH₃)(acetone)]⁺ (**28**) was followed using methylene chloride-*d*₂ as solvent.



Low Temperature Reactions of 13 and 28 with AcFcBF₄. Solutions of complex (0.5 mL of a 5 mM solution in acetone-*d*₆) and 1,1,2-trichloroethane (internal standard, 15 μ L of a 215 mM solution in acetone-*d*₆) were added to a J. Young NMR tube, and an initial ¹H NMR spectrum was taken. The solutions were frozen, and a solution of oxidant or methyl triflate (0.1 mL of a 25 mM solution in acetone-*d*₆) was layered on the frozen complex solution and frozen. The solutions were thawed at -78 °C (acetone/CO_{2(s)} bath) and added to a spectrometer that had been preequilibrated at -80 °C. The temperature of the spectrometer was raised in 20 °C intervals until a reaction was observed.



Reaction of (tpa)Pd^{II}(CH₃)₂ (32**) with PhI(OAc)₂.** The procedure for oxidation by one-electron oxidants was followed only a solution of PhI(OAc)₂ was substituted for the solution of the one-electron oxidant. The reaction was complete within 10 minutes.

4.5 References

- (1) Lersch, M.; Tilset, M. *Chem. Rev.* **2005**, *105*, 2471.
- (2) Conley, B. L.; Tenn, W. J., III; Young, K. J. H.; Ganesh, S. K.; Meier, S. K.; Ziatdinov, V. R.; Mironov, O. Oxgaard, J.; Gonzales, J.; Goddard, W. A., III; Periana, R. A. *J. Mol. Catal. A* **2006**, *251*, 8.
- (3) Shilov, A. E.; Shul'pin, G. B. *Chem. Rev.* **1997**, *97*, 2879.
- (4) Remy, M. S.; Cundari, T. R.; Sanford, M. S. *Organometallics*, **2010**, *29*, 1522.
- (5) Shiotani, A.; Yoshikiyo, M.; Itatani, H. *J. Mol. Catal.* **1983**, *18*, 23.
- (6) Shiotani, A.; Itatani, H.; Inagaki, T. *J. Mol. Catal.* **1986**, *34*, 57.
- (7) Lee, S. H.; Lee, K. H.; Lee, J. S.; Jung, J. D.; Shim, J. S. *J. Mol. Catal. A* **1997**, *115*, 241.

-
- (8) Iretskii, A. V.; Sherman, S. C.; White, M. G.; Kenvin, J. C.; Schiraldi, D. A. *J. Catal.* **2000**, *193*, 49.
- (9) Burton, H. A.; Kozhevnikov, I. V.; *J. Mol. Catal. A* **2002**, *185*, 285.
- (10) Dwight, T. A.; Rue, N. R.; Charyk, D.; Josselyn, R.; DeBoef, B. *Org. Lett.* **2007**, *9*, 3137.
- (11) Lanci, M. P.; Remy, M. S.; Kaminsky, W.; Mayer, J. M.; Sanford, M. S. *J. Am. Chem. Soc.* **2009**, *131*, 15618.
- (12) Khusnutdinova, J. R.; Rath, N. P.; Mirica, L. M. *J. Am. Chem. Soc.* **2010**, *132*, 7303.
- (13) Ye, Y.; Ball, N. D.; Kampf, J. W.; Sanford, M. S. *J. Am. Chem. Soc.* **2010**, *132*, 14682.
- (14) Wang, X.; Truesdale, L.; Yu, J.-Q. *J. Am. Chem. Soc.* **2010**, *132*, 3648.
- (15) Culkin, D. A.; Hartwig, J. F. *Organometallics* **2004**, *23*, 3398.
- (16) Grushin, V. V.; Marshall, W. J. *J. Am. Chem. Soc.* **2006**, *128*, 4632.
- (17) Hughes, R. P.; Ward, A. J.; Rheingold, A. L.; Zakharov, L. N. *Can. J. Chem.* **2003**, *81*, 1270.
- (18) Kieltsch, I.; Dubinina, G. G.; Hamacher, C.; Kaiser, A.; Torres-Nieto, J.; Hutchinson, J. M.; Klein, A.; Budnikova, Y.; Vicic, D. A. *Organometallics* **2010**, *29*, 1451.
- (19) Connelly, N. G.; Geiger, W. E. *Chem. Rev.* **1996**, *96*, 877.
- (20) Seligson, A. L.; Trogler, W. C. *J. Am. Chem. Soc.* **1992**, *114*, 7085.
- (21) Gerdes, G.; Chen, P. *Organometallics* **2004**, *23*, 3031.
- (22) Sloatweg, J. C.; Chen, P. *Organometallics* **2006**, *25*, 5863.
- (23) Canty, A. J.; Done, M. C.; Skelton, B. W.; White, A. H. *Inorg. Chem. Commun.* **2001**, *4*, 648.
- (24) Byers, P. K.; Canty, A. J.; Crespo, M.; Puddephatt, R. J.; Scott, J. D. *Organometallics* **1988**, *7*, 1363.
- (25) Racowski, J. M.; Sanford, M. S. *Top. Organomet. Chem.* **2011**, *35*, 61.
- (26) Wik, B. J.; Lersch, M.; Tilset, M. *J. Am. Chem. Soc.* **2002**, *124*, 12116.
- (27) Wick, D. D.; Goldberg, K. I. *J. Am. Chem. Soc.* **1997**, *119*, 10235.
- (28) Byers, P. K.; Canty, A. J.; Skelton, B. W.; White, A. H. *Chem. Commun.* **1987**, 1093.
- (29) Byers, P. K.; Canty, A. J.; Skelton, B. W.; White, A. H. *Organometallics* **1990**, *9*, 826.
- (30) Racowski, J. M.; Dick, A. R.; Sanford, M. S. *J. Am. Chem. Soc.* **2009**, *131*, 10974.
- (31) Dick, A. R.; Kampf, J. W.; Sanford, M. S. *J. Am. Chem. Soc.* **2005**, *127*, 12790.
- (32) Tappe, K.; Knochel, P. *Tetrahedron: Asymm.* **2004**, *15*, 91.
- (33) Nagao, N.; Egashira, K.; Mogi, D. *Bull. Chem. Soc., Jpn.* **2004**, *77*, 1171.
- (34) Milani, B.; Alessio, E.; Mestroni, G.; Sommazzi, A.; Garbassi, F.; Zangrando, E.; Bresciani-Pahor, N.; Randaccio, L. *Dalton Trans.* **1994**, 1903.
- (35) Byers, P. K.; Canty, A. J.; Jin, H.; Kruis, D.; Markies, B. A.; Boersma, J.; Van Koten, G.; Hill, G. S.; Irwin, M. J.; Rendina, L. M.; Puddephatt, R. J. *Inorg. Synth.* **1998**, *32*, 162.

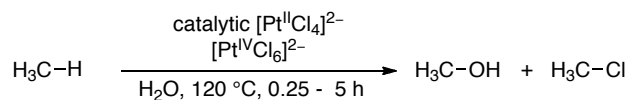
CHAPTER 5

Stoichiometric Studies of Disproportionation, One-Electron Oxidation and Reductive Elimination at Platinum.

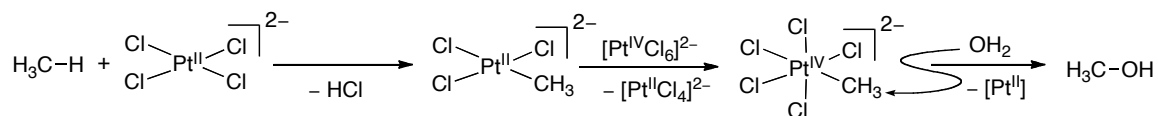
5.1 Background and Significance

In the late 1960s, Shilov demonstrated the first oxidation of methane to methanol by a homogenous, transition metal catalyst (Scheme 5.1).¹⁻³ Chloride salts of platinum were proposed to afford methanol by C–H activation of methane to generate a Pt–CH₃ intermediate with subsequent oxygenation of the CH₃ ligand (Scheme 5.2).^{1,2} Since that time, substantial efforts have been made toward understanding the fundamental steps of methane oxidation in the “Shilov system” with particular attention being paid to the activation of methane by platinum complexes.

Scheme 5.1 Oxygenation of Methane Catalyzed by Platinum Salts.¹



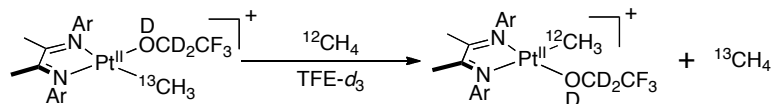
Scheme 5.2 Proposed Mechanism for Shilov System for Oxygenation of Methane.¹



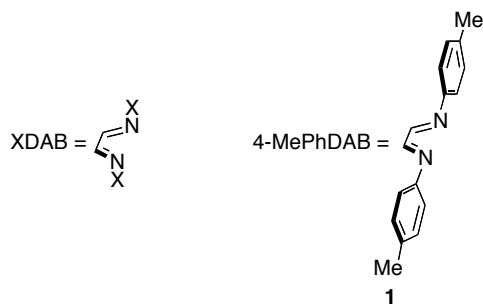
The Bercau and Tilset groups in particular have undertaken mechanistic studies of methane activation using platinum complexes bearing 1,4-diaza-1,3-butadiene (DAB) ligands.⁴ Their studies have shown platinum(II)-DAB complexes to be competent at stoichiometric C–H activation of methane (Scheme 5.3). Because these DAB ligands are shown throughout this chapter, a general abbreviation, XDAB, is introduced here

(Scheme 5.4). In this abbreviation, X = the substituent on the nitrogen. For example, ligand **1** is abbreviated as 4-MePhDAB.

Scheme 5.3 C–H Activation of Methane by Pt(II)-Diimine Complexes.⁴

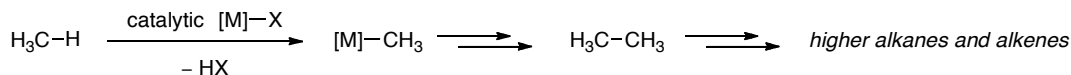


Scheme 5.4 Abbreviation System for 1,4-diaza-1,3-butadiene (DAB) Ligands.



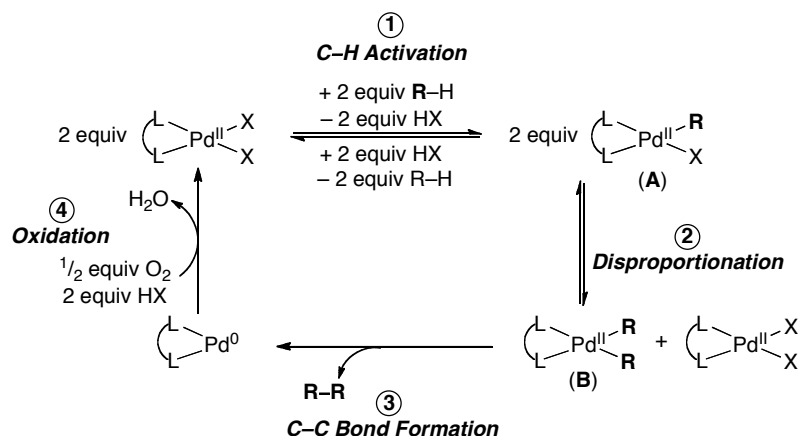
Activation of methane is the key first step not only in methane oxygenation but in any functionalization methane. Our focus is the oligomerization of methane to give heavier, liquid alkanes (Scheme 5.5). Similar to oxygenation of methane, C–H activation of methane is required for homogeneous oxidative oligomerization of methane. Because platinum has such rich precedent for alkane activation, we desired to study its application in the toward homogenous oligomerization of methane.

Scheme 5.5 C–H Activation as a First Step in Oligomerization of Methane.



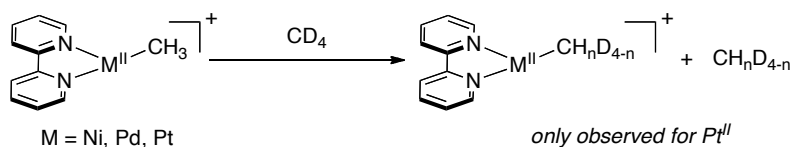
Initial studies toward design of a platinum catalyst for oxidative oligomerization of methane were inspired by the related palladium-catalyzed oxidative homocoupling of arenes (Scheme 5.6).⁵⁻⁹ In this system, the palladium catalyst is proposed to 1) C–H activate the arene, 2) perform an Ar-for-X metathesis called disproportionation, 3) reductively eliminate the biaryl product, and 4) be reoxidized from Pd(0) to Pd(II).

Scheme 5.6 Proposed Catalytic Cycle for Pd(II)-Catalyzed Homocoupling of Arenes.



Palladium has substantial precedent for the C–H activation of sp^2 C–H bonds required to perform this reaction,¹⁰ but there are only a limited number of examples of methane activation by palladium.^{11–15} Gas phase and computational studies of methane activation by Group 10 [(bpy)M(CH₃)]⁺ (2,2'-bipyridine) complexes showed only the platinum complex to be competent for methane activation (Scheme 5.7).¹⁶

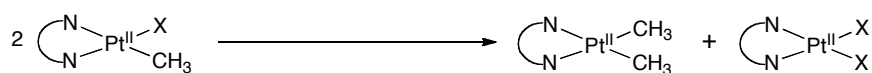
Scheme 5.7 Methane Activation by [(bpy)Pt(CH₃)]⁺.¹⁶



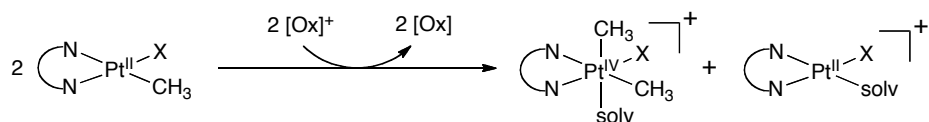
Compelled by this C–H activation precedent for platinum, we undertook studies toward the fundamental steps of oxidative oligomerization of methane by platinum that were guided by our previous successes toward palladium-catalyzed oxidative oligomerization of methane. One of the most substantial challenges met in our studies of palladium toward oxidative oligomerization of methane was generation of a dimethyl intermediate from which C–C formation could occur. Two distinct pathways to overcome this challenge identified in the course of these studies were: disproportionation at palladium(II) (Path A, Scheme 5.8)¹⁷ and one-electron oxidatively-induced methyl transfer (Path B, Scheme 5.8).¹⁸

Scheme 5.8 Two Pathways for Formation of a “Dimethyl”-Platinum Intermediate.

Path A: Disproportionation Driven by Thermodynamics

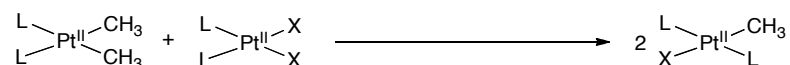


Path B: Methyl Transfer Driven by Oxidation

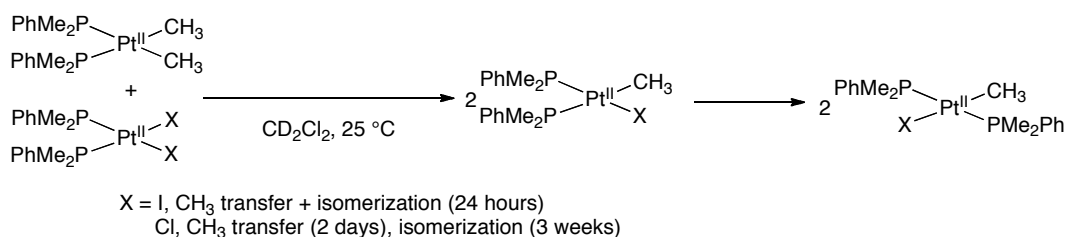


Reported studies of platinum toward path A, methyl disproportionation, were limited to the microscopic reverse comproportionation reaction (Scheme 5.9).^{19–22} Puddephatt had shown in multiple cases, reaction of $(\text{L})_2\text{Pt}(\text{CH}_3)_2$ with $(\text{L})_2(\text{Pt})(\text{X})_2$ produced two equivalents of $(\text{L})_2\text{Pt}(\text{CH}_3)\text{X}$. Initial reports showed that in the reaction of monodentate phosphine complexes $(\text{P}(\text{CH}_3)_2\text{Ph})_2\text{Pt}(\text{CH}_3)_2$ and $(\text{P}(\text{CH}_3)_2\text{Ph})_2\text{Pt}(\text{X})_2$, X-type ligands had a substantial impact on the rate of the reaction (Scheme 5.10).²⁰ When X = iodide, the reaction was complete in 24 h, while when X = chloride, transfer of a methyl group occurred over two days, and subsequent *cis-trans* isomerization occurred over 3 weeks. Based on the isomers observed in the reaction, the authors proposed methyl transfer occurred through a transition state with two five-coordinate platinum centers (Scheme 5.11). Additionally, the authors suggested that the bridging halide in the transition state was responsible for the dramatic difference in rates observed. They posited that iodide was a superior bridging ligand in comparison to chloride, thereby facilitating the interaction of two platinum centers that is required for methyl transfer to occur.

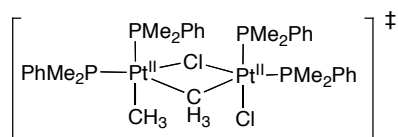
Scheme 5.9 Comproportionation of $(\text{L})_2\text{Pt}(\text{CH}_3)_2$ with $(\text{L})_2(\text{Pt})(\text{X})_2$.



Scheme 5.10 Effect of Halide on Comproportionation Reaction.¹⁹

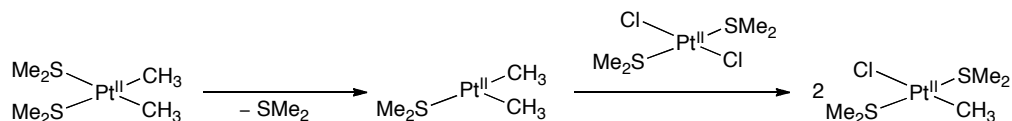


Scheme 5.11 Proposed Transition State for Methyl Transfer between Platinum Complexes.¹⁹



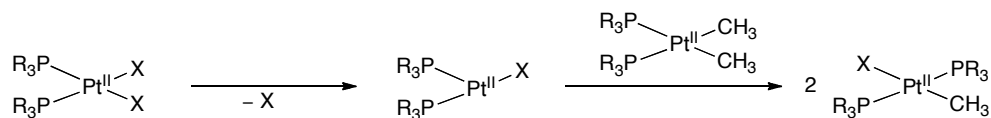
In a related system, Puddephatt and coworkers studied the kinetics of comproportionation (Scheme 5.12).²³ Comproportionation of $(\text{SMe}_2)\text{Pt}(\text{CH}_3)_2$ and $(\text{SMe}_2)\text{Pt}(\text{X})_2$ was shown to occur via equilibrium loss of the labile L-type ligand, SMe_2 . It is not clear whether this mechanism is general to the monodentate phosphine systems or whether the identity of the L-type ligand influenced the mechanism of the reaction. This leaves open the possibility that either phosphine dissociation or X-type ligand dissociation could also lead to methyl transfer (Scheme 5.13).

Scheme 5.12 Mechanism of Comproportionation of $(\text{SMe}_2)_2\text{Pt}(\text{CH}_3)_2$ and $(\text{SMe}_2)_2\text{Pt}(\text{X})_2$.²³

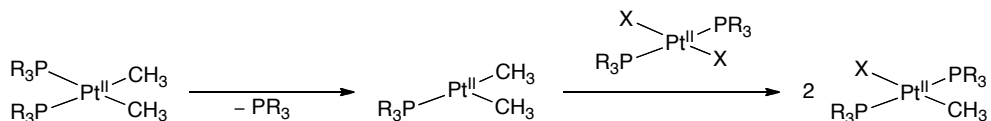


Scheme 5.13 X-type Versus L-type Ligand Dissociation in Methyl Transfer Reactions.

X-Type Ligand Dissociation

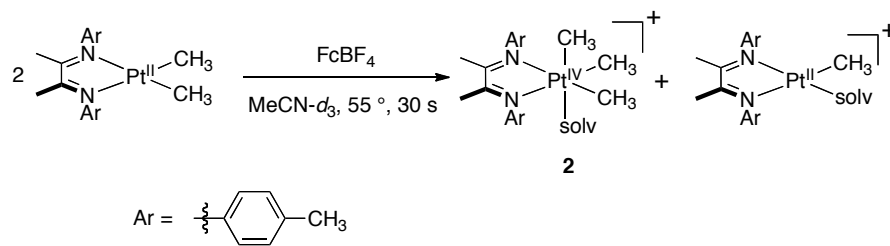


L-Type Ligand Dissociation



Path B, oxidatively-induced methyl transfer, had been previously reported for platinum (Scheme 5.14).²⁴ Tilset showed that (4-MePhDAB)Pt^{II}(CH₃)₂ underwent an oxidatively-induced methyl transfer upon reaction with one-electron oxidant, ferrocenium tetrafluoroborate (FcBF₄). The reaction in acetonitrile yielded stable platinum products, [(4-MePhDAB)Pt^{IV}(CH₃)₃(MeCN)]BF₄ (**2**) and [(4-MePhDAB)Pt^{II}(CH₃)(MeCN)]BF₄.

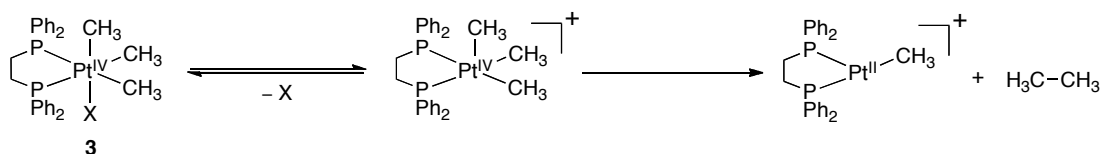
Scheme 5.14 One-Electron Oxidatively-Induced Methyl Transfer from Pt(II).²⁴



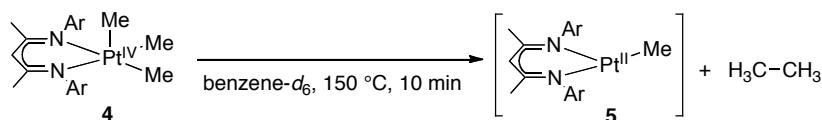
An additional challenge in the platinum system is C–C bond formation to produce ethane. Specifically, the diimine Pt^{IV} complexes, like **2** produced in the one-electron oxidation performed by Tilset are resistant to reductive elimination.^{25–28} More generally, six coordinate Pt^{IV}-trimethyl complexes bearing chelating *sp*² nitrogen donor ligands have not been shown to undergo reductive elimination of ethane. Studies of reductive elimination from related phosphine-ligated complexes, (dppe)Pt(CH₃)₃X (**3**) (dppe = 1,2-bis(diphenylphosphio)ethane), indicated reductive elimination proceeds through a five-coordinate intermediate produced by dissociation of X (Scheme 5.15).^{29–32} Subsequently, carefully designed five-coordinate (N–N)Pt^{IV}(CH₃)₃ complexes were isolated, but even these five coordinate complexes undergo reductive eliminate only at high temperatures

(Scheme 5.16).^{33–35} For example, diketimate complex **4** underwent reductive elimination in benzene to form monomethyl complex **5** only after heating to 150 °C. Complex **5** went on to react with solvent and was not isolated. Importantly, all of the stable five-coordinate Pt^{IV} complexes synthesized to date bear chelating *sp*² nitrogen-donor ligands, illustrative of the stability imparted by such ligands.³⁶ So while there is precedent for diimine ligands promoting C–H activation of methane and one-electron oxidatively-induced methyl transfer, the stability that they impart on Pt(IV)-trimethyl complexes restricts elimination of ethane.

Scheme 5.15 Mechanism of Ethane Elimination from Pt^{IV}-Phosphine Complexes.



Scheme 5.16 Elimination of Ethane from Five-Coordinate Pt^{IV} with *sp*² Nitrogen Chelates.³³



This chapter focuses on addressing the challenges put forth for oxidative oligomerization of methane by platinum. Studies of methyl disproportionation of platinum(II)-methyl complexes were conducted as were studies of one-electron oxidatively-induced methyl transfer. Lastly, we designed simple diimine ligands to promote ethane elimination from platinum(IV).

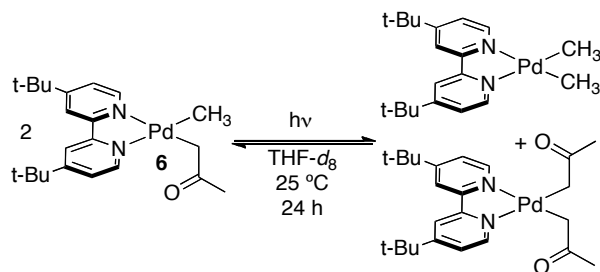
5.2 Results and Discussion

5.2.1 Disproportionation of Pt^{II}-Monomethyl Complexes

Density functional theory (DFT) calculations previously led to the first example of methyl disproportionation at Pd^{II}.¹⁷ By systematically varying ancillary L-type and X-type ligands, in a (L)₂Pd(CH₃)X model, the disproportionation thermodynamics were minimized to show L = *sp*² nitrogen ligands and X = CH₂COCH₃ provided a favorable,

albeit uphill, value for methyl disproportionation. These studies lead to the subsequent synthesis of (^tBu-bpy)Pd(CH₃)(CH₂COCH₃) (**6**) which underwent disproportionation in THF-*d*₈ (Scheme 5.16).

Scheme 5.17 Disproportionation of (^tBu-bpy)Pd(CH₃)(CH₂COCH₃).¹⁷



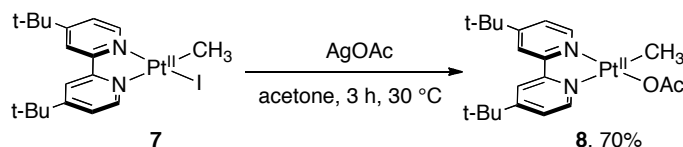
By analogy, DFT calculations were employed on the related Pt^{II} system to minimize ΔG of disproportionation ($\Delta G_{\text{disprop}}$). The functional (B3LYP) and basis set (CEP-31G(d)), shown to be effective for predicting the Pd^{II} system, were extended to the study of the present Pt^{II} system. Chelating diimine ligands were selected for initial examination because they are known to promote C–H activation at group 10 metals^{4,37–41} and were shown to be sufficient model ligands with palladium(II)¹⁷ and platinum(II).⁴² Initial calculations on Pt^{II} focused on modifying the X ligand in a (MeDAB)Pt^{II}(CH₃)X model to minimize $\Delta G_{\text{disprop}}$ (Table 5.1). Interestingly, the thermodynamics for disproportionation were 3.6–4.5 kcal/mol more favorable than the related Pd^{II} disproportionation for all X-type ligands calculated.

Table 5.1 Comparison of $\Delta G_{\text{disprop}}$ for Pt^{II} and Pd^{II} Systems.

X	$\Delta G_{\text{disprop}}$ (kcal/mol)	
	Pt ^{II}	Pd ^{II}
I	8.1	11.8
Br	7.6	12.1
Cl	7.5	11.7
OAc	4.5	8.1

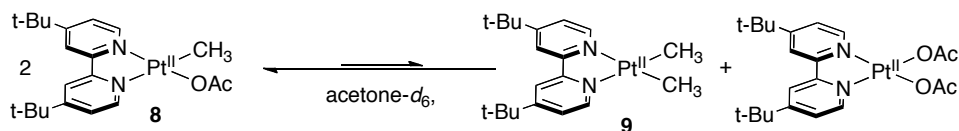
Since $\Delta G_{\text{disprop}}$ was calculated to be lowest for $X = \text{OAc}$, synthesis of the related complex $(^t\text{Bu-bpy})\text{Pt}^{\text{II}}(\text{CH}_3)\text{OAc}$ (**8**) was carried out to test for disproportionation. $(^t\text{Bu-bpy})\text{Pt}^{\text{II}}(\text{CH}_3)\text{OAc}$ (**8**) was synthesized by reacting $(^t\text{Bu-bpy})\text{Pt}^{\text{II}}(\text{CH}_3)\text{I}$ (**7**) with AgOAc (Scheme 5.18).

Scheme 5.18 Synthesis of $(^t\text{Bu-bpy})\text{Pt}^{\text{II}}(\text{CH}_3)\text{OAc}$.



Complex, **8** was weighed into a screw cap NMR tube under N_2 , dissolved in acetone- d_6 and heated to 50°C . The reaction was monitored by ^1H NMR spectroscopy over 16 h. If disproportionation were to occur, the monomethyl platinum complex would generate equilibrium concentrations of $(^t\text{Bu-bpy})\text{Pt}^{\text{II}}(\text{CH}_3)_2$ (**9**) and $(^t\text{Bu-bpy})\text{Pt}^{\text{II}}(\text{OAc})_2$ (Scheme 5.19). No reaction was observed. Further heating of the complex at 90°C over 24 h again showed no evidence for disproportionation.

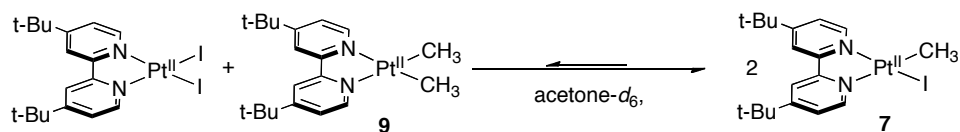
Scheme 5.19 Disproportionation of $(^t\text{Bu-bpy})\text{Pt}^{\text{II}}(\text{CH}_3)\text{X}$.



Complex **8** had the most favorable $\Delta G_{\text{disprop}}$ (4.5 kcal/mol) of the complexes studied, but this ΔG corresponds to an unfavorable K_{eq} of 5.0×10^{-4} . This suggests that either the equilibrium concentration of **9** is too small to observe or the kinetic barrier to methyl transfer is too large to observe methyl transfer from $(^t\text{Bu-bpy})\text{Pt}^{\text{II}}(\text{CH}_3)\text{X}$. To differentiate these two hypotheses, the related comproportionation reaction was run (Scheme 5.20). As the microscopic reverse of disproportionation, the comproportionation reaction should be downhill thermodynamically. Because disproportionation was calculated to be least thermodynamically favored for $X = \text{I}$, we reasoned that comproportionation of **9** and $(^t\text{Bu-bpy})\text{Pt}^{\text{II}}(\text{I})_2$ would be the most likely comproportionation reaction to succeed ($\Delta G_{\text{comprop}} = -\Delta G_{\text{disprop}}$). Importantly, the related

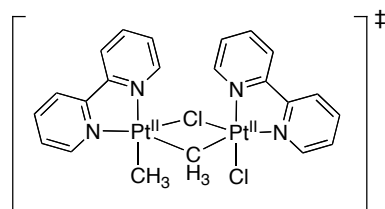
palladium comproportionation reaction gave the expected monomethyl product (Chapter 2) after heating for 16 h at 50 °C. However, when **9** was reacted with platinum complex (^tBu-bpy)Pt^{II}(I)₂ for 16 h at 50 °C no reaction occurred. Further heating at 90 °C for 24 h produced only 10% yield of (^tBu-bpy)Pt^{II}(CH₃)I (**7**). These results suggest that although the thermodynamics of disproportionation of Pt^{II}-methyl compounds is more favorable compared to that of Pd^{II}-methyl disproportionation, the kinetic barrier for disproportionation at Pt^{II} is significantly higher than that at Pd^{II}.

Scheme 5.20 Comproportionation of (^tBu-bpy)Pt^{II}(CH₃)₂ and (^tBu-bpy)Pt^{II}(X)₂.

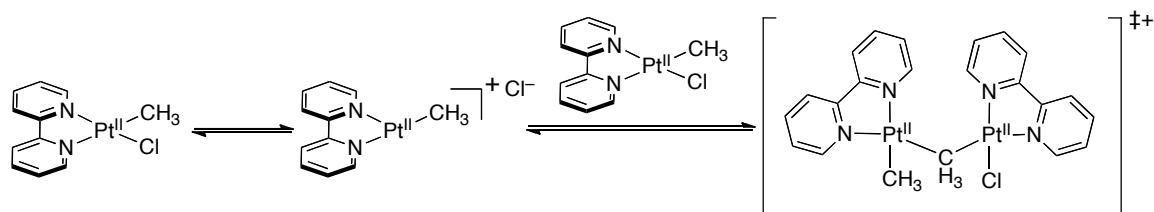


DFT calculations of the methyl transfer mechanism were pursued to further analyze the origin of the observed high kinetic barrier to methyl transfer between Pt^{II} centers. Diimine complex (MeDAB)Pt^{II}(CH₃)Cl was chosen as a model for its simplicity and analogy to thermodynamic calculations. Two mechanisms were considered: a direct exchange of CH₃-for-Cl from five-coordinate Pt (**TS-I**^{Pt}, Scheme 5.21) like that proposed by Puddephatt (Scheme 5.11) and methyl transfer between two square planar platinum complexes where previous dissociation of Cl⁻ from one platinum center had occurred (**TS-II**^{Pt}, Scheme 5.21). Calculation of **TS-II**^{Pt} required inclusion of solvation energy and diffuse basis functions to accurately model the charged species. As such, geometry optimizations for all complexes were calculated in a vacuum using B3LYP/CEP-31G(d). Then single point energy calculations were run with diffuse functions (CEP-31G(d)+) added to all chloride atoms. Solvent corrections were employed using the integral equation formalism of the polar continuum model (IEFPCM) to model the system in acetone solvent. All free energies reported for transition state calculations incorporate these modifications.

Scheme 5.21 Proposed Transition State for Direct Exchange of CH₃-for-Cl.

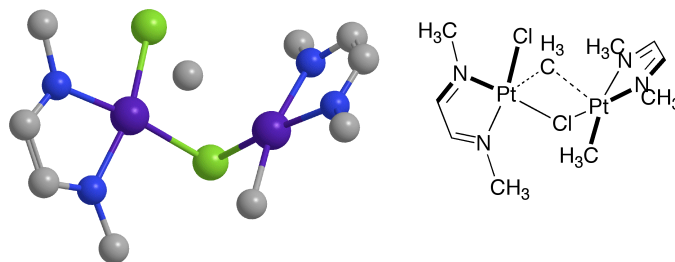


Scheme 5.22 Transition State for Methyl Transfer Following Cl⁻ Dissociation.



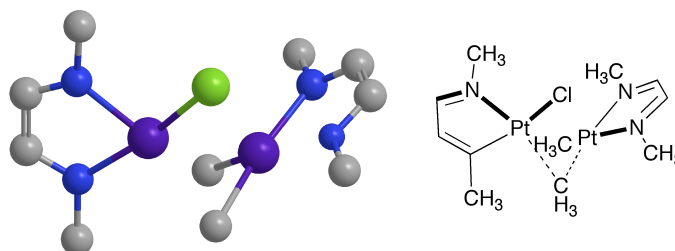
In transition state **TS-I^{Pt}**, two Pt^{II} centers in square pyramidal geometries were bridged by a methyl and chloride atoms in a Pt-Cl-Pt-Me diamond core (Scheme 5.23). Visual inspection of the single imaginary frequency showed the expected transfer of methyl between the two Pt centers, while the bridging chloride atom remained static. This calculation suggested that Cl bridges the two Pt^{II} centers, orienting them for transfer of methyl group. Moving the methyl group along the reaction coordinate toward products followed by geometry optimization produced the expected (MeDAB)Pt^{II}(CH₃)₂ and (MeDAB)Pt^{II}(Cl)₂ products. Similarly, two (MeDAB)Pt^{II}(CH₃)Cl complexes were observed when moving the CH₃ group toward its starting complex. Importantly, although motion of the chloride was not observed in the transition state, the chloride atom breaks its bond with the newly formed (MeDAB)Pt^{II}(CH₃)₂ unit to give the expected (MeDAB)Pt(Cl)₂ product.

Scheme 5.23 Methyl Transfer Transition State **TS-I^{Pt}**.



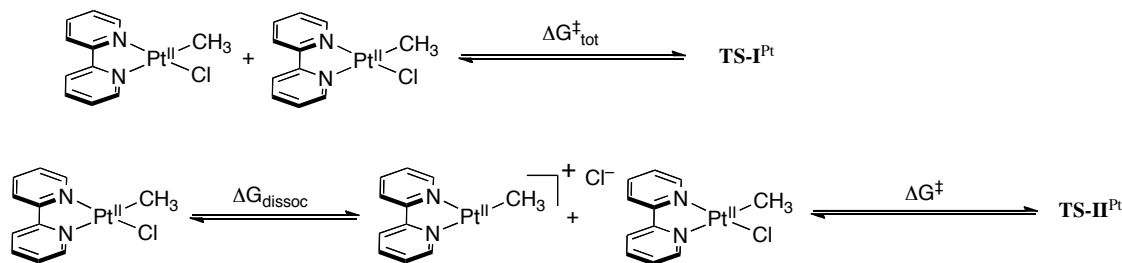
Optimization of **TS-II^{Pt}** gives two square planar Pt^{II} complexes bridged only by a methyl group (Scheme 5.24). The reaction coordinate analysis described for **TS-I^{Pt}** was also applied to **TS-II^{Pt}** and confirmed this to be a methyl transfer transition state.

Scheme 5.24 Methyl Transfer Transition State **TS-II^{Pt}**.



Energies of transition states **TS-I^{Pt}** and **TS-II^{Pt}** can be found in Table 5.2. The energies are defined as ΔG_{dissoc} for dissociation of a chloride from one starting complex and ΔG^\ddagger for the energy required to reach the transition state for methyl transfer. For transition state **TS-I^{Pt}**, where no chloride dissociation occurs, $\Delta G^\ddagger = \Delta G_{\text{tot}}^\ddagger$, and $\Delta G_{\text{tot}}^\ddagger$ is 78.1 kcal/mol. At this $\Delta G_{\text{tot}}^\ddagger$, the Eyring equation predicts the rate to be approaching zero (3.5×10^{-45} mol/s). $\Delta G_{\text{tot}}^\ddagger$ for **TS-II^{Pt}** is a component energy made up of chloride dissociation plus the energy required to reach the methyl transfer transition state. The majority of the energy required to reach transition state **TS-II^{Pt}** is that required for dissociation of Cl⁻ ($\Delta G_{\text{dissoc}} = 31.3$ kcal/mol).

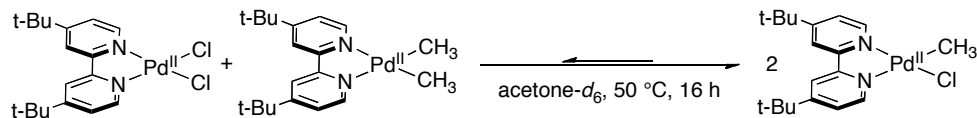
Table 5.2 Transition State Energies from Methyl Transfer at Pt^{II}.



Transition State	ΔG_{dissoc} (kcal/mol)	ΔG^{\ddagger} (kcal/mol)	$\Delta G_{\text{tot}}^{\ddagger}$ ($\Delta G_{\text{dissoc}} + \Delta G^{\ddagger}$)
TS-I ^{Pt}	–	78.1	78.1
TS-II ^{Pt}	31.3	5.0	36.3

These calculations suggest direct CH₃-for-X transfer (TS-I^{Pt}) is not energetically accessible for the disproportionation of methyl groups between platinum atoms. Of the transition states optimized, TS-II^{Pt}, which requires initial dissociation of chloride, is the favored pathway. If this dissociative pathway is the path by which methyl transfer occurs, palladium should have a lower ΔG_{dissoc} than platinum because, palladium, and second row transition metal in general, undergo ligand substitution reactions faster than their third row congeners.⁴³ If ΔG_{dissoc} is lower for palladium than platinum, then $\Delta G_{\text{tot}}^{\ddagger}$ should be lower as well, barring a commensurate rise in ΔG^{\ddagger} . Experiment supports this hypothesis, as comproportionation between (^tBu-bpy)Pd(CH₃)₂ and (^tBu-bpy)Pd(Cl)₂ occurs at 50 °C in acetone-*d*₆ (Scheme 5.25).¹⁷

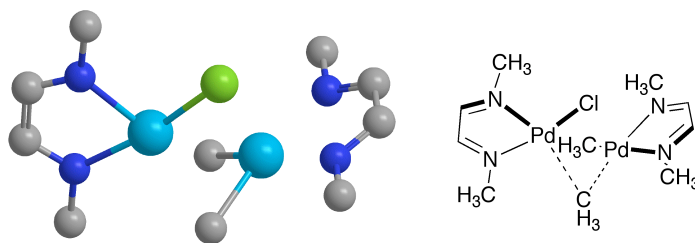
Scheme 5.25 Comproportionation of (^tBu-bpy)Pd(CH₃)₂ and (^tBu-bpy)Pd(Cl)₂.



To see if theory also supports this hypothesis, transition state TS-II^{Pd} (Scheme 5.26) was optimized and dissociation of chloride from (MeDAB)Pd^{II}(CH₃)Cl was calculated by analogy to the Pt^{II} system. A transition state for direct CH₃-for-Cl

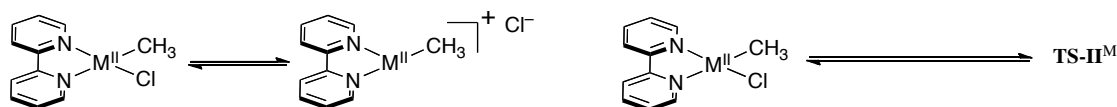
exchange, **TS-I^{Pd}**, could not be found for comparison to **TS-I^{Pt}**. As with the platinum system, dissociation of Cl⁻ gives T-shaped Pd^{II} complex [(MeDAB)Pd^{II}(CH₃)]⁺. Bridging of CH₃ from (MeDAB)Pd^{II}(CH₃)Cl to the T-shaped intermediate gave methyl transfer transition state **TS-II^{Pd}**.

Scheme 5.26 Methyl Transfer Transition State **TS-II^{Pd}**.



Optimized energies are shown in Table 5.3. The calculations demonstrate a lower ΔG_{dissoc} and $\Delta G^{\ddagger}_{\text{tot}}$ for methyl transfer at Pd^{II}. However, while ΔG_{dissoc} is 9.9 kcal/mol lower for palladium, an increase of 7.4 kcal/mol was calculated for ΔG^{\ddagger} to form **TS-II^{Pd}**. These calculations suggest the slow rate of methyl transfer between platinum centers is due in large part to the poor equilibrium for Cl⁻ dissociation from platinum.

Table 5.3 Transition State Energies from Methyl Transfer at Pd^{II} and Pt^{II}.

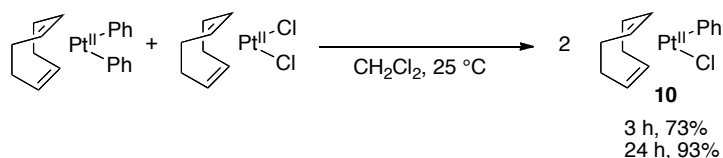


Transition State	ΔG_{dissoc} (kcal/mol)	ΔG^{\ddagger} (kcal/mol)	$\Delta G^{\ddagger}_{\text{tot}}$ ($\Delta G_{\text{dissoc}} + \Delta G^{\ddagger}$)
TS-II^{Pd}	21.4	12.4	33.8
TS-II^{Pt}	31.3	5.0	36.3

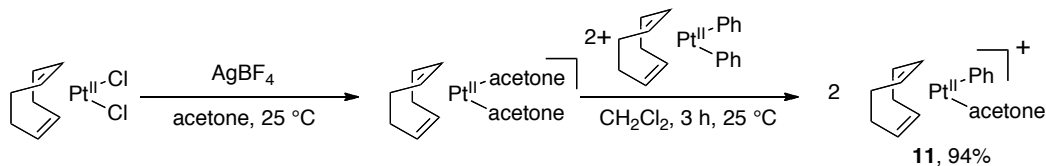
The combination of these theoretical and experimental data suggest that, while Pt^{II}-monomethyl complexes have more favorable thermodynamics for disproportionation than the analogous palladium complexes, the kinetic barrier associated with the methyl transfer is sufficiently large to hinder disproportionation. Calculations indicate that the energy required to dissociate chloride from platinum makes up the majority of the energy cost for methyl transfer.

These hypotheses are borne out by the research of Osakada on comproportionation of Pt-aryl systems (Scheme 5.27).^{44,45} Over the course of 3 h, monophenyl complex **10** was produced in 73% yield. After 24 h, 93% yield of **10** was formed. In this system, COD (1,5-cyclooctadiene) was proposed to labilize the trans X-type ligands and facilitate aryl transfer. Addition of chloride completely inhibited formation of **10**. Conversely, removal of the chloride ligands from (COD)Pt^{II}(Cl)₂ with AgBF₄ allowed monophenyl complex **11** to be formed in 94% yield within 3 h (Scheme 5.28). Further, when 2,2'-bipyridine (bpy) was used as the chelating ligand for the starting dihalide, no reaction occurred under the same conditions (Scheme 5.29). However, when (bpy)Pt^{II}(Ph)₂ was reacted with (COD)Pt^{II}(Cl)₂, the reaction proceeded smoothly to give **11** and (bpy)Pt^{II}(Ph)Cl (Scheme 5.30). Osakada's findings further support the proposed mechanism of halide dissociation followed by methyl transfer, and show that in phenyl transfer reactions, Pt-bpy complexes do not sufficiently facilitate halide dissociation to allow aryl transfer.

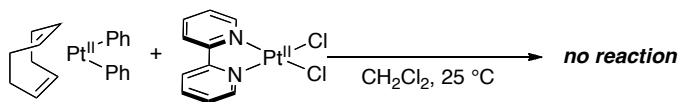
Scheme 5.27 Comproportionation of Phenyl to Give (COD)Pt^{II}(Ph)Cl.⁴⁵



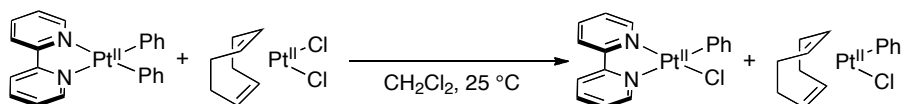
Scheme 5.28 Comproportionation between (COD)Pt^{II}(Ph)₂ and [(COD)Pt^{II}(acetone)₂]⁺.⁴⁵



Scheme 5.29 Comproportionation between (COD)Pt^{II}(Ph)₂ and (bpy)Pt^{II}(Cl)₂.⁴⁵



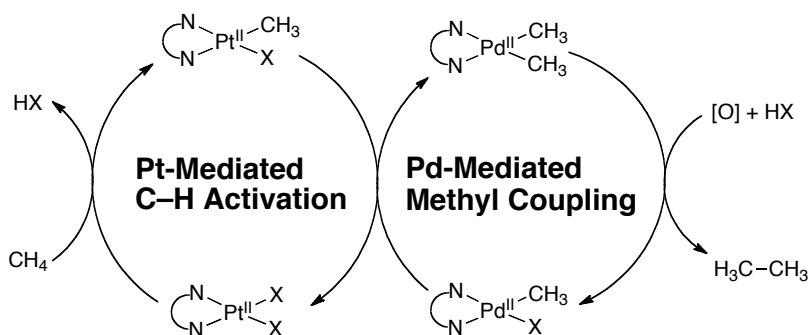
Scheme 5.30 Comproportionation between (bpy)Pt^{II}(Ph)₂ and (COD)Pt^{II}(Cl)₂.⁴⁵



5.2.2 Methyl Transfer from Pt^{II} to Pd^{II}

The computational and experimental studies described above show that disproportionation of monomethyl-Pt^{II} complexes to form the important dimethyl-Pt^{II} intermediate is kinetically unfavorable. However it was still important to consider how C–H activation at Pt^{II}, to yield a Pt-monomethyl complex, could be used productively toward oxidative oligomerization of methane. In light of this, we considered multiple ways to facilitate methyl transfer from monomethyl-platinum complexes. One method considered was the tandem catalysis between platinum and palladium, where CH₃ would be transferred from platinum to palladium, followed by subsequent C–C bond from palladium (Scheme 5.31). In this scheme, methane is activated by platinum to form a platinum-monomethyl complex. A formal disproportionation with a palladium monomethyl would then yield a palladium dimethyl intermediate from which ethane elimination is induced by one-electron oxidation. The oxidation event would also regenerate the palladium-monomethyl for further disproportionation.

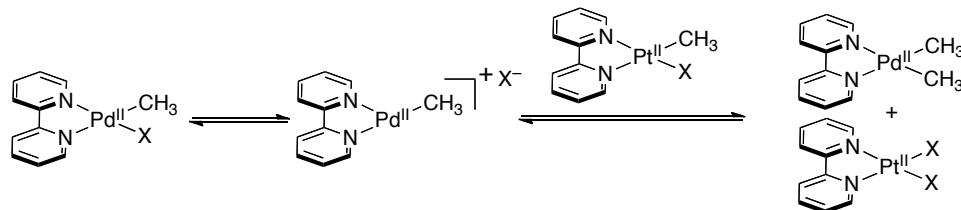
Scheme 5.31 Tandem Palladium and Platinum System for Methane Oligomerization.



Although methyl transfer at Pt^{II} bearing a bpy chelate was shown to be kinetically unfavorable, disproportionation at the analogous Pd^{II} complexes had been achieved.¹⁷ Also, chloride dissociation was calculated to be the largest contributor to $\Delta G_{\text{tot}}^{\ddagger}$ for methyl transfer between platinum centers. In transfer of a methyl to palladium, the palladium methyl complex should be the complex undergoing dissociation of an X-type ligand, which was computed to be more favorable than for the platinum analogue

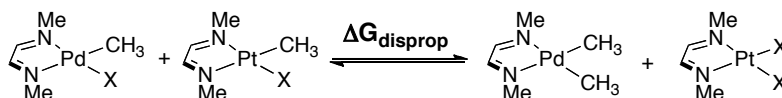
(Scheme 5.32). Based on these observations, it is reasonable to propose that methyl transfer from Pt^{II} to Pd^{II} should be more favorable kinetically than methyl disproportionation between two platinum centers. However, it was unclear whether methyl transfer to generate dimethyl-platinum or dimethyl-palladium would be thermodynamically preferred.

Scheme 5.32 Methyl Transfer from (*t*-Bu-bpy)Pd^{II}(CH₃)Cl to (*t*-Bu-bpy)Pt^{II}(CH₃)Cl.

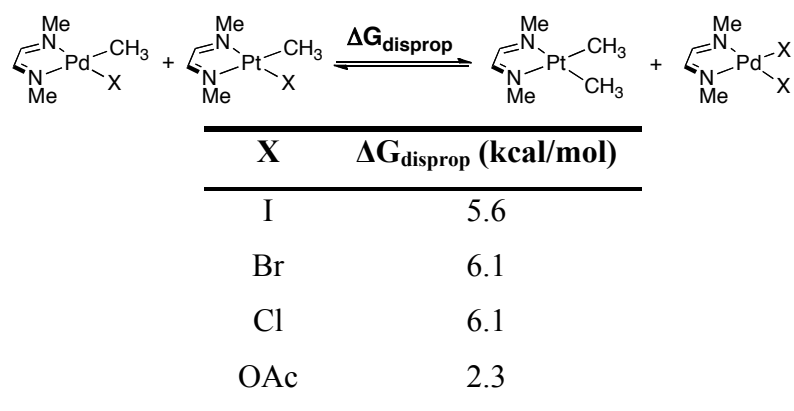


To answer this question, the thermodynamics for formation of a (MeDAB)Pd^{II}(CH₃)₂ (Table 5.4) or a (MeDAB)Pt^{II}(CH₃)₂ (Table 5.5) complex from (MeDAB)Pt^{II}(CH₃)X and (MeDAB)Pd^{II}(CH₃)X were calculated. The computations show that formation of (MeDAB)Pt^{II}(CH₃)₂ is more favorable than formation of (MeDAB)Pd^{II}(CH₃)₂ for all X ligands calculated.

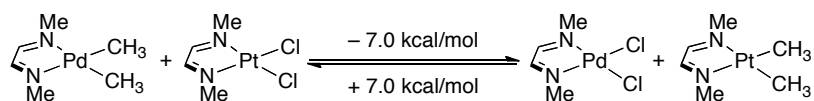
Table 5.4 Methyl Transfer from Pt to Pd to Generate (Me-DAB)Pd(CH₃)₂.



X	$\Delta G_{\text{disprop}}$ (kcal/mol)
I	14.3
Br	13.6
Cl	13.1
OAc	10.3

Table 5.5 Methyl Transfer from Pd to Pt to Generate (Me-DAB)Pt(CH₃)₂.

A comparison of dimethyl and dichloro complexes of palladium and platinum was done by DFT computation to understand the origin of the thermodynamic preference for platinum-dimethyl formation (Scheme 5.33). The (Me-DAB)Pt(CH₃)₂ and (Me-DAB)Pd(Cl)₂ were shown to be 7.0 kcal/mol more favorable than (Me-DAB)Pd(CH₃)₂ and (Me-DAB)Pt(Cl)₂. Presumably, this speaks to the greater thermodynamic stability of (Me-DAB)Pt(CH₃)₂ compared to (Me-DAB)Pd(CH₃)₂ rather than the greater stability of (Me-DAB)Pd(Cl)₂ compared to its platinum analogue.

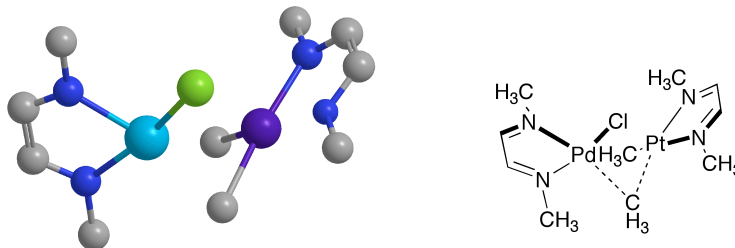
Scheme 5.33 Comparison of Thermodynamic Stability of Pt versus Pd Complexes.

Even though methyl transfer from palladium to platinum was computed to be more thermodynamically favorable than methyl transfer from palladium to platinum, the discussion of methyl transfer kinetics given above suggested methyl transfer to platinum should be kinetically unfavorable. Based on the mechanism above, (L₂)Pt^{II}(CH₃)X would still need to dissociate X ($\Delta G_{\text{dissoc}} = 31.3$ kcal/mol) to allow methyl transfer to occur. However, it was interesting to consider whether transfer of a methyl from palladium to platinum rather than from platinum to platinum would require less energy ($\Delta G_{\text{tot}}^{\ddagger}$).

Calculations of methyl transfer transition states for palladium-to-platinum transfer (TS-II^{Pd-Pt}, Scheme 5.34) and platinum-to-palladium (TS-II^{Pt-Pd}, Scheme 5.35) were

performed as described above for **TS-II^{Pt}** and **TS-II^{Pd}**. Values for ΔG_{dissoc} , ΔG^\ddagger , and $\Delta G_{\text{tot}}^\ddagger$ are tabulated in Table 5.6.

Scheme 5.34 Methyl Transfer Transition State **TS-II^{Pd-Pt}**.



Scheme 5.35 Methyl Transfer Transition State **TS-II^{Pt-Pd}**.

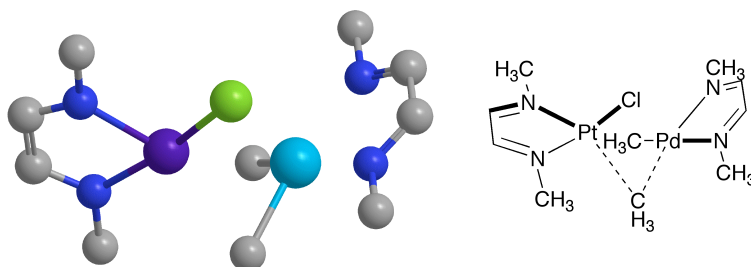


Table 5.6 Transition State Energies from Methyl Transfer between Pd^{II} and Pt^{II}.

Transition State	ΔG_{dissoc} (kcal/mol)	ΔG^\ddagger (kcal/mol)	$\Delta G_{\text{tot}}^\ddagger$ ($\Delta G_{\text{dissoc}} + \Delta G^\ddagger$)
TS-II^{Pd-Pt} (M = Pt, M' = Pd)	31.3	1.4	32.7
TS-II^{Pt-Pd} (M = Pd, M' = Pt)	21.4	17.1	38.5

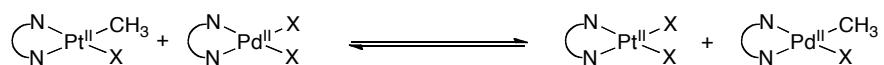
A clear disparity was observed for ΔG^\ddagger . Transfer of a methyl from palladium to platinum (ΔG^\ddagger) was calculated to be 1.4 kcal/mol higher in energy than ΔG_{dissoc} for the Cl- dissociation from platinum. Remarkably, this lowered $\Delta G_{\text{tot}}^\ddagger$ for palladium-to-platinum methyl transfer (32.7 kcal/mol) below $\Delta G_{\text{tot}}^\ddagger$ calculated for methyl transfer

between two palladium centers (33.8 kcal/mol). However, in the desired direction of CH₃ transfer from platinum to palladium, ΔG[‡] is substantially less favorable.

These computational results suggested that disproportionation of (L₂)Pt^{II}(CH₃)X and (L₂)Pd^{II}(CH₃)X would always prefer formation of the (L₂)Pt^{II}(CH₃)₂ over (L₂)Pd^{II}(CH₃)₂. Transition state calculations also indicated transfer of a methyl from palladium to platinum was kinetically favored over methyl transfer from platinum to palladium. However, methyl transfer from platinum to palladium is necessary to take advantage of the ability of platinum(II) to C–H activate methane. Preferential methyl transfer from palladium to platinum would require a palladium catalyst to C–H activate methane and a platinum catalyst to perform C–C coupling. Both of these processes are less favorable than the alternative platinum-mediated C–H activation and the palladium-mediated C–C coupling.

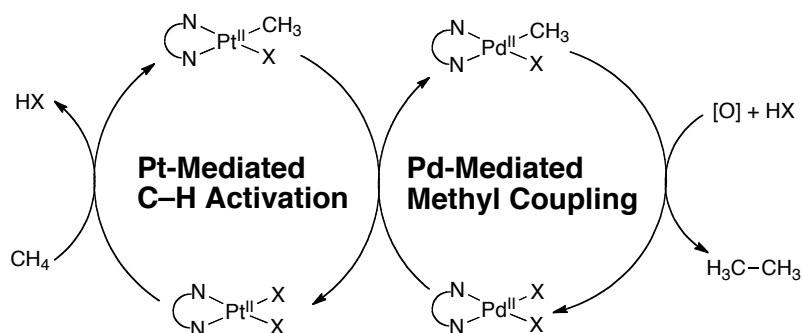
As an alternative to palladium-platinum disproportionation, transfer of a methyl from a monomethyl platinum complex to a Pd(X)₂ species could alleviate the challenges of performing a disproportionative methyl transfer between two monomethyl species (Scheme 5.36). The thermodynamic energy difference between (L₂)Pt^{II}(CH₃)X versus (L₂)Pd^{II}(CH₃)X is expected to be less than the related difference between (L₂)Pt^{II}(CH₃)₂ versus (L₂)Pd^{II}(CH₃)₂ because the additional stability of the Pt–CH₃ bond is imparted on only one CH₃ group rather than two. This could allow a significant equilibrium concentration of (L₂)Pd^{II}(CH₃)X to be generated.

Scheme 5.36 Methyl Transfer from (L₂)Pt^{II}(CH₃)X to (L₂)Pd^{II}(X)₂.



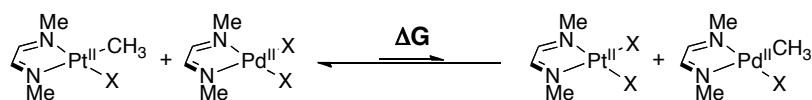
If methyl transfer from Pt to Pd were achieved, one could envision the dual catalyst system pictured in Scheme 5.37. In this proposed system, a Pt^{II} catalyst C–H activates methane to form a Pt-monomethyl complex. Then platinum transfers a CH₃ group to a Pd^{II}(X)₂ catalyst from which ethane is generated via a one-electron oxidation.

Scheme 5.37 Tandem Palladium and Platinum System for Methane Oligomerization.



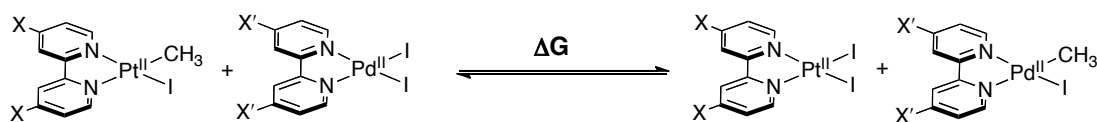
Based on the discussion of $(\text{MeDAB})\text{Pt}^{\text{II}}(\text{CH}_3)_2$ versus $(\text{MeDAB})\text{Pd}^{\text{II}}(\text{CH}_3)_2$ stability given above, we expected an equilibrium of $(\text{MeDAB})\text{Pt}^{\text{II}}(\text{CH}_3)\text{X}$ versus $(\text{MeDAB})\text{Pd}^{\text{II}}(\text{CH}_3)\text{X}$ to favor the $(\text{MeDAB})\text{Pt}^{\text{II}}(\text{CH}_3)\text{X}$. Indeed calculations of methyl transfer between $(\text{MeDAB})\text{Pt}^{\text{II}}(\text{CH}_3)\text{X}$ and $(\text{MeDAB})\text{Pd}^{\text{II}}(\text{X})_2$ showed thermodynamic preference for the platinum-monomethyl complex (Table 5.7).

Table 5.7 Methyl Transfer from $(\text{MeDAB})\text{Pt}^{\text{II}}(\text{CH}_3)\text{X}$ to $(\text{MeDAB})\text{Pd}^{\text{II}}(\text{X})_2$.



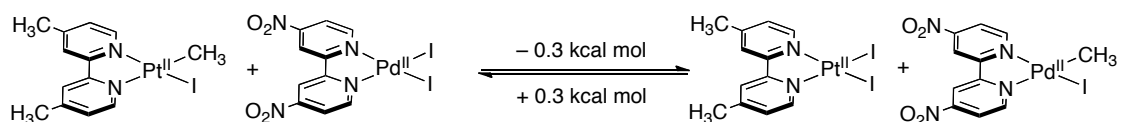
X	$\Delta G_{\text{disprop}}$ (kcal/mol)
I	2.5
Br	1.5
Cl	1.4
OAc	2.2

We reasoned that modification of the ancillary chelating ligand could shift the equilibrium in favor of a palladium-monomethyl species. In particular, we hypothesized that varying the electronics of the complexes could shift the equilibrium in favor of forming $(\text{L}_2)\text{Pd}(\text{CH}_3)\text{X}$. In order to modify the electronics of the ligand, we chose to switch from the MeDAB model system to a 2,2'-bipyridine system so that the 4 and 4' positions of the bpy ligand could be substituted with electronically diverse substituents (Table 5.8). Table 5.8 summarizes DFT calculations of the thermodynamics of methyl transfer between Pt and Pd with electronically diverse bipyridine ligands.

Table 5.8 Methyl Transfer from (X-bpy)Pt^{II}(CH₃)I to (X'-bpy)Pd^{II}(I)₂.

X	X'	$\Delta G_{\text{disprop}}$ (kcal/mol)
NO ₂	CH ₃	6.3
H	CH ₃	4.0
H	H	2.7
CH ₃	H	1.8
CH ₃	NO ₂	-0.3

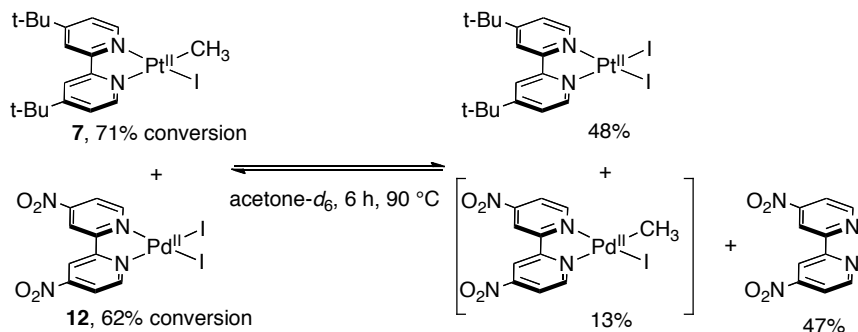
The calculations suggested that electron donating ligands on platinum and electron withdrawing ligands on palladium should give the most favorable thermodynamics for palladium-monomethyl formation. Indeed, the calculated equilibrium between (NO₂-bpy)Pd^{II}(CH₃)I (NO₂-bpy = 4,4'-dinitro-2,2'-bipyridine) and (CH₃-bpy)Pt^{II}(CH₃)I (CH₃-bpy = 4,4'-dimethyl-2,2'-bipyridine) favors (NO₂-bpy)Pd^{II}(CH₃)I (Scheme 5.38).

Scheme 5.38 Methyl Transfer from (CH₃-bpy)Pt^{II}(CH₃)I to (NO₂-bpy)Pd^{II}(I)₂.

To confirm the findings of the calculations, (NO₂-bpy)Pd^{II}(I)₂ (**12**) was synthesized and reacted with (^tBu-bpy)Pt^{II}(CH₃)I (**7**) (Scheme 5.39). In acetone-*d*₆, **12** and **7** were reacted at 25 °C, and the reaction was monitored by ¹H NMR spectroscopy. No reaction occurred over the course of 24 h under these conditions. Reaction at 50 °C for 17 h gave minimal conversion. However, a new methyl resonance was observed as a shoulder to one of the Pt-CH₃ satellite peaks. The solution was further heated to 90 °C, and after 6 h, a new methyl peak was observed at 0.952 ppm (13% yield). This was tentatively assigned to (NO₂-bpy)Pd^{II}(CH₃)I. Significant decomposition occurred during the reaction. The mass balance of platinum complexes (the sum of **7** and (^tBu-

bpy)Pt^{II}(I)₂) was only 77%. Free NO₂-bpy was observed in 47% yield, indicating nearly half of **12** decomposed over the course of the reaction. To further confirm the identity of new species observed by ¹H NMR spectroscopy, attempts were made to independently synthesize (NO₂-bpy)Pd^{II}(CH₃)I. However, unfortunately these synthetic efforts were unsuccessful.

Scheme 5.39 Methyl Transfer from (^tBu-bpy)Pt(CH₃)I to (NO₂-bpy)Pd(I)₂.

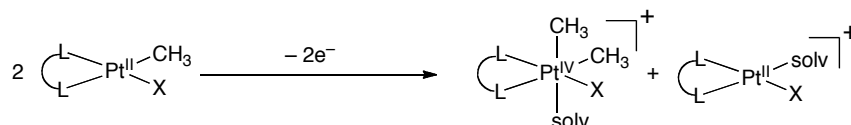


Fundamentally, the transfer of CH₃ from platinum to palladium could allow access to a dual catalyst system for oxidative oligomerization of methane. However, based on these studies, CH₃ transfer between the two metals is limited by the thermodynamic preference for methyl coordination to platinum rather than palladium and by the poor kinetics associated with transfer of a CH₃ to/from platinum. Unfavorable X-type ligand dissociation from platinum was proposed to be the major contributor to the kinetic stability of platinum complexes toward methyl transfer. As an alternative, methyl transfer from a (^tBu-bpy)Pt^{II}(CH₃)X complex to (L₂)Pd^{II}(X)₂ was considered. Calculations indicated that such reactions between platinum bearing electron-donating ligands and palladium bearing electron-withdrawing ligands would have favorable thermodynamics for transfer of CH₃ to palladium. The reaction of (^tBu-bpy)Pt^{II}(CH₃)I and (NO₂-bpy)Pd^{II}(I)₂ provided tentative evidence for the formation of (NO₂-bpy)Pd^{II}(CH₃)I and suggested that modification of the metal electronics could overcome the inherent preference for CH₃ binding to platinum.

5.2.3 Synthesis and One-Electron Oxidation of Monomethyl-Pt^{II} Complexes

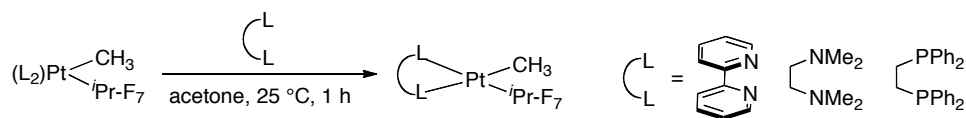
Methyl transfer from platinum to platinum and platinum to palladium were reactions that were solely controlled by the thermodynamics and kinetics associated with transfer of the methyl group. Alternatively, in Chapters 3 and 4, one-electron oxidation was shown to be an efficient method for inducing methyl transfer. To further study platinum in context of methane oligomerization, an efficient method for methyl transfer must be uncovered, and so we turned to one-electron oxidation of platinum-methyl complexes as another means of promoting methyl transfer (Scheme 5.40). Complexes of palladium with the general formula (^tBu-bpy)Pd^{II}(CH₃)X were shown to evolve ethane upon one-electron oxidation (Chapter 4). Specifically complexes where X = OAc, CF₃ gave the most promising results for CH₃ transfer and subsequent elimination of ethane. In light of these results, complexes of monomethyl-platinum with the general formula (L₂)Pt^{II}(CH₃)X (X = OAc, CF₃) were synthesized for study in oxidatively-induced methyl transfer.

Scheme 5.40 Methyl Transfer at Platinum Induced by One-Electron Oxidation.

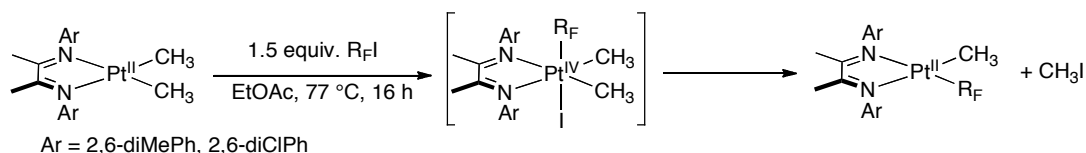


(^tBu-bpy)Pt^{II}(CH₃)OAc (**8**) was synthesized as described above. Syntheses of monomethyl platinum perfluoroalkyl complexes were accomplished by one of two methods (Scheme 5.41). In Method 1, (L₂)Pt^{II}(CH₃)(R_F) (R_F = perfluoroalkyl group, L₂ = labile chelating ligand) complexes were synthesized. The L₂ ligands were then substituted with the desired chelating ligand. For Method 2, (ArDAB)Pt^{II}(CH₃)(R_F) complexes, (ArDAB)Pt^{II}(CH₃)₂ complexes were reacted with a perfluoroalkyl iodide [2-heptafluoropropyl iodide (ⁱPr-F₇I) or 1-nonafluorobutyl iodide (ⁿBu-F₉I)] according to the procedure of Hughes (Method 2, Scheme 5.42).⁴⁶ These latter reactions proceeded via oxidative addition to (ArDAB)Pt^{II}(CH₃)₂ to give (ArDAB)Pt^{IV}(CH₃)₂(ⁱPr-F₇)I followed by reductive elimination of CH₃I.

Scheme 5.41 Synthesis of Platinum-Perfluoroalkyl Complexes by Ligand Displacement.

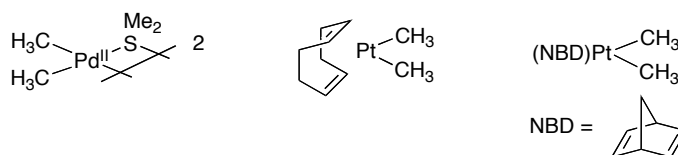


Scheme 5.42 Reaction of (ArDAB)Pt^{II}(CH₃)₂ with Perfluoroalkyl Iodides.⁴⁶



Method 1 required initial synthesis of (L₂)Pt^{II}(CH₃)(R_F) precursor complexes, where L₂ could be easily displaced by desired ligands. For related (L₂)Pt^{II}(CH₃)₂ ligand substitution reactions these precursor complexes bear L₂ ligands such as L₂ = 2 x μ-S(CH₃)₂ or diolefin (Scheme 5.43).^{47,48} Related complexes (NBD)Pt^{II}(CH₃)(CF₃) (**13**)⁴⁹ and (COD)Pt^{II}(CH₃)(ⁿBu-F₉) (**14**)⁵⁰ had previously been synthesized, but only **13** had been used in ligand substitution reactions (Scheme 5.44).

Scheme 5.43 (L₂)Pt^{II}(CH₃)₂ Complexes Used for Ligand Substitution Reactions.



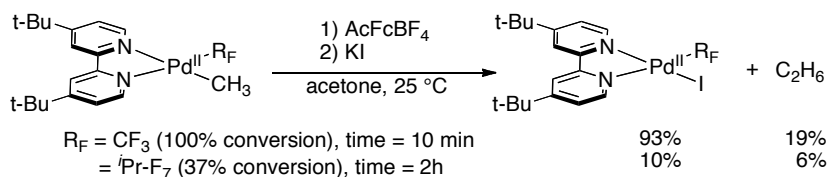
Scheme 5.44 (L₂)Pt^{II}(CH₃)(R_F) Complexes Utilized in Ligand Exchange.



Initially, it was important to synthesize Pt–CF₃ complexes based on the results of related palladium-R_F complexes. In Chapter 4, it was shown that change of R_F from CF₃ to ^tPr-F₇ in the oxidation of (^tBu-bpy)Pd^{II}(CH₃)(R_F) with one-electron oxidant acetylferrocenium tetrafluoroborate (AcFcBF₄) led to lower conversion over longer time (Scheme 5.45). Over 2 h, only 37% of the ^tPr-F₇ complex was converted to 6% of ethane. In contrast, for the CF₃ complex, 100% conversion was observed within 10

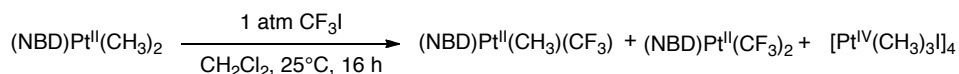
minutes to give 19% yield of ethane. In these reactions, the maximum theoretical yield of ethane was equal to 50% of the conversion of the starting material, because two molecules of starting complex were required to produce one molecule of ethane.

Scheme 5.45 Effect of Perfluoroalkyl Group in One-Electron Oxidation of Pd^{II}.



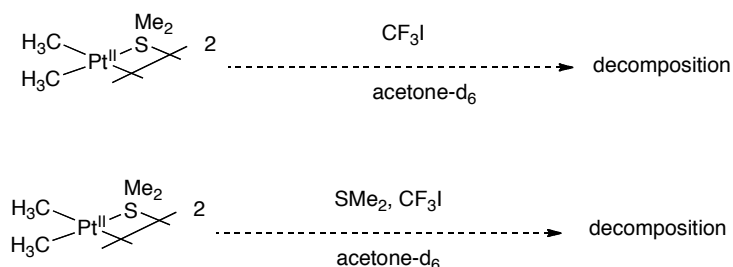
The palladium results suggested initial efforts to synthesize Pt^{II}-R_F complexes should focus on generating Pt^{II}-R_F complexes where R_F = CH₃ rather than larger perfluoroalkyl groups. In the report of the synthesis of **13**, (NBD)Pt^{II}(CH₃)₂ was reacted under 1 atm of gaseous CF₃I in a sealed tube.⁴⁹ Complex **13** was isolated as an intermediate in the formation of (NBD)Pt^{II}(CF₃)₂ (**15**) as a mixture of Pt^{II} products (Scheme 5.46). The mixture included (NBD)Pt^{II}(CH₃)₂, **13**, **15**, and platinum tetramer [Pt^{IV}(CH₃)₃I]₄ that results from the oxidative addition of the methyl iodide byproduct to the starting dimethyl-platinum complex. Subsequent isolation produced a low yield (11%) of **13**. In my hands, isolation of clean samples of **13** could not be obtained.

Scheme 5.46 Products of Oxidation of (NBD)Pt^{II}(CH₃)₂ with CF₃I.⁴⁹



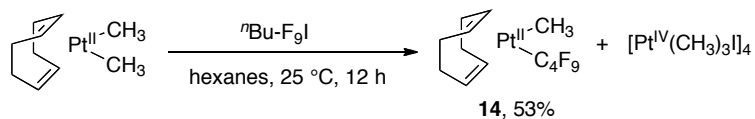
Attempts to synthesize (SMe₂)₂Pt^{II}(CH₃)(CF₃) were carried out using similar methods on a small scale in a J. Young NMR tube (Scheme 5.47). Monitoring the reactions by ¹H NMR spectroscopy always indicated the decomposition of the starting dimethyl-platinum complex without concurrent growth of any resonances indicative of new Pt^{II}-CH₃ complexes.

Scheme 5.47 Attempted Syntheses of $(\text{SMe}_2)_2\text{Pt}^{\text{II}}(\text{CH}_3)(\text{CF}_3)$.



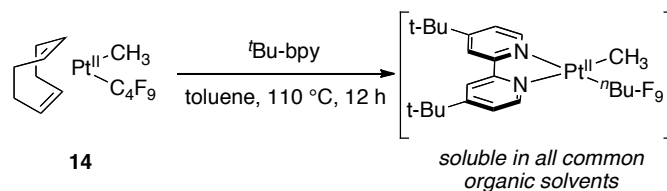
Without a successful route to a $(\text{L}_2)\text{Pt}^{\text{II}}(\text{CH}_3)(\text{CF}_3)$ precursor complex, further synthetic efforts were aimed toward preparation of $(\text{L}_2)\text{Pt}^{\text{II}}(\text{CH}_3)(\text{R}_\text{F})$ complexes where $\text{R}_\text{F} = {}^n\text{Bu-F}_9$ or ${}^i\text{Pr-F}_7$. $(\text{COD})\text{Pt}^{\text{II}}(\text{CH}_3)({}^n\text{Bu-F}_9)$ (**14**) was synthesized by the method of Hughes (Scheme 5.48).⁵⁰ $(\text{COD})\text{Pt}^{\text{II}}(\text{CH}_3)_2$ was reacted with 1.5 equiv of ${}^n\text{Bu-F}_9\text{I}$ at 25 °C for 12 h to produce **14** and $[\text{Pt}^{\text{IV}}(\text{CH}_3)_3\text{I}]_4$. As with synthesis of **13**, $[\text{Pt}^{\text{IV}}(\text{CH}_3)_3\text{I}]_4$ was formed by reaction of the CH_3I byproduct with the starting material followed by displacement of the COD ligand.

Scheme 5.48 Synthesis of $(\text{COD})\text{Pt}^{\text{II}}(\text{CH}_3)({}^n\text{Bu-F}_9)$ (**14**).⁵⁰

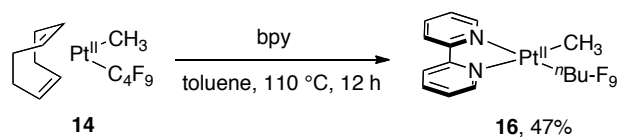


Reaction of **14** with ${}^t\text{Bu-bpy}$ in toluene at 110 °C for 1 h produced a new complex that could not be isolated in solid form (Scheme 5.49). When reacting **14** with 2,2'-bipyridine (bpy) instead, a yellow solid precipitated from solution after 12 h of reaction time (Scheme 5.50). Addition of pentanes further precipitated the product, and $(\text{bpy})\text{Pt}^{\text{II}}(\text{CH}_3)({}^n\text{Bu-F}_9)$ (**16**) could be isolated in 47% yield.

Scheme 5.49 Attempted Synthesis of $({}^t\text{Bu-bpy})\text{Pt}^{\text{II}}(\text{CH}_3)({}^n\text{Bu-F}_9)$.



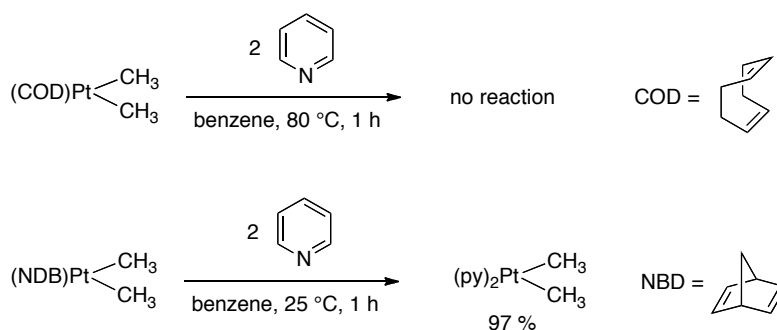
Scheme 5.50 Synthesis of (bpy)Pt^{II}(CH₃)(ⁿBu-F₉) (**16**).



Attempts to synthesize (4-MePhDAB)Pt^{II}(CH₃)(ⁿBu-F₉) by reacting **14** with 4-MePhDAB in a related procedure resulted in decomposition of both ligand and the precursor complex without concurrent formation of (4-MePhDAB)Pt^{II}(CH₃)(ⁿBu-F₉). From this result, it was deduced that COD bound **14** too tightly to be used as a general precursor for synthesis of a diverse series of (L₂)Pt^{II}(CH₃)(R_F) complexes.

In order to synthesize a more general (L₂)Pt^{II}(CH₃)(R_F) precursor complex, it was important to identify an L₂ ligand that could more easily be substituted from platinum. Marks described a comparative study of (COD)Pt^{II}(CH₃)₂ versus (NBD)Pt(CH₃)₂ (NBD = 2,5-norbornadiene) in the synthesis of (py)₂Pt^{II}(CH₃)₂ (py = pyridine, Scheme 5.51).⁵¹ In his study, pyridine did not displace COD even at 80 °C for 1 h in benzene. However, when (NBD)Pt^{II}(CH₃)₂ was used as the starting complex (py)₂(Pt)(CH₃)₂ could be isolated in 97% yield under mild conditions.

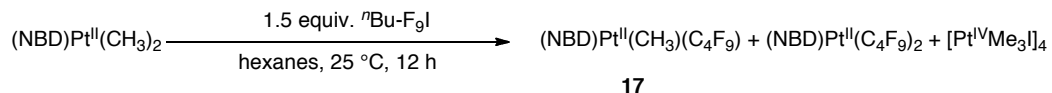
Scheme 5.51 Comparative Study of “Pt^{II}(CH₃)₂” Donors in Synthesis of (py)₂Pt^{II}(CH₃)₂.⁵¹



Based on this precedent, synthesis of (NBD)Pt^{II}(CH₃)(ⁿBu-F₉) (**17**) was undertaken. Using conditions optimized by Hughes for synthesis of (COD)Pt^{II}(CH₃)(ⁿBu-F₉) (**14**), (NBD)Pt^{II}(CH₃)₂ was reacted with 1.5 equivalents of ⁿBu-F₉I in hexanes at 25 °C for 12 h (Scheme 5.52). The resulting reaction mixture contained **17**, (NBD)Pt^{II}(ⁿBu-F₉)₂, and [Pt^{IV}(CH₃)₃I]₄, all methods of isolation attempted led to a

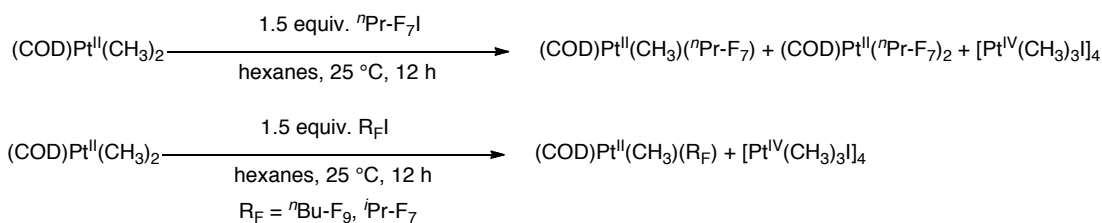
mixture of **17** and $(\text{NBD})\text{Pt}^{\text{II}}(^n\text{Bu-F}_9)_2$. Further reactions with fewer equivalents of $^n\text{Bu-F}_9$ provided the same mixture of products as well as unreacted $(\text{NBD})\text{Pt}^{\text{II}}(\text{CH}_3)_2$. These results show that by changing the COD ligand of $(\text{COD})\text{Pt}^{\text{II}}(\text{CH}_3)_2$ to NBD, the oxidative addition/reductive elimination sequence became unselective, forming a mixture of mono- and di-perfluoroalkylated products.

Scheme 5.52 Attempted Synthesis of $(\text{NBD})\text{Pt}^{\text{II}}(\text{CH}_3)(^n\text{Bu-F}_9)$ (**17**).



A previous study of the oxidative addition of perfluoroalkyl iodides to $(\text{COD})\text{Pt}^{\text{II}}(\text{CH}_3)_2$ indicated that sterics of the perfluoroalkyl iodide had an affect on the distribution of products (Scheme 5.53).⁵² The study showed that $^n\text{Pr-F}_7\text{I}$ gives a mixture of $(\text{COD})\text{Pt}^{\text{II}}(^n\text{Pr-F}_7)_2$ and $(\text{COD})\text{Pt}^{\text{II}}(\text{CH}_3)(^n\text{Pr-F}_7)$. However reaction with $^i\text{Pr-F}_7\text{I}$ and $^n\text{Bu-F}_7\text{I}$ selectively affords the monoperfluoroalkylated product, $(\text{COD})\text{Pt}^{\text{II}}(\text{CH}_3)(\text{R}_\text{F})$ ($\text{R}_\text{F} = ^i\text{Pr-F}_7$ or $^n\text{Bu-F}_7$ respectively). This study suggested that use of a larger perfluoroalkyl iodide might selectively give $(\text{NBD})\text{Pt}^{\text{II}}(\text{CH}_3)(\text{R}_\text{F})$ in the reaction of $(\text{NBD})\text{Pt}^{\text{II}}(\text{CH}_3)_2$ with $\text{R}_\text{F}\text{I}$.

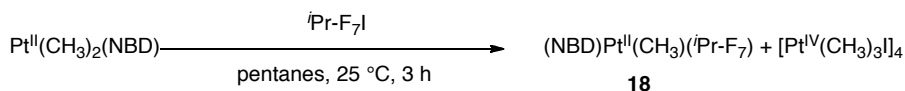
Scheme 5.53 Study of Sterics of $\text{R}_\text{F}\text{I}$ on Product Distribution in $(\text{COD})\text{Pt}^{\text{II}}(\text{CH}_3)_2 + \text{R}_\text{F}\text{I}$.



As anticipated, the reaction of $(\text{NBD})\text{Pt}^{\text{II}}(\text{CH}_3)_2$ with $^i\text{Pr-F}_7\text{I}$ in pentanes at 25 °C for 3 h selectively afforded $(\text{NBD})\text{Pt}^{\text{II}}(\text{CH}_3)(^i\text{Pr-F}_7)$ (**18**) along with $[\text{Pt}^{\text{IV}}(\text{CH}_3)_3\text{I}]_4$ (Scheme 5.54). Previously reported produces for the isolation of the related $(\text{COD})\text{Pt}(\text{CH}_3)(\text{R}_\text{F})$ complexes suggested that filtration of the pentanes solution is sufficient to remove $[\text{Pt}^{\text{IV}}(\text{CH}_3)_3\text{I}]_4$. However in my hands, multiple filtrations, even at low temperature, were insufficient for removal of $[\text{Pt}^{\text{IV}}(\text{CH}_3)_3\text{I}]_4$. Ultimately, removal of

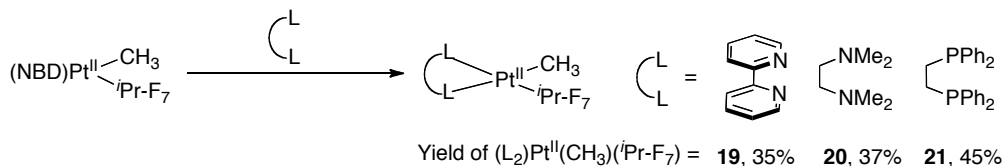
$[\text{Pt}^{\text{IV}}(\text{CH}_3)_3\text{I}]_4$ was accomplished by converting the tetramer into $[\text{Pt}(\text{CH}_3)_3\text{OTf}]_4$ by reaction with AgOTf in benzene. The benzene solution was then extracted with H_2O three times to afford a benzene solution containing pure $(\text{NBD})\text{Pt}(\text{CH}_3)(^i\text{Pr-F}_7)$ (**18**). Concentration of the solution followed by freeze-drying the benzene solvent yielded the desired product as a white powder in 71% yield.

Scheme 5.54 Synthesis of $(\text{NBD})\text{Pt}^{\text{II}}(\text{CH}_3)(^i\text{Pr-F}_7)$ (**18**).



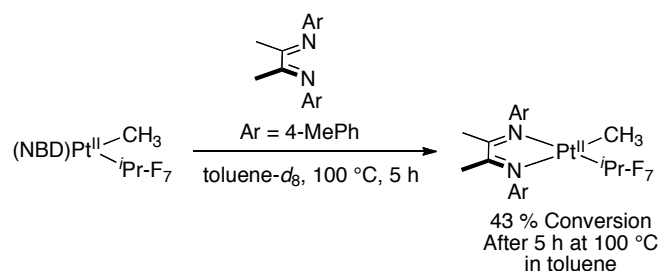
Reaction of **18** with dppe (1,2-bis(diphenylphosphino)ethane), TMEDA (N,N,N',N'-tetramethylethylenediamine), or bpy afforded the related $(\text{L}_2)\text{Pt}^{\text{II}}(\text{CH}_3)(^i\text{Pr-F}_7)$ complexes (Scheme 5.55). Substitution of NBD by bpy (1 h) and TMEDA (20 h) was undertaken in toluene at 110 °C. The ligand dppe substituted NBD over 1 h at 30 °C in acetone.

Scheme 5.55 Displacement of NBD by Chelating Ligands.



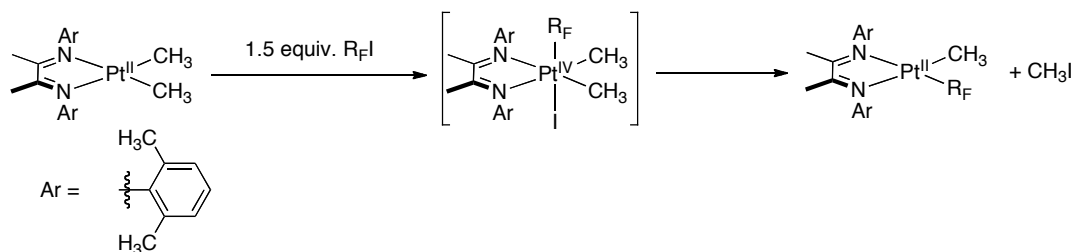
To further test the lability of norbornadiene, $(\text{NBD})\text{Pt}(\text{CH}_3)(^i\text{Pr-F}_7)$ was reacted with the diimine 4-MePhDAB in an NMR tube (Scheme 5.56). A toluene- d_8 solution of **18** and 4-MePhDAB reacted slowly over 5 h at 100 °C to give a new species consistent by ^1H NMR with formation of $(4\text{-MePhDAB})\text{Pt}(\text{CH}_3)(^i\text{Pr-F}_7)$ (**22**) in an 1.3:1 ratio of **18:22**. However prolonged heating did not change the ratio substantially. So while **18** allowed synthesis of a number of $(\text{L}_2)\text{Pt}^{\text{II}}(\text{CH}_3)(^i\text{Pr-F}_7)$ complexes under mild conditions, NBD was still not labile enough for the clean synthesis of platinum complexes of ArDAB ligands.

Scheme 5.56 Reaction of (NBD)Pt^{II}(CH₃)(ⁱPr-F₇) (**18**) with 4-MePhDAB.

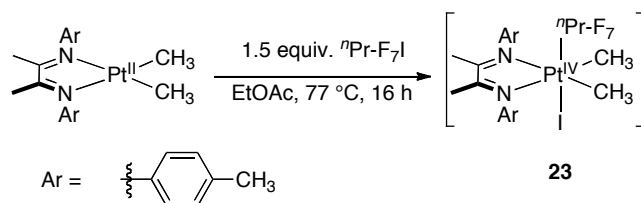


Method 2 is an alternative pathway for the preparation of (ArDAB)Pt(CH₃)(R_F) complexes (Scheme 5.57). Hughes reported this reaction to be limited to ArDAB ligands where the aryl substituents are substituted in the 2 and 6 positions. Reaction of the less sterically congested 4-methyl substituted complex (4-MePhDAB)Pt^{II}(CH₃)₂ with perfluoroalkyl iodides gave only the Pt^{IV} complex, (4-MePhDAB)Pt^{IV}(CH₃)₂(R_F)I (**23**) (Scheme 5.58). Attempts to induce reductive elimination resulted in no reaction or decomposition of **23**. Thus Method 2 is limited to ligands with steric bulk positioned about the Pt center and was not suitable for the complexes prepared by Method 1 without requiring additional synthetic steps.⁵³

Scheme 5.57 Oxidative Addition of R_FI to (ArDAB)Pt^{II}(CH₃)₂.



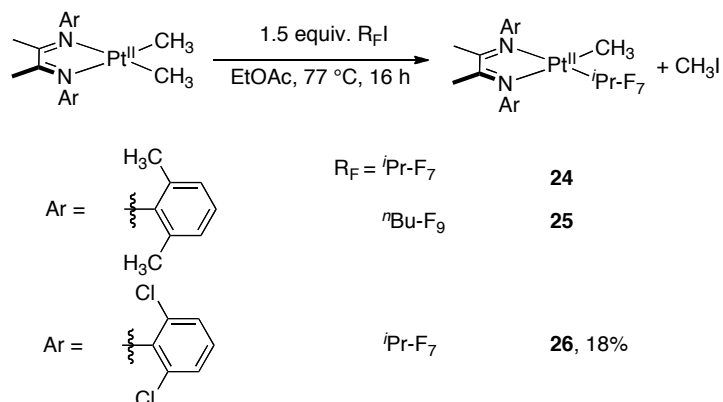
Scheme 5.58 Oxidative addition of R_FI to (4-MePhDAB)Pt^{II}(CH₃)₂.⁴⁶



The complexes (2,6-diMePhDAB)Pt^{II}(CH₃)(ⁱPr-F₇) (**24**), (2,6-diMePhDAB)Pt^{II}(CH₃)(ⁿBu-F₉) (**25**), and (2,6-diClPhDAB)Pt^{II}(CH₃)(ⁱPr-F₇) (**26**) were synthesized by Hughes' procedure (Scheme 5.59). Refluxing (2,6-

diMePhDAB)Pt^{II}(CH₃)₂ or (2,6-diClPhDAB)Pt^{II}(CH₃)₂ with ⁱPr-F₇I or ⁿBu-F₉ in dry ethyl acetate afforded the perfluoroalkyl complexes. Complexes **24** and **25** could not be isolated cleanly. Complex **26** was isolated in 18% yield.

Scheme 5.59 Syntheses of (ArDAB)Pt^{II}(CH₃)(R_F) Complexes, **24**, **25**, and **26**.



With an array of (L₂)Pt^{II}(CH₃)(X) complexes in hand we next sought to examine methyl transfer via one-electron oxidation (Scheme 5.60). The expected products based on one-electron oxidation of (L₂)M^{II}(CH₃)₂ (M = Pd, Pt)^{18,24} were either a 1:1 mixture of [(L₂)Pt^{IV}(CH₃)₂(X)(solvent)]⁺ and [(L₂)Pt^{II}(X)(solvent)]⁺ or a 1:2 mixture of ethane and [(L₂)Pt^{II}(X)(solvent)]⁺. A screen of one-electron oxidants, solvents, and conditions was performed in J. Young NMR tubes. The results of these reactions were determined by ¹H NMR spectroscopic analysis. Table 5.9 summarizes the oxidants, their abbreviations, and their oxidation potentials relative to Fc/Fc⁺ in acetonitrile.⁵⁴ Scheme 5.61 summarizes all of the (L₂)Pt^{II}(CH₃)(X) complexes examined.

Scheme 5.60 Expected Products of One-Electron Oxidation of (L₂)Pt^{II}(CH₃)(X).

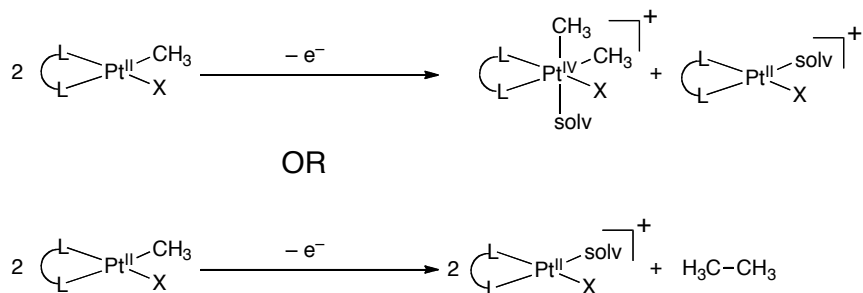
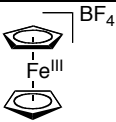
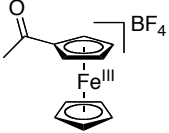
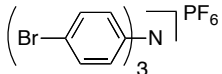
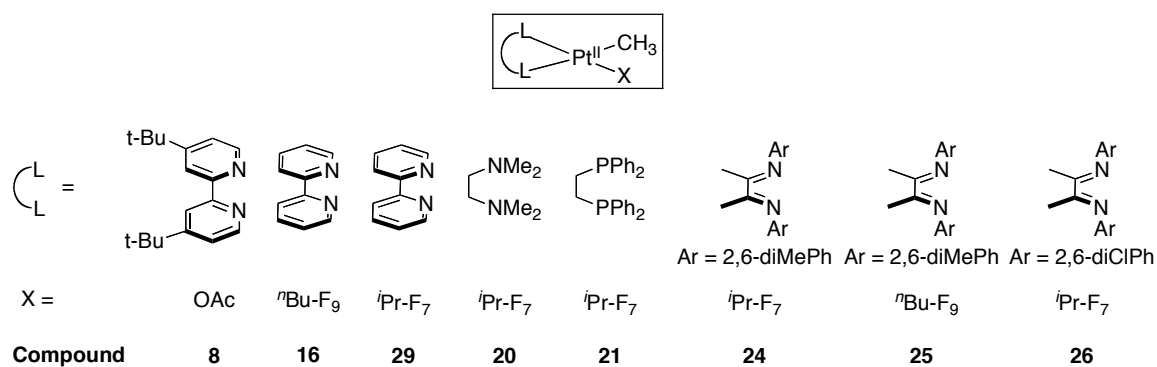


Table 5.9 Oxidation Potentials of One-Electron Oxidants Employed.

Oxidant	Abbreviation	Oxidation Potential (V, vs. Fc/Fc ⁺ in MeCN)
	FcBF ₄	0.0
	AcFcBF ₄	0.27
	(Ar) ₃ NPF ₆	0.67
(NH ₄) ₂ Ce ^{IV} (NO ₃) ₆	CAN	0.88 ^a

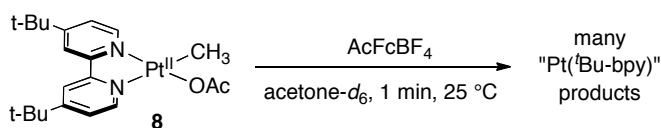
^a oxidation potential determined in H₂O**Scheme 5.61** Summary of all (L₂)Pt^{II}(CH₃)(X) Complexes Synthesized.

For means of comparison, oxidatively-induced methyl transfer at (^tBu-bpy)Pd^{II}(CH₃)₂ (**27**)¹⁸ and (4-MePhDAB)Pt^{II}(CH₃)₂ (**28**)²⁴ were both achieved by oxidation with FcBF₄ under mild conditions. Palladium complex **27** reacted at 25 °C within seconds and platinum complex **28** reacted at 55 °C over only 30 s. In Chapter 4, (^tBu-bpy)Pd^{II}(CH₃)OAc also reacted within seconds at 25 °C but with the stronger oxidant AcFcBF₄. Of the (L₂)Pt^{II}(CH₃)(R_F) complexes screened, only **8** and **16** reacted at room temperature with ferrocene-based oxidants.

Oxidation of **8** with AcFcBF₄ in acetone-*d*₆, dichloromethane-*d*₂, and acetonitrile-*d*₃ produced immediate and quantitative decomposition of **8** (Scheme 5.62). ¹H NMR

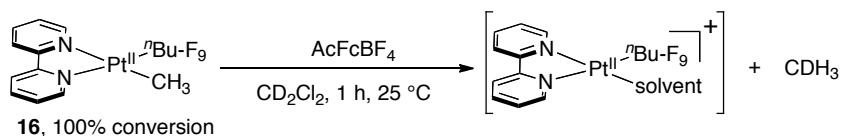
spectroscopic analysis indicated many “(^tBu-bpy)Pt” products were formed, but no Pt–CH₃ resonances were observed. Mass spectrometric analysis showed no evidence for the expected complex [(L₂)Pt^{IV}(CH₃)₂OAc(solvent)]⁺, and neither ethane nor methane were observed.

Scheme 5.62 Reaction of (^tBu-bpy)Pt^{II}(CH₃)OAc with AcFcBF₄.

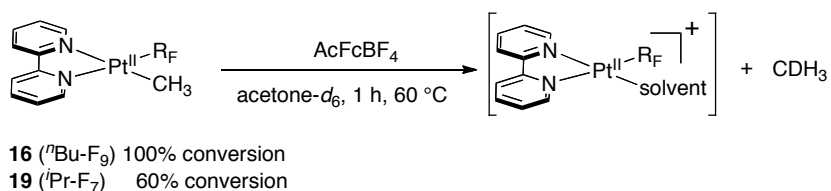


Similarly, complete decomposition of **16** was observed over 1 h at 25 °C when reacted with AcFcBF₄ in dichloromethane-*d*₂ (Scheme 5.63). At the end of the reaction, no Pt–CH₃ resonances were observed, but a trace of methane was detected. In contrast, bpy complex **19** did not react at all at 25 °C. The only difference between **16** and **19** was the perfluoroalkyl group attached to platinum. In **16** R_F = ⁿBu-F₉, and in **19** R_F = ⁱPr-F₇. When compared directly in acetone-*d*₆, **16** and **19** reacted with AcFcBF₄ at 60 °C over 1 h to give 100% conversion and 60% conversion respectively (Scheme 5.64). However, in both reactions no Pt–CH₃ product or ethane resonances were observed, and trace CDH₃ was observed in each case. By ¹H NMR, the platinum products were consistent with [(bpy)Pt^{II}(R_F)(solvent)]⁺, but the identities of the products were unable to be confirmed by mass spectral analysis.

Scheme 5.63 Reaction of **16** with AcFcBF₄ in Dichloromethane-*d*₂.

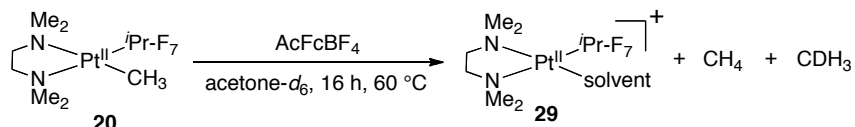


Scheme 5.64 Comparative Oxidation of (bpy)Pt^{II}(CH₃)R_F Complexes **16** and **19**.



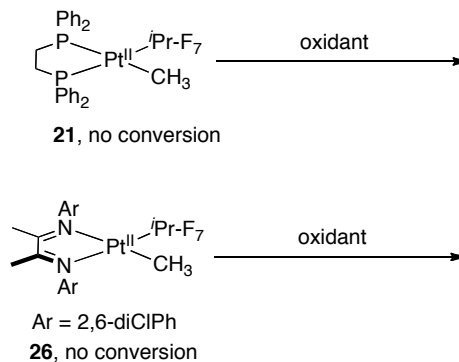
TMEDA complex **20** decomposed less than 10% when reacted with FcBF₄ in acetone-*d*₆ over three days at 60 °C or 1 h at 100 °C. However, **20** reacted similarly to **19** with AcFcBF₄ at 60 °C of 16 h (Scheme 5.65). Starting material was completely converted to give CH₄, CDH₃, and [(TMEDA)Pt^{II}(*i*Pr-F₇)(solvent)]⁺ (**29**) as determined by ¹H NMR and mass spectral analyses, but no ethane was observed.

Scheme 5.65 One-Electron Oxidation of (TMEDA)Pt^{II}(CH₃)(*i*Pr-F₇) (**20**).



The two heptafluoropropyl complexes **21** (L₂ = dppe) and **26** (L₂ = 2,6-diClPhDAB) were completely stable to all oxidation conditions examined (Scheme 5.66). Reaction of **21** with FcBF₄ in acetone-*d*₆ over 3 days at 60 °C or 1 h at 100 °C gave no conversion of starting material. In both acetone-*d*₆ and dichloromethane-*d*₂, **21** and **26** were completely stable over 16 h at 60 °C.

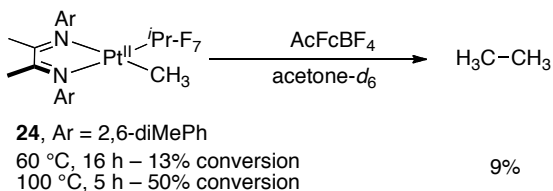
Scheme 5.66 Stability of (dppe)Pt^{II}(CH₃)(*i*Pr-F₇) (**21**) and (2,6-diClPhDAB)Pt^{II}(CH₃)(*i*Pr-F₇) (**26**) to Oxidation.



When reacted with AcFcBF₄ at 60 °C for 16 h in acetone-*d*₆, 2,6-diMePhDAB complex **24** decomposed by 13% to give 9% ethane (Scheme 5.67). Notably, the maximum possible yield of ethane at 13% conversion should be 7%. It is unclear whether an impurity observed in the starting complex decomposed under these conditions to produce the observed ethane in addition to or in lieu of complex **24**. Heating **24** to 100

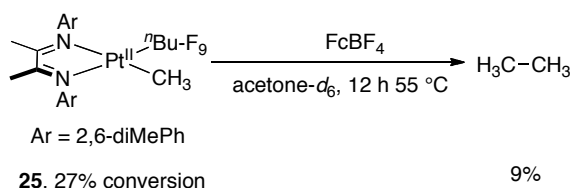
°C with AcFcBF₄, under otherwise identical reaction conditions gave 50% conversion over 5 h, but the yield of ethane remained 9%.

Scheme 5.67 Reaction of (2,6-diMePhDAB)Pt^{II}(CH₃)(ⁱPr-F₇) (**24**) with AcFcBF₄.



In comparison, (2,6-diMePhDAB)Pt^{II}(CH₃)(ⁿBu-F₉) (**25**) reacted with FcBF₄ at 55 °C over 12 h (Scheme 5.68). Complex **25** (27% conversion) reacted to give 9% ethane. Notably, the maximum possible yield of ethane at 27% conversion should be 14%. No new Pt–CH₃ or ⁿBu-F₉ peaks were observed. In the absence of FcBF₄, 100% **25** was observed after 12 h at 55 °C, and no ethane was formed.

Scheme 5.68 Reaction of (2,6-diMePhDAB)Pt^{II}(CH₃)(ⁿBu-F₉) (**25**) with FcBF₄.



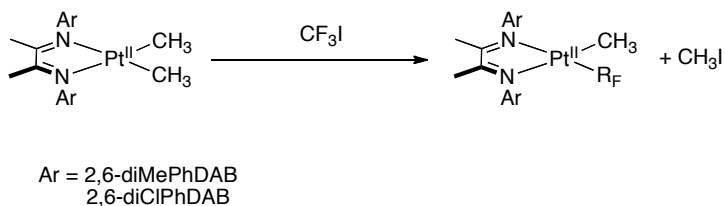
Complexes **24** and **26** were also reacted with stronger oxidant, tris(*p*-bromophenyl)aminium hexafluorophosphate (Ar₃NPF₆), for 16 h at 25 °C in acetone-*d*₆ with no observed decomposition or ethane formation. Reaction of complex **25** with ceric ammonium nitrate (CAN) in acetone-*d*₆ at 25 °C did produce a new Pt–CH₃ resonance (40% yield relative to starting **25**) within ten minutes. However, both **25** and the platinum impurity were decomposed by 34% and 100% respectively, so it is unclear which starting complex, **25** or the impurity, gave rise to the new Pt–CH₃ resonance. Upon standing for 24 h, no further reactivity was observed.

Based on these observations, one-electron oxidations of the monomethyl-platinum complexes studied did not produce the desired methyl transfer for most complexes synthesized. For 2,6-diMePhDAB complexes **25** and **26**, interpretation of the ethane-

producing reactions was complicated by the presence of a impurity that could not be removed after synthesis of **24** or **25**, but was observed to decompose in reactions where ethane formed.

The comparative reactivity of bpy complexes **16** ($R_F = {}^n\text{Bu-F}_9$) and **19** ($R_F = {}^i\text{Pr-F}_7$) and 2,6-diMePhDAB complexes **24** (${}^i\text{Pr-F}_7$) and **25** ($R_F = {}^n\text{Bu-F}_9$) is instructive for further design of $(L_2)\text{Pt}^{\text{II}}(\text{CH}_3)(R_F)$ complexes for oxidatively-induced methyl transfer. In both sets of complexes, the less bulky ${}^n\text{Bu-F}_9$ perfluoroalkyl group allowed decomposition of **16** and **25** under milder conditions than the ${}^i\text{Pr-F}_7$ analogues. In accord with these results, one-electron oxidation of $({}^t\text{Bu-bpy})\text{Pd}(\text{CH}_3)(\text{CF}_3)$ versus $({}^t\text{Bu-bpy})\text{Pd}(\text{CH}_3)({}^i\text{Pr-F}_7)$ indicated bulkier perfluoroalkyl groups required more forcing oxidation conditions to react (Chapter 4). These results suggest further efforts to obtain oxidatively-induced methyl transfer should focus on smaller linear perfluoroalkyl groups (${}^n\text{Pr-F}_7$ or Et-F_5) ligands or CF_3 ligands. Attempts to synthesize $(L_2)\text{Pt}(\text{CH}_3)(\text{CF}_3)$ complexes were unsuccessful in my hands. However, one synthetic pathway that remains unexplored for synthesis of $(L_2)\text{Pt}(\text{CH}_3)(\text{CF}_3)$ is the oxidation of $(2,6\text{-diXDAB})\text{Pt}(\text{CH}_3)_2$ with CF_3I (Scheme 5.69).

Scheme 5.69 Synthesis of $(2,6\text{-diXDAB})\text{Pt}^{\text{II}}(\text{CH}_3)(\text{CF}_3)$.

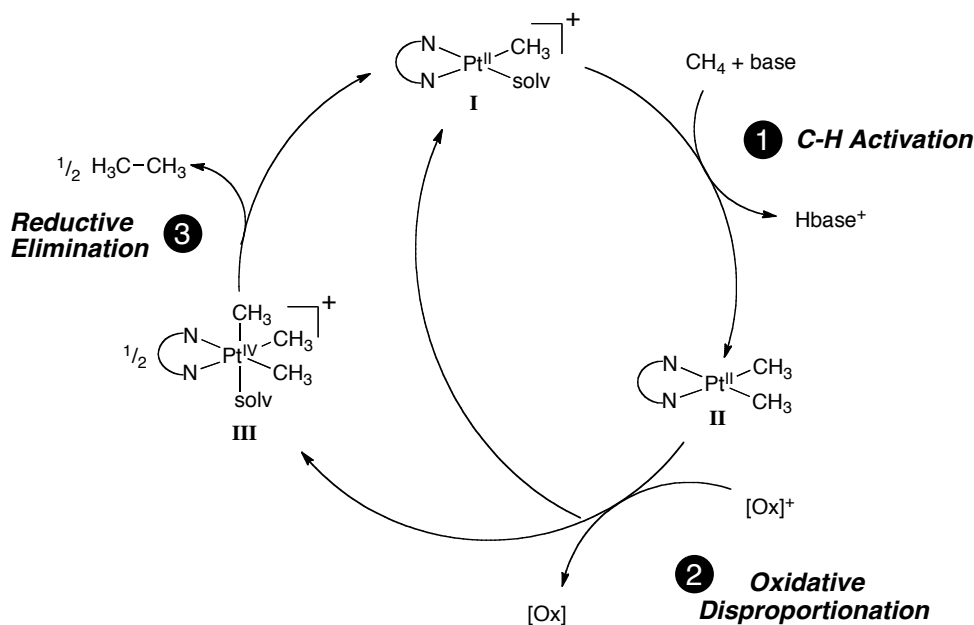


5.2.4 Facile Ethane Elimination from $[(\text{ArDAB})\text{Pt}^{\text{IV}}(\text{CH}_3)_3(\text{solvent})]^+$ Complexes

Methyl transfer between two platinum(II) centers, methyl transfer between platinum(II) and palladium(II), and one-electron oxidatively induced methyl transfer from monomethyl platinum complexes have all been discussed. In each of these cases, the goal was to transfer a methyl between metal centers to make a $\text{Pt}(\text{CH}_3)_n$ ($n > 1$) species from which ethane could be eliminated. For the $(L_2)\text{Pt}^{\text{II}}(\text{CH}_3)(R_F)$ complexes screened, no system was identified that cleanly provided methyl transfer.

As an alternative, C–H activation of CH₄ by a [(L₂)Pt^{II}(CH₃)(solvent)]⁺ complex to generate (L₂)Pt^{II}(CH₃)₂ could circumvent the challenge of generating (L₂)Pt^{II}(CH₃)₂ by methyl transfer at a monomethyl platinum complex (Scheme 5.70). In this cycle, monomethyl-platinum complex **I** performs C–H activation of methane to generate dimethyl-platinum complex **II**. Complex **II** then undergoes one-electron oxidation to generate one half equiv of **I** and one half equiv of platinum(IV) complex **III**. Reductive elimination of ethane from complex **III** generates another half equiv of **I** to complete the catalytic cycle.

Scheme 5.70 Proposed Catalytic Cycle for an [(N–N)Pt^{II}(CH₃)(solvent)]⁺ Catalyst.

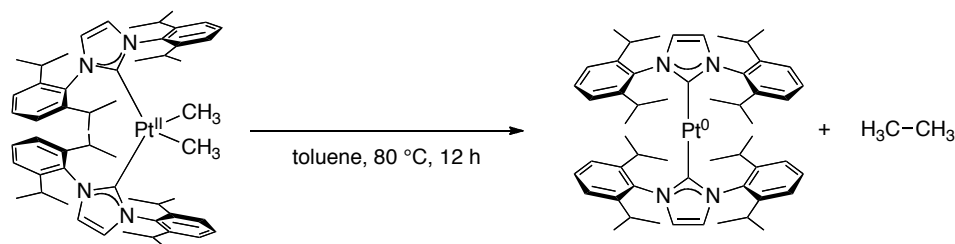


Two challenges needed to be addressed for successful implementation of the proposed catalytic cycle: C–H activation of CH₄ to produce complex **II** and reductive elimination of ethane from intermediate **III**. This section addresses the latter of these two challenges.

Only one example is known of ethane elimination from a platinum(II)-dimethyl complex, and this system utilized sterically encumbered monodentate carbene ligands (Scheme 5.71).⁵⁵ However, many complexes with the general formula (L₂)Pt^{IV}(CH₃)₃X are known to eliminate ethane when L₂ is a chelating diphosphine ligand or two monodentate phosphine ligands.³⁶ However, in considering our entire proposed catalytic

cycle, we were limited to L_2 ligands that had precedent for all steps of the catalytic cycle. Chelating ArDAB are known to facilitate C–H activation of methane⁴ and oxidatively induced methyl transfer.²⁴ However, elimination of ethane from the $(\text{ArDAB})\text{Pt}^{\text{IV}}(\text{CH}_3)_2\text{X}$ complexes produced in oxidatively-induced methyl transfer has not been observed.³⁶ More generally, six coordinate Pt^{IV} -trimethyl complexes bearing chelating sp^2 nitrogen donor ligands have not been shown to undergo reductive elimination of ethane.

Scheme 5.71 Ethane Elimination from Platinum(II).⁵⁵

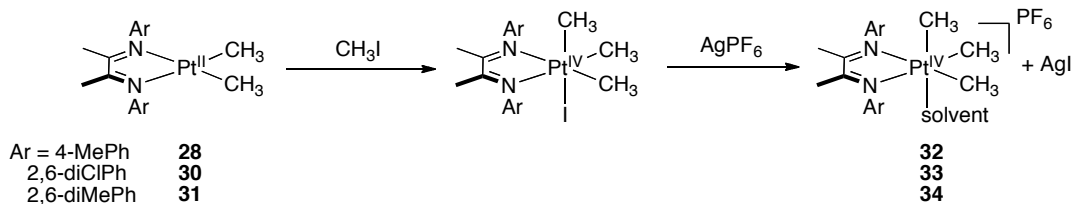


To meet this challenge, we drew inspiration from the report by Hughes on the reductive elimination of methyl iodide from $(2,6\text{-diMePhDAB})\text{Pt}^{\text{IV}}(\text{CH}_3)_2(\text{R}_\text{F})\text{I}$ promoted by the presence of 2,6-substitution of the diimine aryl groups (Scheme 5.56).⁴⁶ Notably, identical reactions with the 4-substituted 4-MePhDAB ligand resulted in isolation of $(4\text{-MePhDAB})\text{Pt}^{\text{IV}}(\text{CH}_3)_2(\text{R}_\text{F})\text{I}$ (Scheme 5.57). Hughes' attempts to promote reductive elimination from $(4\text{-MePhDAB})\text{Pt}^{\text{IV}}(\text{CH}_3)(\text{R}_\text{F})\text{I}$ resulted in no reaction or decomposition of the complex. We hypothesized similarly that 2,6-substitution of the diimine aryl groups might provide enough steric congestion around the Pt metal center to induce reductive elimination of ethane from Pt^{IV} .

To study the effect of ArDAB sterics on ethane elimination, we prepared the cationic $[(\text{ArDAB})\text{Pt}^{\text{IV}}(\text{CH}_3)_3(\text{solvent})]^+$ complexes expected as products from one-electron oxidation of $(\text{ArDAB})\text{Pt}^{\text{II}}(\text{CH}_3)_2$ (Scheme 5.72).²⁴ Known dimethyl complexes, $(4\text{-MePhDAB})\text{Pt}^{\text{II}}(\text{CH}_3)_2$ (**28**), $(2,6\text{-diClPhDAB})\text{Pt}^{\text{II}}(\text{CH}_3)_2$ (**30**), and $(2,6\text{-diMePhDAB})\text{Pt}^{\text{II}}(\text{CH}_3)_2$ (**31**) reacted with methyl iodide in deuterated solvent to generate the respective $(\text{ArDAB})\text{Pt}^{\text{IV}}(\text{CH}_3)_3\text{I}$ complexes *in situ*. Addition of silver hexafluorophosphate (AgPF_6) provided the cationic complexes, $[(\text{ArDAB})\text{Pt}^{\text{IV}}(\text{CH}_3)_3(\text{solvent})]\text{PF}_6$ (Ar = 4-MePh (**32**), 2,6-diClPh (**33**), or 2,6-diMePh

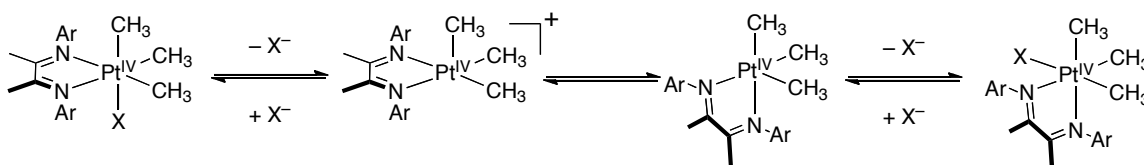
(**34**) in near quantitative yields based on internal standard. It should be noted that all reactions using **31** as starting material were carried out by Dr. Michael Lanci.

Scheme 5.72 *In Situ* Synthesis of $(\text{ArDAB})\text{Pt}^{\text{IV}}(\text{CH}_3)_3(\text{solvent})\text{PF}_6$.



Interestingly, complex **32** displayed resolved axial and equatorial $\text{Pt}-\text{CH}_3$ resonances in acetone- d_6 . In contrast complexes **33** and **34** show one broadened $\text{Pt}-\text{CH}_3$ resonance, indicative of dynamic scrambling of the axial and equatorial methyl positions on the NMR timescale. Similar methyl group scrambling has been observed previously and is attributed to formation of a five-coordinate intermediate at which interconversion of the axial and equatorial positions occurs (Scheme 5.73).²⁶ The observed scrambling at 25 °C for complexes **33** and **34** suggests increased steric congestion about platinum allows favorable equilibrium solvent dissociation to form a five-coordinate complex. If reductive elimination of ethane occurs from five-coordinate intermediate $[(\text{ArDAB})\text{Pt}^{\text{IV}}(\text{CH}_3)_3]^+$ complexes as is reported for phosphine ligands,³⁶ this data suggested that 2,6-substitution of the diimine aryl groups should provide a favorable equilibrium of the five-coordinate complex for further reductive elimination.

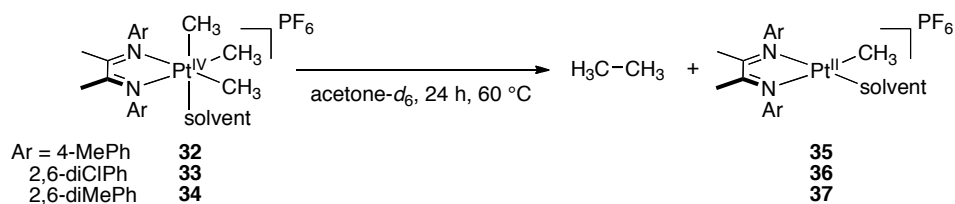
Scheme 5.73 Mechanism of Axial and Equatorial CH_3 Scrambling in $(\text{ArDAB})\text{Pt}^{\text{IV}}\text{CH}_3\text{X}$.



Solutions of **32**, **33**, and **34** were thermolyzed in acetone- d_6 at 60 °C and the reactions were monitored by ^1H NMR spectroscopy for the formation of ethane and $[(\text{ArDAB})\text{Pt}(\text{CH}_3)(\text{solvent})]\text{PF}_6$ (Table 5.10). Thermolysis of **32** in acetone- d_6 for 24 h at 60 °C produced only trace amounts of ethane (< 1%) while generating a new, unidentified

Pt^{IV} complex. The related reaction of **33** in acetone-*d*₆ showed 39% conversion of **33**, 8% yield of ethane, and 2% of complex **36** after 24 h. Complex **34**, when thermolyzed, resulted in complete consumption of starting material, yielding ethane (96%) and complex **37** (82%).

Table 5.10 Summary of [(ArDAB)Pt^{IV}(CH₃)₃(solvent)]PF₆ Thermolysis Results.

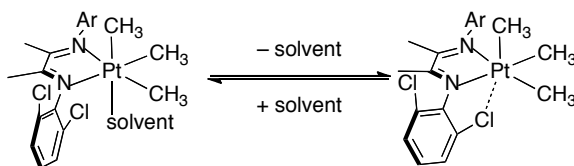


Starting Complex	% Conversion	% Ethane	Monomethyl Complex (% Yield)
33	100	< 1	35 (0)
34	39	8	36 (2)
35	100 ^a	96	37 (82)

^a reaction occurred over 8 h

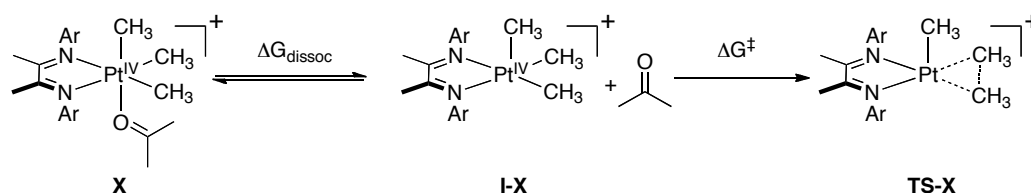
In agreement with our hypothesis, 2,6-diMePhDAB complex **34** produced ethane under moderate conditions while only traces of ethane were formed from 4-MePhDAB complex **32**. Surprisingly, when Ar = 2,6-diClPh (**33**), thermolysis provided only a marginal increase in the amount of ethane formed compared to **32**. It is possible that the chloride lone pair could donate into the empty *dz*² orbital upon dissociation of solvent to stabilize the 5-coordinate intermediate and hinder reductive elimination (Scheme 5.74). Alternatively, π -donation of the chloride lone pair could make 2,6-diClPhDAB a better donor ligand (or worse π -backbonding ligand) providing a more electron rich platinum center compared to **34**. In comparison to **34**, the more electron rich metal center would favor solvent dissociation but disfavor reductive elimination.

Scheme 5.74 Proposed Stabilization of Five-Coordinate Intermediate in **33**.



To study the origin of elimination of ethane promoted by 2,6-diMePhDAB and the disparity in reactivity between **33** and **34**, DFT calculations were employed. For each complex under study, the starting acetone complex (**X**), five-coordinate intermediate (**I-X**), and reductive elimination transition state (**TS-X**) were calculated (Table 5.11). ΔG_{dissoc} was calculated as the difference in free energy between **I-X** and **X**. ΔG^\ddagger is the difference in free energy between **TS-X** and **I-X**. Finally, $\Delta G_{\text{tot}}^\ddagger$ is the sum of ΔG_{dissoc} and ΔG^\ddagger . Dr. Michael Lanci performed calculations on [(2,6-diMePhDAB)Pt^{IV}(CH₃)₃(acetone)]⁺ (**34**) and [(3,5-diMePhDAB)Pt^{IV}(CH₃)₃(acetone)]⁺ (**38**), while I did the related calculations for [(2,6-diClPhDAB)Pt^{IV}(CH₃)₃(acetone)]⁺ (**33**). In this comparison, **38** is a model of 4-MePhDAB substituted **32**.

Table 5.11 Computation of Reductive Elimination of Ethane from [(ArDAB)Pt^{IV}(CH₃)₃(solvent)]⁺.



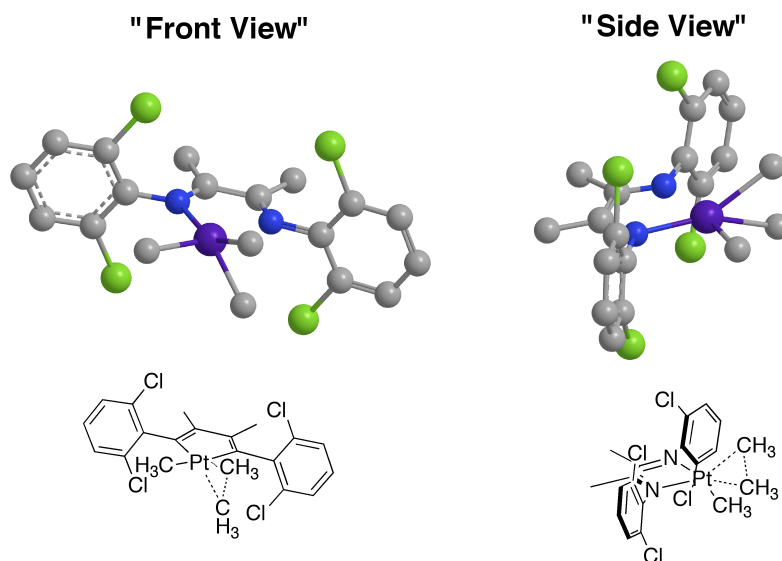
Transition State	ΔG_{dissoc} (kcal/mol)	ΔG^\ddagger (kcal/mol)	$\Delta G_{\text{tot}}^\ddagger$ ($\Delta G_{\text{dissoc}} + \Delta G^\ddagger$)
TS-33	-1.5	26.6	25.1
TS-34	0.1	21.7	21.8
TS-38	5.6	21.6	27.2

A comparison of reductive elimination from **34** and **38** provided evidence for the origin of ethane elimination promoted by (2,6-diXDAB) complexes. The $\Delta\Delta G_{\text{dissoc}}$ between **34** and **38** was 5.5 kcal/mol in favor of complex **34**. Reductive elimination from the five-coordinate complexes **34** and **38** was calculated to have a $\Delta\Delta G^\ddagger$ of only 0.1

kcal/mol. This suggests that the majority of $\Delta\Delta G_{\text{tot}}^{\ddagger}$ for reductive elimination between **34** and **38** is the result of more favorable acetone dissociation from complex **34**. The Eyring equation predicts a difference in rate of 10^4 between **34** and **38**.

Comparison of **33** and **34** showed $\Delta\Delta G_{\text{dissoc}}$ to be 1.6 kcal/mol in favor of 2,6-diCIPhDAB complex **33**. However, unlike **34** and **38** (which had practically identical values for ΔG^{\ddagger}) reductive elimination from **33** was disfavored by 5 kcal/mol. **TS-33** is shown in Scheme 5.75. Examination of the transition state geometry clearly shows no donation of the Cl lone pair into the empty d_{z^2} orbital in the transition state. The nearest chloride is 4.0 Å away from the platinum center. This suggests that the four chlorides are donating lone pair electron density into the aromatic system, making **33** a more electron rich metal center than **34**. The decreased energy of acetone dissociation and increased energy required for reductive elimination are consistent with this proposal.

Scheme 5.75 Reductive Elimination Transition State **TS-33**.

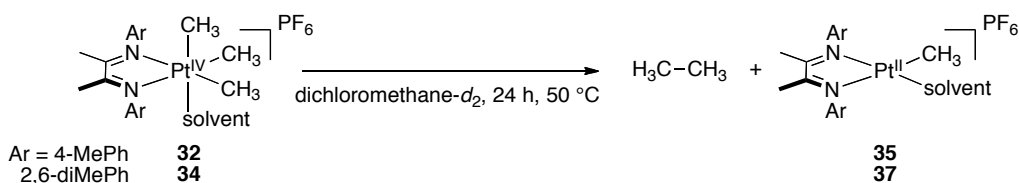


The computational comparison of complexes **34** and **38** suggested that reductive elimination from $[(\text{ArDAB})\text{Pt}(\text{CH}_3)_3(\text{solvent})]\text{PF}_6$ complexes should be even more favorable in a more weakly coordinating solvent. To this end, complexes **32**, **33**, and **34** were prepared in dichloromethane- d_2 under the same conditions as described for reactions in acetone- d_6 . ^1H NMR spectra of **32** exhibited dynamic exchange of axial and equatorial methyl positions in dichloromethane- d_2 in contrast to observations made of **32**

in acetone-*d*₆. Dichloromethane-*d*₂ solutions of **34** were not stable as reductive elimination of ethane was observed even at 25 °C.

Thermolysis of complex **32** in dichloromethane-*d*₂ was performed at 50 °C over 24 h and was monitored by ¹H NMR spectroscopy (Table 5.12). When compared to reaction of **32** in acetone, reaction in dichloromethane produced a higher yield of ethane (16%) and **35** (8%) at 19% conversion of **32**. While the reaction of **32** to produce ethane is still sluggish under these conditions, this results provides further evidence for the role of solvent coordination in the reductive elimination of ethane from trimethyl-Pt^{IV} complexes, [(ArDAB)Pt^{IV}(CH₃)₃(solvent)]PF₆.

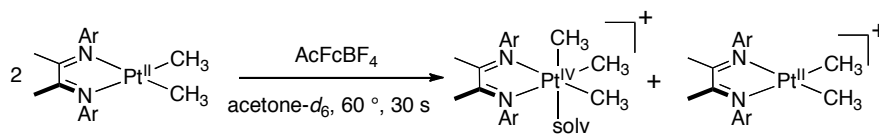
Table 5.12 Thermolysis of [(ArDAB)Pt^{IV}(CH₃)₃(solvent)]PF₆ in Dichloromethane.



Starting Complex	% Conversion	% Ethane	Monomethyl Complex (% Yield)
32	19	16	35 (8)
34	100 ^a	96	37 (82)

Importantly, all of the dimethyl complexes reported above (**28**, **30**, and **31**) undergo oxidatively-induced methyl transfer in acetone-*d*₆ to generate the respective platinum(IV)-trimethyl complexes **32**, **33**, and **34** (Scheme 5.76). These results show that sterically-encumbered platinum complexes bearing ArDAB ligands can accomplish two of the three fundamental steps of our proposed catalytic cycle, oxidatively-induced methyl transfer and elimination of ethane. These studies also clearly show the importance of using a weakly coordinating solvent to maximize the rate of ethane elimination when considering platinum-catalyzed oligomerization of methane.

Scheme 5.76 Oxidatively-Induced Methyl Transfer from (ArDAB)Pt^{II}(CH₃)₂.



5.3 Conclusions

Platinum has the distinct advantage (relative to other group 10 metals) that it is capable of performing C–H activation of methane over other group 10 metals. In order to exploit this advantage toward the oxidative oligomerization of methane, platinum must also be able to also generate new C–C bonds from the activated methyl group. Several pathways toward C–C bond formation from Pt–CH₃ complexes, all involving methyl transfer reactions, were examined in this chapter including: disproportionation of monomethyl platinum complexes, transfer of methyl from platinum to palladium, one-electron oxidation of platinum monomethyl complexes, and one-electron oxidation of platinum-dimethyl complexes.

Disproportionation of (^tBu-bpy)Pt^{II}(CH₃)X complexes was shown via calculations to be more thermodynamically favorable compared to the related disproportionation of (^tBu-bpy)Pd^{II}(CH₃)X complexes. An increase in the kinetic barrier for disproportionation at Pt^{II} was also calculated. The thermodynamically downhill comproportionation reaction between (^tBu-bpy)Pt^{II}(CH₃)₂ and (^tBu-bpy)Pt^{II}(I)₂ required heating at 90 °C for 24 h to provide only 10% (^tBu-bpy)Pt^{II}(CH₃)I giving further credence to an increased kinetic barrier for methyl transfer compared to the analogous palladium complexes.¹⁷

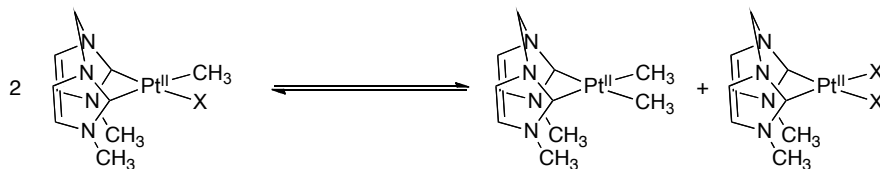
Methyl transfer from (Me-bpy)Pt^{II}(CH₃)I to (NO₂-bpy)Pd(I)₂ was computed to be nearly thermoneutral. The reaction of related complex (^tBu-bpy)Pt(CH₃)I with (NO₂-bpy)Pd(I)₂ produced 13% of a new asymmetric complex over 6 h at 90 °C. This complex was preliminarily assigned as (NO₂-bpy)Pd(CH₃)I based on ¹H NMR spectroscopic analysis.

For Pt-to-Pt disproportionation, the kinetic barrier to methyl transfer is proposed to be greatly affected by the energy required for X-type ligand loss, specifically, X-type ligand loss from the methyl-accepting complex. In trying to circumvent this kinetic

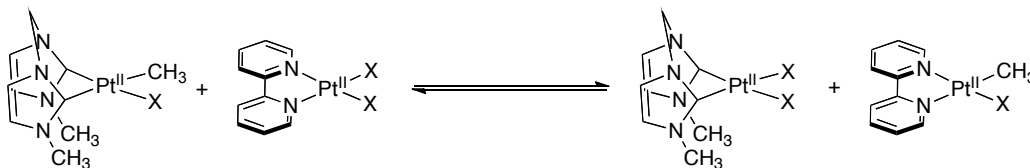
problem by performing Pt-to-Pd methyl transfer, an advantage is gained in X-type ligand dissociation at Pd^{II}, but transfer of CH₃ from Pt to Pd becomes kinetically unfavorable.

One possibility for addressing the challenge of kinetics in methyl transfers with Pt, is to make the complexes more electron rich. Stronger donor ligands should have a greater trans effect, labilizing the X-type ligands. For Pt-to-Pt systems, an example is carbene ligands rather than bipyridine ligands (Scheme 5.77). Likewise, in the Pt-to-Pd methyl transfer, more electron rich ligands on both metals could maintain the thermodynamic neutrality of the system while improving the kinetics. One such example would involve using carbene or *sp*³-nitrogen donor ligands on platinum while using bipyridine instead of NO₂-bpy on palladium (Scheme 5.78). Future experiments along these lines should be pursued.

Scheme 5.77 Electron-Donating Ligands in Platinum(II) Disproportionation.



Scheme 5.78 Electron-Donating Ligands in Platinum-to-Palladium CH Transfer.



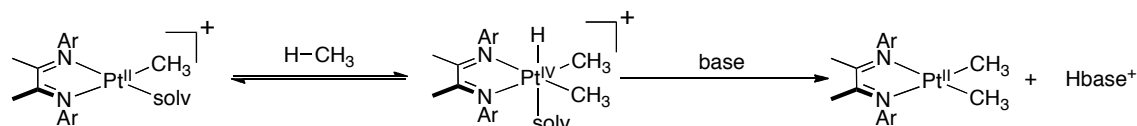
One-electron oxidatively-induced methyl transfer is an alternative option for generating dimethyl-platinum complexes from monomethyl-platinum complexes. In pursuing this pathway, a number of new platinum-perfluoroalkyl complexes of the general formula (L₂)Pt^{II}(CH₃)(R_F) (R_F = nonafluoro-*n*-butyl or heptafluoro-*i*-propyl) were synthesized. Ultimately, the complexes did not produce the desired [(L₂)Pt^{IV}(CH₃)₂(R_F)(solvent)]⁺ complexes upon oxidation under any conditions screened. However, based on comparison of platinum systems to palladium systems the ideal complexes for these reactions should be (L₂)Pt^{II}(CH₃)(CF₃) rather than complexes containing larger perfluoroalkyl substituents. The Pt–CF₃ complexes were not attainable

under any synthetic conditions attempted. However, one synthetic pathway that remains to be explored is reaction of $(\text{ArDAB})\text{Pt}^{\text{II}}(\text{CH}_3)_2$ ($\text{Ar} = 2,6\text{-substituted arene}$) with CF_3I . Hughes has shown this reaction produced $(\text{ArDAB})\text{Pt}^{\text{II}}(\text{CH}_3)(\text{R}_\text{F})$ complexes with concomitant loss of CH_3I for $^n\text{Pr-F}_7\text{I}$, and this could offer an opportunity for entry into $(\text{ArDAB})\text{Pt}^{\text{II}}(\text{CH}_3)(\text{CF}_3)$ complexes.

Lastly, Dr. Michael Lanci and I demonstrated that 2,6-substituted aryl groups in ArDAB ligands were effective at promoting reductive elimination of ethane from $[(\text{ArDAB})\text{Pt}^{\text{IV}}(\text{CH}_3)_3(\text{solvent})]^+$ complexes. Further, $[(\text{ArDAB})\text{Pt}^{\text{IV}}(\text{CH}_3)_3(\text{solvent})]^+$ could be generated by one-electron oxidation of $(\text{ArDAB})\text{Pt}^{\text{II}}(\text{CH}_3)_2$. Upon elimination of ethane, $[(\text{ArDAB})\text{Pt}^{\text{IV}}(\text{CH}_3)_3(\text{solvent})]^+$ produces $[(\text{ArDAB})\text{Pt}^{\text{II}}(\text{CH}_3)(\text{solvent})]^+$. Achieving C–H activation by reaction of methane with $[(\text{ArDAB})\text{Pt}^{\text{II}}(\text{CH}_3)(\text{solvent})]^+$ to yield $(\text{ArDAB})\text{Pt}^{\text{II}}(\text{CH}_3)_2$ would complete all of the fundamental steps necessary for oxidative oligomerization of methane by a platinum catalyst.

To this end, it is important to note that C–H activation by $[(\text{ArDAB})\text{Pt}^{\text{II}}(\text{CH}_3)(\text{solvent})]^+$ has been demonstrated to proceed through an oxidative addition pathway to generate a $[(\text{ArDAB})\text{Pt}^{\text{IV}}(\text{CH}_3)_2(\text{H})(\text{solvent})]^+$ intermediate (Scheme 5.79).⁴ If this intermediate could be trapped by deprotonation of the hydride ligand, the desired transformation to yield $(\text{ArDAB})\text{Pt}(\text{CH}_3)_2$ could be achieved, and with this success, each of the fundamental steps required for platinum-catalyzed oxidative oligomerization of methane would be accomplished.

Scheme 5.79 Generation of a Platinum(II)-Dimethyl Complex Upon Methane Activation.



5.4 Experimental Procedures

5.4.1 Instrumentation

NMR spectra were obtained on a Varian Inova 500 (499.90 MHz for ^1H ; 125.70 MHz for ^{13}C), a Varian Inova 400 (399.96 MHz for ^1H ; 100.57 MHz for ^{13}C , 376.34

MHz for ^{19}F , 161.91 MHz for ^{31}P), or a Varian Mercury 300 (300.07 MHz for ^1H) spectrometer. ^1H and ^{19}F NMR chemical shifts are reported in parts per million (ppm) relative to TMS with the residual solvent peak used as an internal reference. ^{19}F NMR spectra are referenced on a unified scale, where the single primary reference is the frequency of the residual solvent peak in the ^1H NMR spectrum. Multiplicities are reported as follows: singlet (s), doublet (d), doublet of doublets (dd), doublet of doublet of doublets (ddd), and triplet (t).

5.4.2 Materials and Methods

All manipulations were performed using standard Schlenk or glovebox procedures unless otherwise noted. Acetone, acetone- d_6 (Cambridge Isotopes), and methyl iodide were refluxed over calcium sulfate overnight and then distilled, freeze-pump-thaw degassed, and shaken over 4 Å molecular sieves immediately before use. Methylene chloride- d_2 (Cambridge Isotopes) and 1,1,2-trichloroethane were refluxed over CaH_2 overnight and then distilled, freeze-pump-thaw degassed and stored over 4 Å molecular sieves. Silver hexafluorophosphate (Strem) was stored at $-35\text{ }^\circ\text{C}$ in a glovebox freezer. All other solvents were purchased from Fisher or EMD and dispensed from an Innovative Technologies solvent purification system equipped with columns packed with activated alumina, copper catalyst, and molecular sieves. 4,4'-Di-*tert*-butyl-2,2'-bipyridine (*t*Bu-bpy), bpy, and $\text{H}_2\text{Pt}^{\text{IV}}\text{Cl}_6$ were purchased from Aldrich, silver acetate and (COD) $\text{Pt}^{\text{II}}(\text{Cl})_2$ were purchased from Strem, $\text{Na}_2\text{Pd}^{\text{II}}\text{Cl}_4$ and $\text{Pd}^{\text{II}}\text{Cl}_2$ were purchased from Pressure Chemical, $\text{K}_2\text{Pt}^{\text{II}}\text{Cl}_4$ was purchased from Pressure Chemical or Acros, methyl iodide, ferrocene, ceric ammonium nitrate were purchased from Acros, trifluoromethyl iodide was purchased from Matrix Scientific. 1-nonafluorobutyl iodide and 2-heptafluoropropyl iodide were purchased from Acros, and shaken with $\text{Na}_2\text{S}_2\text{O}_3$ to remove I_2 , followed by drying over MgSO_4 and freeze-pump-thaw degassed prior to use. All other materials were used as purchased from Aldrich or Acros.

See Chapter 2 for specific NMR instrumentation settings and particular NMR tubes used in ethane-evolving reactions. Ambient light refers to light emitted from two

fluorescent tube lights in a fume hood. Reactions conducted in the glovebox were conducted at the ambient temperature of the glove box (30 °C) unless otherwise noted.

5.4.3 Computational Methods – Methyl Transfer

See Chapter 2 for details on ground state calculations. To calculate energies for chloride dissociation, a diffuse function was added to chloride ($\xi_{\text{diffuse}} = 0.0483$) in Cl^- and $(\text{MeDAB})\text{M}^{\text{II}}(\text{CH}_3)\text{Cl}$. Solvation energies were applied as a single point energy correction to the optimized structures using the IEFPCM solvation model (see Chapter 2).

Transition states were optimized as saddle points using the Berny algorithm.^{56,57} Transition states were confirmed by visual inspection of the single imaginary frequency. Transition structures were first optimized using B3LYP/CEP-31G(d). A diffuse function was then added to chloride, and single point energies were derived for the optimized structures. Solvation energies were applied as a single point energy correction to the optimized structures using the same methods as for ground state calculations.

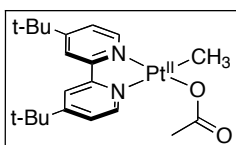
5.4.4 Computational Methods – Reductive Elimination

Molecular geometries were fully optimized at the density functional level of theory (DFT) using Gaussian 03. The restricted (closed shell) calculations were performed using the B3LYP^{58–60} functional. Atomic orbital basis functions employed a triple zeta basis set with effective core potentials and f polarization, LANL2TZ(f),^{61,62,63} on Pt and for C, H, N, and O the 6-31G** basis.⁶⁴ Vibrational frequencies were calculated analytically within the harmonic oscillator approximation.⁶⁵ All minima were characterized by real frequencies unless noted otherwise. Transition states were optimized as saddle points using the Berny algorithm.^{56,57}

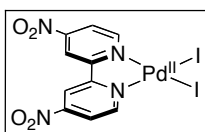
5.4.5 Syntheses

$(\text{SMe}_2)_2\text{Pt}^{\text{II}}(\text{I})_2$,²³ $(^t\text{Bu-bpy})\text{Pt}^{\text{II}}(\text{I})_2$,⁶⁶ $(^t\text{Bu-bpy})\text{Pt}^{\text{II}}(\text{CH}_3)\text{I}$,⁶⁶ $(\mu\text{-SMe}_3)_2\text{Pt}^{\text{II}}_2(\text{CH}_3)_4$,⁴⁷ $(^t\text{Bu-bpy})\text{Pt}^{\text{II}}(\text{CH}_3)_2$,⁶⁷ $(\text{NBD})\text{Pt}^{\text{II}}(\text{Cl})_2$,⁴⁸ $(\text{NBD})\text{Pt}^{\text{II}}(\text{CH}_3)_2$,⁵¹ $(\text{COD})\text{Pt}^{\text{II}}(\text{CH}_3)_2$,⁵¹ $(\text{COD})\text{Pt}^{\text{II}}(\text{CH}_3)(^n\text{Bu-F}_9)$ (**14**),⁵⁰ FcBF_4 ,⁵⁴ acetylferrocene,⁶⁸ AcFcBF_4 ,⁵⁴ 2,6-

diMePhDAB,⁶⁹ 4-MePhDAB,⁷⁰ (4-MePhDAB)Pt^{II}(CH₃)₂ (**28**),⁷¹ and (2,6-diClPhDAB)Pt^{II}(CH₃)₂ (**31**)⁷² were synthesized according to literature procedures. (SMe₂)₂Pt^{II}(CH₃)I was prepared according to the methods of Puddephatt,²³ only the reaction was carried out in acetone instead of methylene chloride, and the acetone solution was used directly in the further synthetic steps without isolation of (SMe₂)₂Pt^{II}(CH₃)I. The ligand NO₂-bpy was prepared by oxidation of bpy to N,N'-bpydioxide⁷³ followed by nitration of the pyridine rings at the 4 and 4' positions and reduction of the N-oxides.⁷⁴ The ligand 2,6-diClPhDAB was prepared according to the procedure for preparation of 4-MePhDAB,⁷⁰ but the yellow precipitate was collected on a frit after only ten minutes of reaction.

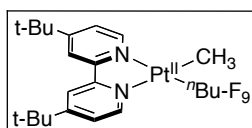


(t-Bu-bpy)Pt^{II}(CH₃)OAc (8): (t-Bu-bpy)Pt^{II}(CH₃)I (106 mg, 0.18 mmol, 1 equiv) was suspended in dry acetone (5 mL). AgOAc (32 mg, 0.19 mmol, 1.1 equiv) and a magnetic stir bar were added, and the reaction was stirred for 3 h at 25 °C. The resulting suspension was passed through a plug of Celite. The acetone filtrate was concentrated under vacuum, and the residue was dissolved in benzene (5 mL). The benzene solution was passed through a plug of Celite, and filtrate was cooled to -32 °C. The frozen benzene solution was dried under vacuum to afford **8** as a pale yellow solid (70 mg, 74%). ¹H NMR (500 MHz, acetone-*d*₆): δ 8.93 (d, ³*J* = 6.5 Hz, *J*_{Pt-H} = 58.5 Hz, 1H), 8.68 (d, ³*J* = 5.5 Hz, 1H), 8.54 (d, ⁴*J* = 1.5 Hz, 1H), 8.47 (d, ⁴*J* = 2.0 Hz, 1H), 7.82 (dd, ³*J* = 5.5 Hz, ⁴*J* = 2.0 Hz, 1H), 7.63 (dd, ³*J* = 6.5 Hz, ⁴*J* = 2.0 Hz, 1H), 1.98 (s, 3H), 1.45 (s, 9H), 1.44 (s, 9H), 0.96 (s, *J*_{Pt-H} = 80.0 Hz, 3H).

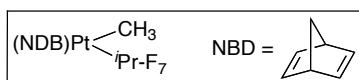


(NO₂-bpy)Pd^{II}(I)₂ (12): An ethanol (2 mL) solution of NO₂-bpy (30 mg, 0.12 mmol, 1.5 equiv) was added to a solution of Na₂Pd^{II}Cl₄ (24 mg, 0.08 mmol, 1 equiv) in H₂O (2 mL).

Immediately, a saturated solution of potassium iodide (181 mg, 1.09 mmol, 13 equiv) in H₂O was added, and the precipitate was allowed to settle overnight. The solid was collected on a frit, washed with H₂O and ethanol, and dried under vacuum to afford **12** as a crystalline red solid (43 mg, 87%). ¹H NMR (300 MHz, acetone-*d*₆): δ 10.29 (d, ³*J* = 5.7 Hz, 2H), 9.66 (d, ⁴*J* = 2.4 Hz, 2H), 8.69 (dd, ³*J* = 6.3 Hz, ⁴*J* = 2.4 Hz, 2H).

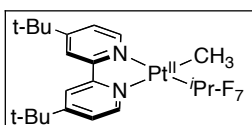


(bpy)Pt^{II}(CH₃)(^{*n*}Bu-F₉) (16): (COD)Pt^{II}(CH₃)(^{*n*}Bu-F₉) (59 mg, 0.11 mmol, 1 equiv) and 2,2'-bipyridine (18 mg, 0.11 mmol, 1 equiv) were dissolved in toluene (1.5 mL) in a 20 mL scintillation vial. A Teflon-coated magnetic stirbar was added, and the vial was fitted with a Teflon-lined cap. The reaction was heated to 110 °C for 12 h. After cooling, the toluene solution was condensed to an oil, and hexanes (15 mL) was added to afford a yellow precipitate. The precipitate was collected on a frit, washed with hexanes, and dried under vacuum to afford **16** as a yellow solid (38 mg, 60%). ¹H NMR (400 MHz, acetone-*d*₆): δ 9.19 (d, ³*J* = 3.6 Hz, 1H), 9.08 (d, ³*J* = 5.6 Hz, *J*_{Pt-H} = 31.6 Hz, 1H), 8.59 (d, ³*J* = 6.8 Hz, 1H), 8.57 (d, ³*J* = 6.8 Hz, 1H), 8.40-8.34 (2 peaks, 2H), 7.85 – 7.78 (2 peaks, 2H), 0.91 (s, *J*_{Pt-H} = 82.8 Hz, 3H). ¹⁹F NMR (376 MHz, acetone-*d*₆): δ -81.8 (s, 3F), -91.9 (s, ²*J*_{Pt-F} = 393 Hz, 2F), -115.6 (s, ³*J*_{Pt-F} = 129 Hz, 2F), -125.5 (s, 2F).

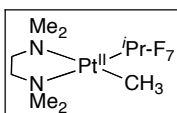


(NBD)Pt^{II}(CH₃)(^{*i*}Pr-F₇) (18): (NBD)Pt^{II}(CH₃)₂ (457 mg, 1.44 mmol, 1 equiv) and ^{*i*}Pr-F₇I (305 μL, 2.15, 1.5 equiv) were suspended in pentanes (75 mL) in a 100 mL Shlenk flask equipped with a Teflon-coated magnetic stirbar. The reaction was stirred in ambient light at 25 °C for 5 h. The solution was exposed to air, and pentanes was removed by rotary evaporator. The residue was dissolved in benzene (5 mL), and silver triflate (370 mg, 1.44 mmol, 1 equiv) was added. The reaction stirred for 30 minutes at 25 °C. The resulting suspension was filtered through Celite, and the filtrate was extracted with H₂O (3 x 10 mL). The benzene layer was dried over MgSO₄, frozen, and the

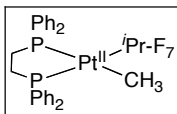
benzene was removed under vacuum to afford **18** as a white solid (481 mg, 71%). ^1H NMR (400 MHz, acetone- d_6): δ 5.66 (t, $^3J = 2.4$ Hz, $^2J_{\text{Pt-H}} = 51.2$ Hz, 2H), 5.54 (t, $^3J = 2.4$ Hz, $^2J_{\text{Pt-H}} = 36.0$ Hz, 2H), 4.23 (multiplet, 2H), 5.66 (t, $^3J = 2.4$ Hz, $^2J_{\text{Pt-H}} = 51.2$ Hz, 2H), 1.84 (multiplet, 1H), 1.82 (multiplet, 1H), 0.63 (s, $^2J_{\text{Pt-H}} = 86.0$ Hz, 3H). ^{19}F NMR (376 MHz, acetone- d_6): δ -69.6 (d, $^3J = 10.5$ Hz, $^3J_{\text{Pt-F}} = 110.9$ Hz, 6F), -192.0 (septet, $^3J = 10.5$ Hz, $^2J_{\text{Pt-F}} = 241.8$ Hz, 1F).



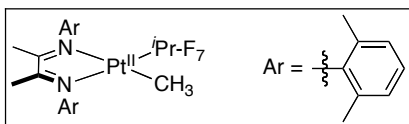
(bpy)Pt^{II}(CH₃)(ⁱPr-F₇) (19): Procedure for synthesis of **16** was followed only reaction was heated to 110 °C for 1 h, and (NBD)Pt^{II}(CH₃)(ⁱPr-F₇) was used as a starting material. (NBD)Pt^{II}(CH₃)(ⁱPr-F₇) (65 mg, 0.14 mmol, 1 equiv), 2,2'-bipyridine (24 mg, 0.15 mmol, 1.1 equiv). Complex **19** was isolated as yellow powder (25 mg, 33%). ^1H NMR (400 MHz, acetone- d_6): δ 9.39 (dd, $J_{\text{H-F}} = 10.0$ Hz, $^3J = 6.0$ Hz, 1H), 9.10 (d, $^3J = 5.6$ Hz, $J_{\text{Pt-H}} = 31.6$ Hz, 1H), 8.57 (d, $^3J = 8.0$ Hz, 1H), 8.56 (d, $^3J = 8.0$ Hz, 1H), 8.39 (dd, $^3J = 7.6$ Hz, $^3J = 6.8$ Hz, 1H), 8.35 (dd, $^3J = 8.0$ Hz, $^3J = 8.0$ Hz, 1H), 7.83 (dd, $^3J = 7.2$ Hz, $^3J = 6.4$ Hz, 1H), 7.78 (dd, $^3J = 7.2$ Hz, $^3J = 5.6$ Hz, 1H), 0.91 (s, $^2J_{\text{Pt-H}} = 82.4$ Hz, 3H). ^{19}F NMR (376 MHz, acetone- d_6): δ -68.0 (d, $^3J = 8.3$ Hz, $^3J_{\text{Pt-F}} = 125.2$ Hz, 6F), -186.2 (septet, $^3J = 8.3$ Hz, $^2J_{\text{Pt-F}} = 97.8$ Hz, 1F).



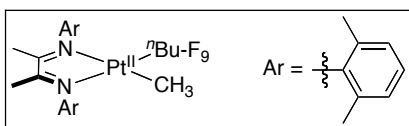
(TMEDA)Pt^{II}(CH₃)(ⁱPr-F₇) (20): Procedure for synthesis of **16** was followed. (NBD)Pt^{II}(CH₃)(ⁱPr-F₇) (100 mg, 0.21 mmol, 1 equiv), TMEDA (60 μL , 0.40 mmol, 2 equiv). Complex **20** was isolated as yellow powder (42 mg, 37%). ^1H NMR (400 MHz, acetone- d_6): δ 4.16 (d, $^3J = 5.6$ Hz, 2H), 2.90 (broad peak, 2H), 2.74 (s, $^3J_{\text{Pt-H}} = 16.8$ Hz, 6H), 2.64 (s, $^3J_{\text{Pt-H}} = 29.2$ Hz, 6H), 0.28 (pentet, $J = 1.6$ Hz, $^2J_{\text{Pt-H}} = 82.8$ Hz). ^{19}F NMR (376 MHz, acetone- d_6): δ -68.3 (d, $^3J = 8.3$ Hz, $^3J_{\text{Pt-F}} = 130.5$ Hz, 6F), -186.5 (septet, $^3J = 8.3$ Hz, $^2J_{\text{Pt-F}} = 108.7$ Hz, 1F).



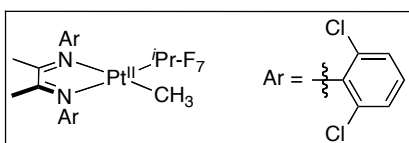
(dppe)Pt^{II}(CH₃)(^{*i*}Pr-F₇) (21): (NBD)Pt^{II}(CH₃)(^{*i*}Pr-F₇) (90 mg, 0.19 mmol, 1 equiv) and dppe (76 mg, 0.19 mmol, 1 equiv) were dissolved in acetone (3 mL). A Teflon-coated magnetic stirbar was added, and the reaction was stirred for 1 h at 30 °C. Pentanes (15 mL) was added to the reaction, and the solution was stored at -32 °C overnight. The resulting precipitate was collected on a frit, washed with pentanes, and dried under vacuum to afford **21** as a white solid (70 mg, 45%). ¹H NMR (400 MHz, acetone-*d*₆): δ 7.80 – 7.70 (multiple peaks, 8H), 7.61 – 7.54 (multiple peaks, 6H), 7.51 – 7.45 (multiple peaks, 6H), 2.34 (multiplet, ²*J*_{P-H} = 65.2 Hz, 4H), 0.44 (t, ³*J*_{P-H} = 6.8 Hz, ²*J*_{Pt-H} = 65.6 Hz, 3H), 2.64. ¹⁹F NMR (376 MHz, acetone-*d*₆): δ -67.6 (t, ⁴*J*_{P-F} = 7.9 Hz, ³*J*_{Pt-F} = 88.4 Hz, 6F), -186.5 (septet, ³*J* = 8.3 Hz, ²*J*_{Pt-F} = 107.5 Hz, 1F). ³¹P NMR (162 MHz, acetone-*d*₆): δ 49.7 (d, *J* = 96.4 Hz, ¹*J*_{Pt-P} = 1874 Hz, 1P), 45.1 (multiplet, ¹*J*_{Pt-P} = 2448 Hz, 1P)



(2,6-diMePhDAB)Pt^{II}(CH₃)₂(^{*i*}Pr-F₇) (24): (2,6-diMePhDAB)Pt^{II}(CH₃)₂ (151 mg, 0.29 mmol, 1 equiv) and ^{*i*}Pr-F₇I (62 μL, 0.44 mmol, 1.5 equiv) were combined in ethyl acetate (10 mL) in a 50 mL Shlenk flask equipped with a Teflon-coated magnetic stirbar and a reflux condenser. The reaction was refluxed for 24 h, but starting material remained. ^{*i*}Pr-F₇I (62 μL, 0.44 mmol, 1.5 equiv) was added a second time and the reaction was refluxed for a further 24 h. Ethyl acetate was removed under vacuum. The residue was taken up in minimal CH₂Cl₂ (< 2 mL), filtered through Celite and pentanes (15 mL) was added. The solution was stored at -32 °C overnight. The resulting precipitate was collected on a frit, washed with pentanes, and dried under vacuum to afford **24** as a red solid (21 mg, 11%). This solid contained an impurity with diagnostic resonances centered at 1.3, 2.2 and between 7.1 to 7.2 ppm by ¹H NMR. ¹H NMR (400 MHz, acetone-*d*₆): δ 7.25 – 7.09 (multiple peaks, 6H), 2.22 (s, 6H), 2.21 (s, 6H), 1.91 (s, 3H), 1.85 (s, 3H), 0.42 (s, ²*J*_{Pt-H} = 81.6 Hz, 3H). ¹⁹F NMR (376 MHz, acetone-*d*₆): δ -68.1 (d, ³*J* = 8.3 Hz, ³*J*_{Pt-F} = 126.3 Hz, 6F), -186.2 (septet, ³*J* = 8.3 Hz, ²*J*_{Pt-F} = 114.3 Hz, 1F).

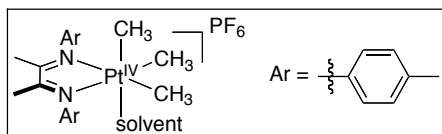


(2,6-diMePhDAB)Pt^{II}(CH₃)(^tBu-F₉) (25): (2,6-diMePhDAB)Pt^{II}(CH₃)₂ (102 mg, 0.20 mmol, 1 equiv) and ^tBu-F₉I (51 μL, 0.30 mmol, 1.5 equiv) were combined in ethyl acetate (10 mL) in a 50 mL Shlenk flask equipped with a Teflon-coated magnetic stirbar and a reflux condenser. The reaction was refluxed for 3 h. Ethyl acetate was removed under vacuum. The residue was taken up in minimal CH₂Cl₂ (< 2 mL), filtered through Celite, and pentanes (35 mL) was added. The solution was stored at -32 °C overnight. The resulting precipitate was collected on a frit, washed with pentanes, and dried under vacuum to afford **25** as a red solid (17 mg, 12%). This solid contained an impurity with diagnostic resonances centered at 1.13 and 7.15 ppm by ¹H NMR. ¹H NMR (400 MHz, acetone-*d*₆): δ 7.24 – 7.05 (multiple peaks, 6H), 2.23 (s, 6H), 2.22 (s, 6H), 1.99 (s, 3H), 1.86 (s, 3H), 0.51 (s, ²J_{Pt-H} = 86.4 Hz, 3H). ¹⁹F NMR (376 MHz, acetone-*d*₆): δ -81.8 (s, 3F), -92.3 (s, ²J_{Pt-F} = 387.3 Hz, 2F), -114.8 (s, J_{Pt-F} = 109.0 Hz, 2F), -125.8 (s, 2F).



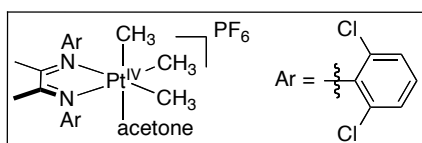
(2,6-diClPhDAB)Pt^{II}(CH₃)(ⁱPr-F₇) (26): (2,6-diClPhDAB)Pt^{II}(CH₃)₂ (68 mg, 0.11 mmol, 1 equiv) and ⁱPr-F₇I (24 μL, 0.17 mmol, 1.5 equiv) were combined in ethyl acetate (10 mL) in a 50 mL Shlenk flask equipped with a Teflon-coated magnetic stirbar and a reflux condenser. The reaction was refluxed for 20 h. Ethyl acetate was removed under vacuum. The residue was taken up in minimal CH₂Cl₂ (< 2 mL), filtered through Celite, and pentanes (15 mL) was added. The solution was stored at -32 °C overnight. The resulting precipitate was collected on a frit, washed with pentanes, and dried under vacuum to afford **26** as a dark green solid (15 mg, 18%). ¹H NMR (400 MHz, acetone-*d*₆): δ 7.79 (d, ³J = 8.4 Hz, 2H), 7.53 (d, ³J = 8.0 Hz, 2H), 7.48 (t, ³J = 8.0 Hz, 1H), 7.37 (t, ³J = 8.4 Hz, 1H), 1.95 (s, 3H), 1.91 (s, 3H), 0.63 (s, ²J_{Pt-H} = 85.2 Hz, 3H). ¹⁹F NMR

(376 MHz, acetone- d_6): δ -68.1 (d, $^3J = 8.3$ Hz, $^3J_{\text{Pt-F}} = 127.8$ Hz, 6F), -185.2 (septet, $^3J = 8.3$ Hz, 1F).



[(4-MePhDAB)Pt^{IV}(CH₃)₃(solvent)]PF₆ (32): A solution of (4-MePhDAB)Pt^{II}(CH₃)₂ (0.34 mL of a 7.4 mM solution, 1 equiv) in deuterated acetone or methylene chloride was added to a J. Young NMR tube containing 0.16 mL of the corresponding solvent. A solution of MeI (0.1 mL of a 32 mM solution, 1.3 equiv) in the corresponding solvent produced a yellow solution within 1 min. at 25 °C. The ¹H NMR spectra were consistent with the tri-methyl Pt^{IV} complex, (4-MePhDAB)Pt^{IV}(CH₃)₃I. ¹H NMR (500 MHz, 25 °C, acetone- d_6): δ 0.66 (s, $^2J_{\text{Pt-H}} = 73.2$ Hz, 3H), 0.80 (s, $^2J_{\text{Pt-H}} = 72.0$ Hz, 6H), 2.40 (s, 6H), 2.45 (s, 6H), 6.82 (broad s, 2H), 7.33 (s, 2H), 7.35 (s, 2H), 7.56 (broad s, 2H). ¹H NMR (500 MHz, 25 °C, dichloromethane- d_2): δ 0.68 (s, $^2J_{\text{Pt-H}} = 81.0$ Hz, 3H), 0.82 (s, $^2J_{\text{Pt-H}} = 71.0$ Hz, 6H), 2.30 (s, 6H), 2.42 (s, 6H), 6.70 (broad s, 2H), 7.31 (broad s, 4H), 7.51 (broad s, 2H).

A solution of AgPF₆ (80 μ L of 36 mM solution, 1.05 equiv.) in acetone- d_6 or methylene chloride- d_2 was added to the NMR tube inside of the glove box. The resulting solution was analyzed by ¹H NMR revealing a new spectrum consistent with the cationic tri-methyl Pt^{IV} complex, [(4-MePhDAB)Pt^{IV}(CH₃)₃(solvent)]PF₆ (32). ¹H NMR (400 MHz, 25 °C, acetone- d_6): δ 0.68 (s, $^2J_{\text{Pt-H}} = 67.2$ Hz, 6H), 1.06 (s, $^2J_{\text{Pt-H}} = 84.0$ Hz, 3H), 2.42 (s, 6H), 2.50 (s, 6H), 6.97 (d, $^3J = 8.4$ Hz, 4H), 7.41 (d, $^3J = 8.4$ Hz, 4H). ¹H NMR (400 MHz, 25 °C, dichloromethane- d_2): δ 0.91 (broad s, $^2J_{\text{Pt-H}} = 67.0$ Hz, 9H), 2.41 (s, 6H), 2.44 (s, 6H), 6.86 (d, $^3J = 8.4$ Hz, 4H), 7.37 (d, $^3J = 8.4$ Hz, 4H).

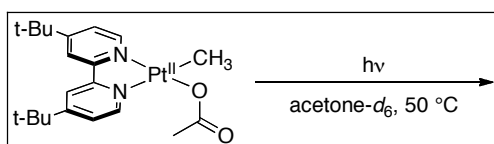


[(2,6-diClPhDAB)Pt^{IV}(CH₃)₃(acetone)]PF₆ (33): A solution of (2,6-diClPhDAB)Pt^{II}(CH₃)₂ (0.5 mL of a 5.0 mM solution, 1 equiv) in acetone- d_6 was added to a J. Young NMR. A solution of MeI (0.1 mL of a 32 mM solution, 1.3 equiv) in the

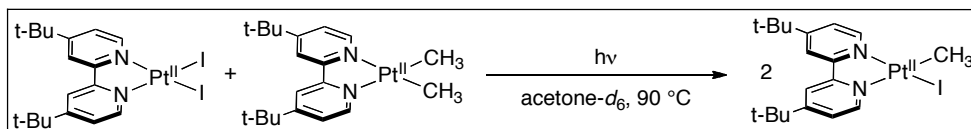
corresponding solvent produced a yellow solution within 1 min. at 25 °C. The ^1H NMR spectra were consistent with the tri-methyl Pt^{IV} complex, $(2,6\text{-diClPhDAB})\text{Pt}^{\text{IV}}(\text{CH}_3)_3\text{I}$. ^1H NMR (500 MHz, 25 °C, acetone- d_6): δ 1.74 (s, $^2J_{195\text{Pt-H}} = 78.0$ Hz, 6H), 1.85 (s, $^2J_{195\text{Pt-H}} = 80.0$ Hz, 3H), 2.15 (s, 6H), 7.21 (t, $^3J = 8.0$ Hz, 2H), 7.52 (d, $^3J = 8.0$ Hz, 4H).

A solution of AgPF_6 (80 μL of 36 mM solution, 1.05 equiv.) in acetone- d_6 was added to the NMR tube inside of the glove box. The resulting solution was analyzed by ^1H NMR revealing a new spectrum consistent with the cationic tri-methyl Pt^{IV} complex, $[(2,6\text{-diClPhDAB})\text{Pt}^{\text{IV}}(\text{CH}_3)_3(\text{acetone})]\text{PF}_6$ (**33**). ^1H NMR (400 MHz, 25 °C, acetone- d_6): δ 1.01 (s, $^2J_{\text{Pt-H}} = 74.8$ Hz, 9H), 2.79 (s, 6H), 7.53 (t, $^3J = 8.4$ Hz, 2H), 7.76 (d, $^3J = 8.4$ Hz, 4H).

5.4.6 Reaction Details

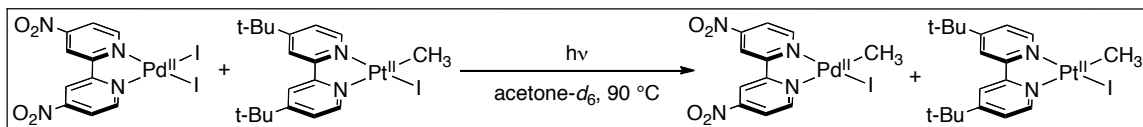


Disproportionation of $(t\text{-Bu-bpy})\text{Pt}^{\text{II}}(\text{CH}_3)\text{OAc}$ (8**).** A solution of **8** (0.6 mL of a 5.0 mM solution in acetone- d_6) was dispensed into a screw cap NMR tube. 1,3,5-trimethoxybenzene (internal standard, 15 μL of a 47.6 mM solution in acetone- d_6) was added, and the tube was sealed with a Teflon-lined cap. The reaction was monitored by ^1H NMR spectroscopy at 25 °C. When not in the NMR spectrometer for data acquisition, the sample was maintained at 50 °C and was exposed to ambient (room) light.

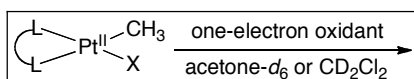


Comproportionation of $(t\text{-Bu-bpy})\text{Pt}^{\text{II}}(\text{CH}_3)_2$ (9**) and $(t\text{-Bu-bpy})\text{Pt}^{\text{II}}(\text{I})_2$.** A solution of **9** (0.15 mL of a 20.3 mM solution in acetone- d_6) and a solution of $(t\text{-Bu-bpy})\text{Pt}^{\text{II}}(\text{I})_2$ (0.45 mL of a 66.6 mM solution in acetone- d_6) were added to a screw cap NMR tube with 1,3,5-trimethoxybenzene (internal standard, 15 μL of a 47.6 mM solution in acetone- d_6). The tube was sealed with a Teflon-lined cap, and the reaction was monitored by ^1H NMR

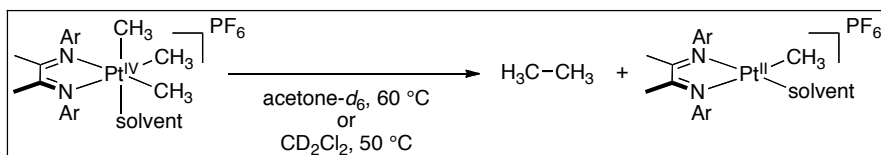
spectroscopy at 25 °C. When not in the NMR spectrometer for data acquisition, the sample was maintained at 50 °C or 90 °C and was exposed to ambient (room) light.



Methyl Transfer from (t-Bu-bpy)Pt^{II}(CH₃)I (7) to (NO₂-bpy)Pd^{II}(I)₂ (12). Solutions of 7 (0.1 mL of a 14.7 mM solution in acetone-*d*₆) and 12 (0.4 mL of a 3.3 mM solution in acetone-*d*₆) were mixed in a screw cap NMR tube with hexamethyldisiloxane (internal standard, 10 μL of 47 mM solution in acetone-*d*₆). The tube was sealed with a Teflon-lined cap, and the reaction was monitored by ¹H NMR spectroscopy at 25 °C. When not in the NMR spectrometer for data acquisition, the sample was maintained at 50 °C or 90 °C and was exposed to ambient (room) light.



One-Electron Oxidation of Platinum Complexes. In the glovebox, the platinum complex (3.0 μmol) was weighed into a J. Young NMR tube and dissolved in deuterated solvent (0.5 mL). A solution of 1,1,2-trichloroethane (internal standard, 15 μL of a 215 mM solution in the corresponding deuterated solvent) was added, and the tube was sealed with a Teflon stopcock. Initial ¹H NMR spectra were taken (and ¹⁹F NMR spectra if the complex had fluorinated ligands). Back in the glovebox, a one-electron oxidant (0.1 mL of a 3.0 mM solution in the corresponding deuterated solvent) was added. The reaction was monitored by ¹H NMR spectroscopy at 25 °C. When not in the NMR spectrometer for data acquisition, the sample was maintained at 25 °C, 55 °C, 60 °C, or 90 °C and was protected from light by wrapping the tube in foil.



Elimination of Ethane from [(4-MePhDAB)Pt^{IV}(CH₃)₃(solvent)]PF₆ (32) or [(2,6-diCIPhDAB)Pt^{IV}(CH₃)₃(acetone)]PF₆ (33). Solutions of **32** and **33** were prepared in J. Young NMR tubes as described in section 5.4.5. The tubes were sealed with a Teflon stopcock, and the reaction was monitored by ¹H NMR spectroscopy at 25 °C. When not in the NMR spectrometer for data acquisition, the samples were maintained at 50 °C (methylene chloride) or 60 °C (acetone) in the absence of light. The yield of ethane evolved in methylene chloride was estimated based on the calibration curve for ethane formation in acetone.

5.5 References

- (1) Shilov, A. E.; Shul'pin, G. B. *Chem. Rev.* **1997**, *97*, 2879.
- (2) Shilov, A. E.; Shul'pin, G. B. *Russ. Chem. Rev.* **1987**, *56*, 442.
- (3) Gol'dshleger, N. F.; Es'kova, V. V.; Shilov, A. E.; Shteinman, A. A. *Zh. Fiz. Khim.* **1972**, *46*, 1358.
- (4) Lersch, M.; Tilset, M. *Chem. Rev.* **2005**, *105*, 2471.
- (5) Ackerman, L. J.; Sadighi, J. P.; Kurtz, D. M.; Labinger, J. A.; Bercaw, J. E. *Organometallics* **2003**, *22*, 3884.
- (6) Konze, W. V.; Scott, B. L.; Kubas, G. J. *J. Am. Chem. Soc.* **2002**, *124*, 12550.
- (7) Yagyu, T.; Hamada, M.; Osakada, K.; Yamamoto, T. *Organometallics* **2001**, *20*, 1087.
- (8) Iretskii, A. V.; Sherman, S. C.; White, M. G.; Kenvin, J. C.; Schiraldi, D. A. *J. Catal.* **2000**, *193*, 49.
- (9) Shiotani, A.; Itatani, H.; Inagaki, T. *J. Mol. Catal.* **1986**, *34*, 57.
- (10) Yeung, C. S.; Dong, V. M. *Chem. Rev.* **2011**, *111*, 1215.
- (11) Strassner, T.; Muehlhofer, M.; Zeller, A.; Herdtweck, E.; Herrmann, W. A. *J. Organomet. Chem.* **2004**, *689*, 1418.
- (12) Periana, R. A.; Mironov, O.; Taube, D.; Bhalla, G.; Jones, C. J. *Science* **2003**, *301*, 814-818.
- (13) Muehlhofer, M.; Strassner, T.; Herrmann, W. A. *Angew. Chem., Int. Ed.* **2002**, *41*, 1745.
- (14) Kao, L. C.; Hutson, A. C.; Sen, A. *J. Am. Chem. Soc.* **1991**, *113*, 700.
- (15) (d) Gretz, E.; Oliver, T. F.; Sen, A. *J. Am. Chem. Soc.* **1987**, *109*, 8109.
- (16) Butschke, B.; Schwarz, H. *Organometallics* **2011**, *30*, 1588.
- (17) Remy, M. S.; Cundari, T. R.; Sanford, M. S. *Organometallics*, **2010**, *29*, 1522.
- (18) Lanci, M. P.; Remy, M. S.; Kaminsky, W.; Mayer, J. M.; Sanford, M. S. *J. Am. Chem. Soc.* **2009**, *131*, 15618.
- (19) Thompson, P. J.; Puddephatt, R. J. *Chem. Commun.* **1975**, 841.
- (20) Puddephatt, R. J.; Thompson, P. J. *J. Chem. Soc., Dalton Trans.* **1975**, 1810.
- (21) Puddephatt, R. J.; Thompson, P. J. *J. Organometallic Chem.* **1976**, *120*, C51.

-
- (22) Puddephatt, R. J.; Thompson, P. J. *J. Chem. Soc., Dalton Trans.* **1977**, 1219.
- (23) Scott, J. D.; Puddephatt, R. J. *Organometallics* **1983**, *2*, 1643.
- (24) Johansson, L.; Ryan, O. B.; Rømming, C.; Tilset, M. *Organometallics* **1998**, *17*, 3957.
- (25) Moret, M.-E.; Chen, P. *J. Am. Chem. Soc.* **2009**, *131*, 5675.
- (26) Hill, G. S.; Yap, G. P. A.; Puddephatt, R. J. *Organometallics*, **1999**, *18*, 1408.
- (27) Hill, G. S.; Puddephatt, R. J. *Organometallics*, **1997**, *16*, 4522.
- (28) Van Asselt, R.; Rijnberg, E.; Elsevier, C. J. *Organometallics* **1994**, *13*, 706.
- (29) Procelewska, J.; Zahl, Liehr, G.; van Eldik, R.; Smythe, N. A.; Williams, B. S.; Goldberg, K. I. *Inorg. Chem.* **2005**, *44*, 7732.
- (30) Williams, B. S.; Goldberg, K. I. *J. Am. Chem. Soc.* **2001**, *123*, 2576.
- (31) Goldberg, K. I.; Yan, J. Y.; Breitung, E. M. *J. Am. Chem. Soc.* **1995**, *117*, 6889.
- (32) Goldberg, K. I.; Yan, J. Y.; Winter, E. L. *J. Am. Chem. Soc.* **1994**, *116*, 1573.
- (33) Luedtke, A. T.; Goldberg, K. I. *Inorg. Chem.* **2007**, *46*, 8496.
- (34) Fekl, U.; Goldberg, K. I. *J. Am. Chem. Soc.* **2002**, *124*, 6804.
- (35) Fekl, U.; Kaminsky, W.; Goldberg, K. I. *J. Am. Chem. Soc.* **2001**, *123*, 6423.
- (36) Grice, K. A.; Scheuermann, M. L.; Goldberg, K. I. *Top. Organomet. Chem.* **2011**, *35*, 1.
- (37) Driver, T. G.; Williams, T. J.; Labinger, J. A.; Bercaw, J. E. *Organometallics* **2007**, *26*, 294.
- (38) Williams, T. J.; Caffyn, A. J. M.; Hazari, N.; Oblad, P. F.; Labinger, J. A.; Bercaw, J. E. *J. Am. Chem. Soc.* **2008**, *130*, 2418.
- (39) Bercaw, J. E.; Hazari, N.; Labinger, J. A.; Oblad, P. F. *Angew. Chem., Int. Ed.* **2008**, *47*, 9941.
- (40) Owen, J. S.; Labinger, J. A.; Bercaw, J. E. *J. Am. Chem. Soc.* **2006**, *128*, 2005.
- (41) Driver, T. G.; Day, M. W.; Labinger, J. A.; Bercaw, J. E. *Organometallics*, **2005**, *24*, 3644.
- (42) Heiberg, H.; Johansson, L.; Gropen, O.; Ryan, O. B.; Swang, O.; Tilset, M. *J. Am. Chem. Soc.* **2000**, *122*, 10831.
- (43) Crabtree, R. H. *The Organometallic Chemistry of the Transition Metals* Hoboken: Wiley Interscience, 1995
- (44) Suzuki, Y.; Yagyu, T. Yamamura, Y.; Mori, A.; Osakada, K. *Organometallics* **2002**, *21*, 5254.
- (45) Suzuki, Y.; Osakada, K. *Bull. Chem. Soc. Jpn.* **2004**, *77*, 139.
- (46) Hughes, R. P.; Ward, A. J.; Rheingold, A. L.; Zakharov, L. N. *Can. J. Chem.* **2003**, *81*, 1270.
- (47) Hill, G. S.; Irwin, M. J.; Levy, C. J.; Rendina, L. M.; Puddephatt, R. J. *Inorg. Synth* **1998**, *32*, 149.
- (48) Drew, D.; Doyle, J. R.; Shaver, A. G. *Inorg. Synth.* **1990**, *28*, 346.
- (49) Appleton, T. G.; Hall, J. R.; Kennard, C. H. L.; Mathieson, M. T.; Neale, D. W.; Smith, G.; Mak, T. C. W. *J. Organometallic Chem* **1993**, *453*, 299.
- (50) Hughes, R. P.; Overby, J. S.; Lam, K.-C.; Incarvito, C. D.; Rheingold, A. L. *Polyhedron* **2002**, *21*, 2357.
- (51) Appleton, T. G.; Hall, J. R.; Williams, M. A. *J. Organometallic Chem.* **1986**, *303*, 139.
- (52) Thomson, J.; Slawin, A. M. Z.; Jain, S. L.; Lobban, J. *Inorg. Chem. Comm.* **2005**, *8*, 782.

-
- (53) Hughes, R. P.; Sweetser, J. T.; Tawa, M. D.; Williamson, A.; Incarvito, C. D.; Rhatigan, B.; Rheingold, A. L.; Rossi, G. *Organometallics* **2001**, *20*, 3800.
- (54) Connelly, N. G.; Geiger, W. E. *Chem. Rev.* **1996**, *96*, 877.
- (55) Fortman, G. C.; Scott, N. M.; Linden, A.; Stevens, E. D.; Dorta, R.; Nolan, S. P. *Chem. Commun.* **2010**, *46*, 1050.
- (56) Reed, A. E.; Weinhold, F. *J. Chem. Phys.* **1983**, *78*, 4066.
- (57) Peng, C.; Ayala, P. Y.; Schlegel, H. B.; Frisch, M. J. *J. Comp. Chem.* **1996**, *17*, 49.
- (58) Becke, A. D. *J. Chem. Phys.* **1993**, *98*, 5648.
- (59) Lee, C.; Yang, W.; Parr, R. G. *Phys. Rev. B* **1998**, *37*, 785.
- (60) Miehlich, B.; Savin, A.; Stoll, H.; Preuss, H. *Chem. Phys. Lett.* **1989**, *157*, 200.
- (61) Hay, J.; Wadt, W. R. *J. Chem. Phys.* **1985**, *82*, 270.
- (62) Hay, P. J.; Wadt, W. R. *J. Chem. Phys.* **1985**, *82*, 284.
- (63) Hay, P. J.; Wadt, W. R. *J. Chem. Phys.* **1985**, *82*, 299.
- (64) Hehre, W. J.; Radom, L.; Schleyer, P. v. R.; Pople, J. A. *Ab Initio Molecular Orbital Theory*; Wiley: New York, 1986.
- (65) Cramer, C. J. *Essentials of Computational Chemistry, 2nd Ed.*, Wiley: Chichester, 2004.
- (66) Levy, C. J.; Vittal, J. J.; Puddephatt, R. J. *Organometallics* **1996**, *15*, 2108.
- (67) Achar, S.; Scott, J. D.; Vittal, J. J.; Puddephatt, R. J. *Organometallics* **1993**, *12*, 4592.
- (68) Tappe, K.; Knochel, P. *Tetrahedron: Asymm.* **2004**, *15*, 91.
- (69) Zhong, H. A.; Labinger, J. A.; Bercaw, J. E. *J. Am. Chem. Soc.* **2002**, *124*, 1378.
- (70) Alcázar, J. Begtrup, M.; de la Hoz, A. *J. Chem. Soc., Perkin Trans.* **1995**, 2467.
- (71) Scollard, J. D.; Labinger, J. A.; Bercaw, J. E. *Helv. Chim. Acta* **2001**, *84*, 3247.
- (72) Gerdes, G.; Chen, P. *Organometallics*, **2003**, *22*, 2217.
- (73) Zhang, D.; Telo, J. P.; Liao, C.; Hightower, S. E.; Clennan, E. L. *J. Phys. Chem. A* **2007**, *111*, 13567.
- (74) ten Brink, G.-J.; Arends, I. W. C. E.; Hoogenraad, M.; Verspui, G.; Sheldon, R. A. *Adv. Synth. Catal.* **2003**, *345*, 497.

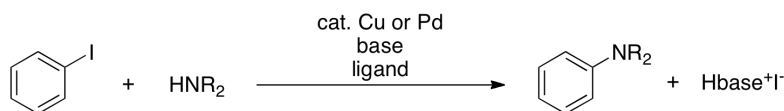
CHAPTER 6

Nitrogen Insertion into Palladium–Carbon Bonds

6.1 Background and Significance

Compounds containing carbon-nitrogen bonds are of great importance in many areas of chemistry, and as a result, transition metal-catalyzed approaches to C–N bond formation have been the subject of intense recent research. In particular, Pd- and Cu-catalyzed aminations of aryl halides have proven to be powerful and widely used synthetic methods for the construction of arylamines (Scheme 6.1).¹ However, despite their great utility, these transformations remain fundamentally limited by the fact that the aryl coupling partner must be prefunctionalized with a halide at the desired position, which increases the number of steps required in a synthetic sequence.

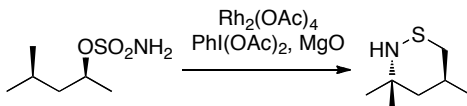
Scheme 6.1 Metal catalyzed amination of aryl halides.



An alternative approach to the synthesis of amines would be the direct conversion of C–H bonds into C–N bonds, an attractive transformation from the standpoints of atom economy and synthetic simplicity.² Several effective methods for the intra- and intermolecular amination of sp^3 C–H bonds have been developed, and these typically utilize rhodium carboxylate, copper homoscorpionate, or metalloporphyrin based catalysts in conjunction with either $\text{PhI}=\text{NR}$ or $\text{PhI}(\text{OAc})_2/\text{MgO}/\text{RNH}_2$ as the aminating reagent (Scheme 6.2).³ The mechanism of these transformations generally involves direct insertion of a metallonitrene into the C–H bond. As a result, the observed selectivities typically parallel those of radical reactions, with preferential amination of activated

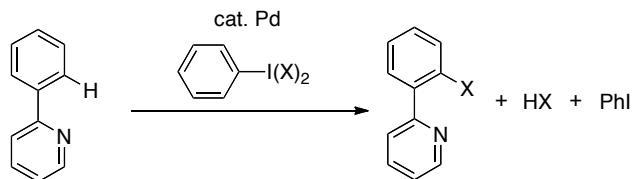
and/or weak C–H bonds (e.g., tertiary, secondary, benzylic, or C–H bonds α to heteroatoms).²

Scheme 6.2 Rh-catalyzed C–H Amination.³

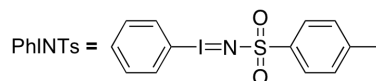


Our group and others have developed a number of Pd-catalyzed processes for converting C–H bonds into C–O,⁴⁻⁸ C–halogen,^{4,9-12} and C–C bonds¹³⁻¹⁵ using iodine(III) reagents as terminal oxidants (Scheme 6.3). In contrast to the aminations described above, these transformations proceed via C–H activation to form discrete organometallic palladacyclic intermediates.¹⁶⁻¹⁹ As such, selectivity is dictated by proximity to a directing group and by steric effects, rather than by the strength/degree of activation of the C–H bonds. We have had a longstanding interest in extending these reactions to C–N bond formation, because such a transformation could serve as a valuable complement to both the amination of aryl halides and the metallonitrene insertion reactions described above. This chapter describes the development of a method for Pd^{II}-mediated oxidative C–H bond amination. We demonstrate that diverse palladacyclic complexes (which were all initially formed by directed C–H activation) undergo stoichiometric amination reactions with PhI=NTs (Scheme 6.4) and related oxidants. Investigations of the scope of these reactions as well as mechanistic insights into the key “NTs” insertion step are described below.

Scheme 6.3 Pd-catalyzed Ligand-Directed Functionalization of C–H Bonds.



Scheme 6.4 Structure of PhI=NTs oxidant.

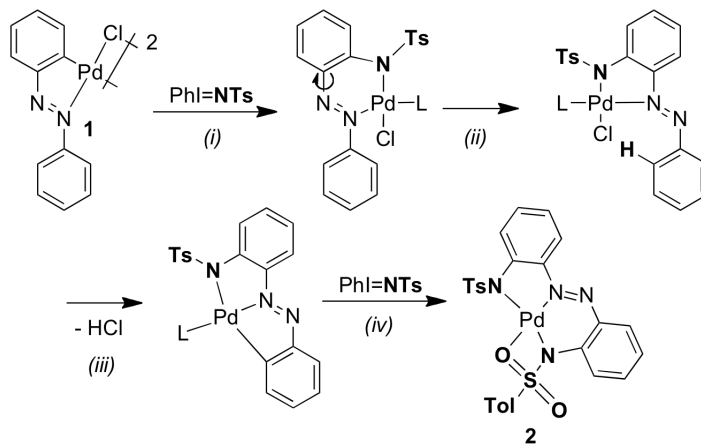


6.2 Results and Discussion

Our initial studies focused on demonstrating the feasibility of the stoichiometric oxidative amination of palladacycles (complexes that are typically formed via directed C–H activation reactions). We selected $\text{PhI}=\text{NTs}$ ²⁰ as the amination reagent on the basis of (i) our previous success using hypervalent iodine compounds in Pd-catalyzed C–H functionalization reactions, (ii) literature precedent for the insertion of “O” into Pd–C bonds using the analogous iodine(III) oxidant $\text{ArI}=\text{O}$,²¹ and (iii) literature precedent for $\text{PhI}=\text{NTs}$ to generate highly reactive metal-imido intermediates.²² The chloride-bridged azobenzene dimer **1** was chosen as the initial substrate, because its reactivity with $\text{ArI}=\text{O}$ had been explored previously.²¹

Dr. Allison Dick demonstrated that reaction of dimer **1** with the hypervalent iodine reagent, $\text{PhI}=\text{NTs}$ resulted in a double-insertion of the “NTs” group to give compound **2** (Scheme 6.1).²³ This reaction was proposed to occur by (i) an initial “NTs” insertion into the Pd–C bond, (ii) decoordination of the azo linkage to form a more favorable five-membered palladacycle, (iii) ortho C–H activation of the adjacent aryl ring, and (iv) a second “NTs” insertion event to afford the final product (Scheme 6.5).

Scheme 6.5 Proposed Mechanism for Double Nitrogen Insertion into Complex **1**.



Subsequently, we turned our attention to palladacycles of benzo[*h*]quinoline, which do not offer the possibility for a second ortho C–H activation event. A series of cyclometalated benzo[*h*]quinoline complexes, including the acetate-bridged dimer **3**, the chloride-bridged dimer **4**, and the *in situ*-generated monomeric pyridine complexes **5** and

6 (Scheme 6.6), were treated with 1.3 equiv of PhI=NTs in MeCN. The crude reactions were then evaporated to dryness, treated with CDCl₃ containing 25% C₅D₅N (in order to convert any halide-and/or acetate-bridged Pd^{II} products to more readily detectable monomers), and assayed by ¹H NMR spectroscopy. With the Pd^{II} starting materials **3-5**, this sequence afforded a complex and largely inseparable mixture of inorganic and organic compounds. However, in all three cases, significant quantities (9-31%) of the desired “NTs” insertion product **7** or **8** were formed. These Pd^{II} complexes were identified in the crude ¹H NMR spectra, by comparison to independently synthesized samples of **7/8**. Interestingly, the organic products **9a/9b**, which result from C–X coupling (X = Cl, OAc depending on the counterion associated with the starting Pd complex), could also be identified in some of these reactions.⁴ As summarized in Table 6.1, chlorinated and/or acetoxyated organic products were formed in yields of up to 18%, and the formation of substantial quantities of these organic side products was inversely correlated to the yield of the desired “NTs” insertion product.

Scheme 6.6 Palladium Complexes of Benzo[*h*]quinoline.

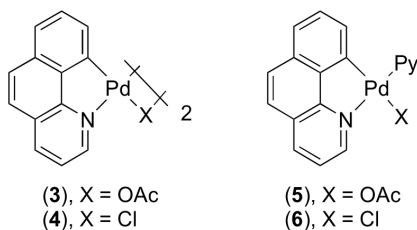
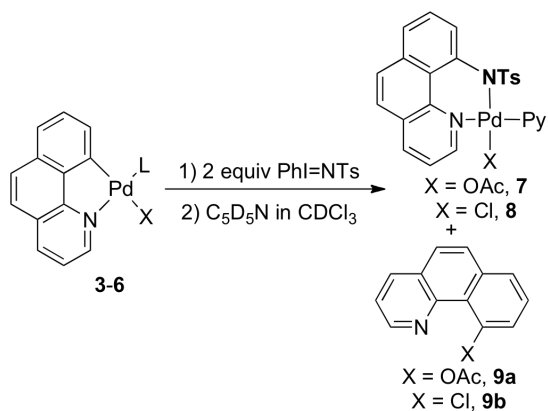


Table 6.1 Major Products Observed from the Reaction of Complexes **3-6** with PhI=NTs.

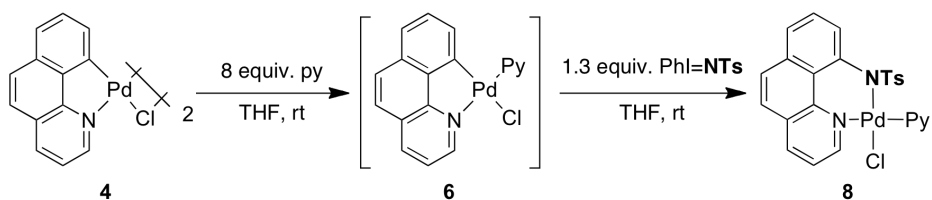


Entry	Complex	Product (yield)	Product (yield)
1	3^a	7 (31%)	9a (0%)
2	4^a	8 (9%)	9b (18%)
3	5^a	7 (16%)	9a (5%)
4	6	8 (51%)	9b (< 2%)

^a Significant quantities of additional unidentified inorganic and organic side products were observed

In contrast to the reactions of **3-5**, the monomeric chloride complex **6** reacted with PhI=NTs to produce a single major inorganic product (**8**) in 51% yield (based on ¹H NMR spectroscopic analysis of the crude reaction mixture), and complex **8** was isolated as a yellow solid in 42% yield. The isolated yield could be improved to 78% when the reaction was conducted in THF (Scheme 6.7). Notably, the C–Cl bond-forming reductive elimination product **9b** was not observed in this transformation.

Scheme 6.7 Reaction Sequence for Synthesis of Complex **8**.



Palladacycle **6** was reacted with PhI=NTs in MeCN-*d*₃ at 25 °C, and the reaction was monitored by ¹H NMR spectroscopy. During the course of the reaction, starting palladacycle **6** and aminated palladacycle **8** were the only benzo[*h*]quinoline products

observed. In the benzyl region of the spectra, resonances were observed corresponding to the benzylic methyl group of the oxidant, the corresponding benzylic methyl resonance of the product **8**, and the methyl resonance of H₂NTs. Interestingly, a second palladium product, (py)₂PdCl₂ (di-pyridine palladium dichloride) was also formed in the reaction. The origin of H₂NTs is presumed to be hydrolysis of the PhI=NTs oxidant. However, the origin of (py)₂PdCl₂ is unclear, as no other palladium byproducts were observed. The ratio of H₂NTs to (py)₂PdCl₂ changed from 1.9:1 to 2.6:1 over the 30 min course of the reaction, suggesting that formation of these byproducts are not related.

The structure of **8** was confirmed by ¹H NMR spectroscopy, which clearly showed the incorporation of a single “NTs” moiety into the starting complex. In addition, crystals suitable for X-ray analysis were obtained by slow diffusion of diethyl ether into a chlorobenzene solution of **8**, and the solid-state structure of **8** is shown in Scheme 6.8. Selected bond distances and bond angles can be found in Table 6.2. In this square-planar palladium(II) complex, the chloride ligand resides trans to the NTs moiety and the pyridine trans to the nitrogen atom of the benzoquinoline ligand. The Pd–N and Pd–Cl bond lengths are comparable to those found in related complexes,^{24,25} and as expected, the bond to the anionic nitrogen is the shorter of the two Pd–N bonds (1.997 versus 2.050 Å). Strikingly, structural analysis reveals that palladium retains a square planar geometry at the expense of planarity of the newly aminated benzo[*h*]quinoline ligand ($\tau_{\text{N1-C13-C12-C11}} = 14.9(7)^\circ$).

Scheme 6.8 ORTEP Diagram for Complex **8**.

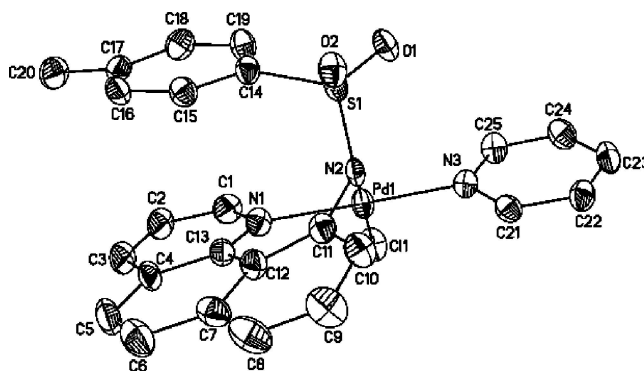
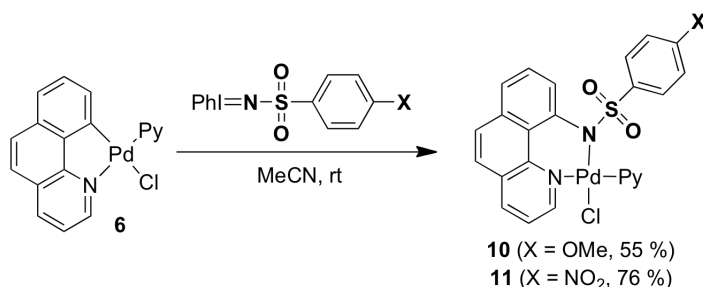


Table 6.2 Selected Bond Distances (Å) and Bond Angles (°) for Complex **8**.

Bond Distances (Å)		Bond Angles (°)	
Pd(1)–N(1)	2.050(4)	N(2)–Pd(1)–N(1)	86.84
Pd(1)–N(2)	1.997(4)	N(2)–Pd(1)–N(3)	89.14
Pd(1)–N(3)	2.026(4)	N(3)–Pd(1)–N(1)	175.97
Pd(1)–Cl(1)	2.3277(12)	N(1)–Pd(1)–Cl(1)	175.04

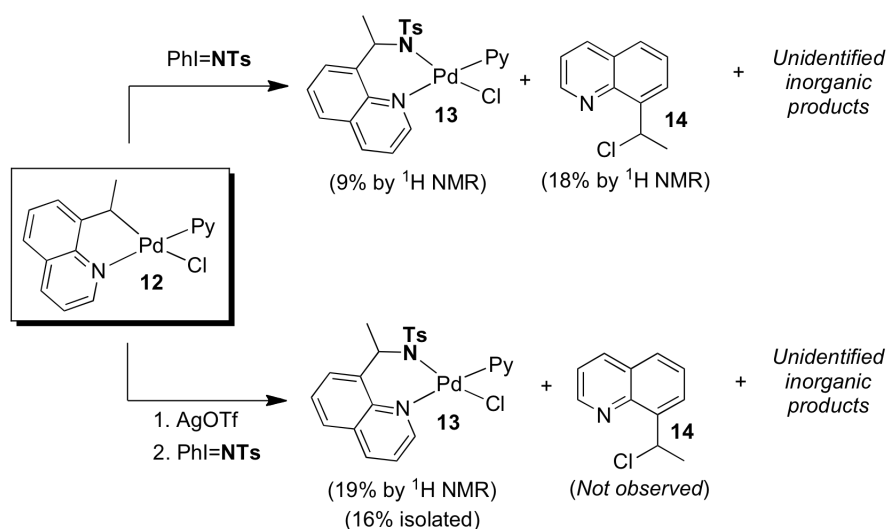
Reactions of the *in situ*-generated palladacycle **6** with hypervalent iodide oxidants derived from electronically diverse benzenesulfonamides were also explored. As summarized in Scheme 6.9, these transformations proceeded in modest to good yields with oxidants containing both electron-donating and electron-withdrawing substituents on the aryl group of the sulfonamide. When the rates of sulfonamide insertion into isolated monomer **6**²⁶ were measured under identical reaction conditions, the formation of **8** was found to proceed to completion within 30 min, while the reactions to form **10** and **11** required 2 and 2.5 h, respectively, to reach complete conversion. However, it is difficult to draw definitive mechanistic conclusions from these kinetic data, due to the dramatically varied solubilities of these iodine(III) aminating reagents as well as their susceptibility toward hydrolysis under the reaction conditions.

Scheme 6.9 Amination of Complex **6** with Electronically Diverse Oxidants.

Analogous NTs insertion reactions were also examined with palladacycles containing *sp*³ Pd–C bonds. For example, the 8-ethylquinoline complex **12** reacted with 1.3 equiv of PhI=NTs to afford **13** in 9% yield (as determined by ¹H NMR spectroscopy) along with a number of unidentified Pd-containing species (Scheme 6.10). Interestingly,

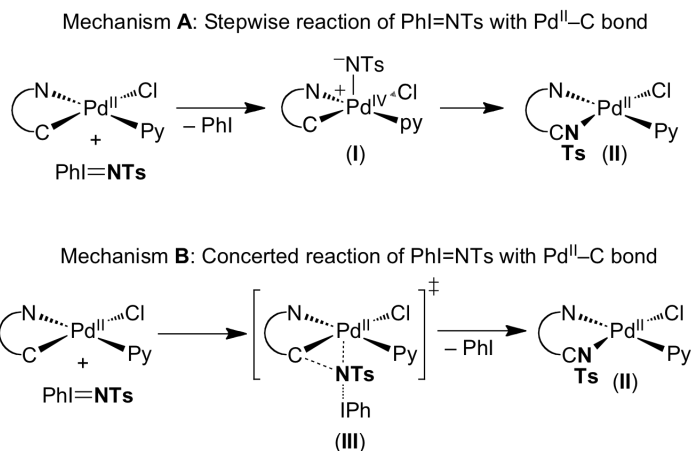
the C–Cl bond-forming reductive elimination product **14** was identified as the major organic byproduct of this reaction. Removal of the chloride ligand from **12** with AgOTf prior to addition of the oxidant eliminated this competing transformation and increased the ^1H NMR yield of aminated palladacycle **13** to 19%. For reactions with and without addition of AgOTf, significant quantities of $(\text{py})_2\text{PdCl}_2$ were also identified by ^1H NMR spectroscopy. Again, the origin of this byproduct is unclear, but it is believed to contribute to the low overall yield of **13**.

Scheme 6.10 Amination of Palladium-8-Ethylquinoline Complex **12**.



There are at least two possible mechanisms for the “ $\text{NSO}_2\text{-Ar}$ ” insertion reactions: a stepwise process (Scheme 6.11, Mechanism A) and a concerted pathway (Scheme 6.11, Mechanism B). The stepwise mechanism would involve (i) initial nucleophilic attack of the Pd(II) center on $\text{PhI}=\text{NTs}$, (ii) loss of PhI to form a discrete Pd(IV) imido intermediate (I), and (iii) collapse of the intermediate to afford the insertion product. Alternatively, the concerted process would proceed by a transition state involving a three-centered interaction between the Pd(II) center, the bound carbon, and the “ NTs ” group (**III** in Scheme 6.11).

Scheme 6.11 Possible Mechanisms for Insertion of “NTs” into the Pd–C Bond.



While these two mechanisms are difficult to definitively distinguish from one another, we currently favor mechanism **A** for several reasons. First, the closely related reaction of ArI=O with palladacycles has been proposed to proceed via a stepwise mechanism similar to **A**.^{27,28} In addition, Pd^{IV}-oxo intermediates analogous to **I** have been proposed as intermediates in the reactions of Pd–C bonds with both inorganic and organic peroxides.^{29,30} Finally, the observation of organic side products **9a**, **9b**, and **14** resulting from C–X coupling (X = OAc, Cl) is also consistent with a mechanism involving Pd^{IV} intermediates. Both C–OAc¹⁸ and C–Cl^{19,31–33} bond-forming reductive elimination have been shown to be facile from Pd^{IV} centers; in contrast, analogous reactions at Pd^{II} complexes are generally kinetically slow and/or thermodynamically unfavorable.^{34,35} As such, we hypothesize that **9b** and **14** are generated by a C–Cl coupling reaction from intermediate **I** that is competitive with “NTs” insertion into the Pd–C bond. Computations inspired by our initial report have subsequently provided additional support for our proposal, indicating that a pathway proceeding through a singlet Pd^{IV}-imido (**I**, Mechanism A) is lower in energy than mechanism B.³⁶ Comparison of **I** to other electronic structures, including a triplet Pd^{IV}-imido, and singlet and triplet nitrene complexes indicates that **I** is indeed the ground state electronic structure.

With optimal conditions for the NTs insertion reaction in hand, we next sought to liberate the newly aminated organic ligands from the Pd center via protonolysis of the

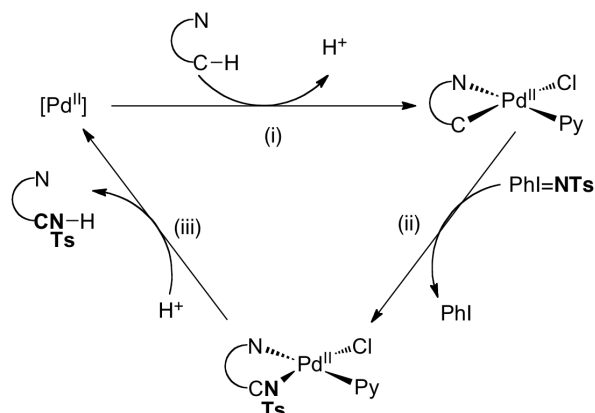
Pd–N bond. A series of acidic reaction conditions were examined to achieve this goal, and the results are reported in Table 6.3. Interestingly, no C–N bond cleavage was observed in neat AcOH at room temperature or at 100 °C (Table 6.3, entries 1 and 2). In contrast, neat trifluoroacetic acid afforded appreciable (~15%) conversion to product **15** at room temperature (entry 3). The addition of 5 equivalents of HCl resulted in quantitative cleavage of the Pd–N bond to afford **15** (entry 5), and analogous conditions were also effective for the release of **16** from complex **13** (entry 6). Notably, with the success of these protonolysis reactions, we have established the feasibility of the three elementary steps (i) cyclopalladation, (ii) oxidative amination, and finally (iii) protonolysis for release of the aminated product (Scheme 6.12).

Table 6.3 Acid Cleavage of Aminated Palladacycles.

Entry	Product	Conditions	% Conversion ^a
1	 TsHN 15	Neat AcOH, 25 °C	n/r
2		Neat AcOH, 100 °C	n/r
3		Neat CF ₃ CO ₂ H, 25 °C	15%
4		1 equiv HCl	80%
5		5 equiv HCl	100%
6	 NHTs 16	5 equiv HCl	42% ^b

(a) % Conversion determined by ¹H NMR spectroscopy; (b) Isolated yield

Scheme 6.12 Proposed Catalytic Cycle for Palladium-Catalyzed Amination of C–H Bonds.



6.3 Conclusions

In summary, we described a new mild reaction for the stoichiometric conversion of C–H bonds into amines via palladacyclic intermediates. This transformation is proposed to proceed via a stepwise mechanism involving a Pd^{IV}-imido intermediate. Notably, while this work was in progress, Che and co-workers reported a related Pd-catalyzed directed oxidative C–H amination reaction that uses K₂S₂O₈ as a stoichiometric oxidant.³⁷ Since, multiple reports have demonstrated the use of Pd^{II/IV} cycles for catalytic conversion of C–H bonds to C–N bonds.^{38–40} The further development of this methodology will provide an attractive complement to existing transformations such as the catalytic amination of aryl halides and nitrene insertion into activated C–H bonds.

6.4 Experimental Procedures

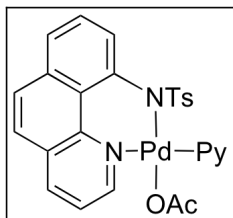
6.4.1 General Procedures

NMR spectra were obtained on a Varian Inova 500 (499.90 MHz for ¹H; 125.70 MHz for ¹³C) or a Varian Inova 400 (399.96 MHz for ¹H; 100.57 MHz for ¹³C) spectrometer. ¹H NMR chemical shifts are reported in parts per million (ppm) relative to TMS, with the residual solvent peak used as an internal reference. Multiplicities are reported as follows: singlet (s), doublet (d), doublet of doublets (dd), doublet of doublet of doublets (ddd), doublet of triplets (dt), triplet of doublets (td), triplet of triplets (tt),

triplet (t), doublet of quartets (dq), quartet (q), multiplet (m), and broad resonance (br). Infrared spectra were obtained on a Perkin-Elmer FT-IR Spectrum BX spectrometer. High resolution mass spectral data were obtained on a Micromass AutoSpec Ultima magnetic sector mass spectrometer.

6.4.2 Materials and Methods

Benzo[*h*]quinoline was purchased from TCI America or Aldrich and used as received. PhI=NTs⁴¹ and the OMe- and NO₂-⁴² substituted variants were prepared according to literature procedures from commercially available sulfonamides. Palladium(II) dimers of benzo[*h*]quinoline^{43,44} and 8-ethylquinoline⁴⁵ were prepared according to literature procedures. Authentic samples of PdCl₂(py)₂ were prepared according to literature procedure.⁴⁶ PdCl₂ and Na₂PdCl₄ were purchased from Pressure Chemical and used as received. Solvents were purchased from Fisher Scientific and used without further purification. All reactions were carried out under ambient atmosphere. Flash chromatography was performed on Silicycle Silica P flash silica gel (40-63 μm particle size, 60 Å pore diameter, 50 m²/g surface area) and thin layer chromatography was performed on EMD TLC plates pre-coated with 250 μm thickness silica gel 60 F₂₅₄.



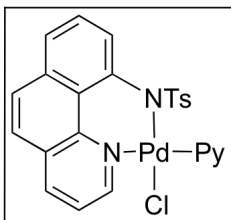
Product 7. Complex **8** (33.1 mg, 0.06 mmol, 1 equiv) was dissolved in 5 mL of CH₂Cl₂ in a 20 mL scintillation vial equipped with a Teflon stirbar. Silver acetate was added, and the mixture was stirred for 30 min. AgCl was removed by filtration through Celite, and the Celite pad was washed with CH₂Cl₂ (3 × 5 mL). The yellow solution was concentrated, and a solid was precipitated with Et₂O. The yellow solid was collected on a fritted filter (21.1 mg, 61% yield). ¹H NMR (CDCl₃): δ 8.96 (2H, dt, *J* = 5.1, 1.6 Hz), 8.68 (1H, dd, *J* = 5.5, 1.6 Hz), 8.04 (1H, dd, *J* = 8.0, 1.5 Hz), 7.88-7.72 (5H, multiple peaks), 7.47-7.41 (3H, multiple peaks), 7.31 (1H, dd, *J* = 7.9, 5.5 Hz), 7.14 (2H, d, *J* = 8.1 Hz), 6.48 (2H, d, *J* = 7.9 Hz), 1.99 (3H, s), 1.79 (3H, s). ¹³C NMR (CDCl₃): δ 177.54,

151.78, 151.30, 141.92, 140.44, 139.57, 139.13, 138.49, 137.96, 135.97, 130.28, 130.06, 129.11, 127.79, 127.39, 126.71, 126.36, 125.61, 124.91, 124.02, 121.69, 23.86, 21.06. HRMS-electrospray (m/z): calcd for $[C_{27}H_{23}N_3O_4PdS - C_5H_5N + Na^+]$, 534.9920; found, 534.9928.

Products 7 and 9a (Procedure to determine yield by 1H NMR spectroscopy). Complex **3** (12.5 mg, 0.02 mmol, 1 equiv) and PhINTs (17.6 mg, 0.5 mmol, 1.3 equiv relative to [Pd]) were weighed into six 4 mL vials. Each vial was equipped with a Teflon stirbar, and 2 mL MeCN was added to each vial. Pyridine (25 μ L, 0.33 mmol, 36 equiv relative to [Pd]) was added to 3 vials to generate complex **7** in situ. Reactions were stirred overnight. Solvent was removed under vacuum, and the resulting oil was dissolved in 0.7 mL of a 3:1 $CDCl_3:C_5D_5N$ solution containing 1,3,5-trimethoxybenzene as an internal standard. For each vial, yields of **7** and **9a** were determined by 1H NMR, and average yields were calculated for reactions from **3** and **5**.

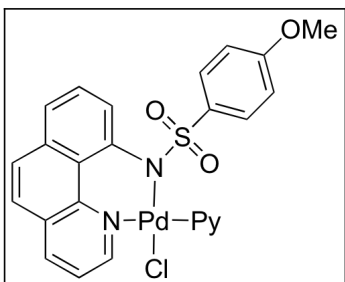
Products 8 and 9b (Procedure to determine yield by 1H NMR spectroscopy). The same procedure was followed as that used for determination of **8** and **9b** yields, only complex **4** (11.6 mg, 0.02 mmol, 1 equiv) was used instead of complex **3**.

Products 8, 10, and 11 (General Procedure). Complex **4** (51.2 mg, 0.08 mmol, 1 equiv) was suspended in MeCN or THF (8 mL) in a 20 mL scintillation vial equipped with a Teflon stirbar. Pyridine (50 μ L, 0.66 mmol, 8 equiv) was added to convert **4** to the corresponding monomer **6**, and the reaction mixture was stirred until all of the solids dissolved. The iminoiodinane reagent (0.21 mmol, 2.6 equiv, 1.3 equiv per [Pd]) was added, and the reaction mixture was stirred at 25 $^{\circ}C$ for between 4 and 18 h. The solvent was removed under vacuum, and the product was purified by recrystallization. The reaction times and purification conditions varied between substrates and are reported in detail below.



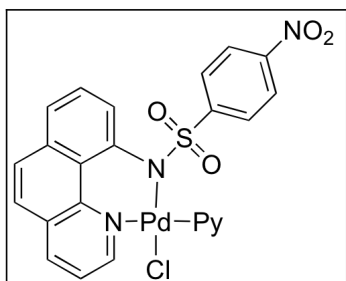
Product 8. Procedure 1 (in MeCN). Reaction time: 4 h. The product was recrystallized twice from CH₂Cl₂/Et₂O. Each crop of crystals was collected on a fritted filter and washed with ether (3 × 25 mL). Product **8** was obtained as a pale yellow solid (48.2 mg, 42% yield).

Procedure 2 (in THF). Reaction time: overnight. The product was recrystallized from CH₂Cl₂/hexanes, collected on a fritted filter, and washed with a 60/40 mixture of hexanes and isopropyl alcohol (3 × 20 mL). Product **8** was obtained as a pale yellow solid (70.9 mg, 78% yield). ¹H NMR (CDCl₃): δ 9.16 (1H, dd, *J* = 5.5, 1.6 Hz), 9.00 (2H, dt, *J* = 5.1, 1.6 Hz), 8.05 (1H, dd, *J* = 8.0, 1.6 Hz), 7.88-7.73 (5H, multiple peaks), 7.47-7.42 (3H, multiple peaks), 7.33 (1H, dd, *J* = 7.9, 5.5 Hz), 7.05 (2H, dt, *J* = 8.5, 2.0 Hz), 6.48 (2H, dd, *J* = 8.4, 0.4 Hz), 1.99 (3H, s). ¹³C NMR (CDCl₃): δ 154.24, 152.59, 141.96, 140.61, 139.33, 138.93, 138.58, 138.16, 136.01, 130.39, 129.86, 128.39, 127.86, 127.64, 126.68, 126.22, 125.60, 125.04, 124.15, 121.96, 21.08. Anal. Calcd for C₂₅H₂₀ClN₃O₂PdS: C, 52.83; H, 3.55; N, 7.39. Found: C, 52.56; H, 3.26; N, 7.10.

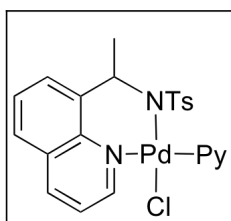


Product 10. Reaction time: overnight. Note: 4 equiv of oxidant per [Pd] was used. The product was recrystallized three times from CH₂Cl₂/Et₂O. Notably, the first addition of Et₂O to a CH₂Cl₂ solution of **6** resulted in the precipitation of an unidentified black solid. The yellow solution was decanted away from this solid, and further addition of ether led to crystallization of the desired product **10**. None of this black solid was observed in subsequent recrystallizations. Each crop of crystals was collected on a fritted filter and washed with ether (3 × 25 mL). Product **10** was obtained as a light yellow solid (51.4 mg,

55% yield). ^1H NMR (CDCl_3): δ 9.21 (1H, dd, $J = 5.5, 1.6$ Hz), 9.00 (2H, dt, $J = 5.2, 1.6$ Hz), 8.08 (1H, dd, $J = 7.9, 1.5$ Hz), 7.88-7.72 (5H, multiple peaks), 7.47-7.43 (3H, multiple peaks), 7.35 (1H, dd, $J = 7.9, 5.5$ Hz), 7.09 (2H, dt, $J = 8.9, 2.9$ Hz), 6.17 (2H, dt, $J = 8.9, 2.9$ Hz), 3.56 (3H, s). ^{13}C NMR (CDCl_3): δ 160.89, 154.25, 152.57, 141.97, 138.97, 138.58, 138.41, 136.00, 134.30, 130.41, 129.88, 128.41, 128.07, 127.67, 126.77, 125.60, 125.03, 124.25, 122.09, 112.44, 55.37. Anal. Calcd for $\text{C}_{25}\text{H}_{20}\text{ClN}_3\text{O}_3\text{PdS}$: C, 51.38; H, 3.45; N, 7.19. Found: C, 51.54; H, 3.46; N, 7.08.



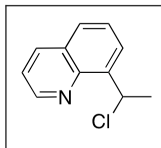
Product 11. Reaction time: 8 h. The product was recrystallized twice from $\text{CH}_2\text{Cl}_2/\text{Et}_2\text{O}$. Each crop of crystals was collected on a fritted filter and washed with ether (3 x 25 mL). Product **11** was obtained as a bright yellow solid (72.6 mg, 76% yield). ^1H NMR (CDCl_3): δ 9.20 (1H, dd, $J = 5.4, 1.6$ Hz), 8.96 (2H, dt, $J = 4.9, 1.4$ Hz), 8.07 (1H, dd, $J = 8.0, 1.5$ Hz), 7.93-7.79 (5H, multiple peaks), 7.53-7.44 (5H, multiple peaks), 7.39 (1H, dd, $J = 8.0, 5.7$ Hz), 7.32 (2H, dt, $J = 8.7, 2.3$ Hz). ^{13}C NMR (CDCl_3): δ 154.15, 152.52, 148.30, 147.29, 141.63, 138.89, 137.85, 136.15, 130.69, 130.09, 128.33, 127.14, 126.95, 126.86, 126.25, 125.27, 124.47, 122.50, 122.35. Note: only 19 (rather than the expected 20) carbon resonances were observed for **11**, presumably due to overlapping peaks. Anal. Calcd for $\text{C}_{24}\text{H}_{17}\text{ClN}_4\text{O}_4\text{PdS}$: C, 48.09; H, 2.86; N, 9.35. Found: C, 48.27; H, 2.91; N, 9.38.



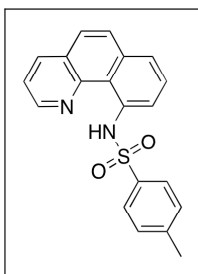
Product 13. Complex **12** (400 mg, 1.1 mmol, 1 equiv) was dissolved in MeCN (80 mL) in a 100 mL round-bottom flask equipped with a Teflon stirbar. AgOTf (545 mg, 2.1 mmol, 2 equiv) was added, and the reaction mixture was stirred for 30 min. The resulting

suspension was filtered through Celite to remove AgCl, and the Celite pad was washed with MeCN (80 mL). PhI=NTs (515 mg, 1.4 mmol, 1.3 equiv) was added, and the resulting suspension was stirred for 8 h at 25 °C. The reaction mixture was filtered through Celite, and LiCl (90 mg, 2.1 mmol, 1.7 equiv) was added to the resulting orange solution. The reaction mixture was stirred for 30 min, and then the solvent was removed under vacuum. The crude oil was dissolved in CH₂Cl₂ (50 mL), and the organic layer was washed with H₂O (3 x 100 mL) and brine (1 x 100 mL). The organic layer was dried with MgSO₄, filtered, and concentrated under vacuum. The product was recrystallized twice from CH₂Cl₂/Et₂O, and each crop was collected on a fritted filter and washed with Et₂O (3 x 50 mL). The resulting mixture contained complex **13** and a second Pd^{II} species [(py)₂PdCl₂] in a 1:1.5 ratio by ¹H NMR spectroscopy (calculated yield: 93 mg (16%)). Removal of py₂PdCl₂ was accomplished by two additional recrystallizations from THF/Et₂O. The isolated yield of pure **13** was very low (~ 4%) as a result of these multiple recrystallizations; however, the crude yield of this reaction was determined by ¹H NMR spectroscopy to be 19%. ¹H NMR (CDCl₃): δ 9.61 (1H, dd, *J* = 5.4, 1.6 Hz), 9.16 (2H, dt, *J* = 4.9, 1.5 Hz), 8.02 (1H, dd, *J* = 8.2, 1.6 Hz), 7.82 (1H, tt, *J* = 7.8, 1.6 Hz), 7.63 (1H, dd, *J* = 7.2, 1.4 Hz), 7.54 (1H, dd, *J* = 8.1, 1.5 Hz), 7.46 (1H, dd, *J* = 7.2, 0.8 Hz), 7.42 (2H, ddd, *J* = 7.7, 5.1, 1.4 Hz), 7.28 (2H, dt, *J* = 8.7, 2.2 Hz), 7.23 (1H, dd, *J* = 8.1, 5.4 Hz), 6.36 (2H, d, *J* = 8.1 Hz), 4.39 (1H, q, *J* = 7.2 Hz), 2.42 (3H, d, *J* = 7.1 Hz), 1.96 (3H, s). ¹³C NMR (CDCl₃): δ 157.2, 153.2, 140.6, 140.2, 140.0, 139.9, 139.3, 138.4, 132.1, 129.7, 128.2, 127.2, 127.0, 126.3, 125.0, 120.6, 56.0, 28.8, 21.0. HRMS-electrospray (*m/z*): calcd for [C₂₃H₂₂ClN₃O₂PdS - C₅H₅N + Na⁺], 488.9632; found, 488.9636.

Determination of ¹H NMR Yields for the Reactions of “NTs” Insertion Products with Acid. A 20 mL scintillation vial equipped with a Teflon stirbar was charged with Pd complex **8** (0.04 mmol). A mixture of MeCN (8 mL) and an appropriate amount of HCl (added as 1 M HCl in ether) was added, and the reaction mixture was stirred for 24 h. The resulting mixture was diluted with H₂O (3 mL), and the organic products were extracted into EtOAc (3 x 5 mL). The organic layers were combined, dried with MgSO₄, filtered, and evaporated to dryness. The resulting oils were analyzed by ¹H NMR spectroscopy in order to determine the percent conversion. Notably, the reactions with AcOH and TFA were carried out using the acid as the solvent.

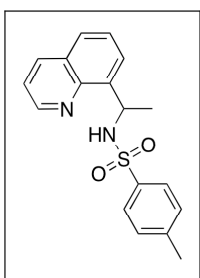


Product 14. This product was observed by ^1H NMR spectroscopy in reactions of **12** with $\text{PhI}=\text{NTs}$ in the absence of AgOTf . The identity of **14** was confirmed by preparation of an authentic sample *via* Pd-catalyzed chlorination of 8-ethylquinoline with CuCl_2 .⁴ Product **14** was purified by chromatography on silica gel ($R_f = 0.15$ in 95% hexanes, 5% ethyl acetate) and was isolated as a white solid (41.2 mg, 9% yield). ^1H NMR (CDCl_3): δ 8.96 (1H, dd, $J = 4.2$ Hz, 1.8 Hz), 8.17 (1H, dd, $J = 8.3$ Hz, 1.8 Hz), 8.02 (1H, dd, $J = 7.3$ Hz, 1.4 Hz), 7.78 (1H, dd, $J = 8.3$ Hz, 1.4 Hz), 7.59, (1H, dd, $J = 7.8$ Hz, 7.6 Hz), 7.43 (1H, dd, $J = 8.3$ Hz, 4.2 Hz), 6.66 (1H, q, $J = 6.8$ Hz), 1.99 (3H, d, $J = 6.9$ Hz). ^{13}C NMR (CDCl_3): δ 150.0, 144.9, 141.1, 136.5, 128.3, 128.1, 127.1, 126.6, 121.4, 53.3, 26.5. HRMS-electrospray (m/z): M^+ calcd for $\text{C}_{11}\text{H}_{10}\text{ClN}$, 191.0502; found, 191.0495.



Product 15. Complex **8** (61.0 mg, 0.11 mmol, 1 equiv) was weighed into a 20 mL scintillation vial equipped with a Teflon stirbar. MeCN (8 mL) and HCl (as a 1 M solution in Et_2O , 5 equiv) were added. The reaction was stirred for 24 h, and then diluted with saturated NaHCO_3 (50 mL). The aqueous layer was extracted with ethyl acetate (3 x 50 mL), and the combined organic layers were dried with MgSO_4 , filtered, and evaporated to dryness. The resulting solid was purified by chromatography on silica gel ($R_f = 0.14$ in 80% hexanes, 20% ethyl acetate). The product **15** was isolated as a pale yellow solid (12.1 mg, 32% yield). Note: this reaction proceeded to 100% conversion as determined by ^1H NMR spectroscopy. ^1H NMR (CDCl_3): δ 8.98 (1H, dd, $J = 4.5$ Hz, 1.4 Hz), 8.25 (1H, dd, $J = 8.0$ Hz, 1.6 Hz), 7.91 (1H, dd, $J = 7.4$ Hz, 1.3 Hz), 7.80 (2H, d, $J = 8.25$ Hz), 7.74 (1H, d, $J = 8.8$ Hz), 7.63 (1H, d, $J = 8.8$ Hz), 7.61-7.52 (3H, multiple

peaks), 7.09 (2H, d, $J = 8.5$ Hz), 2.23 (3H, s), -0.72 (1H, br s). ^1H NMR (C_6D_6): δ 8.39 (1H, dd, $J = 8.0$ Hz, 1.0 Hz), 8.33 (1H, dd, $J = 4.5$ Hz, 1.8 Hz), 7.96 (2H, dt, $J = 8.5$ Hz, 1.7 Hz), 7.33 (1H, dd, $J = 8.0$ Hz, 1.8 Hz), 7.27 (1H, t, $J = 7.9$ Hz), 7.21 (1H, d, $J = 8.8$ Hz), 7.12 (1H, dd, $J = 7.9$ Hz, 0.6), 6.95 (1H, d, $J = 8.8$ Hz), 6.68 (1H, dd, $J = 8.8$ Hz, 4.5 Hz), 6.49 (2H, d, $J = 8.0$ Hz), 1.59 (3H, s), -0.49 (1H, br s). ^{13}C NMR (CDCl_3): δ 147.56, 145.97, 143.27, 138.73, 137.41, 136.85, 135.29, 129.52, 129.24, 128.80, 127.43, 127.37, 125.51, 122.89, 121.32, 117.49, 116.28, 21.55. HRMS-electrospray (m/z): $[\text{M}+\text{H}]^+$ calcd for $\text{C}_{20}\text{H}_{17}\text{N}_2\text{O}_2\text{S}$, 349.1011; found, 349.1018.



Product 16. Complex **12** (34.7 mg, 0.064 mmol, 1 equiv) was weighed into a 20 mL scintillation vial equipped with a Teflon stirbar. MeCN (8 mL) and HCl (as a 1 M solution in Et₂O) were added. The reaction was stirred for 24 h, and then diluted with saturated NaHCO₃ (50 mL). The aqueous layer was extracted with ethyl acetate (3 x 50 mL), and the combined organic layers were dried with MgSO₄, filtered, and evaporated to dryness. Analysis of the crude reaction mixture by ^1H NMR spectroscopy showed multiple aromatic products. The crude mixture was purified by chromatography on silica gel ($R_f = 0.12$ in 80% hexanes, 20% ethyl acetate), and the product (**16**) was isolated as a white solid (8.6 mg, 42% yield). ^1H NMR (CDCl_3): δ 8.78 (1H, dd, $J = 4.2$ Hz, 1.8 Hz), 8.02 (1H, dd, $J = 8.3$ Hz, 1.8 Hz), 7.62 (1H, br d, $J = 9.9$ Hz), 7.53 (1H, dd, $J = 7.5$ Hz, 2.1 Hz), 7.36 (1H, dd, $J = 8.3$ Hz, 4.2 Hz), 7.30-7.22 (4H, multiple peaks), 6.67 (2H, d, $J = 7.9$ Hz), 4.86 (1H, dq, $J = 9.9$ Hz, 7.1 Hz), 2.12 (3H, s), 1.70 (3H, d, $J = 7.1$ Hz). ^1H NMR (C_6D_6): δ 8.24 (1H, dd, $J = 4.2$ Hz, 1.8 Hz), 7.53 (1H, br d, $J = 9.7$ Hz), 7.45 (2H, dt, $J = 8.4$ Hz, 1.9 Hz), 7.27 (1H, dd, $J = 8.3$ Hz, 1.8 Hz), 7.00 (1H, dd, $J = 8.1$ Hz, 1.5 Hz), 6.92 (2H, dd, $J = 7.0$ Hz, 1.4 Hz), 6.83 (1H, dd, $J = 7.1$ Hz, 1.0 Hz), 6.58 (1H, dd, $J = 8.3$ Hz, 4.2 Hz), 6.30 (2H, d, $J = 8.0$ Hz), 5.12 (1H, dq, $J = 9.9$ Hz, 7.1 Hz), 1.67 (3H, s), 1.61 (3H, d, $J = 7.0$ Hz). ^{13}C NMR (CDCl_3): δ 148.7, 145.5, 142.0, 138.4, 137.5,

136.8, 128.9, 128.6, 128.4, 127.4, 126.5, 126.2, 121.1, 56.0, 24.4, 21.3. HRMS-electrospray (m/z): $[M+H]^+$ calcd for $C_{18}H_{19}N_2O_2S$, 327.1167; found, 327.1152.

Kinetic Measurements for Reaction of Differentially Substituted Iminoiodinane reagents with benzo[*h*]quinoline monomer 6. Complex **6** (3.0 mg, 0.0075 mmol, 1 equiv) and the iminoiodinane reagent (0.03 mmol, 4.0 equiv) were weighed into each of 24 vials. CD_3CN (0.6 mL) was added, and the reactions were stirred at 25 °C for various time intervals. The contents of each vial were transferred to an NMR tube, and a 1H NMR spectrum was recorded immediately.

Structure Determination for 8. Structure Determination. Yellow needles of **mr17** were grown from a chlorobenzene/diethyl ether solution at 22 deg. C. A crystal of dimensions 0.44 x 0.06 x 0.04 mm was mounted on a standard Bruker SMART 1K CCD-based X-ray diffractometer equipped with a LT-2 low temperature device and normal focus Mo-target X-ray tube ($\lambda = 0.71073$ Å) operated at 2000 W power (50 kV, 40 mA). The X-ray intensities were measured at 123(2) K; the detector was placed at a distance 4.969 cm from the crystal. A total of 2740 frames were collected with a scan width of 0.5° in ω and ϕ with an exposure time of 45 s/frame. The integration of the data yielded a total of 36204 reflections to a maximum 2θ value of 49.70° of which 3897 were independent and 2847 were greater than $2\sigma(I)$. The final cell constants (Table 1) were based on the xyz centroids of 6997 reflections above $10\sigma(I)$. Analysis of the data showed negligible decay during data collection; the data were processed with SADABS and corrected for absorption. The structure was solved and refined with the Bruker SHELXTL (version 6.12) software package, using the space group $C2/c$ with $Z = 8$ for the formula $C_{25}H_{20}N_3O_2SCIPd$. All non-hydrogen atoms were refined anisotropically with the hydrogen atoms placed in idealized positions. Full matrix least-squares refinement based on F^2 converged at $R1 = 0.0375$ and $wR2 = 0.0822$ [based on $I > 2\sigma(I)$], $R1 = 0.0676$ and $wR2 = 0.0942$ for all data.

Sheldrick, G.M. SHELXTL, v. 6.12; Bruker Analytical X-ray, Madison, WI, 2001.

Sheldrick, G.M. SADABS, v. 2.10. Program for Empirical Absorption Correction of Area Detector Data, University of Gottingen: Gottingen, Germany, 2003.

Saint Plus, v. 7.01, Bruker Analytical X-ray, Madison, WI, 2003.

6.5 References

- (1) Muci, A. R.; Buchwald, S. L. *Top. Curr. Chem.* **2002**, *219*, 131.
- (2) Dick, A. R.; Sanford, M. S. *Tetrahedron* **2006**, *62*, 2439.
- (3) Espino, C. G.; DuBois, J. *Modern Rodium-Catalyzed Organic Reactions*; Wiley: New York, 2005; p. 379.
- (4) Kalberer, E. W.; Whitfield, S. R.; Sanford, M. S. *J. Mol. Catal. A* **2006**, *251*, 108.
- (5) Kalyani, D.; Sanford, M. S. *Org. Lett.* **2005**, *7*, 4149.
- (6) Desai, L. V.; Hull, K. L.; Sanford, M. S. *J. Am. Chem. Soc.* **2004**, *126*, 9542.
- (7) Dick, A. R.; Hull, K. L.; Sanford, M. S. *J. Am. Chem. Soc.* **2004**, *126*, 2300.
- (8) Yoneyama, T.; Crabtree, R. H. *J. Mol. Catal. A* **1996**, *108*, 35.
- (9) Kalyani, D.; Dick, A. R.; Anani, W. Q.; Sanford, M. S. *Tetrahedron* **2006**, *62*, 11483.
- (10) Kalyani, D.; Dick, A. R.; Anani, W. Q.; Sanford, M. S. *Org. Lett.* **2006**, *8*, 2523.
- (11) Hull, K. L.; Anani, W. Q.; Sanford, M. S. *J. Am. Chem. Soc.* **2006**, *128*, 7134.
- (12) Giri R.; Chen, X.; Yu, J.-Q. *Angew. Chem., Int. Ed.* **2005**, *44*, 2112.
- (13) Deprez, N. R.; Kalyani, D.; Krause, A.; Sanford, M. S. *J. Am. Chem. Soc.* **2006**, *128*, 4972.
- (14) Kalyani, D.; Deprez, N. D.; Desai, L. V.; Sanford, M. S. *J. Am. Chem. Soc.* **2005**, *127*, 7330.
- (15) Daugulis, O.; Zaitsev, V. G. *Angew. Chem., Int. Ed.* **2005**, *44*, 4046.
- (16) Stowers, K. J.; Sanford, M. S. *Org. Lett.* **2009**, *11*, 4584.
- (17) Deprez, N. D.; Sanford, M. S. *J. Am. Chem. Soc.* **2009**, *131*, 11234.
- (18) Racowski, J. M.; Dick, A. R.; Sanford, M. S. *J. Am. Chem. Soc.* **2009**, *131*, 10974.
- (19) Dick, A. R.; Kampf, J. W.; Sanford, M. S. *J. Am. Chem. Soc.* **2005**, *127*, 12790.
- (20) Halfen, J. A. *Curr. Org. Chem.* **2005**, *9*, 657.
- (21) Bhawmick, R.; Biswas, H.; Bandyopadhyay, P. *J. Organometallic Chem.* **1995**, *498*, 81.
- (22) Mahy, J. P.; Battioni, P.; Bedi, G.; Mansuy, D.; Fisher, J.; Weiss, R.; Morgenstern-Badarau, I. *Inorg. Chem.* **1988**, *27*, 353.
- (23) Dick, A. R.; Remy, M. S.; Kampf, J. W.; Sanford, M. S. *Organometallics* **2007**, *26*, 1365.
- (24) Bugarčić, Z. D.; Liehr, G.; van Eldik, R. *J. Chem. Soc., Dalton Trans.* **2002**, 951.
- (25) Peters, J. C.; Harkins, S. B.; Brown, S. D.; Day, M. W. *Inorg. Chem.* **2001**, *40*, 5083.
- (26) Cockburn, B. N.; Howe, D. V.; Keating, B. F.; Johnson, B. F. G.; Lewis, J. J. *J. Chem. Soc., Dalton Trans.* **1973**, *40*, 5083.
- (27) Kamaraj, K.; Bandyopadhyay, D. *Organometallics* **1999**, *18*, 438.
- (28) Kamaraj, K.; Bandyopadhyay, D. *J. Am. Chem. Soc.* **1997**, *119*, 8099.
- (29) Valk, J.-M.; Boersma, J. van Koten, G. *Organometallics* **1996**, *15*, 4366.
- (30) Alsters, P. L.; Teunissen, H. T.; Boersma, J.; Spek, A. L.; van Koten, G. *Organometallics* **1993**, *12*, 4691.

-
- (31) Alsters, P. L.; Engel, P. F.; Hogerheide, M. P.; Copijn, M.; Spek, A. L.; van Koten, G. *Organometallics* **1993**, *12*, 1831.
- (32) Lagunas, M.; Gossage, R. A.; Spek, A. L.; van Koten, G. *Organometallics* **1998**, *17*, 731.
- (33) Fahey, D. R. *J. Organometallic Chem.* **1971**, *27*, 283.
- (34) Roy, A. H.; Hartwig, J. F. *J. Am. Chem. Soc.* **2003**, *125*, 13944.
- (35) Roy, A. H.; Hartwig, J. F. *J. Am. Chem. Soc.* **2001**, *123*, 1232.
- (36) Ke, Z.; Cundari, T. R. *Organometallics* **2010**, *29*, 821.
- (37) Thu, H.-Y.; Yu, W.-Y.; Che, C.-M. *J. Am. Chem. Soc.* **2006**, *128*, 9048.
- (38) Mei, T. S.; Wang, X.; Yu, J. Q. *J. Am. Chem. Soc.* **2009**, *131*, 10806.
- (39) Li, J. J.; Mei, T. S.; Yu, J. Q. *J. Angew. Chem., Int. Ed.* **2008**, *47*, 6452.
- (40) Jordon-Hore, J. A.; Johansson, C. C. C.; Gulia, M.; Beck, E. M.; Gaunt, M. J. *J. Am. Chem. Soc.* **2008**, *130*, 16184.
- (41) Yamada, Y.; Yamamoto, T.; Okawara, M. *Chem. Lett.* **1975**, 361.
- (42) Södergren, M. J.; Alonso, D. A.; Bedekar, A. V.; Andersson, P. G. *Tetrahedron Lett.* **1997**, *38*, 6897-6900.
- (43) Nonoyama, M.; Suzuki, K.; Yamasaki, K. *Proc. Japan Acad.* **1969**, *45*, 605-608.
- (44) Selbin, J.; Gutierrez, M. A. *J. Organometallic Chem.* **1983**, *246*, 95.
- (45) Holcomb, H. L.; Nakanishi, S.; Flood, T. C. *Organometallics* **1996**, *15*, 4228-4234.
- (46) Rajput, J.; Moss, J. R.; Hutton, A. T.; Hendricks, D. T.; Arendse, C. E.; Imrie, C. *J. Organometallic Chem.* **2004**, *689*, 1553.